

GEOMAR REPORT



RV SONNE

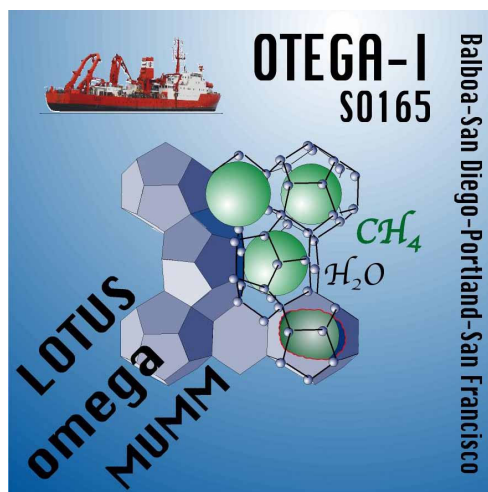
CRUISE REPORT SO165

OTEGA-I

LOTUS – OMEGA – MUMM

Balboa-San-Diego-Portland-San Francisco

June 29 – August 20, 2002



112

GEOMAR REPORT



**FS/RV SONNE
FAHRTBERICHT SO165
CRUISE REPORT SO165**

OTEGA I

LOTUS - OMEGA - MUMM

BALBOA - SAN DIEGO- PORTLAND - SAN FRANCISCO

JUNE 29 - AUGUST 20, 2002

**Edited by
O. Pfannkuche, A. Eisenhauer, P. Linke & C. Utecht
with contributions of cruise participants**

GEOMAR
Forschungszentrum
für marine Geowissenschaften
der Christian-Albrechts-Universität
zu Kiel

**KIEL 2003
GEOMAR REPORT 112**

GEOMAR
Research Center
for Marine Geosciences
Christian Albrechts University
in Kiel

Preface	1
1. Introduction.....	2
2. Objectives	4
3. Participants and participating institutions	6
4. Narrative	8
5. Preliminary Results	12
5.1 DTS-1 deep-towed sidescan sonar	12
5.2 Seafloor mapping (Bathymetry).....	23
5.3 The Fate of Methane	27
5.3.1 Methane analyses in the water column.....	27
5.3.2 CTD profiling of oceanographic parameters	36
5.3.3 METS-Mooring: Methane measurements by sensors	37
5.3.4 Flare Imaging	43
5.3.5 GasQuant.....	50
5.3.6 ADCP water current profiling.....	53
5.4 The Fluid Flux Observatory (FLUFO)	57
5.5 Deep-sea Observation System (DOS)	64
5.6 Deployment of the novel observatories BIGO and FLUFO	70
5.7 Controlled hydrodynamics inside the chambers of BIGO	82
5.8 Sediment Geochemistry	86
5.9 Hydrate Detection and Stability Determination (HDSD)	98
5.10 Sediment coring and physical properties	104
5.11 In-situ Measurements with GSPT.....	115
5.12 Sediment coring with autoclave technology.....	120
5.13 Sampling of gas hydrates and investigation of their internal structure	123
5.14 Authigenic Carbonates.....	127
5.15.1 Microbial Ecology	130
5.15.2 Beggiatoa mats at Hydrate Ridge.....	139
5.15.3 Microbial Ecology and Physiology	141
5.15.4 Molecular Ecology.....	143
5.16 Benthic foraminifera	146
6. References.....	149
7. List of stations	152

Preface

O. Pfannkuche

Natural gas hydrates represent an immense hydrocarbon resource underlying large portions of the world's ocean margins. There is increasing evidence that natural gas hydrates played a significant role in enhancing the pace of past global climate change through the release of methane, a greenhouse gas some 20 times more active than carbon dioxide. Thus the understanding of the origin, structure, and behaviour of near-surface gas hydrates and their interaction with the sedimentary and oceanic environment is critical in evaluating and quantifying their role in the global carbon cycle. International interest in science and engineering research on natural gas hydrates has been remarkably enhanced in the last decade. German investigation namely by GEOMAR contributed substantially to our present knowledge on marine gas hydrates. The finding of near sediment surface gas hydrate deposits at Hydrate Ridge (Cascadia Subduction Zone off Oregon, USA) resulted in two large international campaigns TECFLUX I (Tectonically Induced Material Fluxes) in 1999 and TECFLUX II in 2000. Investigations were mainly carried out by Canadian, German and US scientists. Results of these campaigns gave direction to the establishment of a special research focus "Gas hydrates in the Geosystem" funded by the German Ministry of Education and Research within the research topic "Geotechnologies", <http://www.geotechnologien.de/>.

Marine geo-science and biogeochemical investigations of naturally occurring gas hydrates are an overall focus at the GEOMAR Research Centre, <http://www.gashydrate.de/>. In this context the following three collaborative projects as part of the national programme "Geotechnologies" are co-ordinated here:

- **INGGAS** - Integrated Geophysical Characterisation and Quantification of Gas Hydrates, <http://www.geomar.de/~mbreitzk/inggas/index.html>
- **OMEGA** - Shallow Marine Gas Hydrates: Dynamics of a Sensitive Methane Reservoir, <http://www.gashydrate.de/projekte/omega/index.html>
- **LOTUS** - Long-term Observatory for the Study of Control Mechanisms of the Formation and Destabilisation of Gas Hydrates, http://www.geomar.de/~jgreiner/web_LOTUS/index.html.

OMEGA and LOTUS are closely co-operating with the Max Planck Institute for Marine Microbiology: The MPI coordinates the collaborative gas hydrate project:

- **MUMM** - Methane in Gashydrate-bearing Marine Sediments –Turnover Rates and Microorganisms, <http://www.mpi-bremen.de/deutsch/biogeo/mumm2.html>.

This cruise report presents the working programme, station list and first results of OMEGA, LOTUS and MUMM investigations on near sediment surface gas hydrates at Hydrate Ridge gained during SONNE Cruise No.165 (June 29 –August 21, 2002).

Acknowledgements

On behalf of all participants we would like to thank the master of FS SONNE, H. Andresen and his crew for the continued interest, flexibility and their contribution to provide an always pleasant and professional atmosphere on board. The expedition was financed by the Federal Ministry of Education and Research in Bonn (BMBF) grant no. 03G0165A. Project review and scheduling of the SONNE cruise was handled efficiently by the Projektträger Jülich.

1. Introduction

O. Pfannkuche

Understanding the origin, structure, and behaviour of near-surface gas hydrates and their interaction with the sedimentary and oceanic environment is critical in evaluating and quantifying their role in the global carbon cycle. Previous investigations have shown that massive gas hydrates close to the sediment/water interface may act as a sensitive C-reservoir due to their exposed position near the stability limit. These hydrates generate extremely high and variable fluxes of methane and influence their immediate and far-field environments.

There is growing evidence that the destabilization of gas hydrates and the resulting release of methane may be one of the most powerful influences on past abrupt climatic changes of the earth system. However, in climate research the release of methane from gas hydrates has hardly been considered in model calculations since little information exists on the geochemical cycle of methane in marine hydrates. It is not clear which proportion of methane released at the sediment-water interface reaches the atmosphere or whether the passage of large amounts of methane into the atmosphere is prevented by oxidization in the sediment boundary layer or in the overlying water column by methane-oxidizing organisms. Previous results from the TECFLUX programme suggest that a large proportion of the methane released from deeper sediments is oxidized to CO₂ in the upper sediment layers. The pathways of methane oxidation and the micro-organisms involved have not been identified yet, thus, the regulation of methane turnover in marine sediments is not understood. This is partly due to sampling problems since the quick decomposition of gas hydrates and the outgassing of methane during retrieval destroys the natural zonation of microbial and chemical processes.

Furthermore it is not known whether the exhalation of methane from the sediments into the water column represents a constant flux or if variations occur that are controlled by environmental factors. In addition, little information exists concerning the life time and temporal activity of gas hydrate deposits and methane vents, and therefore no quantitative evaluation of temporal oscillations in gas hydrate source strengths has been possible to date. Even the residence time of methane in the form of gas hydrate is totally unknown.

These deficiencies in our knowledge on marine gas hydrates led to the establishment of the collaborative research projects MUMM, LOTUS and OMEGA within in the German national research focus GEO-Technologies which combined their efforts in SONNE Cruise No. 165/OTEGA I.

Shallow gas hydrates are known from sediments of several areas of the world but there are few sites known so far where massive gas hydrate layers outcrop at the sediment water interface. At "Hydrate Ridge" on the continental margin off Oregon (Fig 1.) mixed methan-sulfide hydrates and carbonates form a massive pavement along the crest of a ridge at water depths between 600 and 1000m which are partly exposed. Vent fields from which methane charged low salinity fluids containing sulfide, ammonia, ⁴He and isotopically light CO₂ are associated with these exposures. The discharge of fluids stimulates an extraordinary large benthic carbon turnover that is in the order of one magnitude higher than at comparable ocean depth. Extensive coverage of the seafloor by bacterial mats, *Calyptogena* clams with

hydrogen sulfide immediately below the sediment water interface demonstrate the intimate relationship between, hydrate exposure, fluid discharge, biological community structure and benthic carbon turnover rates. Substantial discharge of methane bubbles into the water column was observed on the Northern and Southern Summit of Hydrate Ridge during previous expeditions (e.g. SO110, SO143, SO148) creating plumes several hundred meters in height and several kilometres in width. The wide spread carbonate pavement of Hydrate Ridge as well as frequent chemoherms result from bacterial methane oxidation and subsequent precipitation of a variety of carbon mineral phases and fabrics leading to the recognition of a class of carbonates with considerable diagnostic features related to gas hydrates.

The formulation of scientific questions for our investigations, sampling strategies and site selection during SO165 were mainly based on the results of our investigations during the TECFLUX Programme (SO143, Bohrmann et. al. 2000; SO148, Linke & Suess 2001).

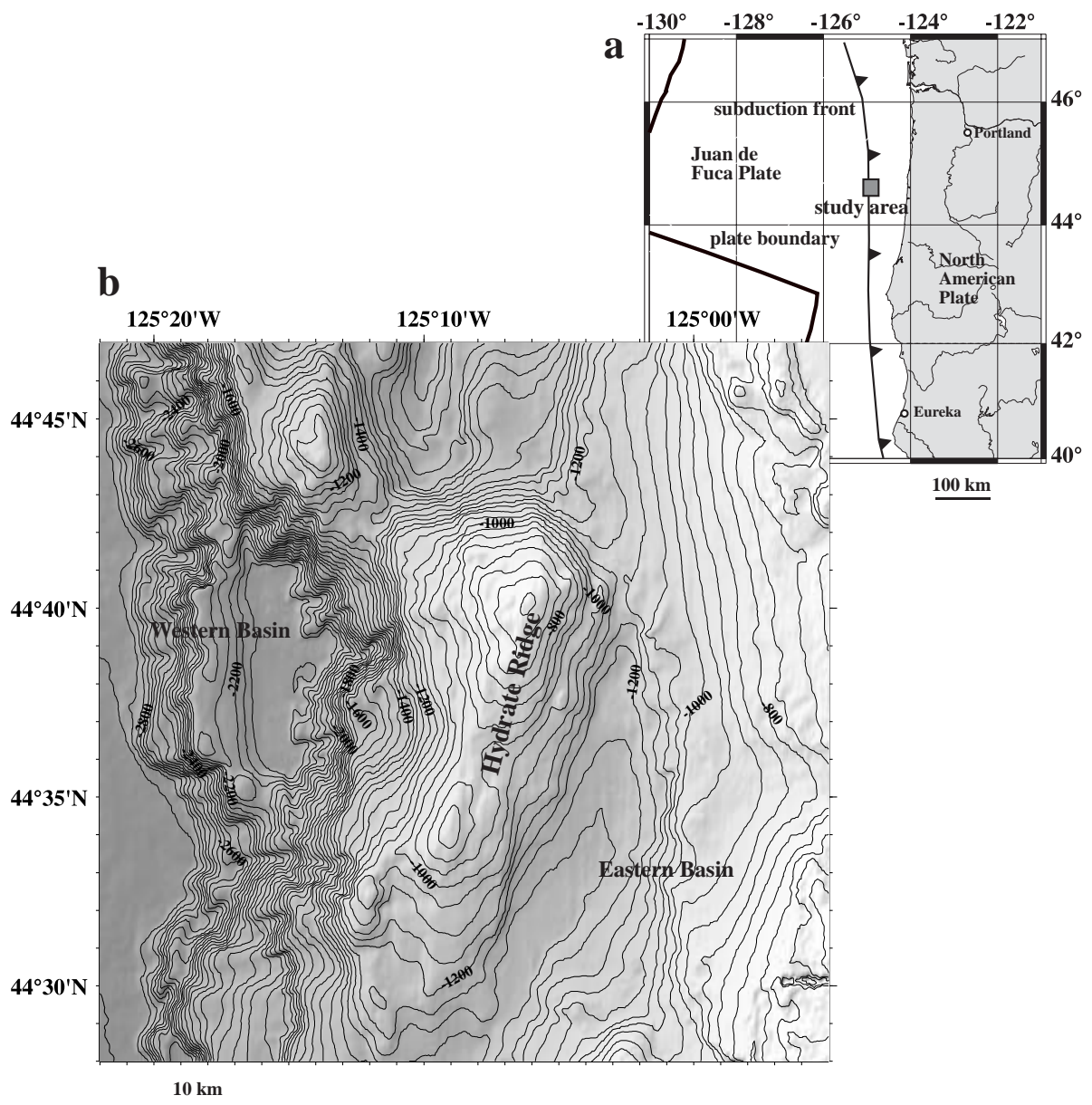


Fig. 1.1. Location and bathymetry of Hydrate Ridge.

2. Objectives

O. Pfannkuche

R/V SONNE cruise SO165/ OTEGA I represented the first joint expedition of the collaborative projects LOTUS, OMEGA and MUMM to study the gas hydrate province at Hydrate Ridge (Oregon continental margin). All three projects are funded as a part of the research initiative "Gas Hydrates in the Geo-System" within the scope of the "Geotechnologien" programme of the German Ministry of Education and Research (BMBF).

Main objectives were:

- deployments of long-term observatories to measure fluid flows and to monitor mechanisms that control the formation and dissociation of gas hydrate.
- exploration of near-surface gas hydrates structure and the conditions leading to their formation and dissociation.
- determination of the biogeochemical turnover and the role of micro-organisms in marine sediment containing gas hydrate.

The cruise was divided into two legs.

Leg 1 started in Balboa (Panama) with a short stop in San Diego and ended Portland/ Oregon.

Leg 2 started in Portland and ended in San Francisco (California).

2.1 Objectives Leg 1

Several objectives were addressed during leg 1 which was solely restricted to the Hydrate Ridge proper.

A dense lawn mower style grid was mapped with the high-resolution side scan sonar. The side scan sonar uses frequencies of 75 and 710 kHz with a 5-6 fold coverage to image the surface of Hydrate Ridge with a resolution in the range of decimetres up to centimetres.

Benthic long-term observatories were deployed to record the temporal variability of physicochemical and biogeochemical processes associated with the dissociation and formation of gas hydrate. While the conventional point-by-point and short-term measurements only record such processes on time scales of hours (biological decomposition processes) or days (fluid venting), the new observatories expand the recording times to scales corresponding to the natural controlling mechanisms.

Multiple corer samples were analysed for geochemical sediment properties. Among other things depth profiles of nutrients and chloride provided information about material flux and gas hydrate deposits in deeper parts of the sediment column.

Another focus was the assessment of methane in sediment and water. Several techniques were employed to measure methane concentrations. In addition to conventional chemical analyses of water samples, new methane sensors were deployed for the first time in a mooring. Since methane is also abundant in the bottom near water column in the form of gas bubbles building up discrete gas flares two hydroacoustic methods were used to estimate the volume of gas bubbles and thus the amount of methane by flare imaging with a ship-borne and lander-integrated system (GasQuant).

The microbiological investigations included incubation experiments to determine microbial turnovers of methane and sulfate (anaerobic oxidation of methane,

=AOM; sulfate reduction, =SR) in the sediment above gas hydrate using radio tracers. Vertical zonation of bacterial species, their composition and biomass in bacterial mats (*Beggiatoa* mats) in dependence to sulfide, nitrate and oxygen profiles was examined. Micro-electrodes were employed to measure high-resolution profiles (oxygen, pH, sulfide) in multiple corer samples. Apart from incubation experiments to determine sulfate reduction rates, a method was used for high-resolution imaging of the intensity and zonation of sulfate reduction in sediments hosting bacterial mats.

2.2. Objectives Leg 2

Leg 2 mainly focussed on sampling and processing gas hydrates. Apart from conventional sampling devices such as the TV-Multicorer, TV-grab, gravity corer and piston corer, a newly developed Multi-Autoclave Corer (MAC) was deployed for the first time. The use of autoclave technology enabled us for the first time to recover sediment cores under in situ pressure. Pressure preservation means that gas hydrate will not dissociate and sediment structure is maintained as it usually does due to changes of pressure and temperature during retrieval. Thus, we obtained pore water profiles with minimized effects of gas hydrate dissociation. One important feature was the analysis of positive chloride anomalies around gas hydrate layers. Pore water profiles obtained so far from the gas hydrate deposits of Hydrate Ridge were always affected by decompression and the time-consuming dissection of samples. An advanced stage of dissociation, which had been reached before small samples could be taken, was expressed by a marked freshening of the samples (negative chloride anomalies). After berthing in San Francisco autoclave samples were examined by computer tomography to image the internal structure of gas hydrates under in situ conditions.

Another topic was the measurement of basic physical properties of sediments containing gas hydrate. A SwordFish system developed by Christian Situ, Vancouver/ Ca. was deployed for this purpose. This remotely controlled, 6 m long penetrating lance with sensors collects information on several parameters such as in situ pore water pressure, permeability, density, water content and shear wave velocity. It can also take pore water samples (water and gas), preserving their hydrostatic pressure. Samples serve for calculating the amounts of fluid and gas escaping from the sediment into the hydrosphere on diffuse pathways. The microbiological programme was continued with radio tracer incubation experiments for the determination of microbial turnover of methane and sulfate and extended with studies on the AOM activity in sediments above gas hydrate and directly within gas hydrate layers under in vitro conditions. Furthermore, samples were taken to cultivate the AOM consortium and develop AOM active mesocosms. The experiments will be complemented by molecular biological analyses of the diversity of microbial symbiotic consortia within the sediment and an identification and quantification of micro-organisms directly associated with gas hydrate at the MPI Bremen.

3. Participants and participating institutions

Leg 1 (Balboa – San Diego – Portland): 28.6.-3.8.02, San Diego 9.7.02

1.	Pfannkuche	Olaf	GEOMAR
2.	Bannert	Bernhard	OKTOPUS
3.	Bellier	Frederic	IXSEA Oceano
4.	Drews	Manuela	GEOMAR
5.	Greinert	Jens	GEOMAR
6.	Gubsch	Stefan	TU-HH
7.	Hägele	Daniela	GEOMAR
8.	Heinz	Petra	IfG Tübingen
9.	Jakobi	Fabian	MPI Bremen
10.	Kähler	Anja	BioLab
11.	Keir	Robin	GEOMAR
12.	Klaucke	Ingo	GEOMAR
13.	Kriwanek	Sonja	GEOMAR
14.	Linke	Peter	GEOMAR
15.	Mählich	Birte	GEOMAR
16.	Mörz	Tobias	GEOMAR
17.	Pieper	Martin	BioLab
18.	Poser	Michael	Oktopus
19.	Preisler	Andre	MPI Bremen
20.	Queisser	Wolfgang	GEOMAR
21.	Sommer	Stefan	GEOMAR
22.	Treude	Tina	MPI Bremen
23.	Türk	Mathias	GEOMAR
24.	Viergutz	Thomas	TU-HH
25.	Ziebis	Wiebke	SCRIPPS

Leg 2 (Portland – San Francisco): 3.8.02 - 21.8.02

1.	Eisenhauer	Anton	GEOMAR
2.	Abbegg	Friedrich	GEOMAR
3.	Albrecht	Ingrun	GEOMAR
4.	Brückmann	Warner	GEOMAR
5.	Christian	Harold	ChristianSitu
6.	Drews	Manuela	GEOMAR
7.	Fürhaupter	Karin	Marilim
8.	Greinert	Jens	GEOMAR
9.	Hohnberg	Hans-Jürgen	MAT-TUB
10.	Liebetau	Volker	GEOMAR
11.	Lösekan	Tina	MPI Bremen
12.	Luff	Roger	GEOMAR
13.	Lunau	Angela	BioLab
14.	Mählich	Birte	GEOMAR
15.	Mudrack	Horst	MAT-TUB
16.	Nauhaus	Katja	MPI
17.	Petersen	Asmus	KUM
18.	Polansky	Julia	MPI
19.	Treitschke	Michaela	GEOMAR
20.	Treude	Tina	MPI

Participating Institutions

BioLab	Forschungsinstitut, Kieler Str. 51, 24594 Hohenwestedt.
Christian Situ	Geotechnical & Geoenvironmental Consulting, Vancouver, Canada V6E 1Y8
GEOMAR	Forschungszentrum für marine Geowissenschaften, Wischhofstr. 1-3, 24148 Kiel
IfG Tübingen	Institut für Geowissenschaften, Universität Tübingen, Sigwartstr. 10, 72076 Tübingen
KUM GmbH	Wischhofstr. 1-3, 24148 Kiel
Marilim GmbH	Gewässeruntersuchung, Wischhofstr. 1-3, 24148 Kiel
MAT-TUB	Maritime Technik, Technische Universität Berlin, Müller-Breslau-Str., 10623 Berlin
MPI	Max-Planck-Institut für Marine Mikrobiologie, Celsiusstr.1, 28359 Bremen
IXSEA Oceano	Rue Rivoalon, Sainte-Anne du Portzic, 29200 Brest
Oktopus GmbH	Kieler Str. 51, 24594 Hohenwestedt
SCRIPPS	Institution of Oceanography, 9500 Gilman Drive, La Jolla, Ca.92093
TU-HH	Ocean Engineering 1, Technical University Hamburg Harburg, Lämmersieth 72, 22305 Hamburg

4. Narrative

4.1 Narrative Leg 1

O. Pfannkuche

Leg 1 of cruise SO-165 started in Balboa (Panama) on 28.06.02 when the scientific vanguard consisting of nine persons boarded RV SONNE at 9.00h. In the course of the day eight containers with the scientific equipment for leg 1 were unloaded and stored on the ship. The sea safe storage of the equipment was continued in the morning of 29-06. At 12.30h (local time) RV. SONNE left Balboa and started its transit to Hydrate Ridge. From 30-06 to 08-07 the ship continued its transit along the mid-American coast. Scientific activity mainly comprised of the assembly of the lander systems, preparation of video-controlled launch and survey systems, programming of control units, test runs of observatory chambers in a test tank and sensor calibrations (Fig 4.1.1).

The transit to the working area was interrupted on 09-07 when the vessel called in for an intermediate stop at San Diego (California). RV SONNE was moored at San Diego harbour shortly after 09.00h (local time). The main group of scientists (15 persons) and a service technician for the POSIDONIA System from OCEANO boarded the vessel. Scientific equipment transported by air freight was taken on board. At 22.00h we left San Diego and continued our transit to Hydrate Ridge. Cruising speed of the ship decelerated by head winds. Scientists continued the preparation of instruments and laboratories.

We reached Hydrate Ridge at 05.00h local time on 13-07 and started station work immediately with two CTD/Ro casts.

On 14-07 at 08.00h we disembarked the service technician from OCEANO 1nm off Newport to a small vessel sent from ashore.

Stations work in the area of Hydrate Ridge was performed until 01-08. Benthic investigations focussed on three areas, the Northern and Southern Summit of Hydrate Ridge and to the eastern slope of the Eastern Basin (Fig. 4.2). A grid of CTD/Ro stations to study the meso-scale distribution of methane in the water column was established covering ca. 1000 square nautical miles in the Hydrate Ridge area (Fig. 4.2). A total of 149 Stations were sampled during leg 1 including 50 CTD/Ro casts, 37 TV-MUC sediment samples, 19 Lander deployments, several transects with towed gear (OFOS, Side Scan Sonar), 18kHz/Parasound surveys, multi-beam echo-sounding profiles and a variety of other gear employments (compare list of stations, app.).

Two more U.S. American research vessels worked at Hydrate Ridge during our stay, which required mutual agreements especially for activities on the Southern Summit, where methane hydrates outcrop at the sediment surface. The drilling ship JOIDES RESOLUTION was present during the entire period of our activities. RV ATLANTIS in combination with the submersible ALVIN occupied Hydrate Ridge from 26. to 29.07.

Station works in the area of Hydrate Ridge ended in the afternoon of 01-08. RV SONNE headed north to the mouth of the Columbia River and steamed upstream to Portland (Oregon). The ship berthed in Portland in the early afternoon of 02-08. In the course of 03-08 a part of the scientific equipment was unloaded and new equipment for leg 2 was taken on board. Leg 1 of cruise SONNE 165 ended on 03-08.

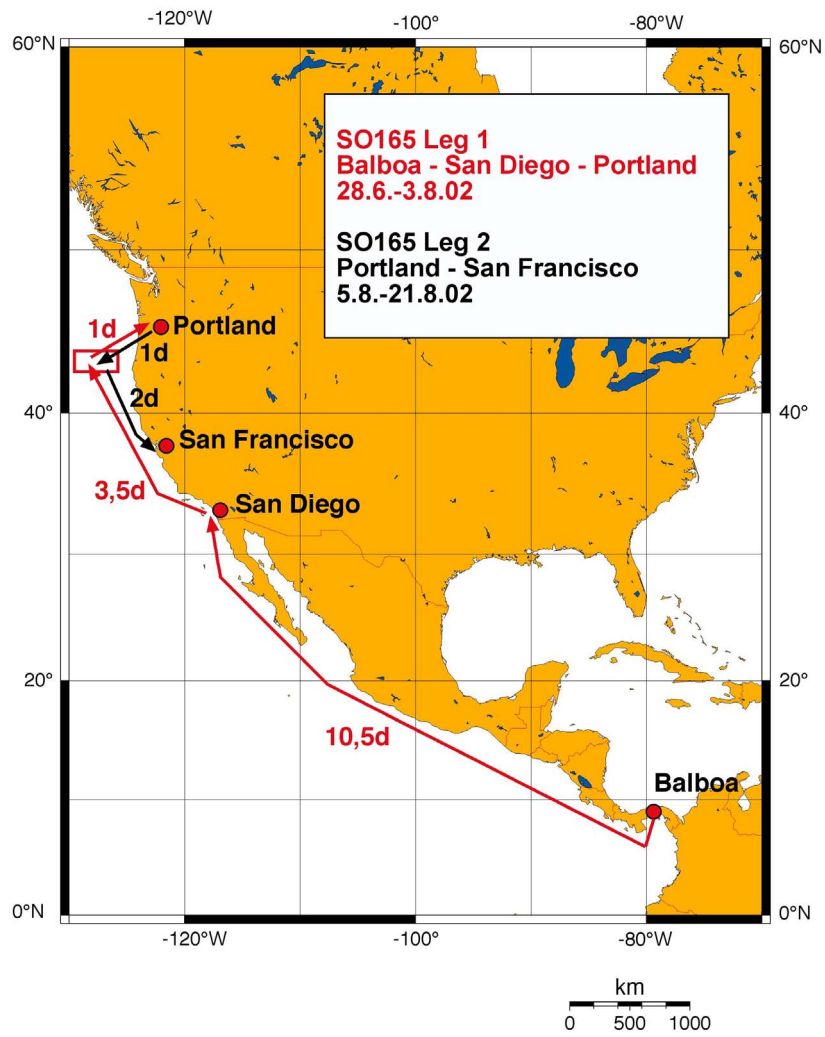


Fig. 4.1: Cruise tracks and harbours of SONNE cruise No. 165.

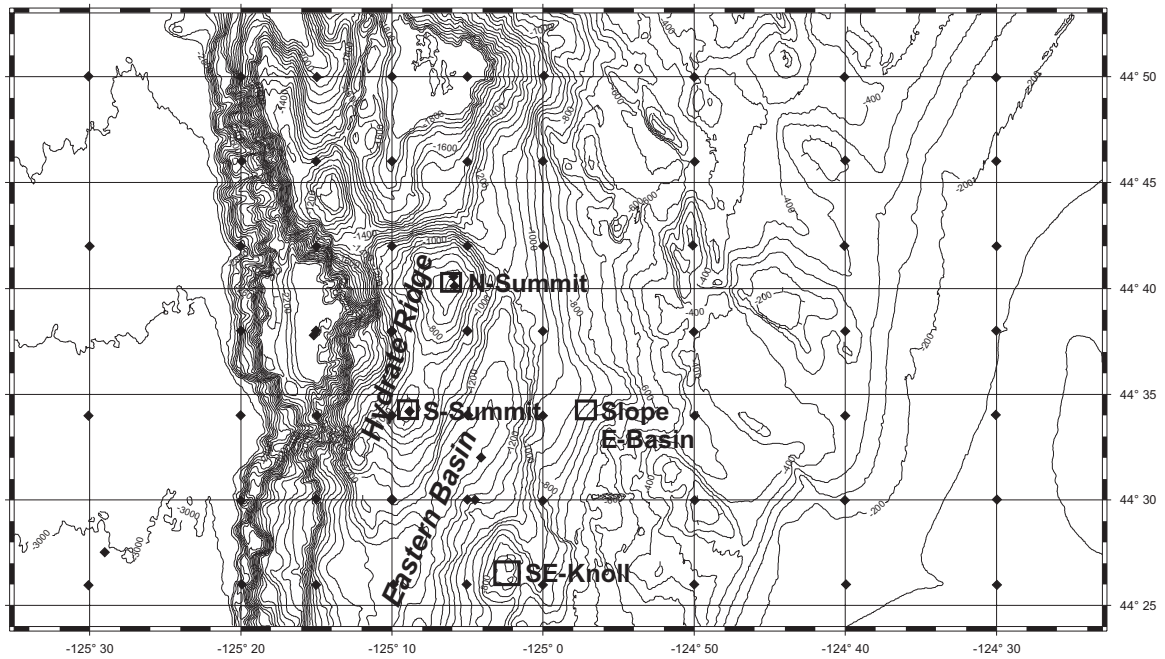


Fig. 4.2: Working areas of cruise SONNE 165 (benthos surveys indicated by boxes, CTD/Ro sampling grid indicated by diamonds)

4.2 Narrative Leg 2

A. Eisenhower

On Monday, 5. August RV SONNE left Portland harbour. During the 8 hour transit to the Pacific through the picturesque Columbia River Gorge the different working groups on board began preparing scientific equipment and laboratories. After entering the Pacific Leg 165-2 started with a CTD profile carried out near the Northern Summit of Hydrate Ridge early on the 6. August. After JOIDES Resolution completed drilling at ODP Leg 204 Site HR4b we occupied the first site on the Southern Summit of Hydrate Ridge and began operations with several MUC and one TV-grab deployment. During this first and two further deployments of the TV-grab we successfully recovered large amounts of massive gas hydrate, quickly satisfying the need for samples of the biology and geochemistry groups on board. The whole scientific crew worked jointly sifting through several cubic meters of sediment to salvage a large number of samples of hydrate and carbonates. The first deployment (station 155) of the GSPT push-in tool intended to determine in situ sediment permeability on the 6. August was unsuccessful. The lower part of the "stinger" broke off after penetrating the sediment to 1 m, a leaky pressure housing flooded part of the electronics package. The newly designed multi-autoclave corer MAK was assembled and deployed the first time on the 7. and 8. August (stations 161 and 170). During the first week of SO165-2 several unsuccessful attempts were made to recover sediment cores with gravity corers. Two Lander systems for methane flare detection and quantification deployed during Leg1 were recovered. The "Flare imaging" (station 158) detected several sources of methane bubbles on the northern Hydrate Ridge (Gusher Site), an observation that was verified with CTD profiles in this area. Sea floor observations using OFOS on the slope of the northern Hydrate Ridge near the Gusher Site (station 164) confirmed earlier results on the distribution of carbonate blocks. Observations also showed that bacterial mats and associated clam fields are less abundant than on the Southern Summit.

During the second week of cruise SO165-2, 12. to 18. August, RV Sonne was accompanied by three other research vessels (JOIDES Resolution, New Horizon, Ewing) operating in the immediate vicinity, showing the great attention Hydrate Ridge has gained in the geomarine research community. Through close coordination of our operations with the other vessels we were able to continue with our scheduled program on the southern summit of Hydrate Ridge during most of this week.

During several deployments of the TV grab system we were able to recover large amounts of gas hydrate. The recovered hydrate boulders showed a great diversity in physical appearance, from almost massive blocks to fragile, honeycomb-like structures. Due to the large amount of hydrate recovered we almost run out of cryo storage capability aboard ship.

In this week we successfully deployed the MAC (Multi Autoclave Corer), designed and build by colleagues from TU Berlin. For the first time they were able to retrieve sediment cores under in situ pressure conditions from the sea floor. The successful recovery of two pressurized sediment cores for further shore-based X-ray analysis was greeted with standing ovations from the science party assembled on deck.

During this week we also continued recovering sediments with a gravity corer and TV guided multiple corer for sedimentological, geochemical and biological work groups. However, due to indurated clay and carbonate layers only 1-2 m long cores could be retrieved on the southern Hydrate Ridge.

Several OFOS deployments on the top of SE Knoll showed that it is made up of layered carbonates and massive carbonate boulders. Using the TV grab system of Sonne we were able to secure two large block of layered carbonate for shore-based analysis. Using the CTD we continued our water column sampling program, night time operations were mostly dedicated to complete the swath bathymetry mosaic on the southern Hydrate Ridge and surrounding basins.

Cruise SO165-2 terminated its program at Hydrate Ridge on Sunday 18. August at 1800h after a final TV grab deployment on the SE Knoll. On Tuesday, 20. August the cruise SO165-2 ended after entering San Francisco harbour in the early morning.

5. Preliminary Results

5.1 DTS-1 deep-towed sidescan sonar

I. Klaucke, J. Greinert, B. Mählich

Introduction

The deep-towed high-resolution sidescan sonar investigations of Hydrate Ridge build upon previous geoacoustic studies with GLORIA (Carson et al., 1994) and SeaMARC-I sidescan sonar (Johnson and Goldfinger, 2002). These studies allowed to identify the best targets for more detailed, high-resolution studies during this cruise. Sidescan sonar mapping is a well-established technique and based on the interaction of an acoustic beam with the seafloor. The principle of sidescan sonar is that an acoustic beam is scattered at targets on the seafloor and the amount of scattering that is directed back to the instrument is recorded (Figure 5.1.1). The amount of back-scattering is related in decreasing order to the regional slope, the microtopography of the seafloor and the physical properties of the material on the seafloor. Knowing the regional slope, it is in principle possible to relate the backscatter signal to lithology, as long as the backscatter return is correctly calibrated. For more detailed information about sidescan sonar principles and data processing, refer to Blondell and Murton (1998). Compared to the previous low-resolution instruments, high-resolution DTS-1 data should provide the possibility to map the extent of near-surface gas-hydrates and associated features, such as carbonate crusts or clam fields. This surface information can then be integrated with very high-resolution subbottom information of the uppermost sedimentary layer, therefore allowing volume estimates of sedimentary units at the seafloor. Based on maps resulting from such an approach it will be subsequently possible to more clearly relate these features to the underlying structures that are believed to act as fluid conduits. Then knowing the extent of different facies related to gas hydrates, it will be possible to determine regional methane fluxes in combination with other approaches used during this cruise.

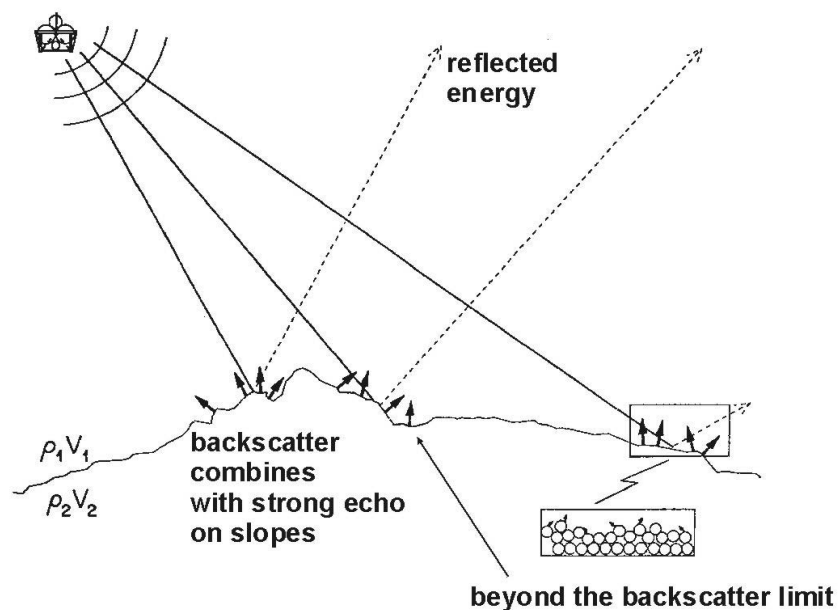


Fig. 5.1.1: General principles of backscattering of acoustic energy at the seafloor (from Johnson and Helferty, 1990).

Technical description of the instrument

Underwater set-up

The DTS-1 sidescan sonar (Fig. 5.1.2) is an EdgeTech Full-Spectrum (FS-DW) dual-frequency, chirp sidescan sonar working with 75 and 410 kHz centre frequencies. The 410 kHz sidescan sonar emits a pulse of 40 kHz bandwidth and 2.4 ms duration (giving a range resolution of 1.8 cm) and the 75 kHz sidescan sonar provides a choice between two pulses of 7.5 and 2 kHz bandwidth and 14 and 50 ms pulse length, respectively. They provide a maximum across-track resolution of 10 cm. Due to towing speeds in the range of 2.5 to 3.0 knots and a range of 750 metres during this cruise, maximum along-track resolution is of the order of 0.75 metres. In addition to the sidescan sonar sensors, the DTS-1 contains a 2-16 kHz, chirp subbottom penetrator providing a choice of three different pulses of 20 ms pulse length each: a 2-10 kHz pulse, a 2-12 kHz pulse and a 2-15 kHz pulse giving nominal vertical resolution between 6 and 10 cm. The sidescan sonars and the subbottom penetrator can be run with different trigger modes: internal, external, coupled and gated triggers. Coupled and gated trigger modes also allow to specify trigger delays. The sonar electronics provide four serial ports (RS232) in order to attach up to four additional sensors. One of these ports is used for a Honeywell altitude sensor providing information on heading, roll and pitch. Finally, there is the possibility of recording data directly in the underwater unit through a mass-storage option with a total storage capacity of 30 Gbyte.

The sonar electronic is housed in a titanium pressure vessel mounted on a towfish of 2.8m x 0.8m x 0.9m in dimension (Fig. 5.1.2). The towfish houses a second titanium pressure vessel containing the wet-end of the SEND DSC-Link telemetry system and the bottom PC of the seismic streamer data acquisition system (see also section on deep-tow streamer). In addition, a Posidonia capable OCEANO releaser with separate receiver head and a NOVATECH emergency flash and VHF transmitter are included in the towfish. The towfish can also be equipped with a forward-looking sonar, but this sensor has been removed for the present cruise in order to gain additional buoyancy at the nose of the fish. Additional syntactic foam has also been placed in the front of the towfish in order to further improve the towing behaviour. For the same reason, the towfish has been fitted with a deflector at the rear. This deflector has five positions from 0 to 5 and is designed to reduce the pitch of the towfish.

The towfish is connected to the ship's cable via the depressor (2 tons weight) through a 40 m long umbilical cable (Fig. 5.1.2). The umbilical cable is tied to a buoyant rope that takes up the actual towing forces. An additional rope has been taped to the buoyant rope and serves to pull in the instrument during recovery.

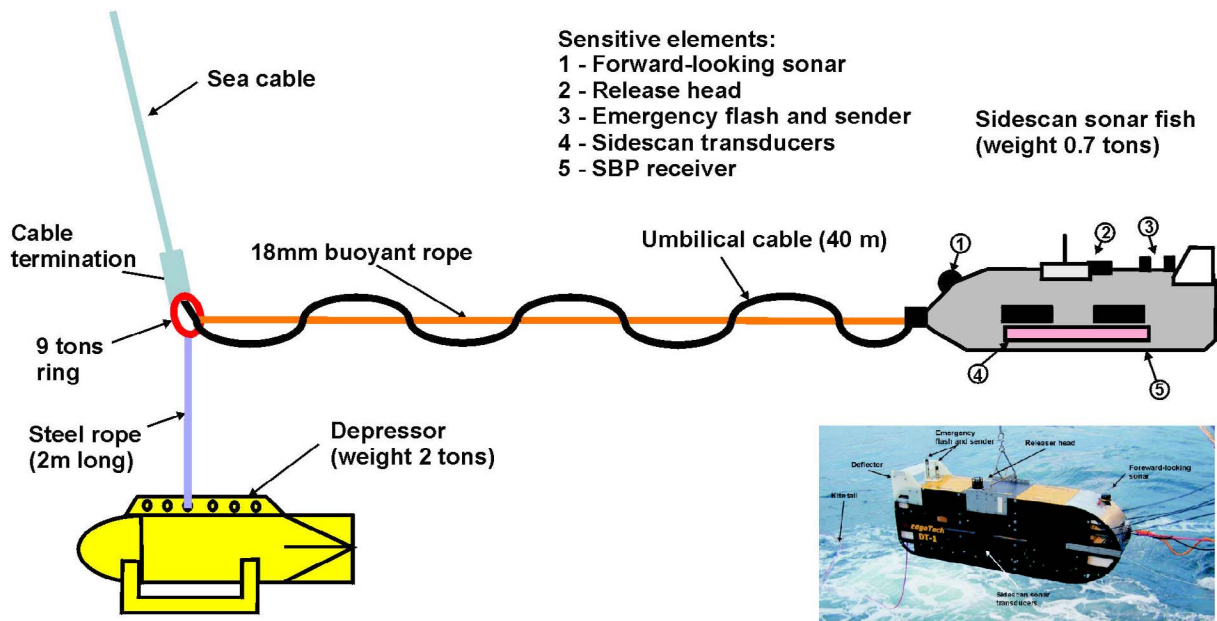


Fig. 5.1.2: The DTS-1 towing configuration and towfish.

Laboratory set-up

The laboratory set-up consists of four elements: the dry-end of the SEND DSC-Link telemetry, the topside PC of the streamer acquisition system, the EdgeTech surface interface unit FS-IU and the topside unit running ELAC Hydrostar Online software (Fig. 5.1.3). In the absence of the deep-towed seismic streamer, the only function of the bottom and topside PC of the streamer acquisition system is to provide a serial link between the OCEANO releaser operating in responder mode and the Posidonia topside unit. Hydrostar Online allows general running of the sidescan sonar and subbottom penetrator operations as well as onscreen display of a subset of the acquired data. Unfortunately some additional settings such as the trigger mode or data window size can only be changed by accessing the underwater electronics directly via the FS-IU. The FS-IU also runs JStar, a diagnostic software tool, that also allows running some basic data acquisition and data display functions.

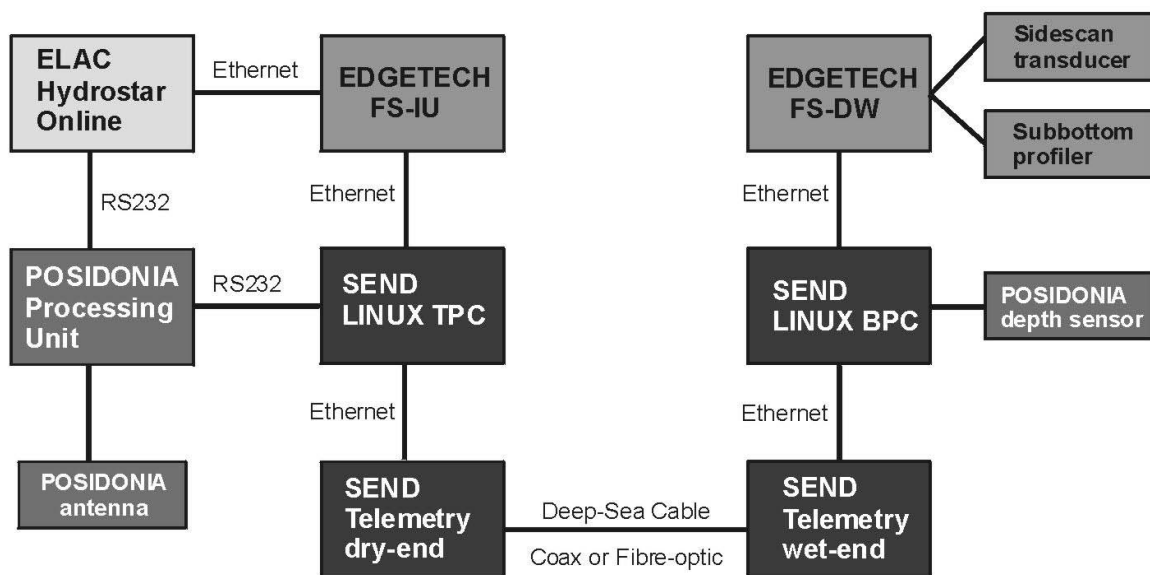


Fig. 5.1.3: The DTS-1 laboratory and electronics set-up.

Software

The main operations of the DTS-1 sidescan sonar are essentially run using HydroStar Online, a multibeam bathymetry software developed by ELAC Nautik GmbH and recently adapted to the acquisition of EdgeTech sidescan sonar data. Since cruise SO-163 a new version of HydroStar Online (version 3.3.4 beta 8) with improved onscreen data representation and time synchronisation has been available. This software package allows onscreen representation of the data, of the fish's attitude, and of the towfish's navigation when connected to the POSIDONIA system. It also allows setting some principle parameters of the sonar electronics, such as the selected pulse, the range, the power output, the gain, the ping rate, and the range of registered data. However, this version does not allow to set the trigger mode or the master subsystem in coupled trigger mode. HydroStar Online also allows to start and stop data storage either in XSE-format on the HydroStar Online computer or in JSF-format on the FS-DW. Simultaneous storage in both XSE and JSF-formats. HydroStar Online creates a new XSE-file when a file size of 10 Mb is reached, while a new JSF-file is created every 20 Mb. How fast this file size is reached depends on the amount of data generated, which in turn essentially depends on the use or not use of the high-frequency sidescan sonar. The amount of data generated is also a function of the sidescan sonar and subbottom pulses and of the data window that is specified in the sonar.ini file on the FS-DW. The data window specifies the range over which data are sampled. Proper selection of this parameter strongly depends on the selected range of the sidescan sonar system in order to avoid "good" data to be cut-off, or to prevent too large amounts of useless data using up storage space. It also proved practical to switch off data recording during turns of the ship. During the present cruise a new file was created every 3 minutes, resulting in a total of 1025 files or 2.1 Gbyte of data.

Further handling of the data is still problematic as neither the XSE nor the JSF data format can be read directly by our sidescan sonar and seismic (for the subbottom penetrator) processing software. At present patches have been developed to read sidescan sonar data into both PRISM (a software package from Southampton Oceanography Centre) and CARAIBES (a software package from IFREMER) and to read subbottom profiler data into SEISMOS.

USBL Underwater positioning

Underwater navigation of the towfish was carried out using a POSIDONIA deployable acoustic array from OCEANO Technologies, for which a number of upgrades have been made at the beginning of the cruise. The POSIDONIA system is based on a bi-directional exchange of submarine acoustic signals between one or several acoustic transponders and the acoustic array consisting of 1 transmission transducer and two pairs of hydrophones (Fig. 5.1.4). The acoustic transponders are interrogated by an acoustic signal and send a 25ms M-FSK (multi-frequency shift keying) reply. The 25ms M-FSK signal is a succession of ten monochromatic pulses (each 2.5ms long) of ten different frequencies ranging from 14.5 to 17.5 kHz. The order of frequencies during the pulse is determined by the M-FSK code. For the optimum detection of the signal with Posidonia, codes 22 or 23 should be selected. The four reception hydrophones of the array receive this signal that is then transmitted to the processing unit, which measures the phases of the signals and the time between interrogation and reply in order to deduce the relative position of the transponder and calculate its geographical position. The minimum ping interval

depends on the range of the transponder. It was kept constant at 5 s during this cruise.

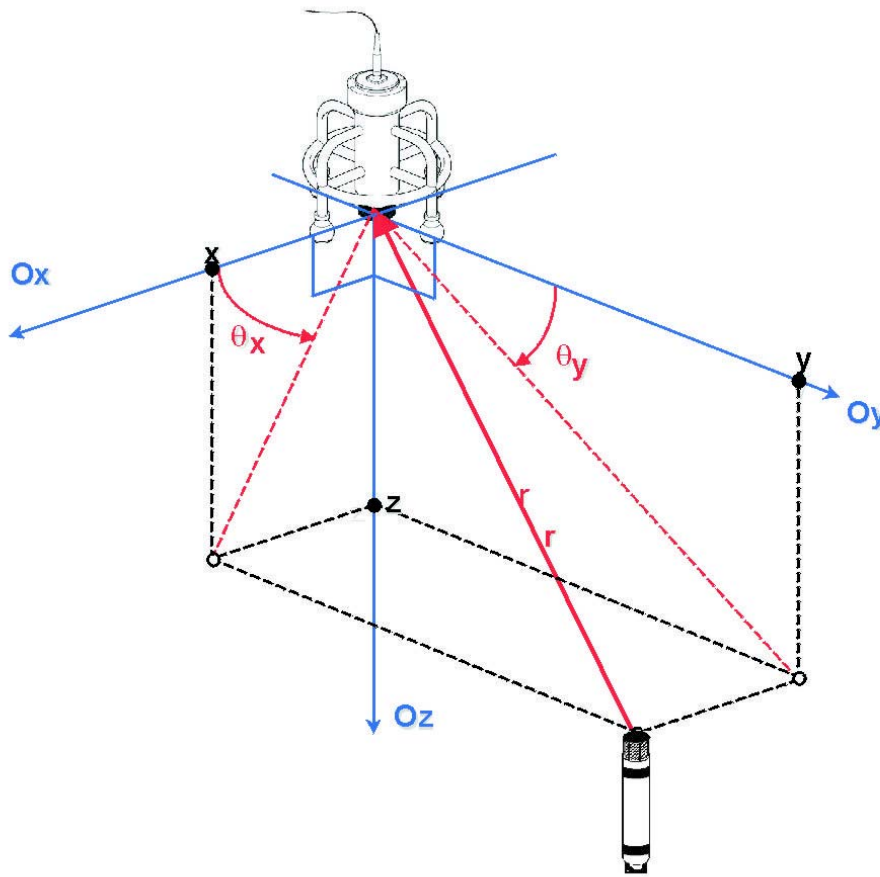


Fig. 5.1.4: The operating principles of the Posidonia USBL system.

The POSIDONIA positioning system runs in two different modes: the free mode and the towed-fish mode. In the free mode all four hydrophones are used to calculate the position of the transponder. In the towed-fish mode only the hydrophones aligned with the towed vehicle are used together with depth information provided by a built-in depth sensor. The free mode should be used when the transponder is located in a cone of 60 degrees underneath the ship, but this mode will work fine up to an angle of 120 degrees. Beyond this angle the towed-fish mode should be used. As the Posidonia antenna is not fixed permanently to the hull of the ship, the antenna has to be calibrated prior to using the Posidonia system. For this calibration an acoustic transponder has to be moored on the seafloor in water depths ranging from 1000-2000 metres, but free from any acoustic shadows, i.e. ideally some metres above ground. The ship will then describe a figure of an eight above the mooring point in order to interrogate the transponder at any angle and from either side of the vessel. The dimension of the eight figure depends on the water depth and is designed to obtain a minimum of 1000 data points. The Posidonia software then allows to calculate correction factors of roll, pitch and yaw in order to correctly position the transponder. The latest version of the software Abyss also allows setting of filters in order to eliminate bad navigation points from the final data file. This filter function also allows smoothing of the underwater navigation, a feature particularly interesting for towed instruments.

Deployment and recovery procedures

Operations for deployment and recovery of the sidescan sonar are a demanding task and require relatively calm sea for a handling that is safe for both crew and instrument. Five persons are ideal for safe operation, but during this cruise only four people were available including the responsible scientist. The deployment and especially recovery procedure could only be successful thanks to calm sea conditions. The sidescan sonar instrument should ideally be towed from the A-frame. With no speed made by the ship the kite tail is first thrown into the water and let to drift away. Then the sidescan towfish is lowered into the water (Fig. 5.1.5) and released with a special hook allowing to detach the crane cable. The sidescan fish then also drifts astern with minimal speed made by the ship. Meanwhile, the buoyant rope is secured. Then the depressor is put in place below the A-frame with the buoyant towing rope fitted to the end termination of the sea cable and the umbilical cable connected to the sea cable. Any loose ends are securely tied up and the depressor, with the towfish attached to it, is deployed. At this stage it is important that no strain is exerted on the cable connection.

During recovery, first the depressor is pulled in and secured on deck. Then the towfish is pulled close to the stern of the ship with the additional rope taped to the umbilical cable. In this way the towfish can be recovered with the air-pressure winches on the A-frame. This technique proved practical under good weather conditions, but for a short time during recovery, the sidescan sonar fish is only secured at one point and can turn freely along its long axis.

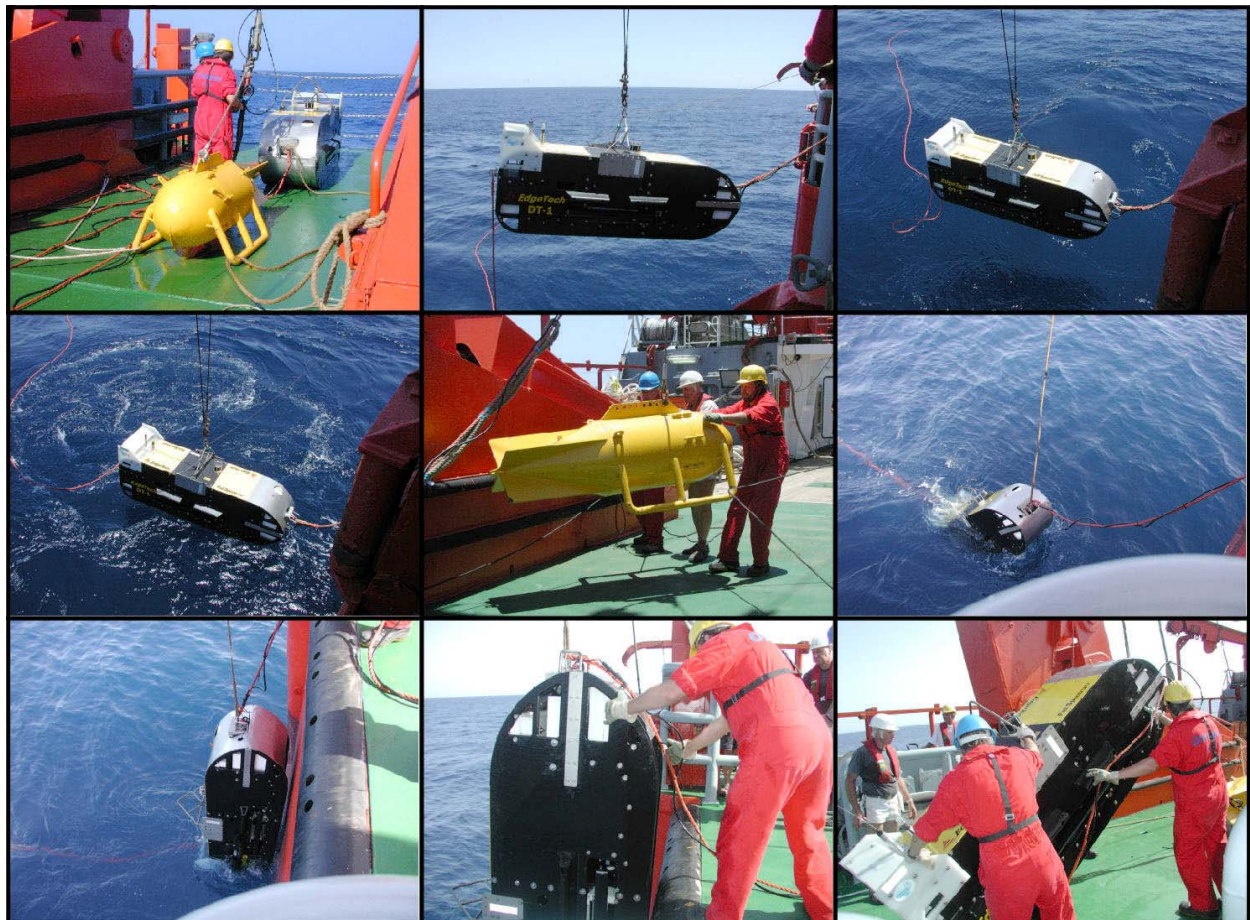


Fig. 5.1.5: The DTS-1 towfish and the depressor during deployment and recovery.

Operational settings and data quality

The DTS-1 has been deployed six times during the cruise (stations 53, 58, 79, 86, 95 and 111). Unfortunately only four of these deployment have been successful (stations 53, 58, 86, 95) while the other two deployments encountered problems with the power and data connection to the towfish. In one case (station 79) the umbilical cable broke near the connector, but could be replaced by a spare fiber-optic umbilical cable. Unfortunately, immediately after this replacement the cable on FS SONNE also broke and operations had to be stopped. The final attempt of deployment of the DTS-1 (station 111) also failed due to a not yet identified problem with the data connection to the towfish. As this problem could not be solved onboard, further deployments of the DTS-1 have not been possible.

During all deployments the principal parameters or operational settings have been kept constant in order to obtain data of similar characteristics. These settings are:

Sidescan pulse: 7.5 kHz bandwidth, 14 ms duration

Sidescan sonar range: 750 m

Sidescan sonar data window: 26000 samples

Subbottom profiler pulse: 2-10 kHz bandwidth, 20 ms duration

Subbottom profiler data window: 6000 samples

Trigger mode: coupled (sidescan was master trigger)

Ping repetition rate: 0.49 s

The four successful deployments resulted in 7 N-S trending profiles across both the northern and southern summits of Hydrate Ridge (Fig. 5.1.6). The quality of the data obtained during these deployments was overall rather satisfactory (e.g. Fig. 5.1.7), but strong acoustic interference may prove difficult to be filtered out during processing. These interferences result from the interrogation of the Posidonia transponder although the latter is working at much lower frequencies (14.5 - 17.5 kHz) than the 75 kHz sidescan sonar. These Posidonia pings are also present in the subbottom profiler data (2-10 kHz). These high-amplitude interferences at fixed intervals can be easily filtered during processing of the data. On profiles across the northern summit of Hydrate Ridge additional, strong interference patterns have been observed (Fig. 5.1.8). These interferences are not yet fully explained, but it appear likely that they were generated by 200 kHz ADCP that had been deployed as part of the DOS-Lander in this area.

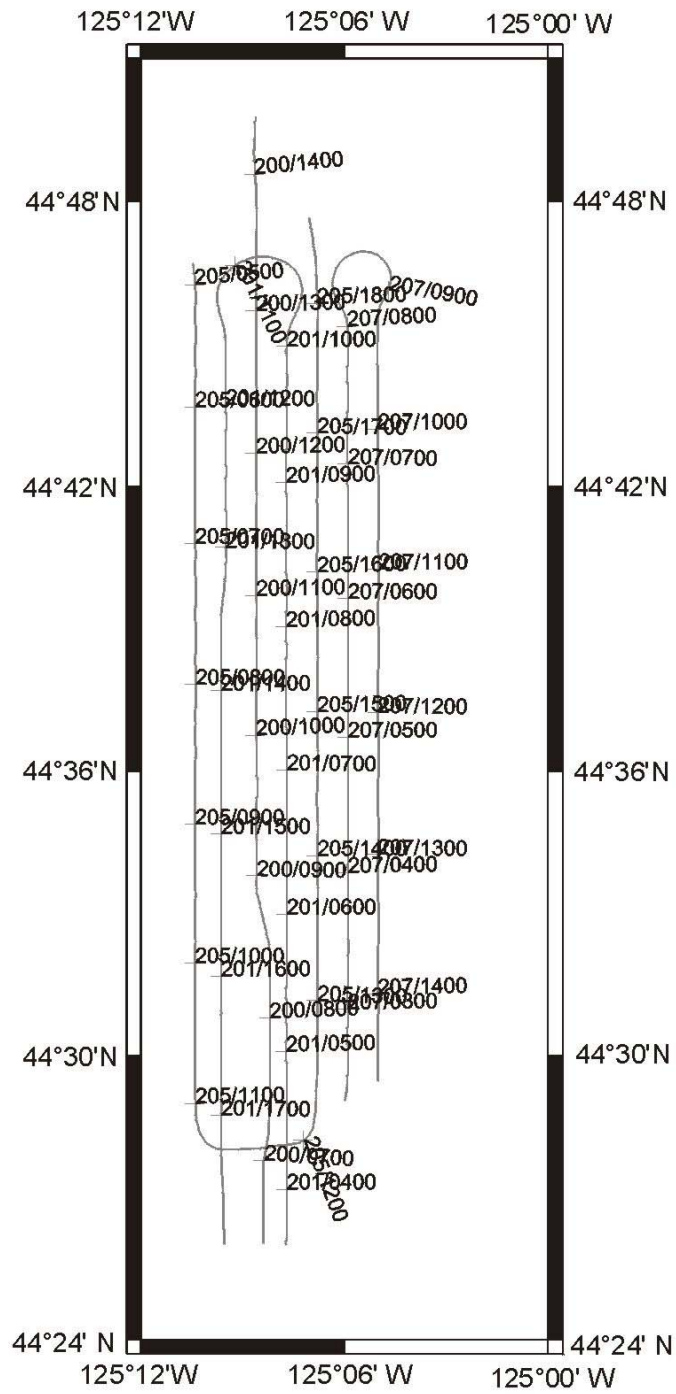


Fig. 5.1.6: Track-plot during the DTS-1 deployments.

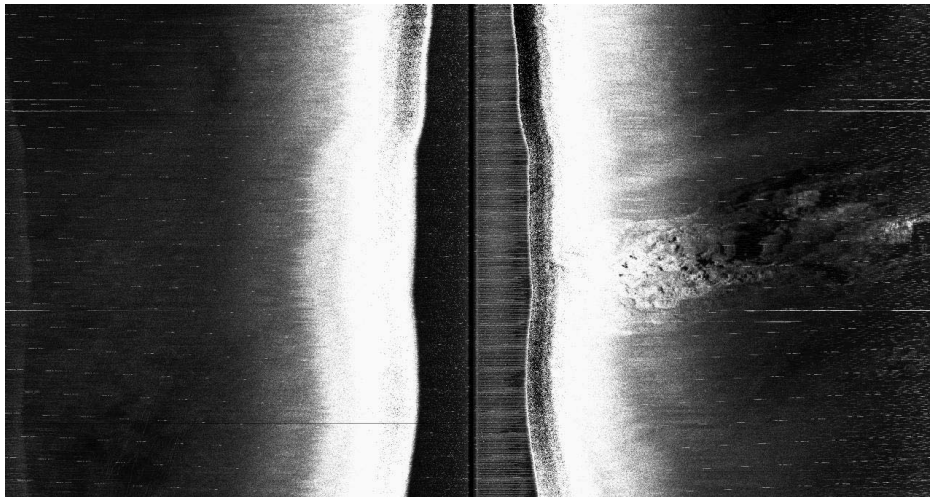


Fig. 5.1.7: Example of raw DTS-1 sidescan sonar data.

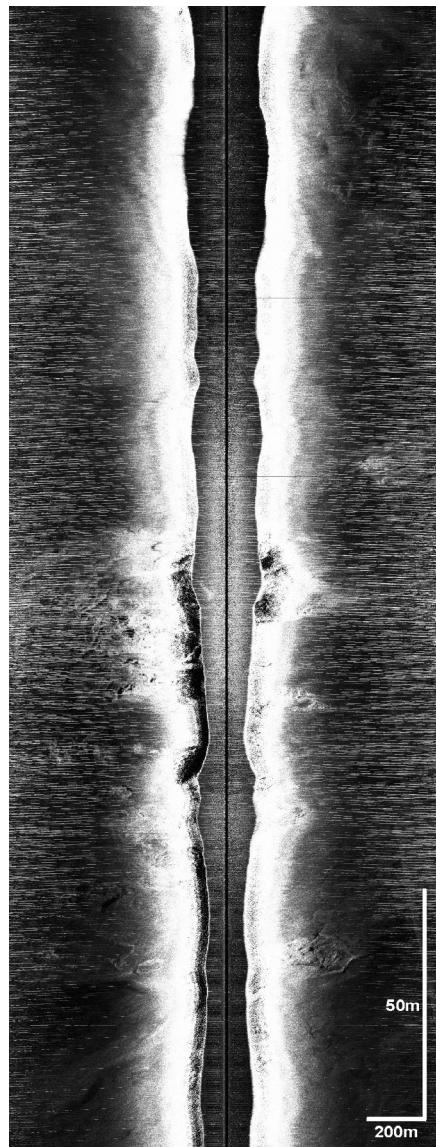


Fig. 5.1.8: Example showing strong interferences on the 75 kHz sidescan sonar imagery at the northern summit. This interference is believed to result from 200 kHz ADCP running on the seafloor.

Preliminary results

Processing and interpretation of the high-resolution sidescan sonar data are still in progress and only preliminary results can be made at this point. High-backscatter patches that are possibly related to the features we are interested in (Fig. 5.1.9) are concentrated on the two summits. For the rest of Hydrate Ridge they are still present, but distributed rather patchily. The correct correspondence between different backscatter intensities and gas hydrate related facies can only be determined after full processing of the data and integration with ground-truthing data. In addition to the various patches of high backscatter, NNE-SSW trending lineations between the two summits have also attracted our attention (Fig. 5.1.10). They might be either the surface expression of faults or sedimentary bedforms related to currents on Hydrate Ridge. This will also be investigated further in the coming months.

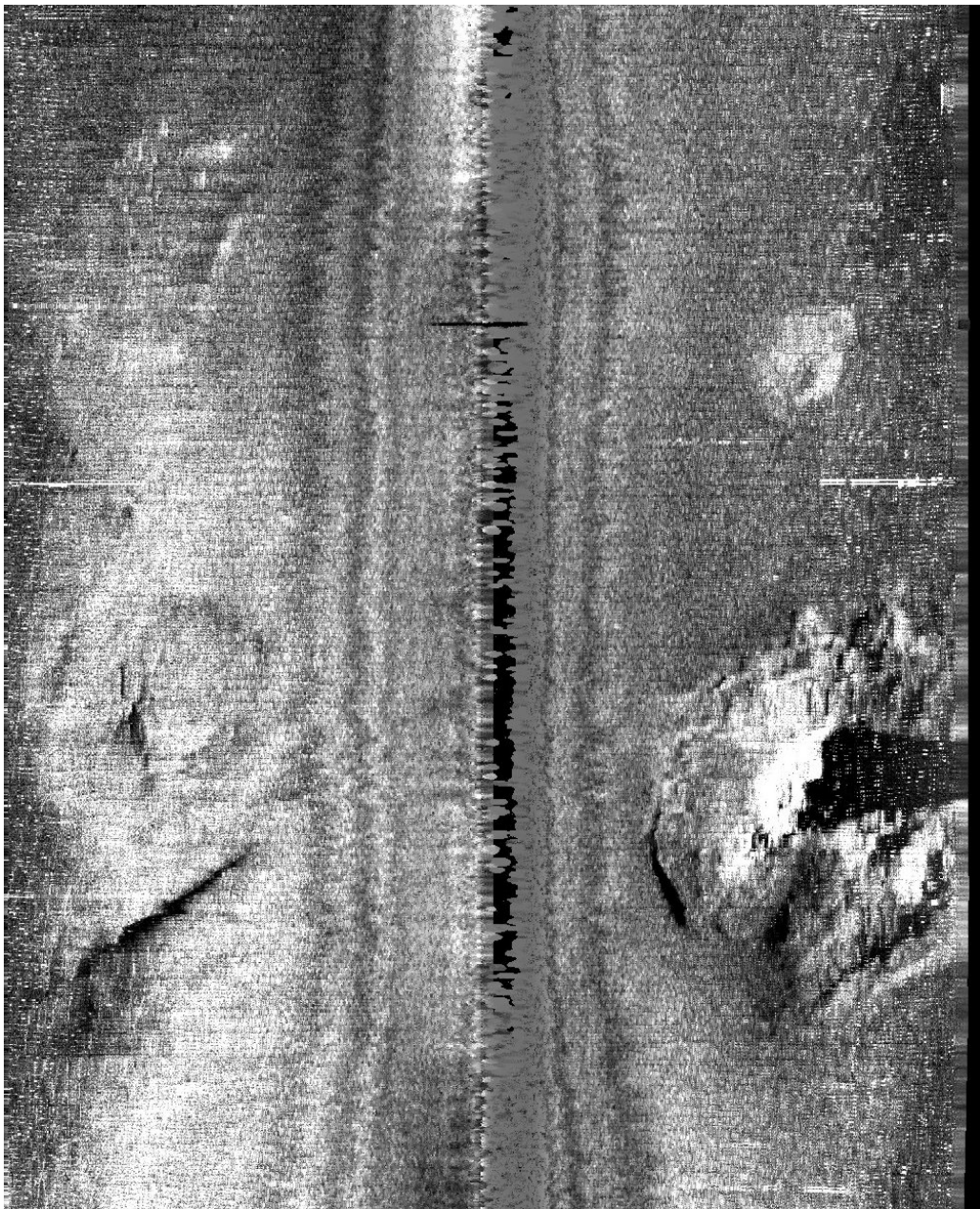


Fig. 5.1.9: Processed 75 kHz sidescan sonar profile showing several, not yet fully identified features near the southern summit of Hydrate Ridge.



Fig. 5.1.10: Processed 75 kHz sidescan mosaic showing an area with intensive lineations on the northern flank of the southern summit of Hydate Ridge

5.2 Seafloor mapping (Bathymetry)

J. Greinert, I. Klauke

We employed a new EM 120 System to map the bathymetry during both OTEGA legs. The data provides an upgrade of previous surveys in the region.

Brief technical description

The system is capable of emitting and receiving 191 beams. It was run with 50° swath width only. Resulting in a higher resolution compared to data recorded during the previous cruises. All maps shown here are based on pre-processed data. These data were statistically cleaned by the NEPTUNE software onboard RV SONNE with a grid space of 30 or 50 m. A sound velocity profile was taken from CTD-2. Pre-processed xyz and backscatter data were saved on CDs, raw data were saved on DAT tapes; both data types are stored at GEOMAR.

Results

The Hydrate Ridge itself was mapped during SO165-1 parallel to side-scan sonar surveys; additional mapping at the NW-Knoll and SE-Knoll were undertaken parallel to Flare-Imaging surveys during SO 165-1 and 2 and in advance of the TVG sampling at the SE-Knoll. An overview of the mapped areas and the cruise track during both legs are given in Figure 5.2.1 and 5.2.2. That the new SIMRAD EM 120 system has much better data quality as compared to the old Hydrosweep system is exemplified by the results from the SE-Knoll area. An overview image of the mapped area is shown in Figure 5.2.3. The map in Figure 5.2.4A was created from a 111m x 111m grid (0.001 / 0.001 degree) of the Hydrosweep data. Figure 5.2.4B shows the same area with a 15.4m x 15.4m grid (0.5 / 0.5 seconds) of the new, but only pre-processed, SIMRAD data. It becomes obviously that the uppermost pinnacle-like structure was and could not be detected by the Hydrosweep system. However, this chemoherm structure is clearly visible in the EM 120 data.

The pinnacle-like shape of the upper most top of the SE-Knoll becomes more clear in the 3D view of Figure 5.2.5A. The area and volume of this aragonite-rich chemoherm-complex above the 628 m countour line (Figure 5.2.5B) can be calculated (GMT, grdvolume) and results in 0.03556 km² (188m x 188m) and a volume of 285742 m³ (a cube of 66 m edge length). Using this volume one can estimate the carbon amount stored in this chemoherm. This estimate represents a minimum, as the volume of the SE-Knoll pinnacle is probable much bigger because the volume of the north flank below the 628 m countour is not included in the volume calculation. Assuming a carbonate content of 75 vol.% results in 632203 tons of aragonite (density 2.95 g/cm³) or 252881 tons of carbon stored in the upper cap of the SE-Knoll pinnacle. Such estimates provide a figure of the how much methane-derived carbon is fixed in chemoherm carbonates.

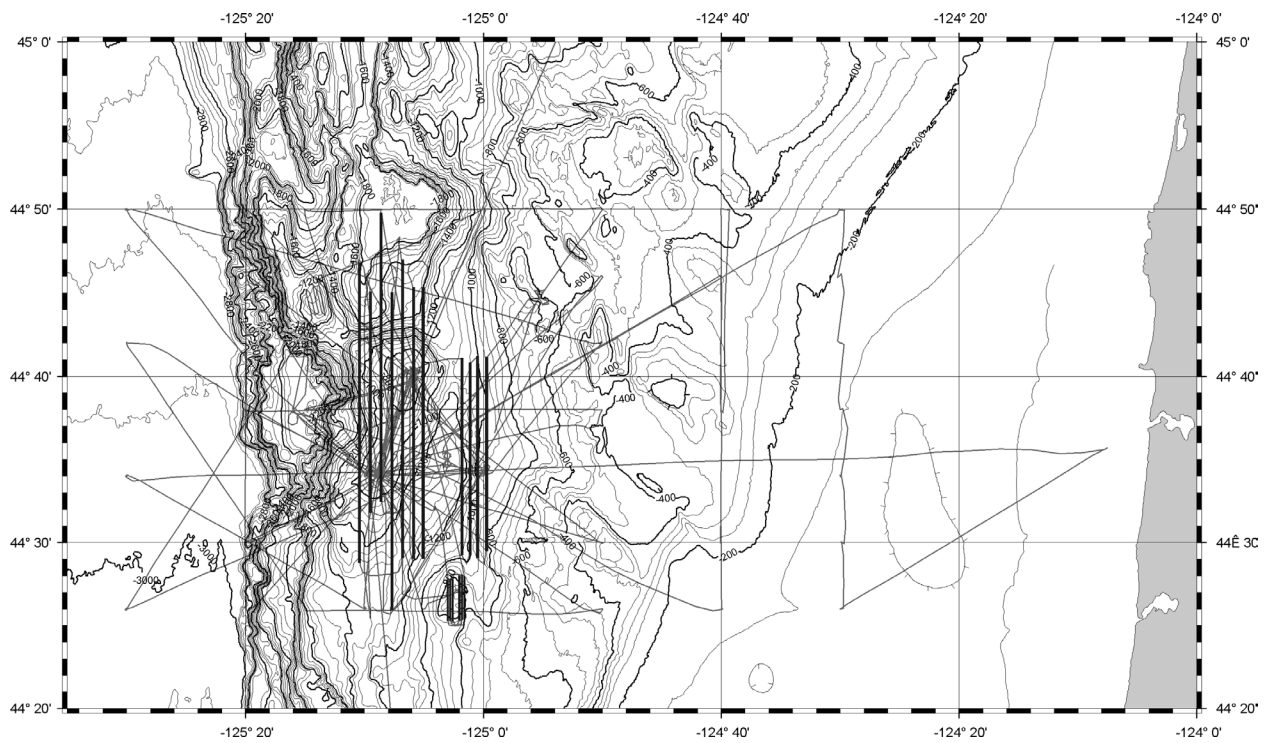


Fig. 5.2.1: Bathymetric map of the Hydrate Ridge area with cruise track of OTEGA Leg 1, SO 165-1. The broader lines mark the profiles undertaken as bathymetric station. Shown in light grey is the cruise track during SO 165-1.

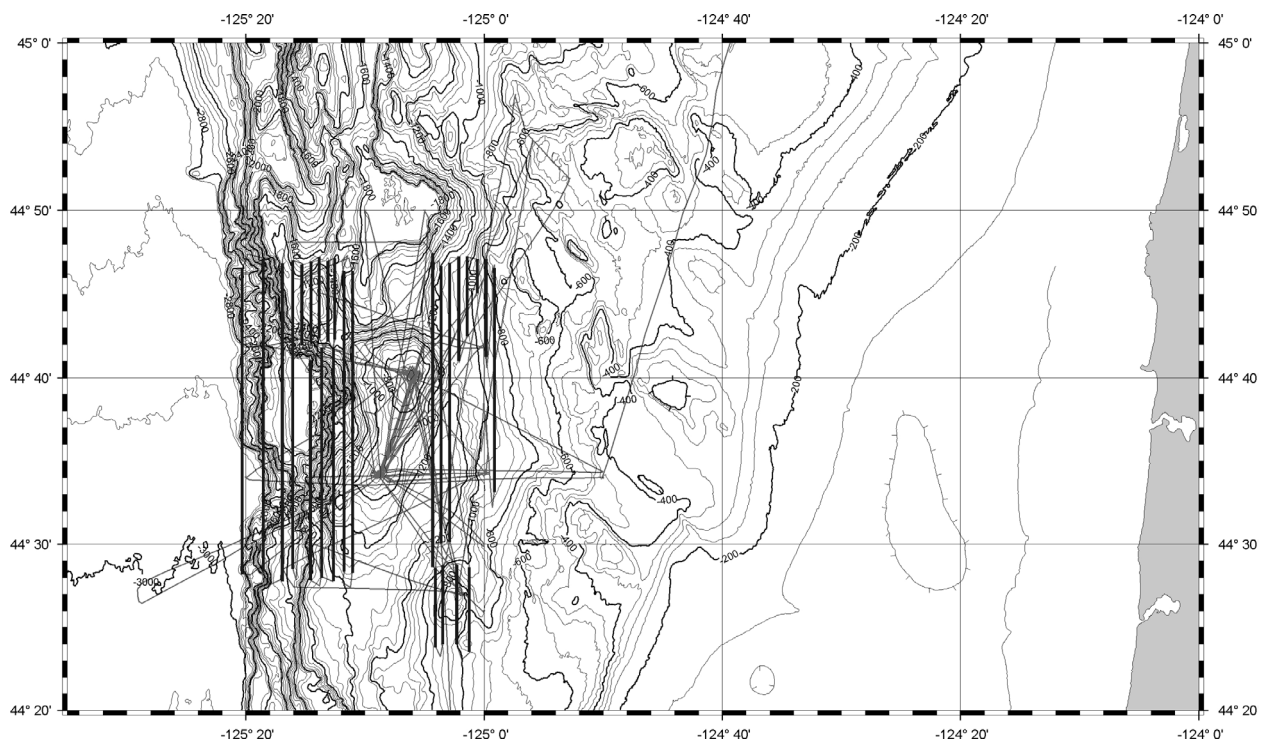


Fig. 5.2.2: Bathymetric map of the Hydrate Ridge area with cruise track of OTEGA Leg 2, SO 165-2. The broader lines mark the profiles undertaken as bathymetric station. Shown in light grey is the cruise track during SO 165-2.

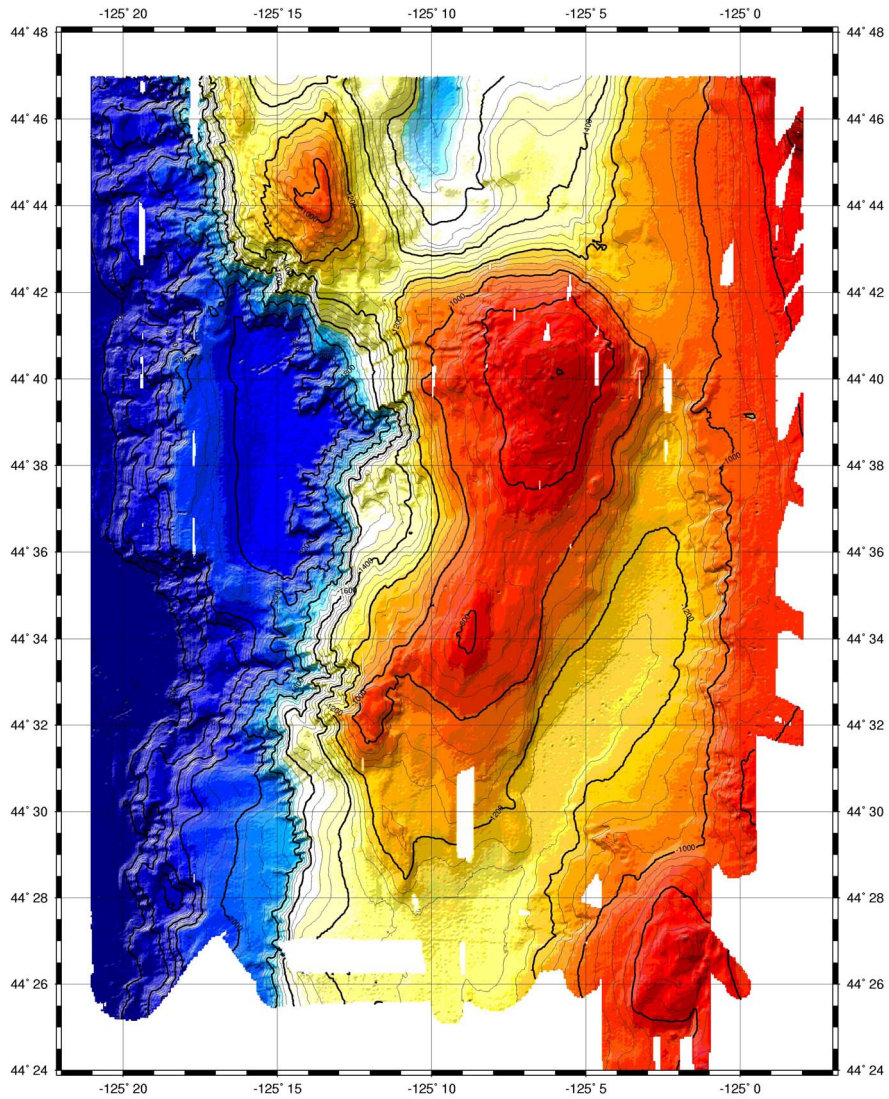


Fig. 5.2.3: Bathymetric overview of the Hydrate Ridge area using the pre-cleaned EM 120 data.

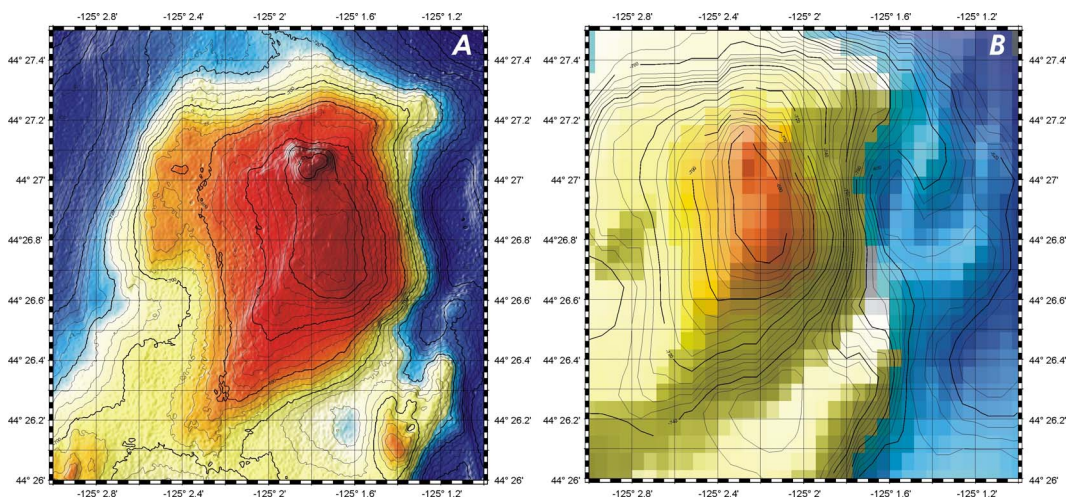


Fig. 5.2.4: The advanced data quality and resolution of the new SIMRAD system (A) shows a additional pinnacle-like structure which could not be detected with the old Hydrosweep system (B).

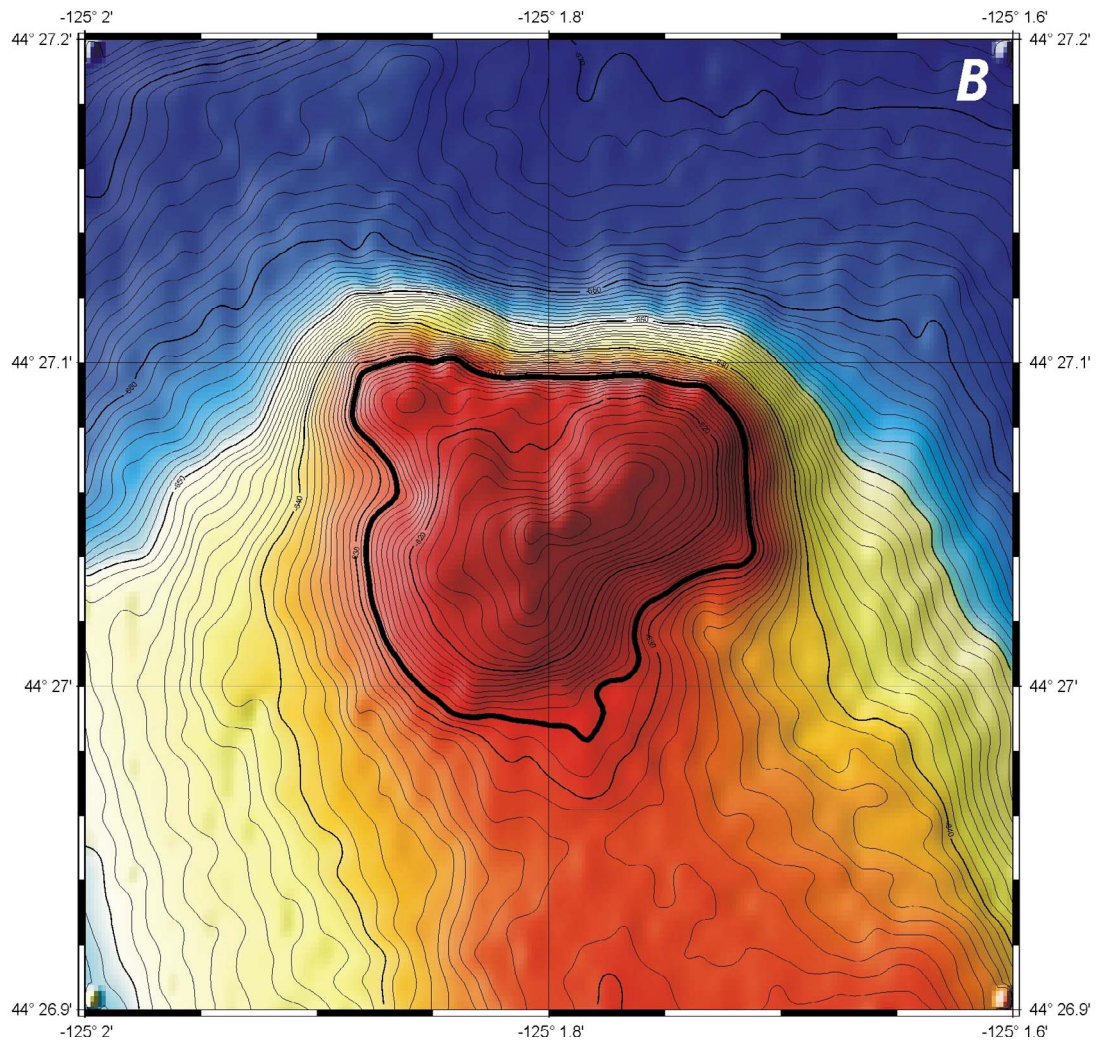
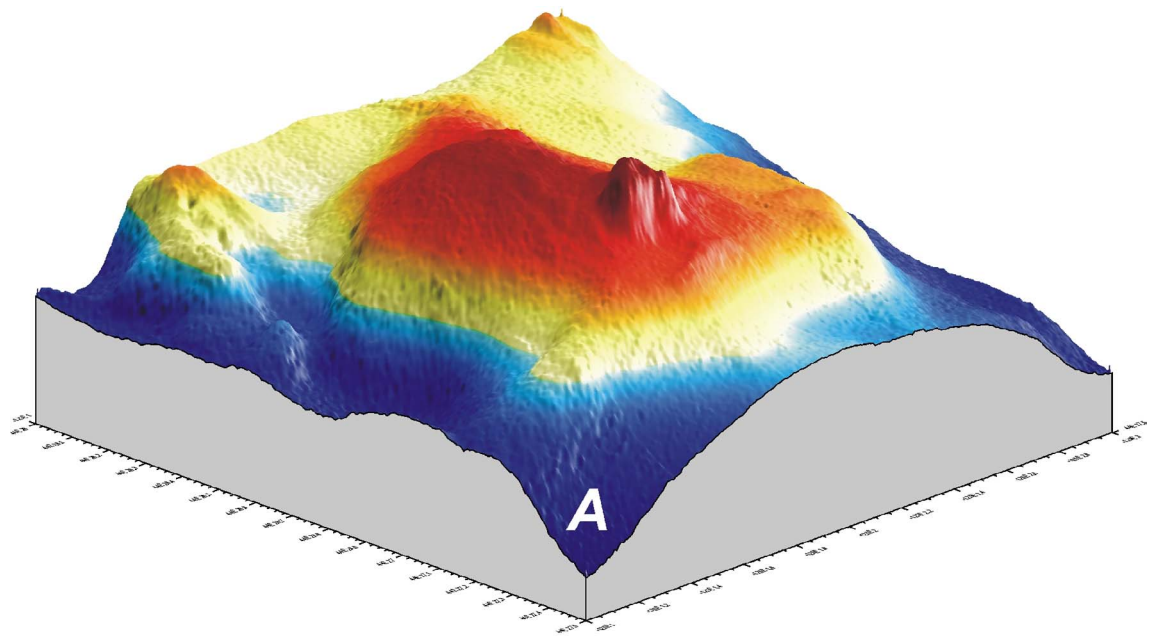


Fig. 5.2.5: A) 3D view of the SE-Knoll showing the pinnacle-like top, which is built up from aragonite-rich chemoherm carbonates. B) Detailed map of the top region of the SE-Knoll used to calculate the area and volume of the chemoherm complex.

5.3 The Fate of Methane

Geochemical and hydroacoustic investigations of the water column

J. Greinert

Introduction

Cold vents on collisional margins supply large amounts of methane to the upper sediment and water column. This influences the local benthic ecology and can result in hydrate formation when the water depth is sufficient for the clathrate stability. It has been suggested that the methane emitted may also affect the level of greenhouse gases in the atmosphere and thereby climate as well. We investigated both dissolved and free gas methane in the water column at Hydrate Ridge using the following methodology: (a) measurements of dissolved methane on water samples taken from the CTD-Rosette, (b) methane sensors, (c) a lander-deployed hydro-acoustic system, and (d) echo-sounding to detect the presence of bubble iflaresî from the bottom.

5.3.1 Methane analyses in the water column

J. Greinert, R. Keir, K. Führhaupter, B. Mählich

The goal of the methane analyses was to investigate the regional influence of vent-released and shelf-derived methane. Previous surveys have shown that the emission of methane from vents is very variable in time and space in the region around Hydrate Ridge (TECFLUX Reports 93 & 98; Heeschen, Ph.D. Thesis, 2002). In order to survey the general distribution, methane was analyzed on a grid of hydrographic stations during both legs of SO165. We sampled an area 40 by 70 kilometers with a grid of 9 by 7 sections (Figure 5.3.1.1). Additional water samples were taken for post-cruise aerobic oxidation rate measurements. This grid extends the area investigated previously eastward to the continental shelf.

Technical description

We used a SeaBird 911 CTD equipped with oxygen and METS-methane sensors. Water samples were collected with a 24-bottle carousel. Power to the METS sensor was supplied by one of the free analog ports of the CTD. This port inserts the voltage of the methane sensor and the voltage of the temperature sensor into the data string sent by the CTD telemetry to the deck unit. The recorded data are processed preliminarily with the SeaBird software using the data conversion and bin averaging tools only. The CTD raw data are stored at GEOMAR.

Methane analyses

The water samples were drawn into 2-liter pre-evacuated glass bottles. Methane from water samples was analyzed by first separating the gas and liquid phases under vacuum, recompressing the gas into a burette, and injecting a gas sample into a chromatograph equipped with a flame ionization detector. The remaining gas in the burette was transferred to a glass vial and sealed for subsequent isotopic analysis.

To convert the GC measured methane concentrations in ppmv to nmol/L the total gas volume released from the sampled water must be determined. This total gas volume is calculated as the sum of the dissolved N₂, Ar, and O₂ concentrations. The

first two are calculated from their solubilities at in-situ temperature and salinity assuming equilibrium with the atmospheric mole fractions. Dissolved oxygen was measured by the Beckmann sensor, which we calibrated against oxygen determined by Winckler titration (calibration see Figure 5.3.1.2).

The total gas volume can be calculated as following:

$$\text{total gas volume} = \text{N}_2\text{-volume} + \text{Ar-volume} + \text{O}_2\text{-volume}$$

With:

Temperature as potential temperature: T in °K

$$\text{N}_2 \text{ ml/L} = \text{EXP}(-172.4965 + 248.4262*(100/T) + 143.0738*\text{LN}(T/100) - 21.712*(T/100) + \text{Salinity}*(-0.049781 + 0.025018*(T/100) - 0.0034861*(T/100)^2)$$

$$\text{Ar ml/L} = \text{EXP}(-173.5146 + 245.451*(100/T) + 141.8222*\text{LN}(T/100) - 21.802*(T/100) + \text{Salinity}*(-0.034474 + 0.014934*(T/100) - 0.0017729*(T/100)^2)$$

The multiplication of the total gas volume per litre and the analysed methane concentration in ppmv results in a methane concentration in nl/L. Dividing the nl/L concentrations by 22.4 results in methane concentrations in nmol/L.

Results

A total of 75 CTD casts were conducted at the 63 grid-points and on the northern and southern summits of Hydrate Ridge (Figure 5.3.1.1). Three positions were sampled twice because of high amount of contaminated analyses (CTD 2 and 71, 7 and 60, 65 and 75). Four stations were undertaken to observe the methane concentration at the northern and the southern summit (CTD 29, 54 in a flare, 63 and 68; Figure 5.3.1.8). Six CTDs were deployed only for water sampling to fuel the reservoir of the BIGO lander. CTD 64 was undertaken to solve technical problems with the winch. CTD 73 was half deployed at a wrong position and no water samples were taken (not shown in Figure 5.3.1.2).

Results of our methane analyses are summarized in oceanographic sections shown in figures 5.3.1.3 and 5.3.1.6. Most of the measurements lie in a range of 0.5 to 32 nmol/L. Concentrations greater than 8 nmol/L are restricted to water depths above 700 m. From the east-west sections (Figures 5.3.1.3, 5.3.1.4), it appears that the greatest release of methane occurs on the upper continental slope near the shelf edge, in water depths of about 150 to 400 meters. In this region concentrations above 20 nmol/L are often found.

The emission of gas bubbles was observed with the Parasound at the southern summit of Hydrate Ridge. We conducted a “to-yo” hydrocast (CTD 54) at this location and observed a rising methane concentration as one ascends through the bubble flare. Most of the rise occurred within the upper 25 meters of the flare. The maximum concentration of 82 nmol/L was reached at the “top” of the flare where the acoustic backscatter had almost disappeared at a water depth of about 600

meters (Figure 5.3.1.7). One hundred meters deeper in the flare, dissolved methane concentrations were much lower, although somewhat variable. It appears that methane diffuses out of the bubbles slowly at first when they rise, up to a depth where the bubbles suddenly collapse and the gas is dissolved. This may be in part due to a hydrate “skin” lining the bubble until a depth is reached when the hydrate becomes unstable (Heeschen et al., in prep.). The methane injected into the water column at the southern summit appears to spread horizontally in a thin lens, which appears at about the 550 m level in sections 3, 4 and 5 (Figure 5.3.1.5 and 6). The concentration in the core of this lens is generally less than in the methane plumes produced near the shelf edge. In Section 3, two more lenses with higher concentrations appear overtop the one produced at the southern summit. In all of the east-west sections, “eddies” with high methane concentration appear in the upper 400 meters at various depths. This may be due to shelf-produced methane that has been carried offshore.

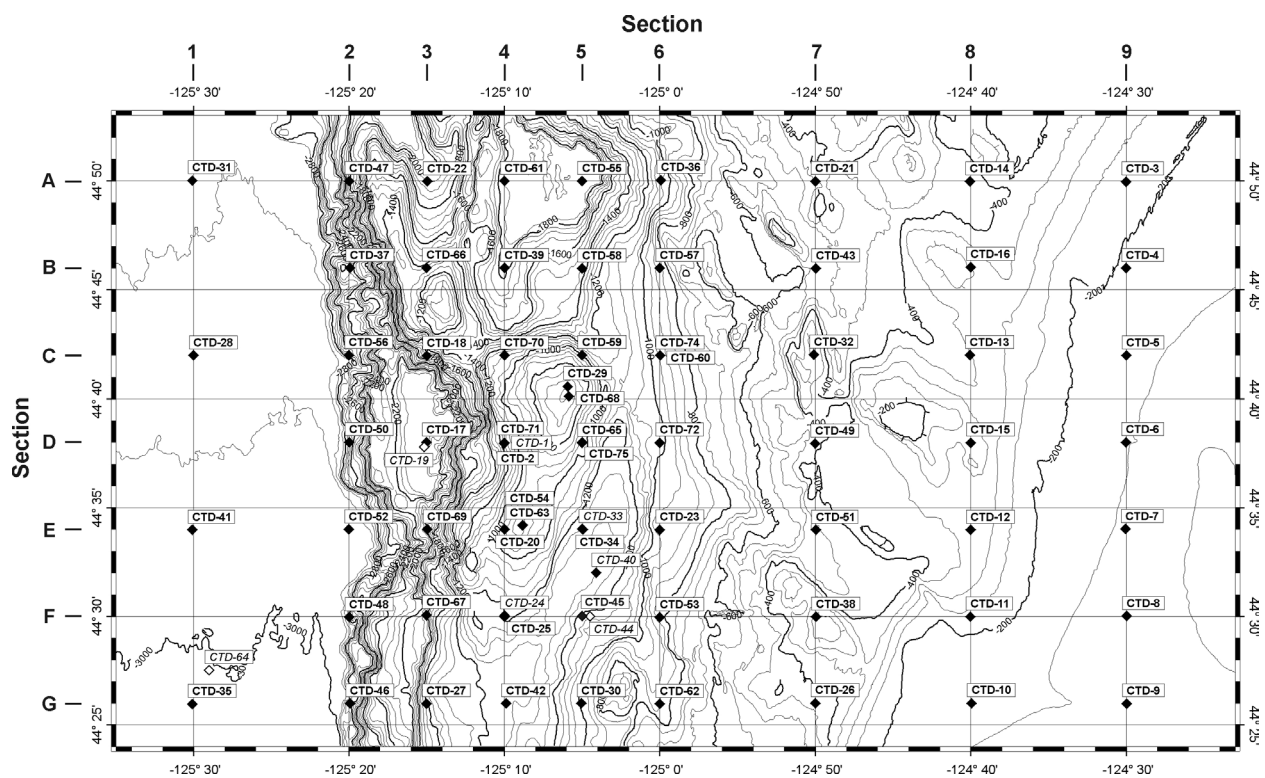


Fig. 5.3.1.1: Bathymetric map of the investigated area with all 74 CTD sampling positions (SO 165-1 & 2). Closed diamonds are sites where water samples were analysed for methane. Open diamonds (and italic labels) are water sampling stations for the reservoir of the Bigo lander system. Station CTD 64 was run because of technical problems with the winch.

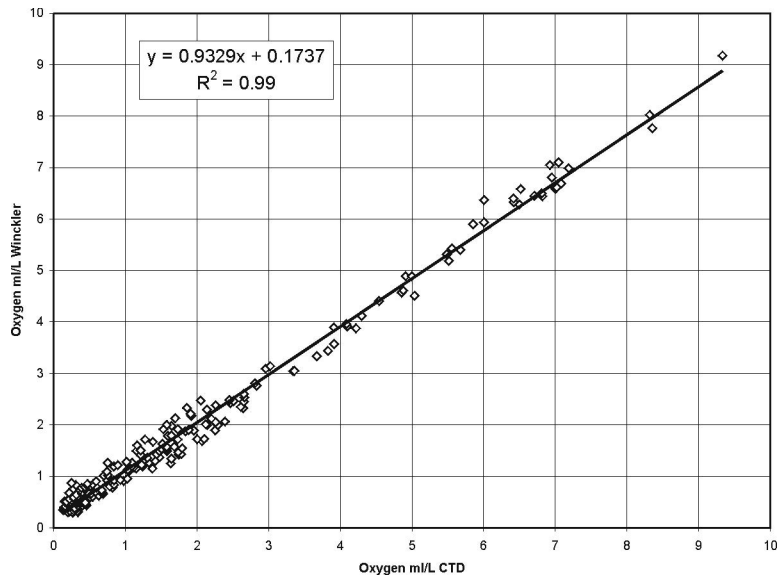


Fig. 5.3.1.2: Correlation between the oxygen content analysed by Winckler titration and the data measured by the Beckmanns oxygen sensor at the CTD.

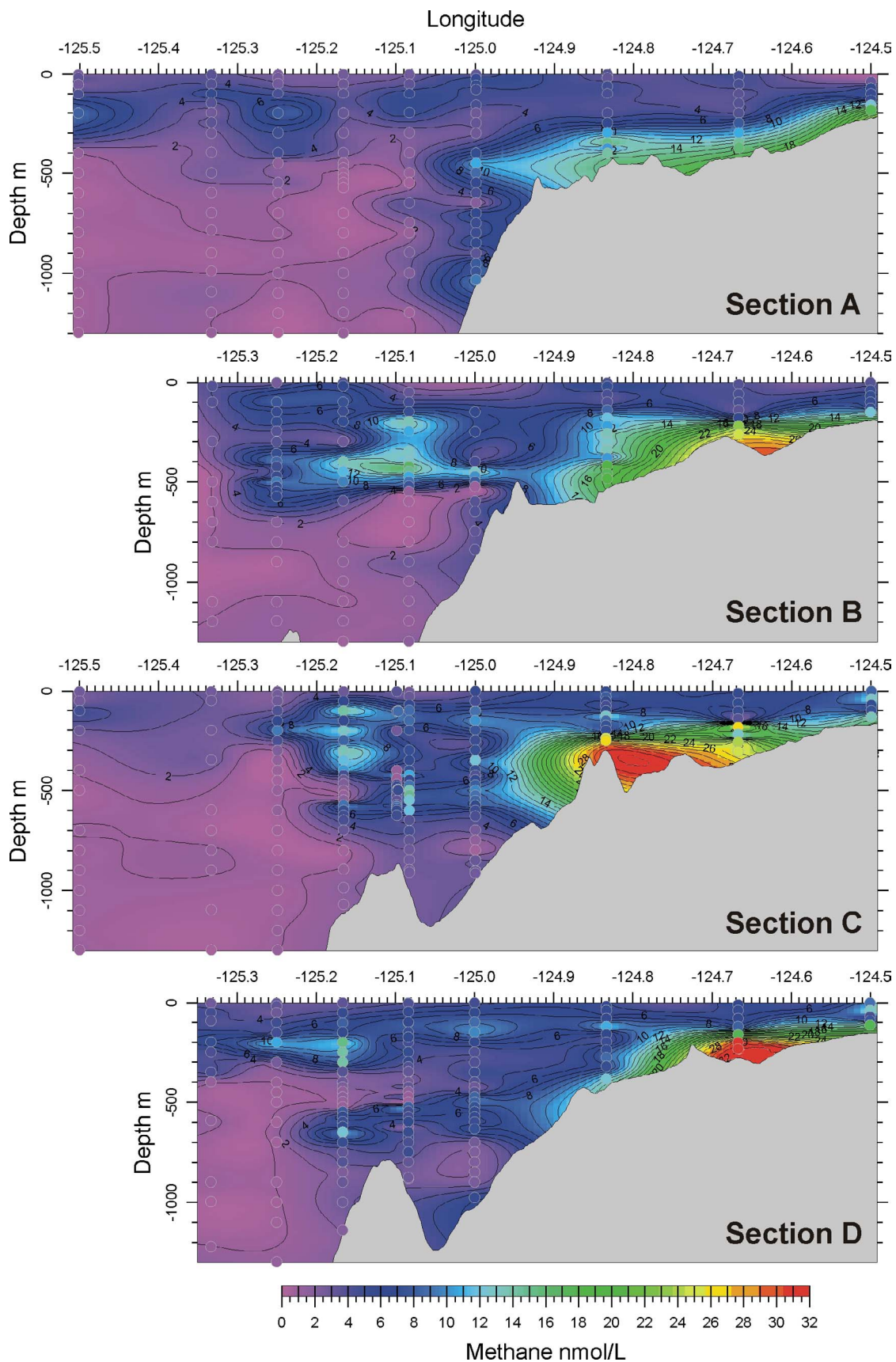


Fig. 5.3.1.3: W-E sections of the methane distribution across the Hydrate Ridge area (Sections A to G). Hydrate Ridge itself lies between -125.25 and -125.10 degrees longitude. Depicted are the concentrations above 1300 m water depth, the concentrations below range from 1 to 2 nmol/L.

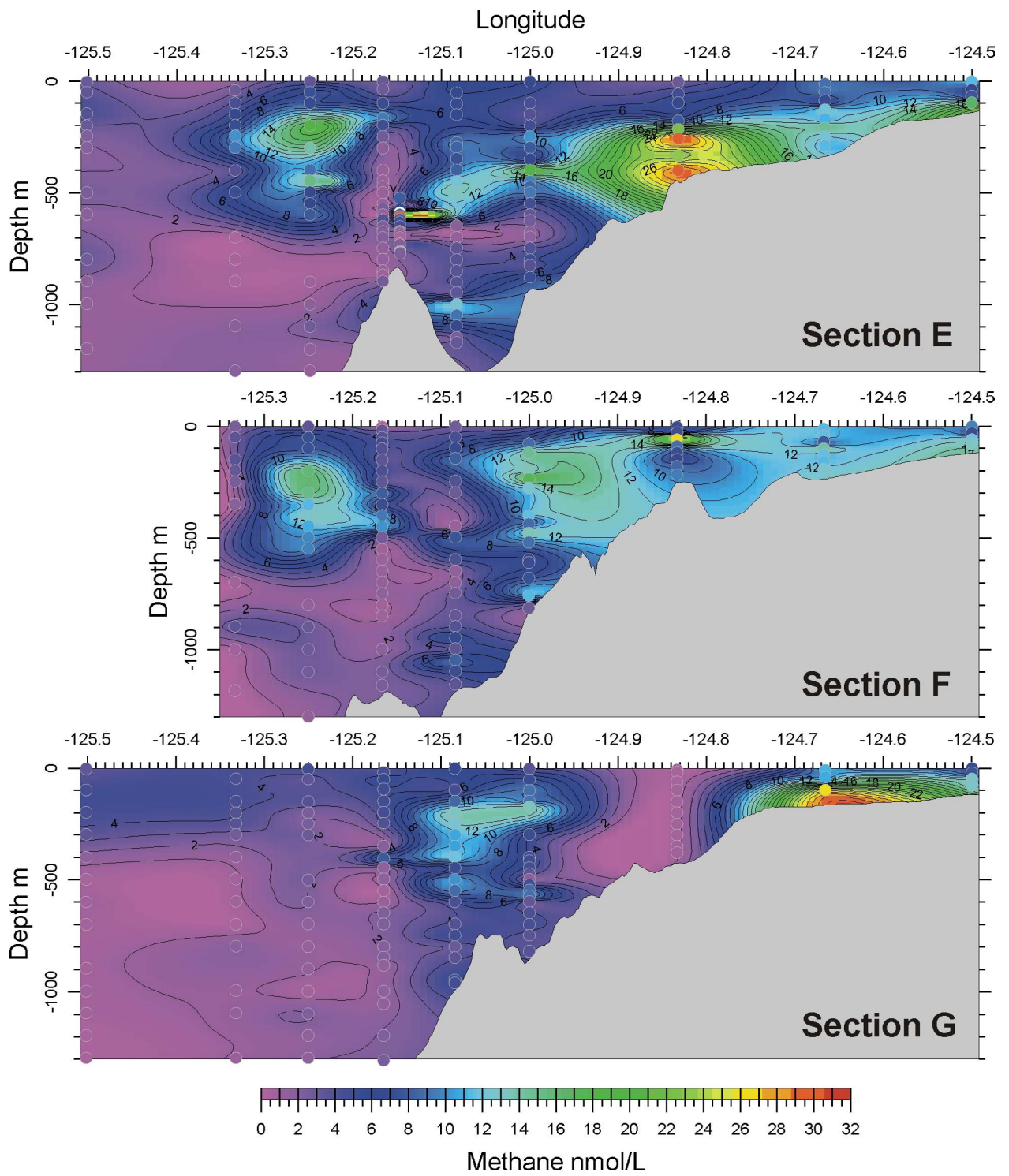


Fig. 5.3.1.4: See figure caption 5.3.1.3.

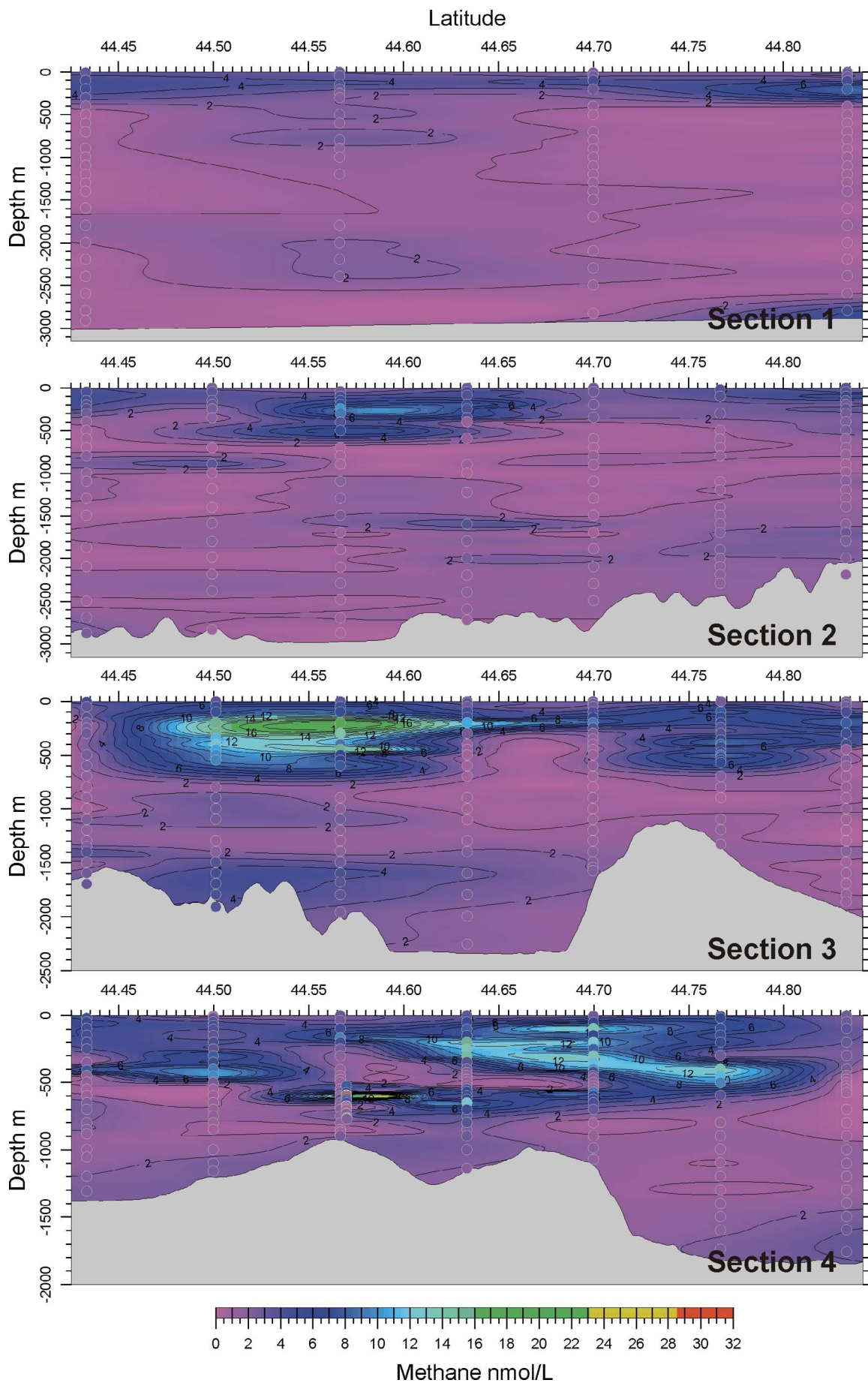


Fig. 5.3.1.5: N-S sections of the methane distribution across the Hydrate Ridge area (Sections 1 to 9).

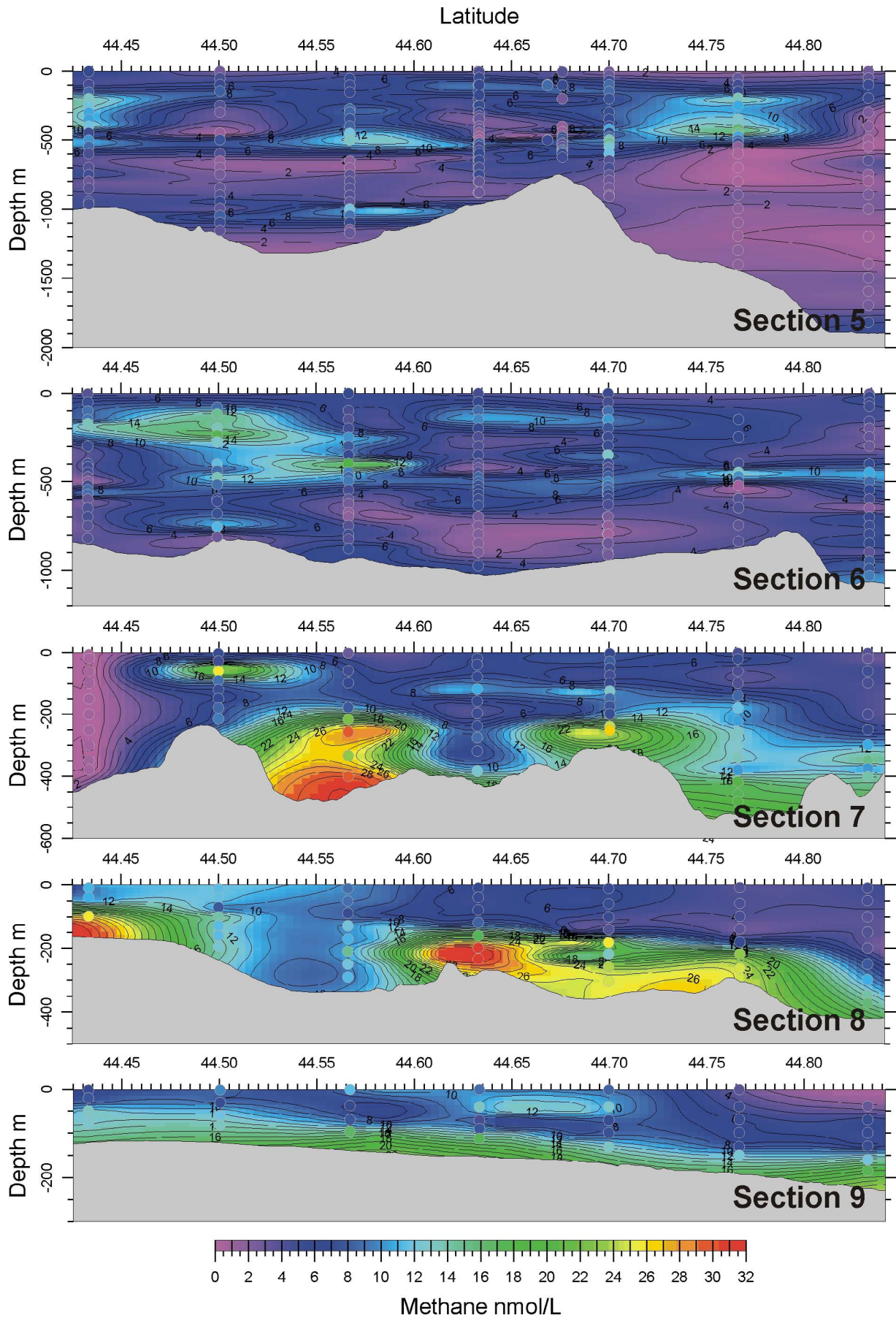


Fig. 5.3.1.6: See figure caption 5.3.1.5.

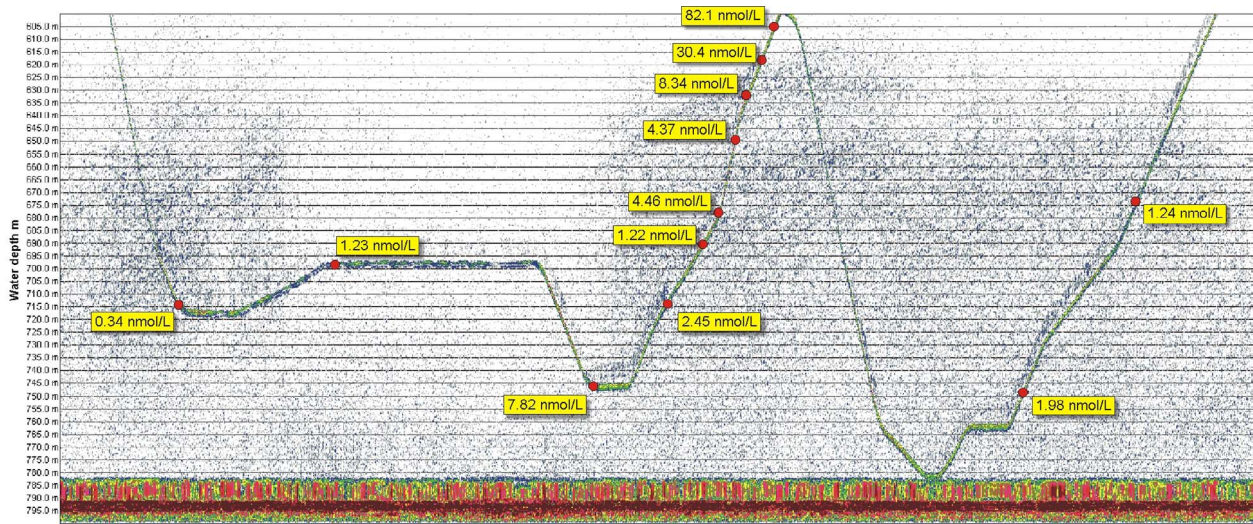


Fig. 5.3.1.7: Flare image of the Bubble Flare at the Southern Summit during CTD 54. The strong reflector in the water column represents the position of the CTD.

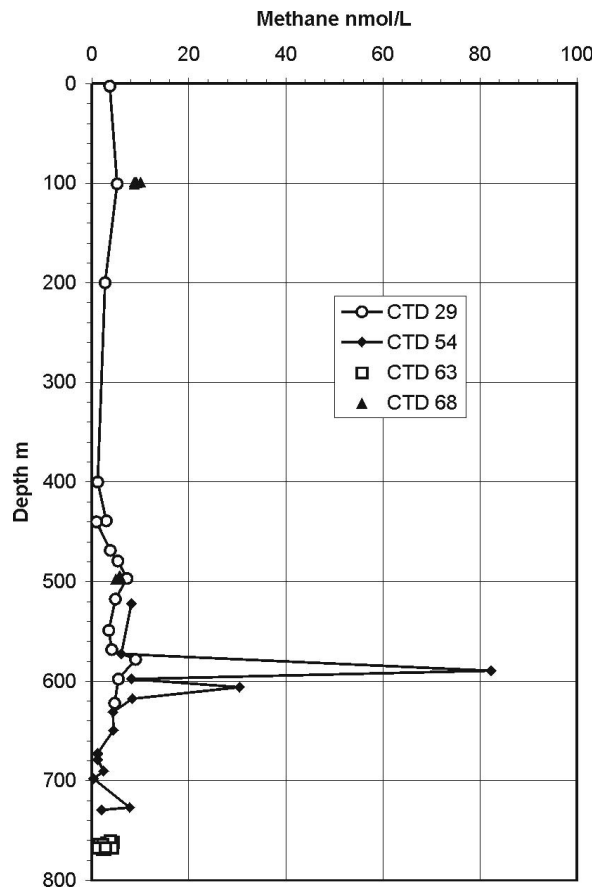


Fig. 5.3.1.8: Methane analyses of CTDs that were not part of the wide spread sampling grid. CTD 29 and 68 are from the Northern Summit. CTD 54 and 63 are from the Southern Summit. However, they were also used for the grid calculations shown in Figure 5.3.1.3 to 5.3.1.6.

5.3.2 CTD profiling of oceanographic parameters

J. Greinert, B. Mählich

General oceanographic parameters of some selected CTD casts are summarized in Figure 5.3.2.1. Also shown are the results of the METS methane sensor. Unfortunately, these data cannot be used for the accurate determination of the methane concentration. The strong hysteresis between down and up cast may have been caused by a slow temperature change of the sensor itself relative to the surrounding water and the general slow decreasing time.

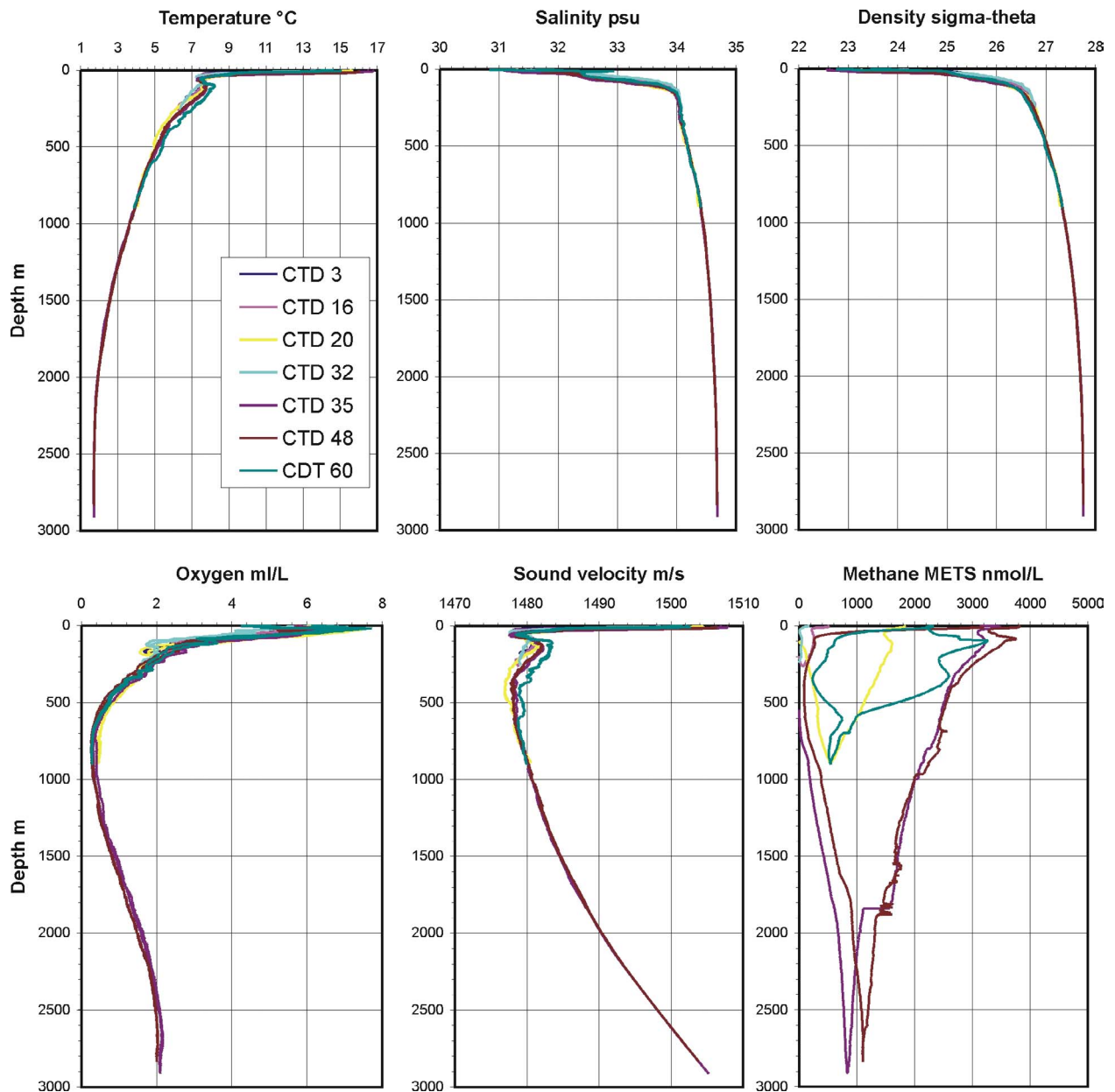


Fig. 5.3.2.1: General oceanographic parameters and METS methane sensor data of 7 CTDs in the investigated area.

5.3.3 METS-Mooring: Methane measurements by sensors

J. Greinert, M. Poser

For the first time GEOMAR deployed a methane sensor mooring to investigate the temporal variability of methane in a definite water depth. The methane sensors itself were the latest generation of METS sensors manufactured by CAPSUM. Although there were problems with the quantitative determination of methane, we aimed to recognize at least qualitatively the temporal variation of methane in the water column during the deployments of 2 and 8 days (Table 5.3.3.1).

Tab. 5.3.3.1: METS-mooring deployments during SO 165.

Station	Date / Time	Position	Sample Depth m	Site
<i>METS 1</i> # 73 / 94 SO 165-1	Deployed: 22.07. / 17:35 Released: 25.07. / 23:51	44:40.546 N 125:5.900 W 630 m wd	596, 566	0.35 Nm north of Gusher Site <i>NO DATA AVAILABLE</i>
<i>METS 2</i> # 104 / 119 SO 165-1	Deployed: 27.07. / 13:45 Released: 29.07. / 13:07	44:33.900 N 125:8.700 W 788 m wd	754, 724	0.2 Nm south of Bubble Site <i>NO DATA AVAILABLE</i>
<i>METS 3</i> # 149 / 159 SO 165-1&2	Deployed: 01.08 14:02 Released: 07.08. / 14:44	44:40.400 N 125:6.000 W 616 m wd	612, 582, 552, 522	0.2 Nm NNW of Gusher Site
<i>METS 4</i> # 177 / 204 SO 165-2	Deployed: 10.08. / 00:35 Released: 13.08. / 22:34	44:40.150 N 125:5.890 W 589 m wd	585, 555, 525, 495	at Gusher Site
<i>METS 5</i> # 217 / 235 SO 165-2	Deployed: 15.08. / 17:45 Released: 18.08. / 16:40	44:40.889 N 125:5.799 W 610 m wd	606, 576, 546, 516	0.37 Nm south of Gusher Site

Technical description

The mooring includes four separate METS units that consist of an energy supply and data logging package mounted in a glass flotation sphere (Figure 5.3.3.1), and an additional flotation sphere (Figure 5.3.3.2).

Ni-Cd batteries with a total capacity of 56 Ah and 12 V were used as power supply for the METS sensor (energy supply of approx. 120 mA/h) and data logger unit. The data logger unit was developed at GEOMAR and uses a PHYTEC microprocessor with 1 MB RAM to hold the program and store the data. The sampling rate of the data logger can be changed from 1 to 59 seconds. A rate of 20 sec. was used for all METS mooring deployments.

The METS sensor is connected to the data logger via a RS232 serial connection. On request of the data logger the sensor sends a data string composed of methane, temperature and humidity data (HEX numbers of the voltage: 0 – 5 V) that is recorded. The methane sensor itself is a heated n-type SnO₂ semi conductor, which is supposed to be sensitive for methane. Unfortunately this sensor needs a

minimum amount of oxygen to work (more than 50 $\mu\text{mol/L}$; the correct methane detection is even influenced at higher concentration, shown by recent test undertaken by CAPSUM) and senses methane only above (9 nmol/L , the lowest concentration used for calibration)

In addition to the four METS units, the mooring itself also consists of a top buoy and a releaser unit. The latter is composed of two Oceano releasers - borrowed from the IfM – that are fixed in a frame together with two flotation spheres. Figure 5.3.3.3 shows a sketch of the complete mooring setting.

Deployments

We deployed and recovered the METS mooring successfully five times (Table 5.3.3.1). The first two deployments, north of the Gusher Site and north of the Bubble Site, were carried out with only two METS units as the other energy/data storage units were in use on the BIGO and FLUFO lander. Unfortunately it came out just after the second deployment, that the data logger software was not able to store more than 10552 data (2.5 days at 20 sec logging interval) and we recovered the second METS mooring the next day to fix this problem. Because of this bug we could not retrieve usable data from METS-Mooring 1 and 2.

After the software bug was fixed, METS-Mooring 3 was deployed for more than one week north of Gusher Site during the time RV SONNE steamed to Portland. METS-Mooring 4 and 5 were also deployed at the northern summit of Hydrate Ridge (Figure 5.3.4.6).

Results

Unfortunately the results of all METS sensors deployed on the mooring are poor. One general reason might be the detection limit of the sensors (the specification sheets gives a range from 20 nmol/L to 1 mmol/L). Our sensors had a calibration range from 9 nmol/L to 11 $\mu\text{mol/L}$. The lower range is high in comparison to 'normal' methane concentrations in the sea. Previous methane analyses at Hydrate Ridge gave a background concentration of about 1 to 2 nmol/L . Higher concentrations during SO 165 vary from 10 to 20 nmol/L and only once 82 nmol/L were analysed from one depth from CTD 54 at the southern summit (5.3.1.7). However, the concentrations analysed during the mooring deployments are much higher than the geochemical analysed data (Figure 5.3.3.4 to 5.3.3.6). The reason for this is still unknown. Possible explanations might be:

- the sensors are calibrated in fresh water and not in salt water
- the dissolved oxygen concentration was too low
- the influence of H_2S is unknown

In addition to these possible influences, all sensors showed a highly variable voltage level of the temperature sensor, which should stay more or less stable through the time. One possible reason might be an error during the data logging and the downloading process to the PC. Because these variations occur randomly and after periods of correct (reasonable) values it is unlikely that transmission errors or storage errors occurred. Another reason may be that something in the sensor itself the voltage variability; this has to be discussed in greater detail together with the CAPSUM technicians.

The preliminary data show a higher variability through time and between the different depth horizons. Some times a correlation to the low tide signal from Newport (grey line in Figure 5.3.3.4 to 6) seems to appear.

Conclusion

The new developed mooring proofed as an easy to handle tool that can be used as multi-purpose platform for various kinds of sensors and devices. All METS sensors used during SO165 as long-term observation tool did not work as expected from the specifications. The significant concentration-discrepancy between sensors of one deployment could not be found in our geochemical analyses. It is still questionable whether the METS sensors can be really used to detect and quantify methane in the marine environment.

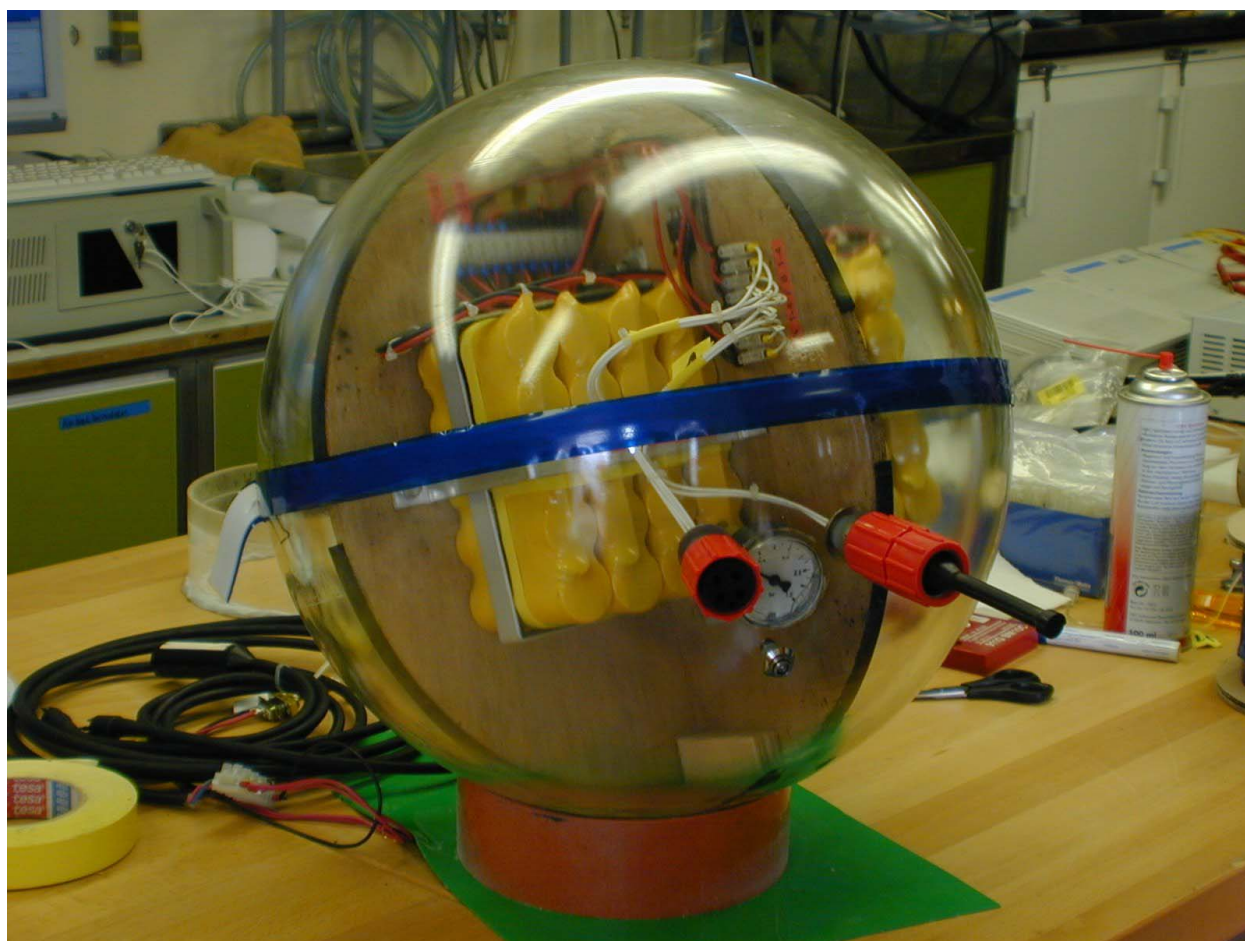


Fig. 5.3.3.1: Glass sphere with the data logger and energy supply for the METS methane sensors



Fig. 5.3.3.2: Three METS units fixed on deck of RV SONNE.

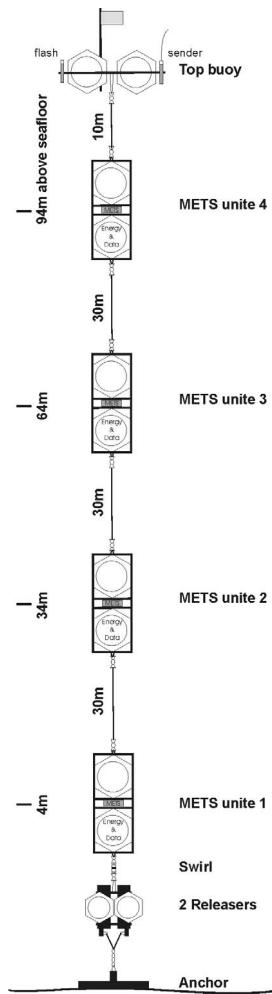


Fig. 5.3.3.3: Scheme of the METS Mooring used during SO 165.

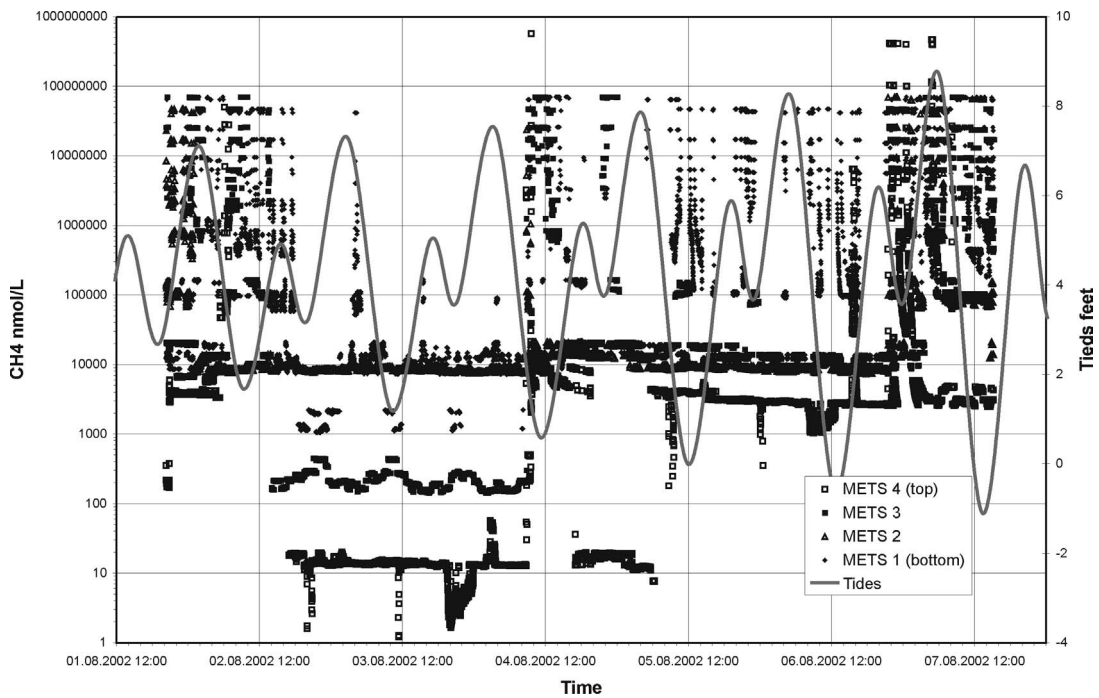


Fig. 5.3.3.4: METS-Mooring 3 deployed for 6 days north of Gusher Site. Starting at the end of the 3rd August the data may indicate a tide-dependent variation with higher concentrations occurring at low tide.

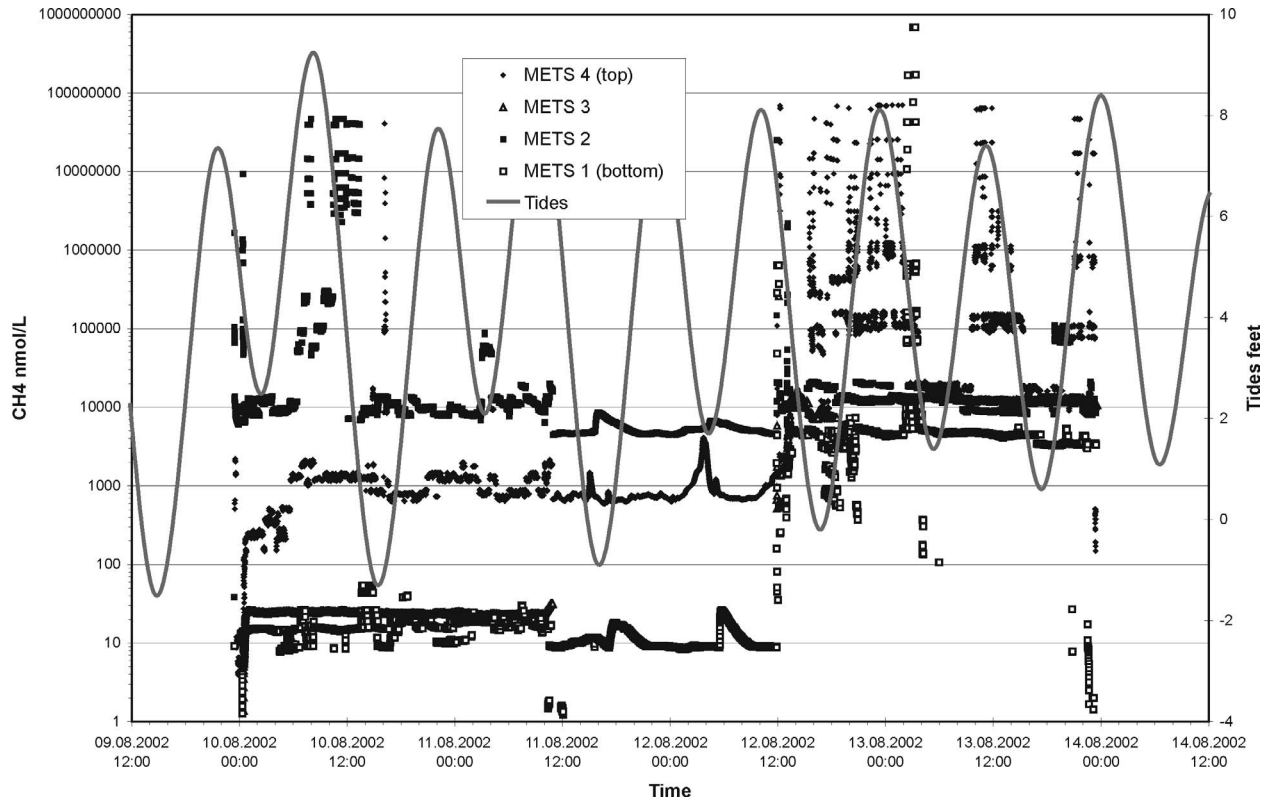


Fig. 5.3.3.5: METS-Mooring 4 deployed at Gusher Site. Notable is the strong increase of the methane concentration in all 4 sensors around 12:00 at the 12th August.

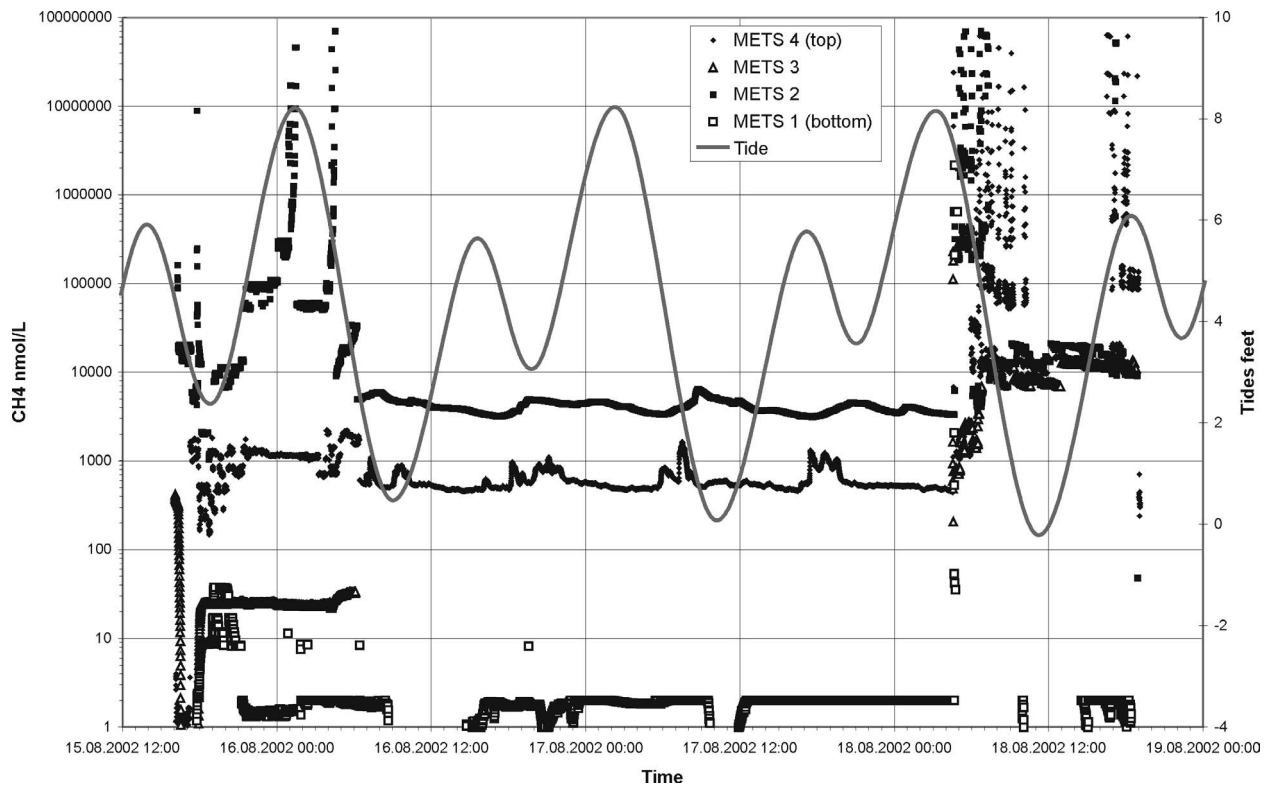


Fig. 5.3.3.6: METS-Mooring 5 deployed south of Gusher site. It is odd that very low concentrations below 1 nmol/L are indicated by sensor METS 1 and METS 3.

5.3.4 Flare Imaging

J. Greinert, B. Mählich

The hydroacoustic detection of gas (methane) bubbles by a ship-mounted single beam echo sounder is one of the monitoring techniques employed in LOTUS subproject 2 (Figure 5.3.4.1). For this purpose we used the 18 kHz NBS signal of the Parasound system to investigate five areas at Hydrate Ridge and the vicinity (Figure 5.3.4.2, Table 5.3.4.1). Bubbles reflect and as well as resonate acoustic signals that can be easily detected with single beam echo sounders. Bubbles released from the bottom at cold vent sites produce an acoustic reflection in the shape of a flare, from which comes the name, Flare-Imaging.

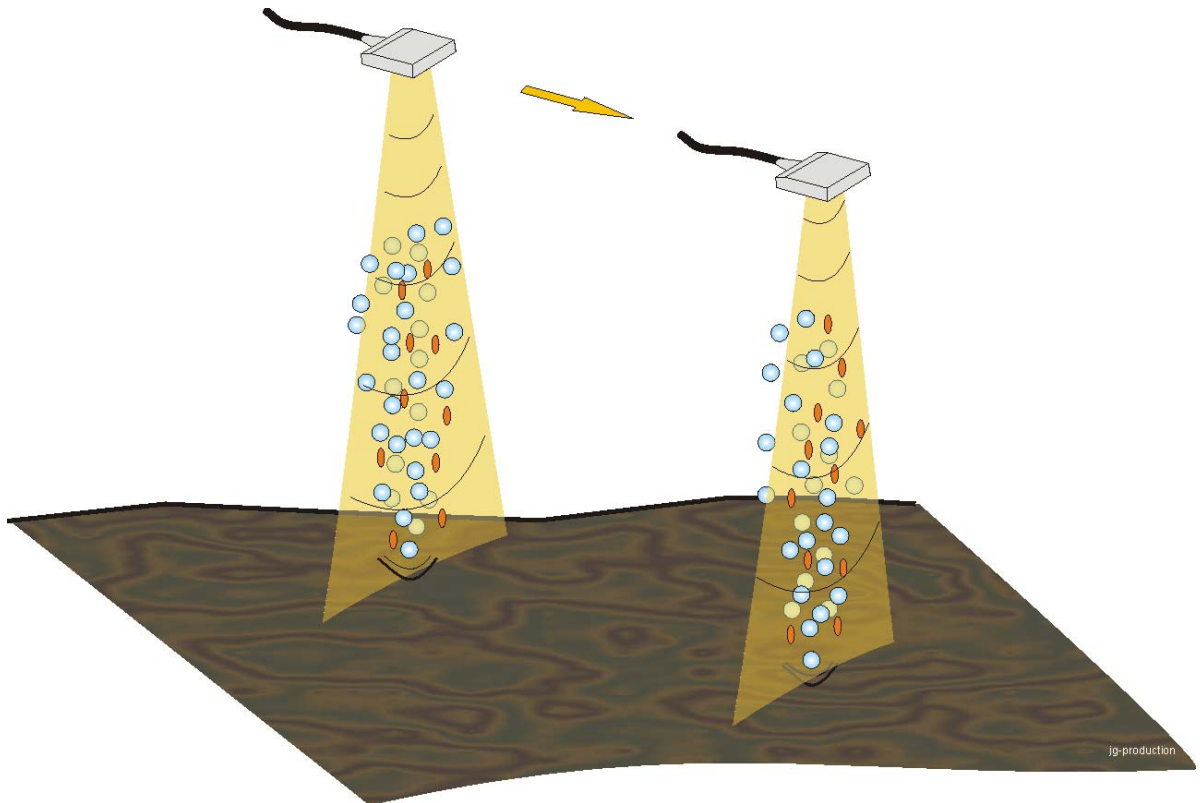


Fig. 5.3.4.1: Scheme of the Flare Imaging; during the ships movement a single beam echo sounder records signals backscattered from different depth of the water column

Technical description

For the Flare Imaging during So 165 we used the unprocessed analog 18kHz NBS signal of the ship's Parasound system. This signal was taken from "the small box on the wall below the ParaDigMa desk" in the hydroacoustic laboratory on RV SONNE. The recording was done by a second ParaDigMa unit composed of a HP 3852 DAU for digitising and a DOS computer to run the ParaDigMa software (FS SONNE compiled!). The necessary position string (position, heading, speed, etc.) was sent a second time from the 'old' VAX system, the Parasound parameter string (frequency, window, range, etc.) was doubled from the original string for the Parasound registration by a Y-cable.

Most of the time we ran the system with a range of 200 m (the usual Parasound range), 50 kHz sample-frequency and a sample interval of 266 millisecond. This

results in 13300 samples per ping that were stored by ParaDigMa and later visualized by the WaveLens software written by Yuriy Artemov, Sevastopol. Good online visualization was achieved with a Gain of 100 and a band pass filter of 6 to 8 kHz (the used 18 kHz signal is down-sampled to a frequency of 7 kHz). The beam angle of the 18 kHz signal was set to 20° as the other smaller angles gave very weak backscatter signals from the water column.

Results

During SO 165-1 & 2 Flare Imaging surveys were run at the northern and southern summit of Hydrate Ridge, at the NW-Knoll and SE-Knoll as well as at a site (Shelf flare) where a possible flare was recognized during transit (Figure 5.3.4.2; Table 5.3.4.1).

Tab. 5.3.4.1: Flare Imaging surveys

Date / Time	Station	Area
16. 7.2002 / 05:15 - 11:00	18kHz - #30	Gusher Site (1)
22. 7.2002 / 14:11 - 16:01	18kHz - #71-3	Gusher Site (2)
27. 7.2002 / 14:53 - 18:35	18kHz - #105	Gusher Site (3)
31. 7.2002 / 14:20 - 20:08	NTTA-1 # 136	Gusher Site (inverse trap)
06.08.2002 / 13:40 - 17:11	18kHz - #152	Gusher Site (4)
16.08.2002 / 21:59 - 2:30	18kHz - #224	Gusher Site (5)
17. 7.2002 / 07:20 - 13:06	18kHz - #37	Bubble Site (1)
06.08.2002 / 18:38 - 19:20	18kHz - #153-1	Bubble Site (2)
07.08.2002 / 10:50 - 12:38	18kHz - #157	Bubble Site (3)
12.08.2002 / 15:23 - 15:58	18kHz - #193	Bubble Site (4) 33 kHz used
22. 7.2002 / 01:45 - 04:38	18kHz - #71-1	Shelf Flare
23. 7.2002 / 01:02 - 3:00	18kHz - #78	SE-Knoll (1)
28. 7.2002 / 10:10 - 17:04	18kHz - #111-3	SE-Knoll (2)
25. 7.2002 / 16:02 - 19:35	18kHz - #92	NW-Knoll

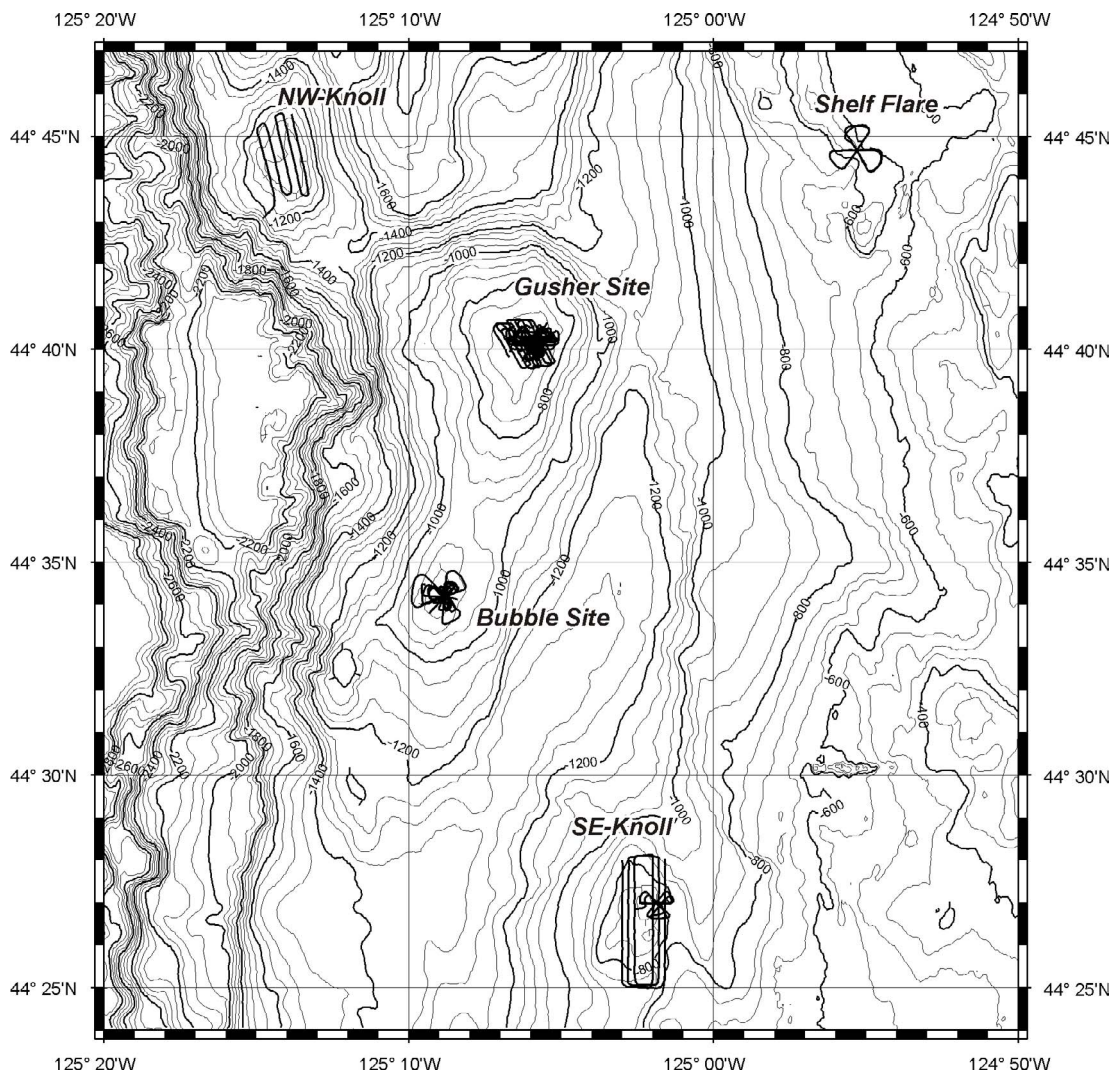


Fig. 5.3.4.2: Location and tracks of the 18 kHz Flare Imaging surveys during SO-165 1 & 2.

NW-Knoll

During the NNW-SSE trending survey lines of station 92 we did not observe any signs of flares.

Shelf Flare

Unfortunately the possible flare seen during the transit to CTD 21 was not recognized again during Flare Imaging station 71-1.

SE Knoll

Two surveys were run at the SE-Knoll and three times we saw a flare at the uppermost top of the pinnacle-like summit of SE-Knoll. Figure 5.3.4.3 shows one flare, all three can be seen in Figure 5.3.4.6. During TVG sampling of this chemoherm complex we observed small bacterial patches and clam colonize mainly localized in deep gullies or cracks that crisscross the entire pinnacle.

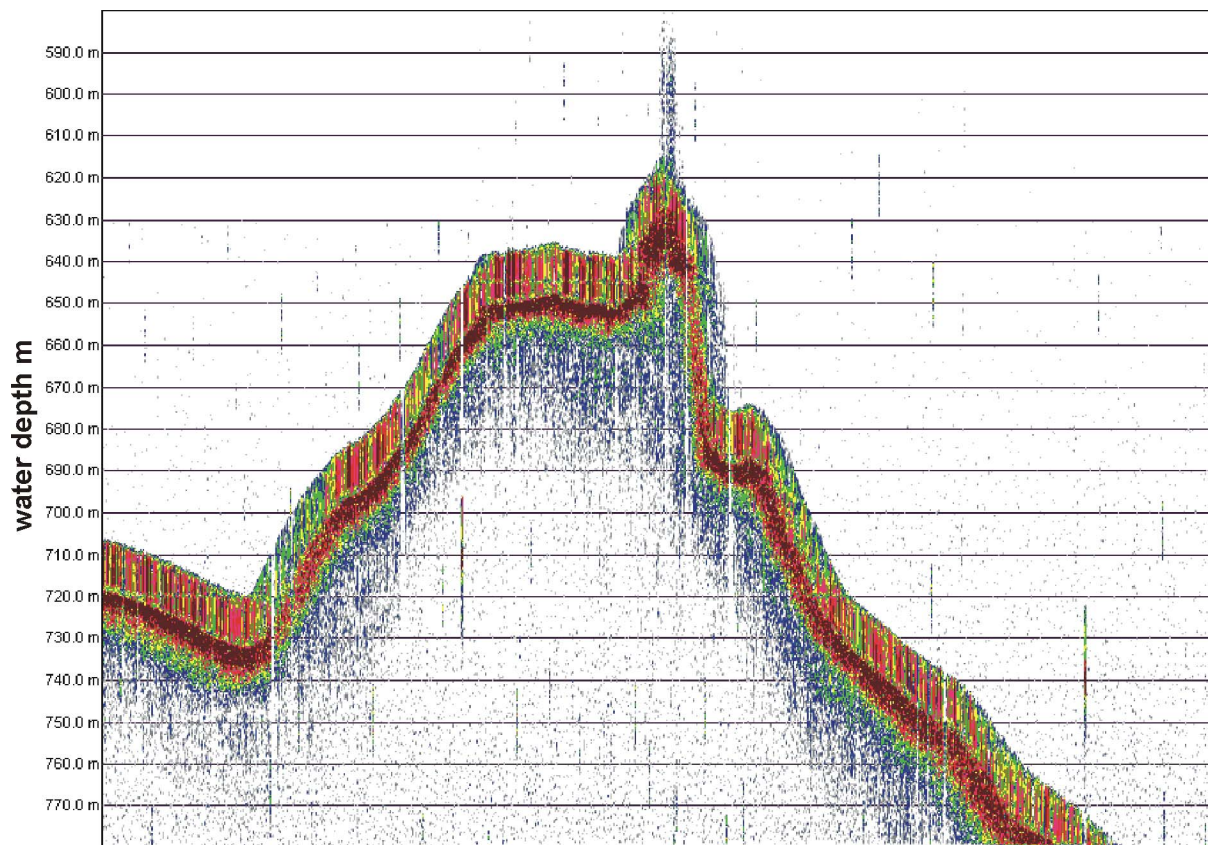


Fig. 5.3.4.3: Flare at the top of the SE-Knoll at 44° 27.0513' N / 125° 1.8027' W; note the nearly perpendicular north flank of this chemoherm

Bubble Site (Southern Summit)

At the upper most top of the southern summit we observed a permanent active flare that was first discovered during SO 148 (Bubble Flare; Figure 5.3.4.4). During our repeated surveys, which covered a greater area at the southern summit, no other flares were detected. During station #193 we used the 33 kHz signal of the NBS sounder, but did not cross the Bubble Site because of limited station time.

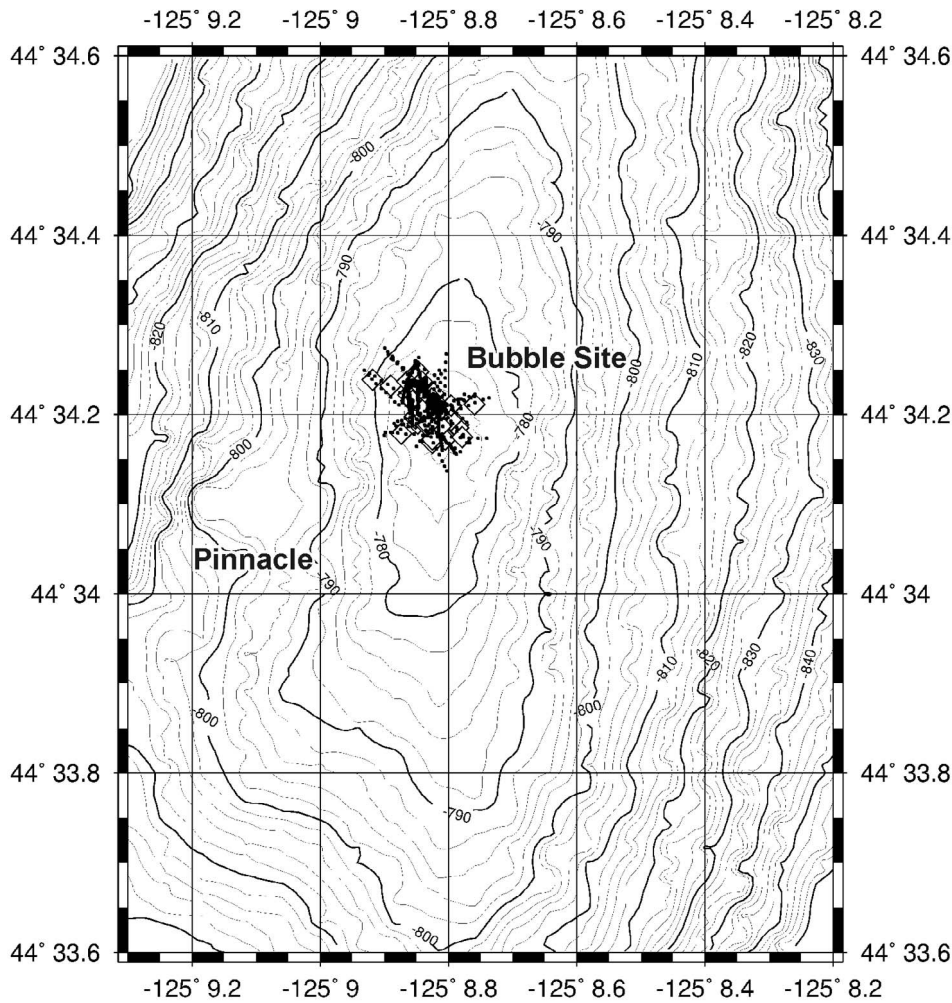


Fig. 5.3.4.4: Bathymetric map of the southern summit of Hydrate Ridge with the Bubble Site position. Grey circles mark the position of rooted flares; black lines represent the occurrence of flares in the water column. No flares were seen at the Pinnacle SW of the Bubble Site.

Gusher Site (Northern Summit)

Most Flare Imaging surveys were done at the northern summit at the Gusher Site area. Figure 5.3.4.6 shows data from the NTTA 1 station with prominent flares at Gusher Site and another location slightly south of it. The distribution of flares, which are rooted at the seafloor (open diamonds) and of all observed flares (black dots) shows a strong association with the crest of the ridge or knoll. Some of these crests are already known to be chemoherms. The Gusher Site has a larger proportion of diagenetic carbonates than chemoherm-type carbonates, but still the expulsion of methane into the water column has been observed at this site as well.

A detailed investigation as to whether the flares depend on the tide still needs to be done. A preliminary 3D image is shown in Figure 5.3.4.7. The processing of such images should become standard procedure because the real distribution of gas bubbles in the water column can not be understood with only time vs. depth images (as in Figure 5.3.4.6).

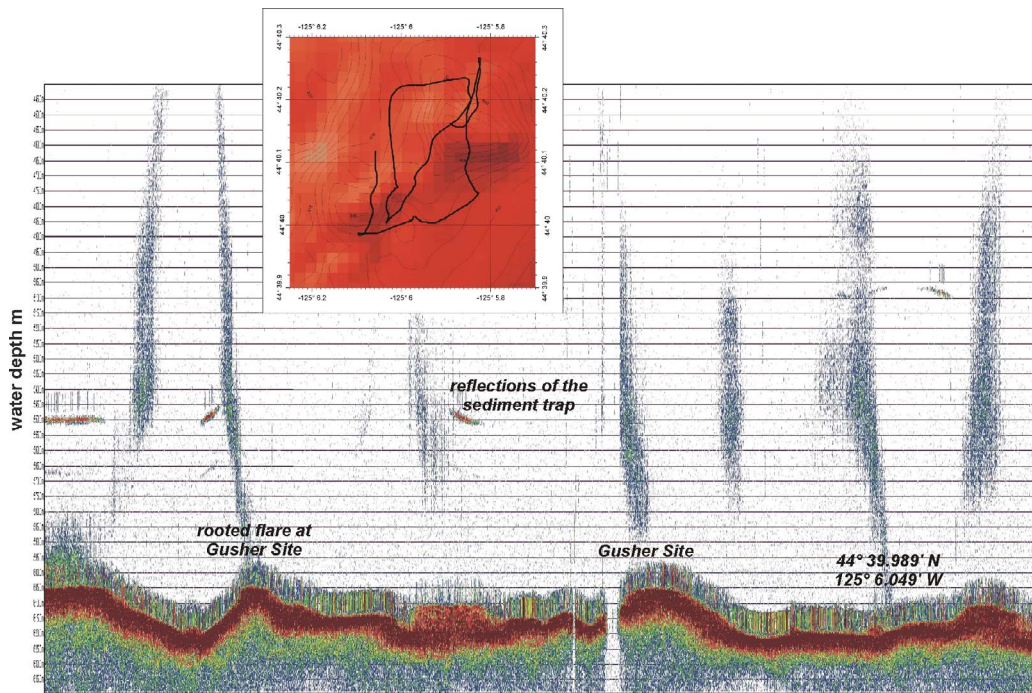


Fig. 5.3.4.5: Flare Imaging during the inverse sediment trap station NTTA-1 #136. The Gusher Site was crossed several times and from different directions. The vertical reflections just above the bottom are artefacts

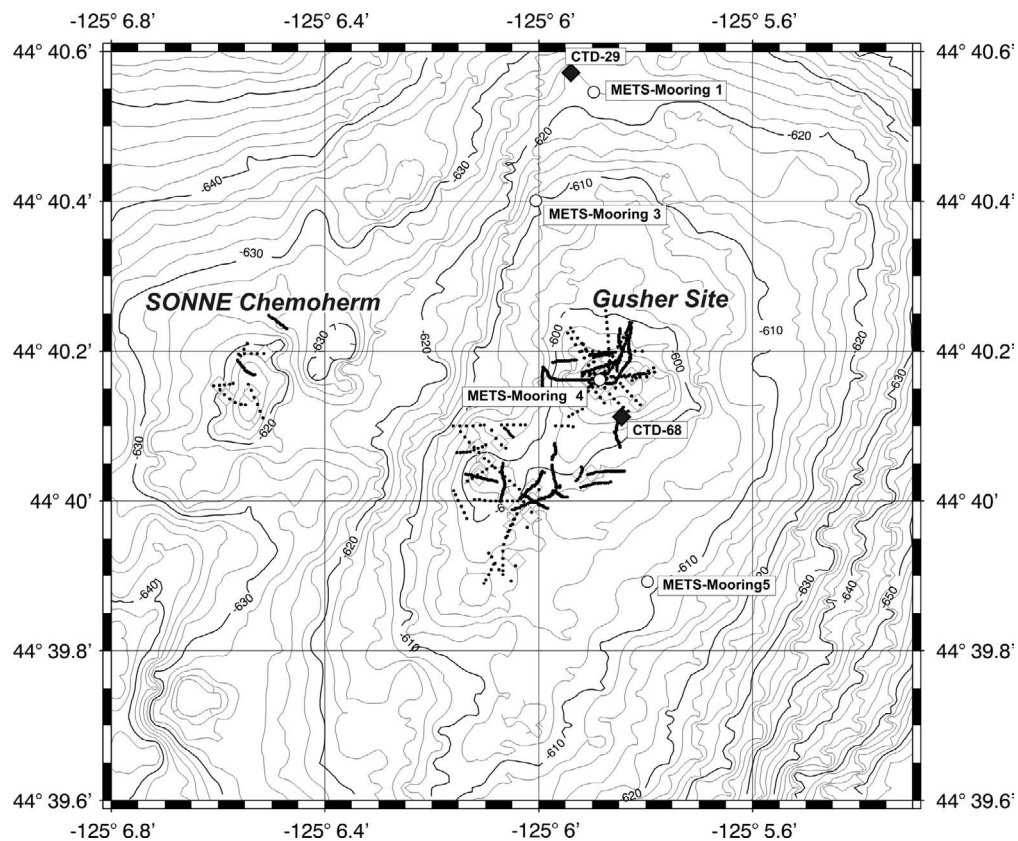


Fig. 5.3.4.6: Bathymetric map of the northern summit of Hydrate Ridge at the Gusher Site area. Open diamonds are the position of rooted flares observed during several Flare Imaging surveys. Also shown are the station positions of four METS-Moorings and two CTDs casts.

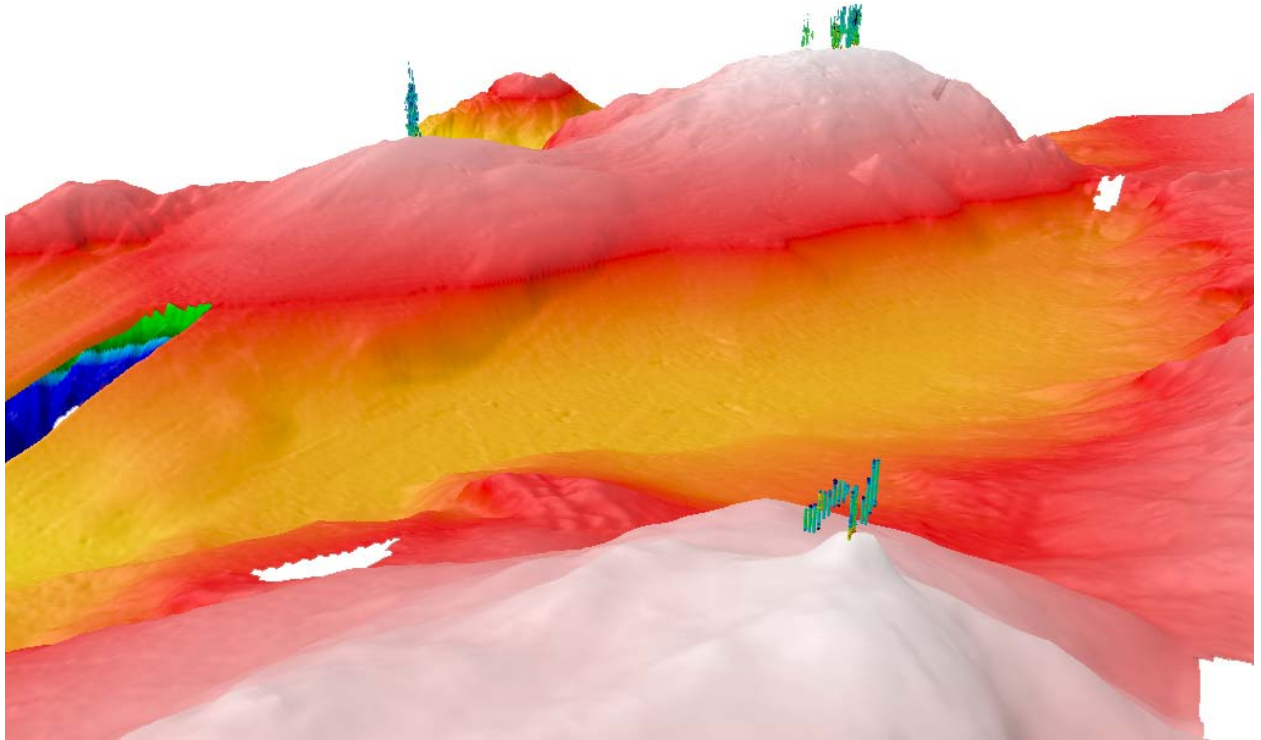


Fig. 5.3.4.7: 3D view of the Hydrate Ridge area from the SE-Knoll towards the southern and northern summit. Flares are shown colour coded by the backscatter intensity.

5.3.5 GasQuant

J. Greinert

It became clear during the TECFLUX campaigns that the emission of free gas bubbles is a very important transport mechanism of methane from the sediment into the water column. Because of their rapid upward migration methane in the bubbles cannot be readily consumed by bacteria in sediments and at the sediment-water interface, and thus most of the bubble emitted gas dissolves in the water column. To quantify the volume discharged through bubbles, a new hydroacoustic system was developed in close cooperation with ELAC-Nautik in Kiel. This system is based on a 'normal' but pressure resistant swath bathymetry transducer that looks horizontally and detects bubbles due to the backscattered acoustic signal (Figure 5.3.5.1). This system, known as GasQuant, is deployed by a lander and can be accurately placed in front of known bubble sites to investigate the periodicity and the amount of gas rising from the seafloor for more than one week.

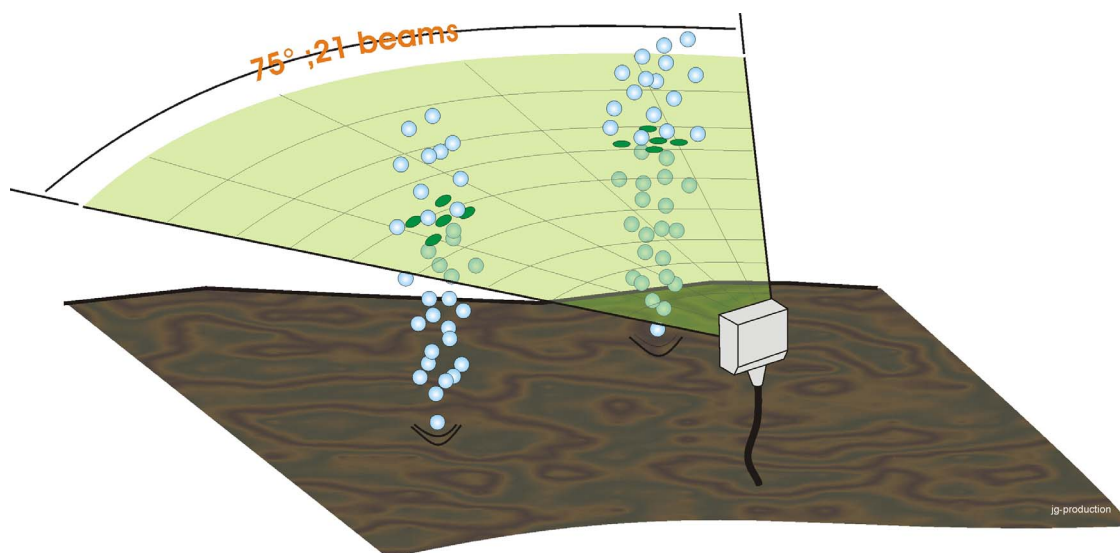


Fig. 5.3.5.1: Scheme of the GasQuant System detecting two bubble sites by the back scattered signal.

Technical description

GasQuant is an autonomous system composed of newly designed pressure resistant (100 bar) 180 kHz swath transducer (75° opening angle with 21 beams; resolution of each beam 3° horizontal and 1.5° vertical), an electronic transducer unit (SEE 30; Transmitting and Receiving Unit), a data acquisition PC, and four deep sea batteries for power supply. The transducer is fixed in a frame at the upper buoyancy circle of the lander (Figure 5.3.5.2, 5.3.5.3). The SEE 30 and the data acquisition PC are both stored in a titanium barrel (40 in diameter and 80 cm long; Figure 5.3.5.4) that is fixed at the tool-frame of the lander. The four deep-sea batteries with 230 Ah and 12 V each are fixed beside this titanium barrel. The SEE 30 was modified to run with batteries in a low power mode (several high power capacitors were removed). The data acquisition PC is a common micro-computer (Windows NT), which controls the system and records the data via the Hydrostar Online software of ELAC-Nautik. Special software was written to restart the computer and the entire system if the PC crashes or the SEE stops unnoticed.



Fig. 5.3.5.2: View of the GasQuant Lander with launcher on top ready for deployment. The tool frame at the base of the lander carries four deep sea batteries and the SEE electronics in a titanium barrel. A compass, observed by one of the two launcher-cameras, was used to control the lander heading during the deployment.



Fig. 5.3.5.3: The pressure resistant 180 kHz transducer of the GasQuant system fixed in a cardanic frame.

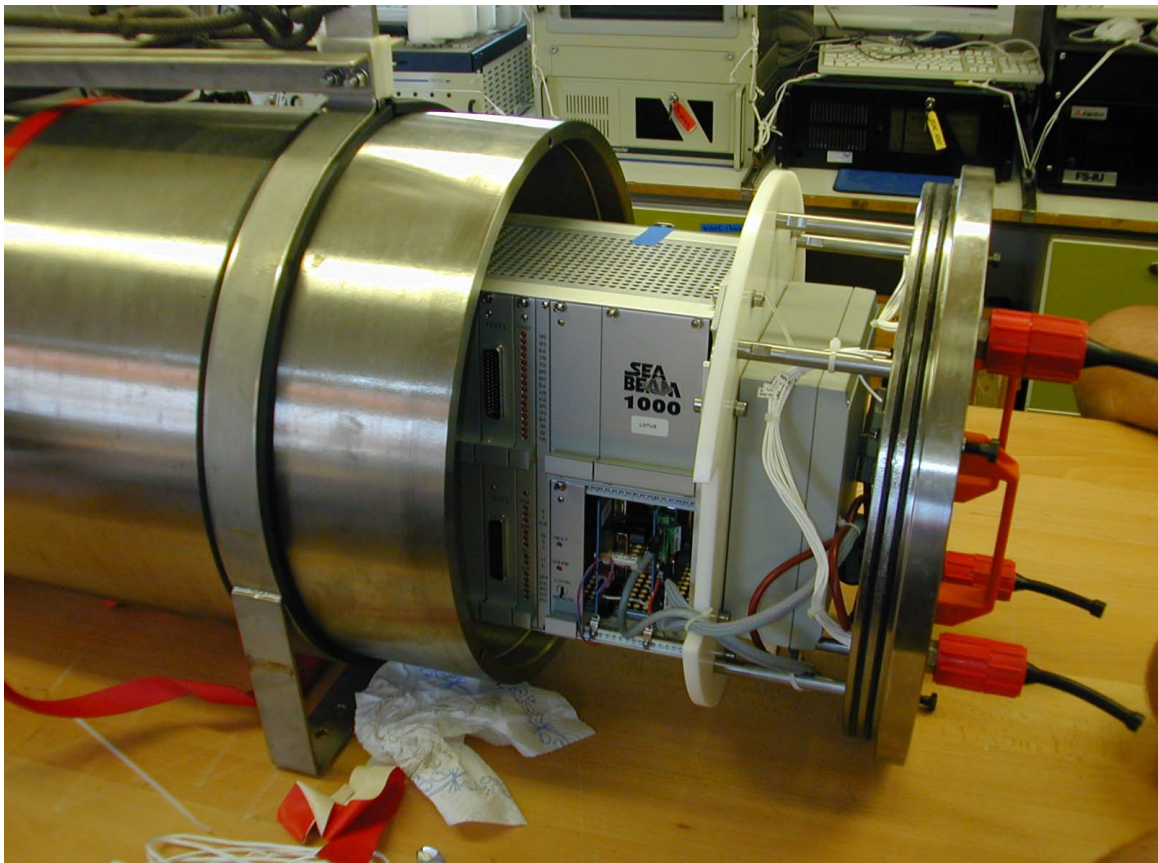


Fig. 5.3.5.4: The titanium barrel and the SEA 30 control and data acquisition unit

Results

The GasQuant system was successfully deployed three times at the northern and southern summit. Even if the Hydrostar Online program or the Windows NT system crashed during the deployment, the entire system started again and recorded in total more than 2 GB of data.

Tab. 5.3.5.1: Positions of the three GasQuant deployments

Station	Date / Time	Position	Heading	Site
GQ 1 # 47 / 68	18.07. 19:54 / 21.07. 18:40	44:40.158 / - 125:5.855	west	Gusher Site
GQ 2 # 84 / 122	24.07 02:08 / 29.07. 23:45	44:34.180 / - 125:8.837	north	Bubble Site
GQ 3 #148 / 166	01.08. 20:06 / 08.08 15:37	44:40.147 / - 125:5.878	north	Gusher Site

The raw data have to be converted and the algorithms for this must be fine-tuned in order to detect and quantify the amount of free gas. This has not yet been completed and thus no results can be shown here.

5.3.6 ADCP water current profiling

J. Greinert, B. Mählich

In addition to aerobic oxidation of methane, water currents are a major factor that impacts the distribution of methane in the water column. Thus the knowledge of the actual water current direction and velocity are of essential need for the understanding of measured methane concentrations.

Technical description

For this purpose we used a new 75 kHz ADCP manufactured by RDI. This “work horse” ADCP (LongRanger) enables measurements up to a distance of 550 m. The ADCP was deployed by a separate Lander. Unfortunately the LongRanger flooded after 2.5 days during the first deployment (Station #2) and could not be used for the rest of the cruise. The LongRanger was sent to RDI for inspection from Portland and the inspection showed that an O-ring of the pressure sensor was defective or not correctly installed. The data were collected with the following settings (*: automatically set):

Number of bins:	100
Bin length:	5.00 m
Blank after transmit:	7.04 m*
Pings per ensemble	100
Time per ping:	6.00 sec*
Distance to first bin:	13.42 m*
Transmit length:	5.76 m*

Measurements were conducted with the 300 kHz and 1200 kHz ADCP's on the DOS Lander Station (#32). The 300 kHz ADCP was also using during the third GasQuant station (#148) and was mounted and lowered on the CTD frame during the second leg (casts 57-72).

Results

Data from LR 1 (deployed between the northern and the southern summit) show again that currents at Hydrate Ridge depend on the tidal cycle (Figure 5.3.6.1, 5.3.6.2). The majority of the time, the currents were oriented to the north. However, the highest velocities of nearly 60 cm/s were directed to the west (Figure 5.3.6.3). Similar mean velocities were observed at Station GQ 3 (deployed at the Gusher Site), and much higher velocities sometimes occurred (the very high velocities of around 1.5 to 2 m/s may, however, be incorrect). Drawing the trajectories from 7 different depths of station GQ 3 indicate a mainly northward direction of the currents. The trajectories also show how the tidal component causes small eddies that progressively migrate to the north.

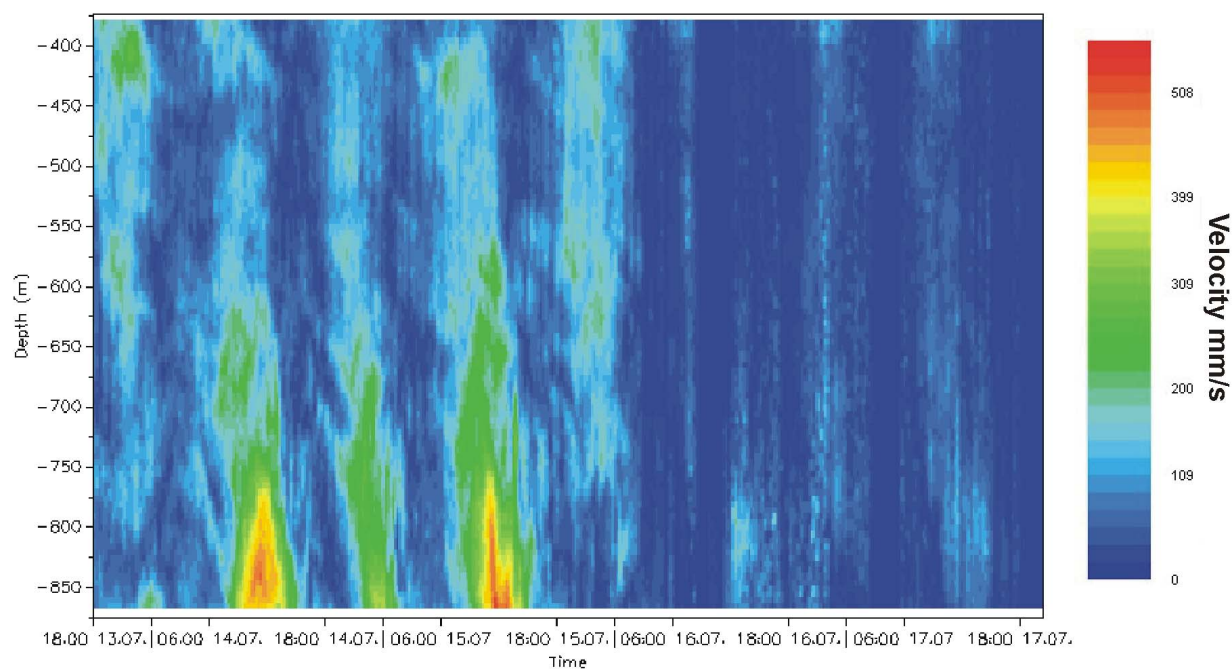


Fig. 5.3.6.1: Water current velocities, measured during station #2 with the LongRanger ADCP. Data after midnight of the 15th are not correct, because of the flooding of the system.

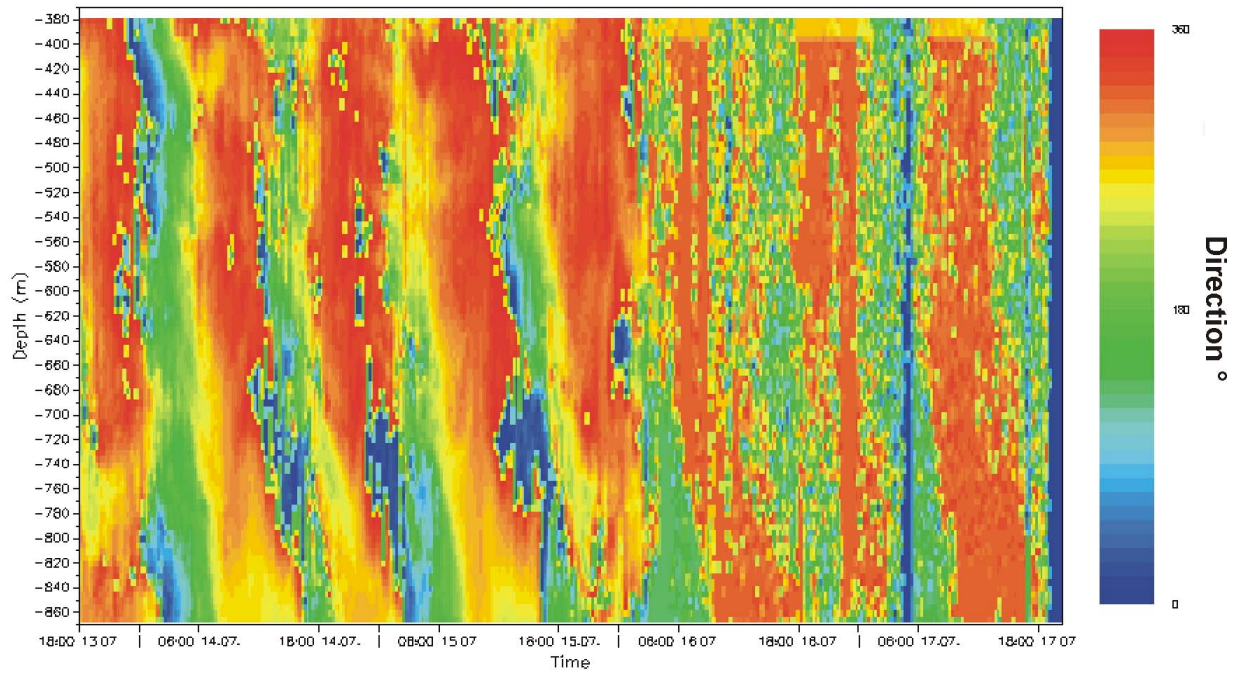


Fig. 5.3.6.2: Water current directions during station #2 (given in degrees).

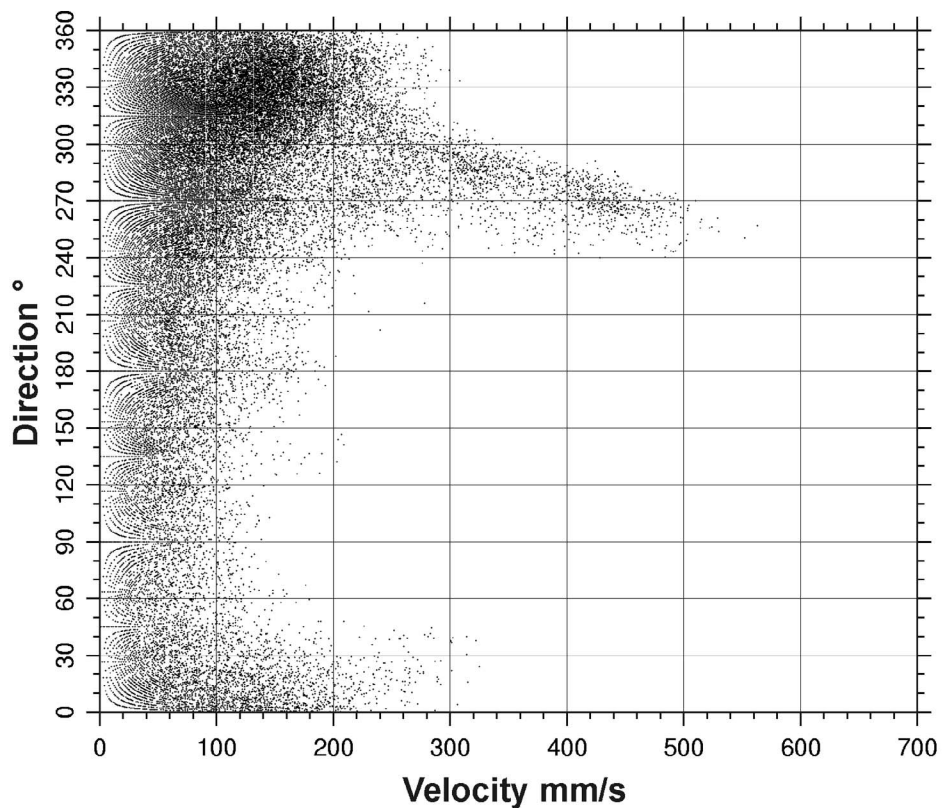


Fig. 5.3.6.3: Velocity vs. direction diagram of all recorded data of station LR 1 (75 kHz ADCP).

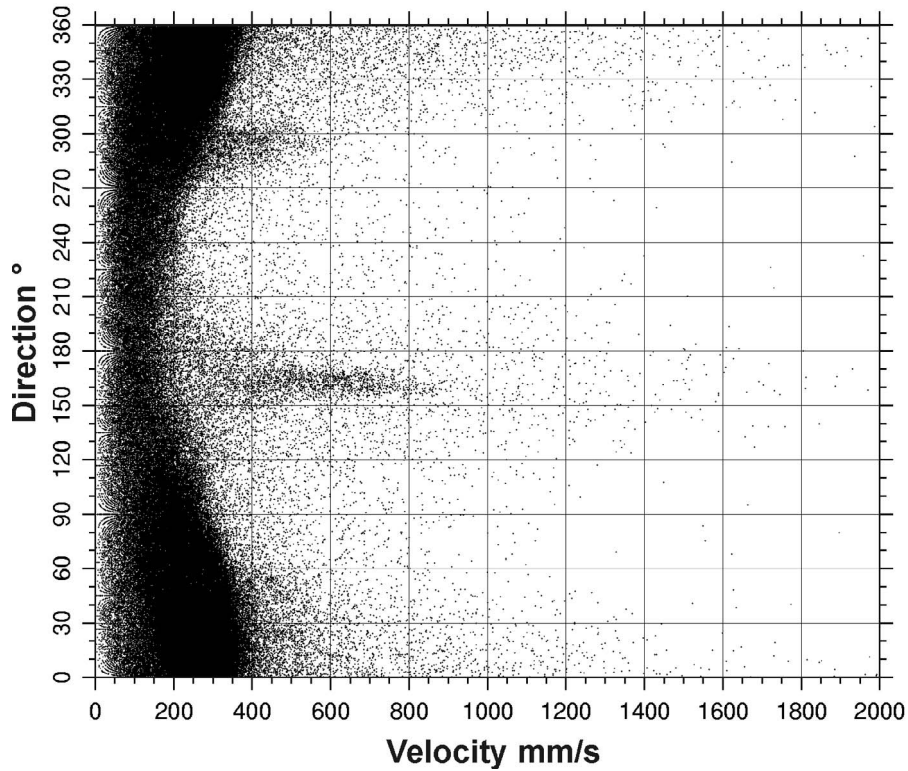


Fig. 5.3.6.4: Velocity vs. direction diagram of all recorded data of station GQ 3 (300kHz ADCP).

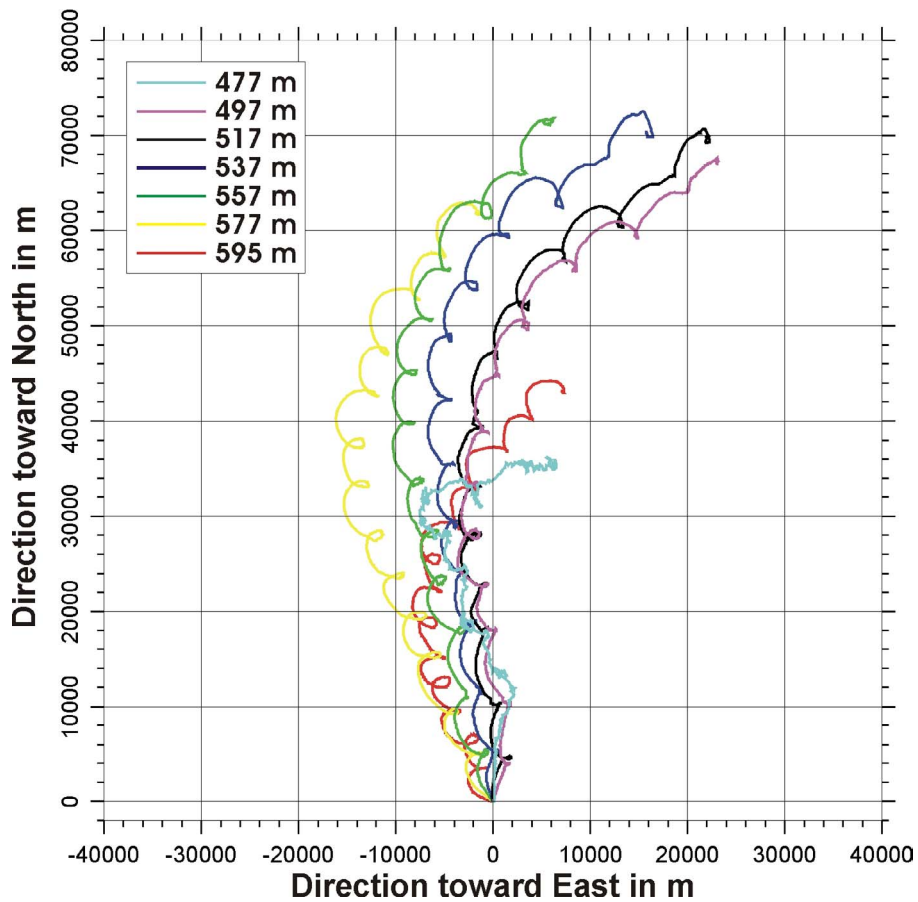


Fig. 5.3.6.5. Trajectories at given depths of station GQ 3 (300 kHz ADCP). Induced by changing current directions the northward directed current shows smaller eddies. The data were recorded between 01.Aug 23:00 and 08.Aug 16:10.

5.4 The Fluid Flux Observatory (FLUFO)

P. Linke, S. Gubsch, S. Sommer, B. Bannert, M. Poser, T. Viergutz

Introduction

Within the international TECFLUX project, multiple measurements of aqueous and chemical fluxes in regions of active fluid seeps and gas vents on Hydrate Ridge, Cascadia accretionary prism, have been performed. These measurements indicated that flow in this environment is highly heterogeneous in both time and space with areas of inflow, outflow, and outflowing fluids with both altered and seawater-like composition. While tectonics is the dominant underlying driving force in fluid expulsion, the shallow expression of this flow might be modulated by more complex hydrological processes. These dynamic processes may include: gas expulsion driven, pumping and aqueous entrainment in migrating gas; buoyancy-driven fracturing of overlying sediments; rapid changes in the permeability distribution due to the injection of gas and the formation of gas hydrates; migrating flow conduits and tidally driven flow oscillations. With this complex scenario in mind FLUFO was designed to quantify the different types of fluxes at the benthic boundary layer of sediments overlying near surface gas hydrates and to monitor relevant environmental parameters as temperature, pressure and near bottom currents. The development and application of the FLUFO-System are part of the LOTUS project. Responsibilities for construction and application of the technical sub-systems were shared in subproject 1 by Geomar (FLUFO-Lander / FLUFO- Peripherals) and TUHH / MT1 (FLUFO Chamber Units (Fig. 5.4.2))

Operational Principle and Configuration of the FLUFO System

The central part of FLUFO are 2 Chamber Units which are carried by a Lander (Fig. 5.4.1). Each Chamber Unit can be separated into two major parts: a cylindrical benthic chamber (30cm diameter) and a measurement and control set up. The measurement and control set up comprises different mechanical and electronically parts as gas separator, flow sensors, control electronics and records the discharge fluid type and its rates. To each chamber syringe samplers with seven 50 ml-syringes are attached.

Both Chambers Units separate the gas phase from the aqueous phase and measure their individual contribution to the total fluid flux. Whereas the first (reference) Chamber Unit measures the aqueous flux without obtaining information about their direction, the second (FLUFO) Chamber Unit measures the aqueous flux including the flow direction. By switching a central valve, the FLUFO Chamber Unit can operate in 4 different modes:

1. Leakage test of the chamber / measurement of permeability of the sediment
2. High-resolution fluid flux measurement (0,1 – 60 ml/min)
3. Average resolution fluid flux measurement (50 – 1000 ml/min)
4. Simulation of the external current regime

Both Chamber Units are controlled by an intelligent electronic control system. The central data management and parameter control is obtained with an ONSET Tattletale 8 controller with 660 Mbyte Flash memory. This configuration enables long-term deployments without loss of data by drained batteries and external control of data/status through communication with an acoustic modem.



Fig.5.4.1: FLUFO attached to the launcher during deployment.

The operational principle of the FLUFO Chamber Unit is shown in Figure 5.4.2. After deployment of the Lander with a video-guided Launcher on a selected site on the seafloor both chambers are slowly driven 15cm into the sediment by a motor. That procedure is followed by a leakage test.

For execution of this test, bottom water is pumped from outside through valve ports I1 and O1 into the benthic chamber passing flow sensor 3 (see Fig. 5.4.2). The pumped bottom water leaves the benthic chamber either through the sediment or by passing the gas separator and flow sensor 2 (valve I4-O4). The comparison between the two flow measurements of the sensors enables a check for leakage of the benthic chamber and an evaluation of the sediment permeability.

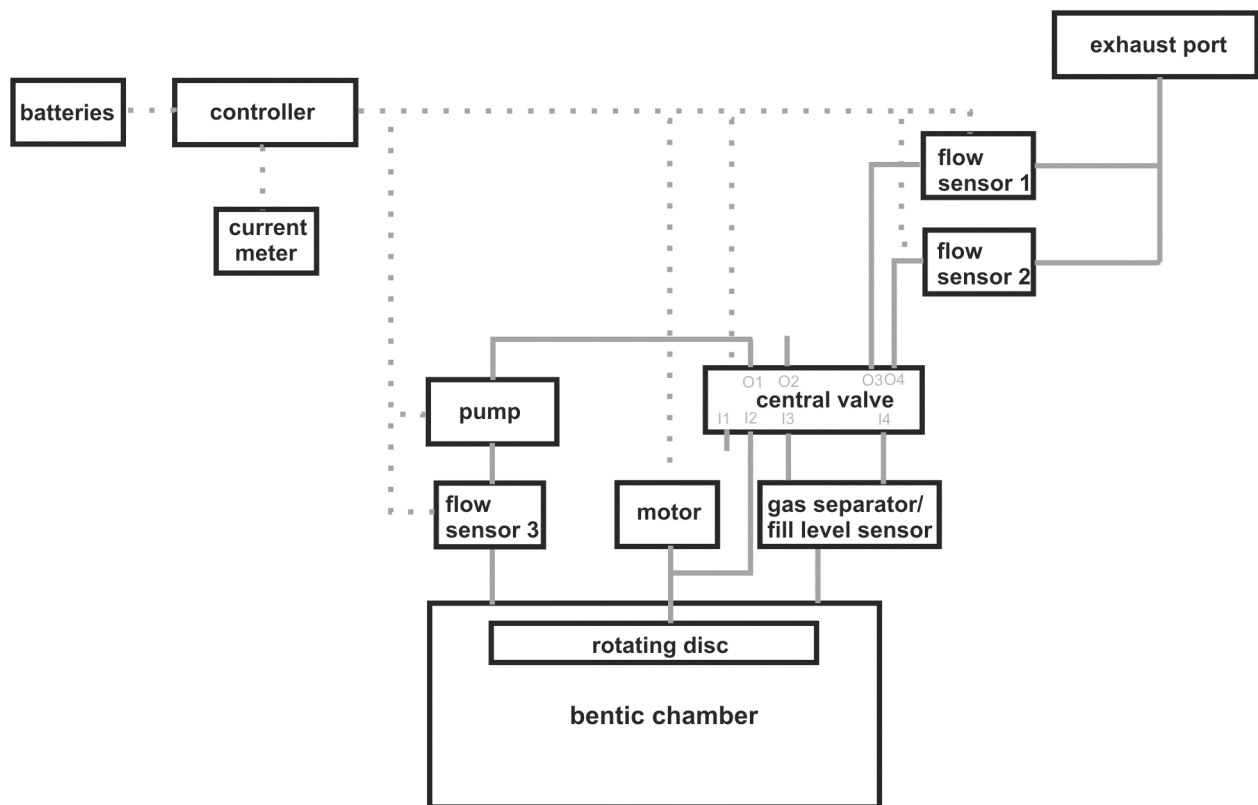


Fig. 5.4.2: Operational scheme of the FLUFO Chamber Unit.

After this check the valve is switched to open the connection between the exit of the gas separator and flow sensor 1 for the flux measurement (valve I4-O3). Thus, discharged fluid will be caught inside the benthic chamber and conducted into the gas separator. Here the gaseous phase is separated from the aqueous phase. The gas separator contains a sensor which measures the absolute gas level. After reaching a defined level, the gas is released by the valve into the surrounding bottom water. The aqueous phase leaves the system by passing the optical flow sensor 1 (patent pending DE 10220088A1). If the out- or inflowing water reaches a defined flow value, the valve is switched from flow sensor 1 to 2. The direction of the fluid flow is measured optically after dye injection.

During measurement the benthic chamber can be operated either with or without rotating disc and a pumping recirculation system which permits to control internal pressure and bottom shear stress pattern.

In order to measure vertical flow with a system exposed to lateral benthic boundary layer (BBL) currents, the design of the chamber required particular care to prevent (or at least reduce) influences of BBL currents. Most of the crucial parts were tested and optimized in a flume. The exhaust port of the chamber orients itself into the prevailing bottom current. Furthermore, the outlet holes are located along the venting tube. As a result the influence of the bottom current is minimised. During the measurement the system can be switched to mode 4 to vary the bottom stress regime like in the BIGO system (see chapter 5.6). In contrast to the BIGO chambers the FLUFO chambers permit deeper sediment penetration to minimize fluid exchange processes by lateral bottom currents at the chamber wall. A shutter like in the BIGO system to retrieve the incubated sediment was not available during this time.

External Sensors

MAVS-3 3axis acoustic current meter

The MAVS current meter is a true 3 axis current meter which employs a differential travel time measurement technique. The current meter takes measurements across 4 acoustic axes to provide a true vector averaged velocity measurement. Programmable burst mode and triggered sampling provide a flexible use. The controller is an ONSET Tattletale 8 which is mounted beneath the main circuit board. System configuration, deployment parameters and data are logged on flash card. The combination of small sensor geometry and differential travel time technique provide reduced disturbances to water flow and low speed measurement accuracy in the 0.03 cm/sec to 10 cm/sec range.

The MAVS-3 employs a faired sensor head with central strut and a 9.5 cm acoustic path length. The 4 acoustic axes are each defined by a pair of transducers, one located on the proximal sensor ring (the ring closest to the pressure housing) and one located on the distal ring (the ring furthest from the pressure housing, Figure 5.4.3). Each axis crosses the ring planes at a 45° angle. The axes are spaced 90° apart around the circumference of the rings. Flow along an acoustic axis is defined to be positive when it flows from the transducer on the distal ring towards the transducer on the proximal ring. The orientation of the sensors (including pitch, roll, compass) in respect to the pressure housing are stored in the system configuration and several options can be chosen to display the different velocity components.

The radial alignment hole of the current meter pressure housing (6000 m) was oriented opposite to the central column of the lander with the distal transducer ring 50 cm above ground with the Lander resting on the ballast weights. This height is equivalent to the top of the retrieved chamber.

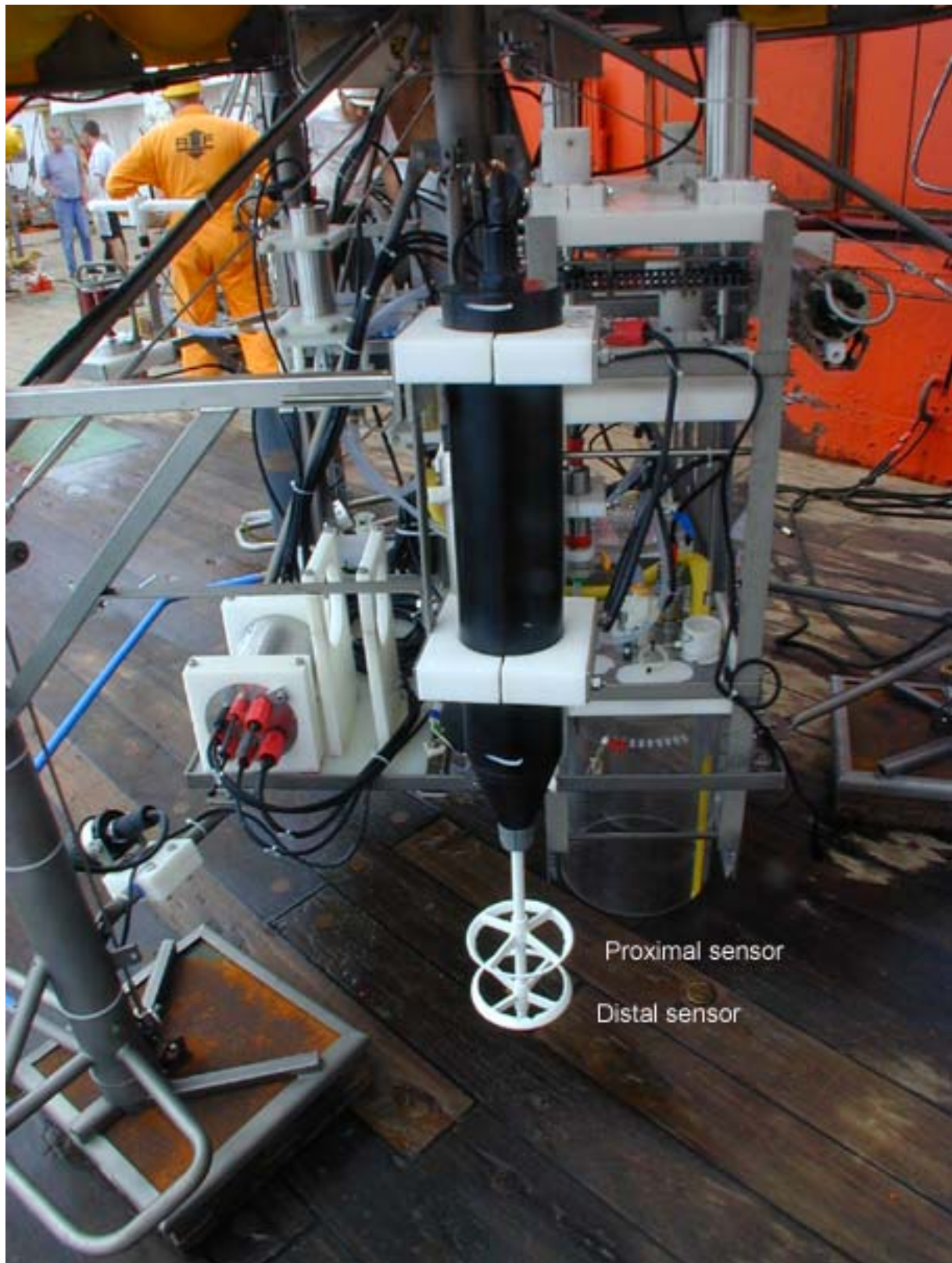


Fig.5.4.3: Sideview of FLUFO with the MAVS current meter attached to one of the 3 legs of the lander. On the right hand side in the back, the FLUFO chamber can be seen.

SBE 16plus SEACAT

The SEACAT is designed to measure conductivity, temperature and pressure in moored applications at depths up to 7000 meters. For precise pressure measurements the SEACAT is equipped with a quartz pressure sensor with temperature compensation. It can be programmed to acquire and record in memory (8 Mbyte FLASH RAM) time series measurements at sample rates of once every 5 seconds to once every 4 hours, adjustable in one-second increments. Setup, diagnostics, and data extraction are performed without opening the titanium housing (Figure 5.4.4.)

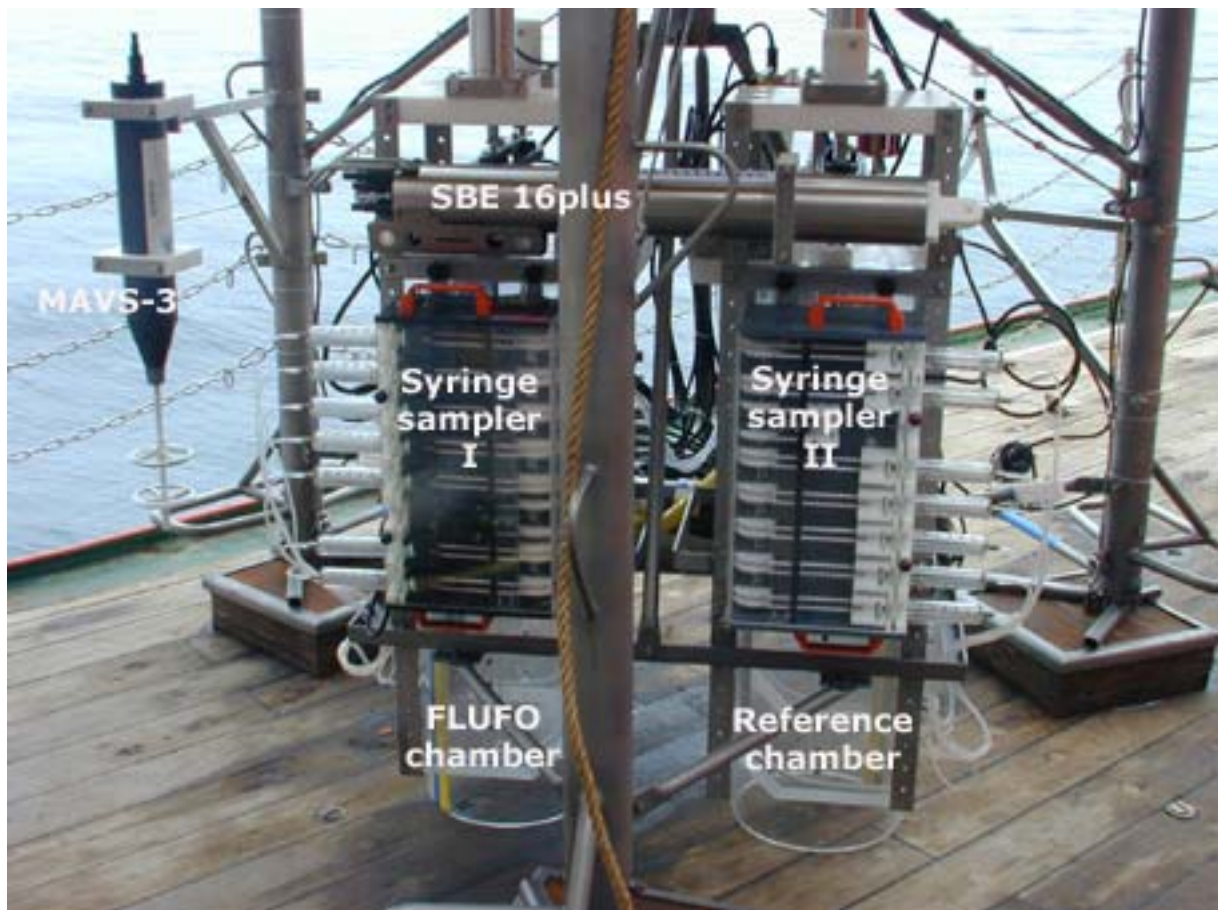


Fig.5.4.4: Backview of FLUFO with SEACAT mounted horizontally on top of the 2 syringe samplers.

Acoustic Telemetry Modem (ATM-880)

The Benthos ATM-880 Series Acoustic Telemetry Modems provide wireless digital communications between underwater instrument packages and surface or subsea platforms. The modems employ two independent multiple frequency shift keying (MFSK) modulation techniques: 1-of-4 MFSK for high speed communications and Hadamard MFSK, which is slower but more reliable in a high multipath environment.

The ATM-880 Series Acoustic Telemetry Modems used on OTEGA consist of three parts: the ATM-881 Deck Box, the remote AT-408 omnidirectional transducer and the subsea ATM-887 Acoustic Telemetry Modem with an omnidirectional (or directional) transducer for full ocean depth applications. The deck box is connected

with a 25-meter cable to the remote transducer to communicate with the subsea modem which is connected via an RS-232 serial interface with the controller on FLUFO.

Results and Discussion

The FLUFO System was deployed five times. The system was sequentially placed on bacterial mats (indicators for near-surface gas hydrates), clam fields, and areas with non-visible chemo-synthetic biological activity (reference station). The measurement periods varied from 12 up to 72 hours. For interpretation of fluid flux rates, auxiliary data as bottom current and static pressure were measurements. In addition water samples from the benthic chamber were taken during each deployment.

The analyses of the data sets reveals a high spatial and temporal variability of flux rates at the Hydrate Ridge. There were three different vertical flux regimes observed: areas with increased outflow from the sediment, areas with increased inflow into the sediment and areas with an alternating flows per tidal phase. All data sets exhibit a significant periodicity. As expected a correlation between tide signal and flux rate prevailed (Figure 5.4.5). In addition there is a significant correlation between vertical flux rate and bottom current. A first analysis of the data sets suggests a high influence of the bottom current on the vertical flow. This feature has to be fully established in upcoming experimental and theoretical work.

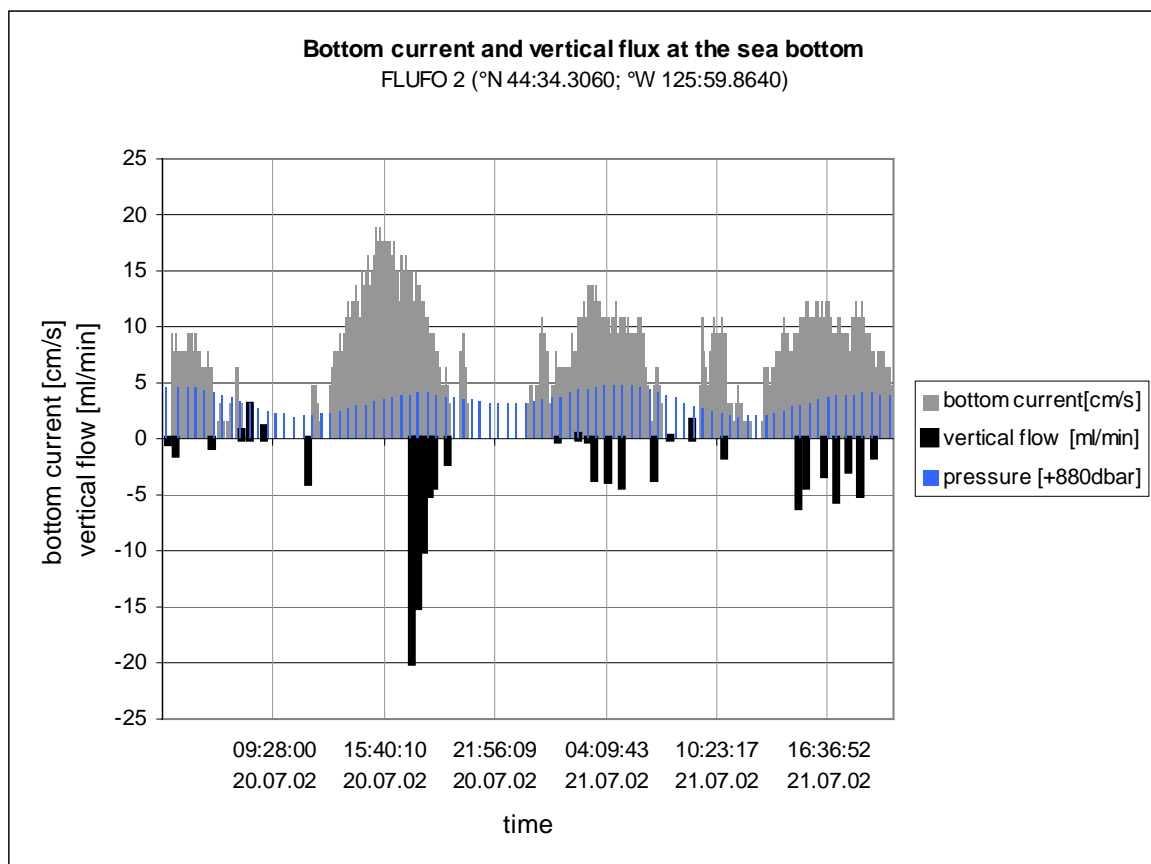


Fig.5.4.5. Bottom current and vertical flow regime at the sea floor (positive values: discharge; negative values: inflow).

5.5 Deep-sea Observation System (DOS)

P. Linke, O. Pfannkuche, B. Mählich, T. Viergutz

Objectives

Bottom water currents with changes in velocity and direction as well as fluctuations in hydrostatic pressure, due to tidal or meteorological influences are expected to have an impact on the exchange processes and biological interactions at the sediment/water interface and the distribution of gas flares expelled from active seep sites into the water column. To monitor these oceanographic control parameters in combination with particle flux and megabenthic biological activity the Deep-sea Observation system (DOS) was deployed.

Instrumentation

Like all other landers DOS was deployed video-guided with a launching system carrying 1 color and 1 b/w video camera (OSPREY & SIMRAD), 2 spotlights (DEEP-SEA POWER & LIGHT) and the telemetry unit for power, video- and data transmission via the ship's hybrid (fiberoptic/coaxial) cable to the winch and telemetry operators on board the vessel. A spotlight was mounted in front of each lander to improve the visibility of small-scale topographic features. The whole system was towed in view, approx. 1.5 m above, the seafloor and the lander was disconnected from the launcher by electric command to a mechanic release (NICHYU GIKEN KOGYO). After deployment, the launcher was retrieved and prepared for the deployment of the next lander.

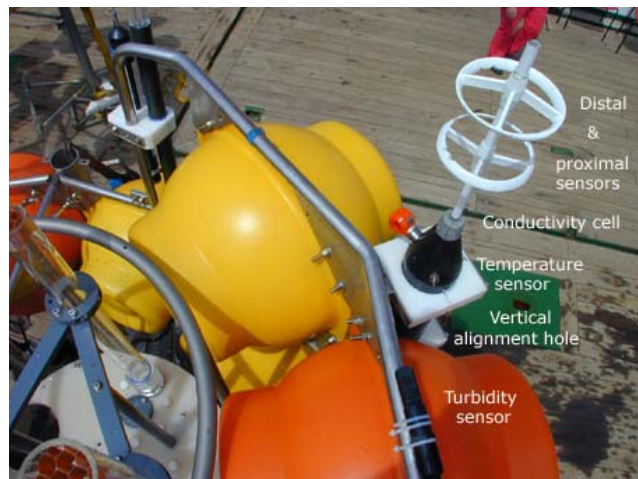
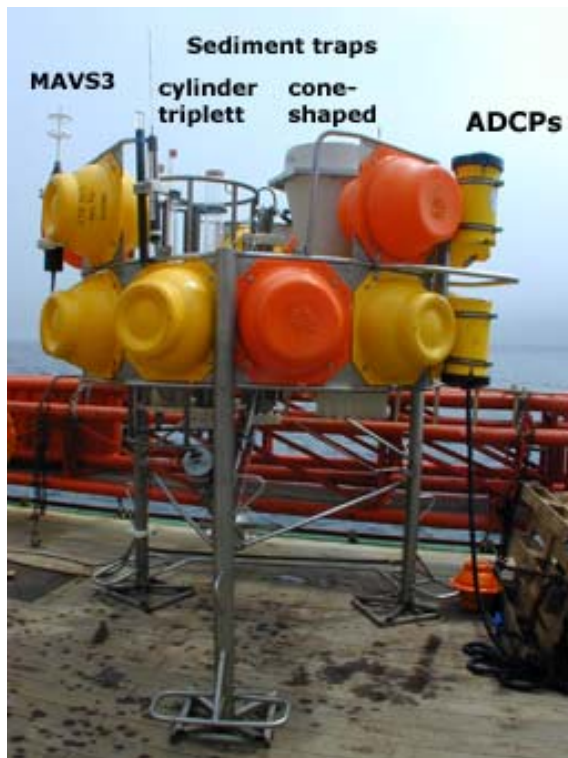


Fig. 5.5.2: View from above. Position of the MAVS3 and the attached sensors.

Fig. 5.5.1: The DOS-Lander after recovery from the 12-day deployment. The acoustic module (ADCPs and MAVS3) and the pair of sediment traps are integrated within the top part of the lander, whereas the optical module is mounted beneath the floatation spheres.

The DOS-Lander system (Fig. 5.5.1) was equipped with 3 major modules:

- 1) an acoustic module with two broadband acoustic doppler current profilers (up-looking 300 kHz and down-looking 1200 kHz ADCP, RD-Instruments) and a 3 axis MAVS current meter (NOBSKA, Fig. 5.5.2) ,
- 2) a pair of sediment traps (Fig. 5.5.3), a cylinder tripllett (TUHH) and a cone-shaped trap (K.U.M.) , and
- 3) an optical module (Fig. 5.5.5) with a stereo still camera and flash (BENTHOS).



Fig. 5.5.3: Position of the two sediment traps (tripllett and cone).



Fig. 5.5.4: View from below on the 12 bottles of the cone-shaped trap after recovery.



Fig. 5.5.5: Arrangement of the optical module with flash and stereo camera.

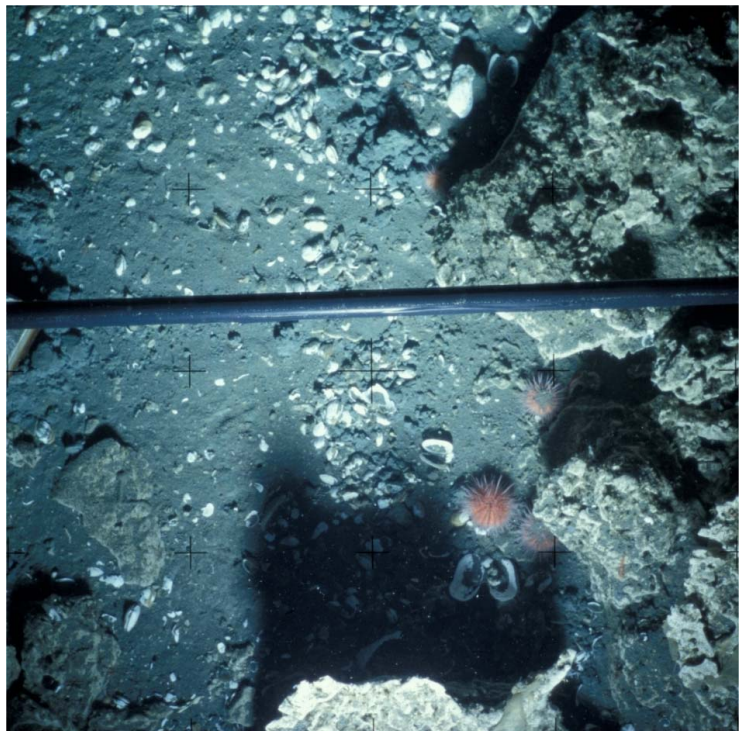


Fig. 5.5.6: Photograph from the deployment site on a clam field at the Northern Summit. Note the carbonate blocks on the surface.

Conducted work

The DOS Lander was deployed for 12 days on a clam site on the Northern Summit to avoid any impacts or conflicts with the drilling operation of JOIDES RESOLUTION. The vertical measurement cells or bins (depth cells) over which the ADCPs measure velocity and collect data were set to 1 m within a range of 3 to 123 m up-looking and down-looking to 5 cm with a range of 60 to 300 cm, respectively. The traps were pre-programmed to obtain particle flux samples with a change of sampling cups in 23 h-intervalls in the cone trap respectively 46h-intervalls in the cylinder trap. Cups were changed simultaneously in the cylinder triplet. Both traps worked successfully as demonstrated in Fig 5.5.4 for the cone trap.

Times of cup rotation cone trap:

Date	Time (UTC)
Cup 1 - 16.07.02	19:00:00 until
Cup 2 - 17.07.02	18:00:00 until
Cup 3 - 18.07.02	17:00:00 until
Cup 4 - 19.07.02	16:00:00 until
Cup 5 - 20.07.02	15:00:00 until
Cup 6 - 21.07.02	14:00:00 until
Cup 7 - 22.07.02	13:00:00 until
Cup 8 - 23.07.02	12:00:00 until
Cup 9 - 24.07.02	11:00:00 until
Cup 10 - 25.07.02	10:00:00 until
Cup 11 - 26.07.02	09:00:00 until
Cup 12 - 27.07.02	08:00:00 until 28.07.02 07:00:00

Times of cup rotation cylinder trap:

Cup 1 - 16.07.02	19:00:00 until
Cup 2 - 18.07.02	17:00:00 until
Cup 3 - 20.07.02	15:00:00 until
Cup 4 - 22.07.02	13:00:00 until
Cup 5 - 24.07.02	11:00:00 until
Cup 6 - 26.07.02	09:00:00 until 28.07.02 07:00:00

The optical module was programmed to obtain stereo photographs of the seafloor area beneath the lander in one hour intervals (Fig. 5.5.6).

Results

The ADCP data from the deployment have been processed at GEOMAR with Matlab routines and will be merged with other data sets obtained during this cruise. The data sets from both ADCPs clearly show the impact of tides in respect of current speed and direction (Figs. 5.5.7 and 5.5.8). In both data sets current speeds of up to 30 cm/s occur which demonstrate large hydrodynamical amplitude on this exposed summit. Unfortunately, the current meter data of the MAVS-3 can not be used since the instrument was deployed up-side-down without the appropriate calibration of the sensor. However, the data of the auxillary sensors are processed right now at GEOMAR.

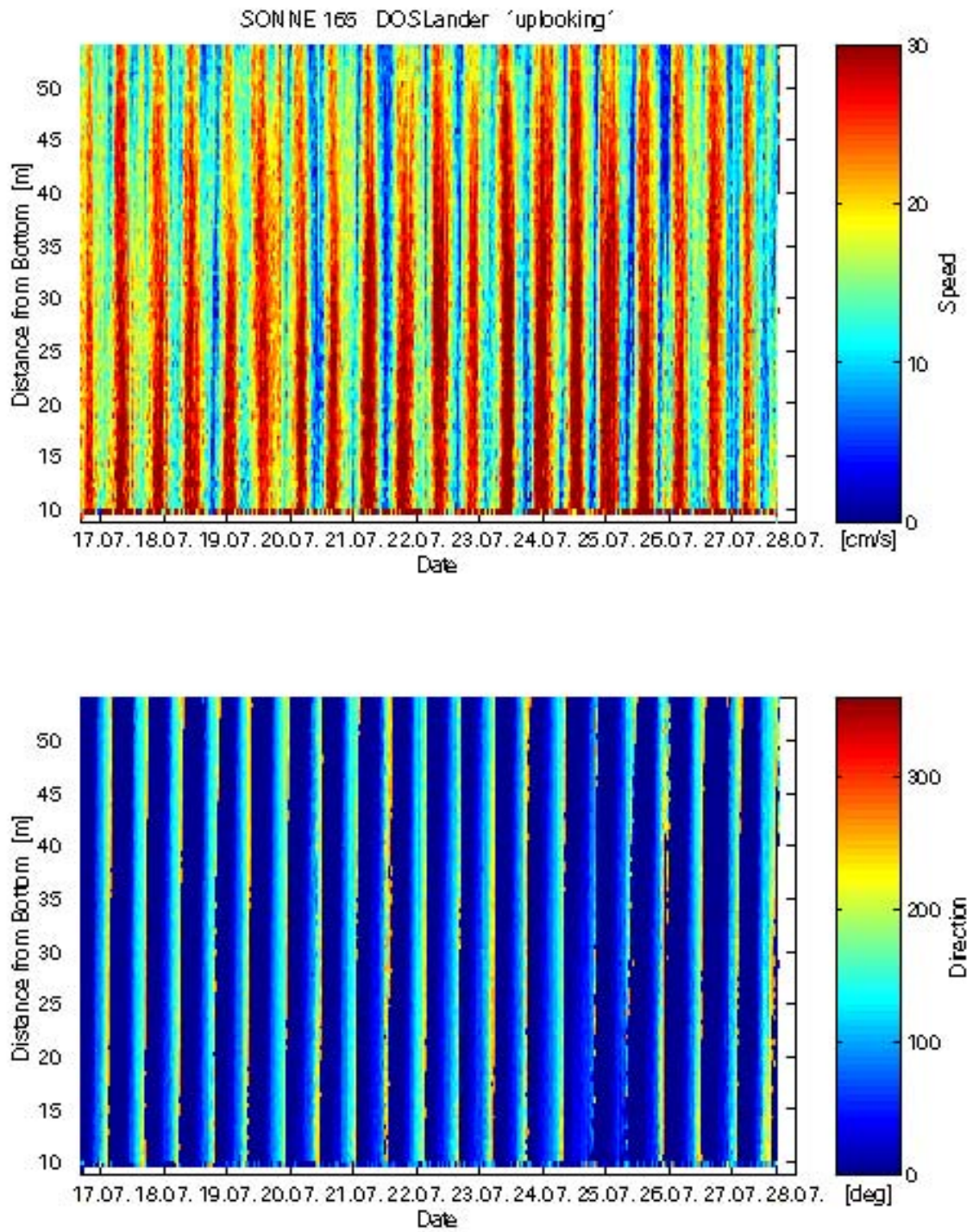


Fig. 5.5.7: Plot of data from the up-looking ADCP in 10 to 55 meters above the seafloor. Current speed and direction clearly show the impact of tides.

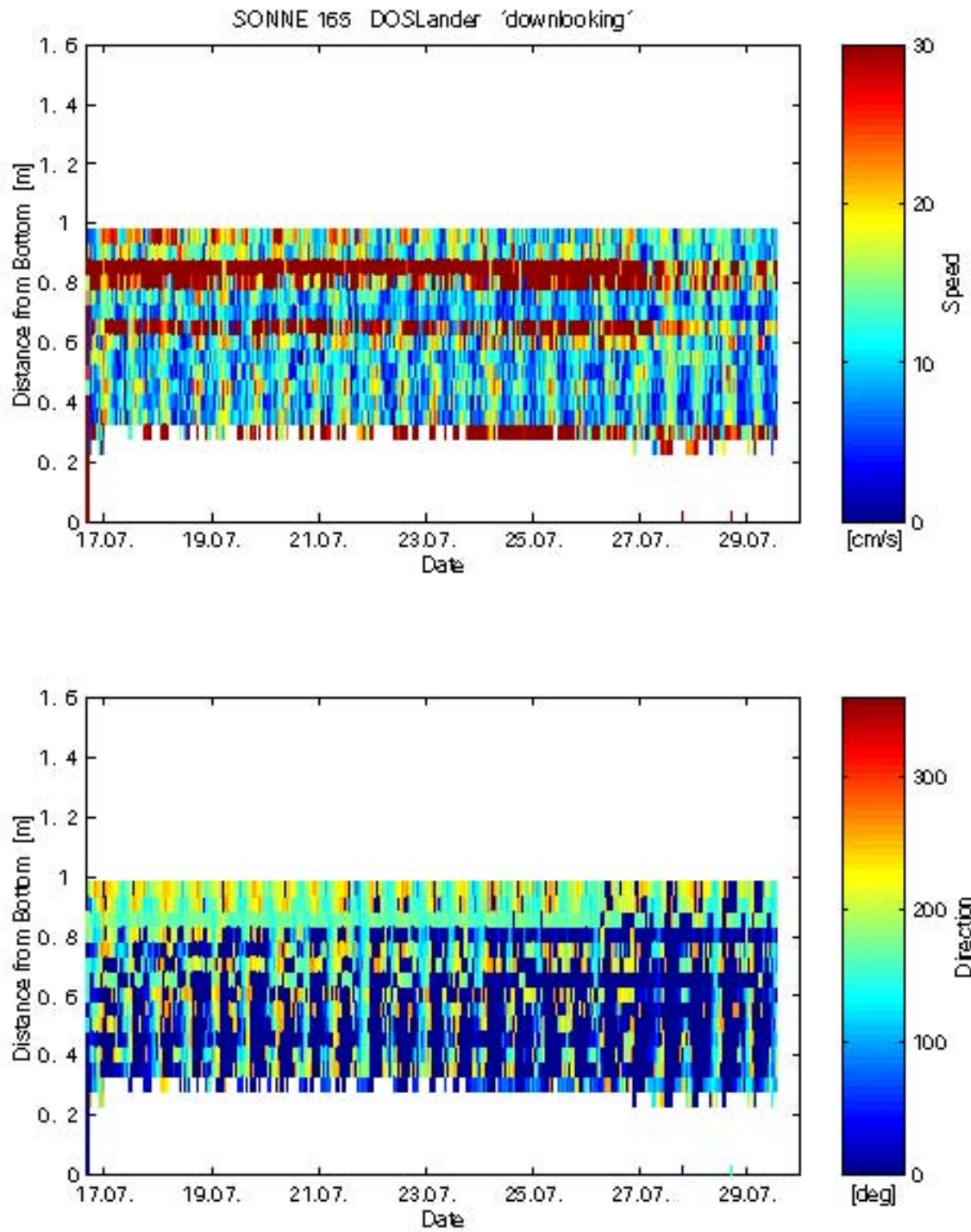


Fig. 5.5.8: Plot of data from the down-looking ADCP in 1 to 0.3 meters above the seafloor. Current speed and direction clearly show the impact of tides.

Sediment traps

A new trap array was provided by TUHH/MT1 to determine the in-situ particle flux at Hydrate Ridge at approx. 2.5 m a.b. and to compare the trap collection rates with those from a small conical trap (aperture area $1/4 \text{ m}^2$) of GEOMAR. The NTTA (new trap technology array) consists of a multiplett of 3 cylindrical tubes of minimum aspect ratio $h/D = 8$, with D at 46, 70, 100 mm for the tubes. Sampling cup rotation intervals were synchronized between the two trap types, with a total collection time of yy days. Two scientific missions were pursued: one to obtain reliable field data to compare a new trapping protocol, by which the in-situ particle flux is obtained from cylinder trap collection rates, with results obtained from rates with the cone trap following the JGOFS trapping protocol. The second mission was to quantify the local sinking-particle flux which is available to the bacterial mats. Both trap arrays functioned well during the experiment and all additional flow parameters were obtained to apply the trapping protocols once the trap calibrations for the particle yield are completed (see Gust and Kozerski (2000) for details of the new protocol). After retrieval of the DOS-Lander, the NTTA was deployed upside-down on a hydrowire overnight at station no 136 to test if raising gas bubbles could be detected/collected. Samples analysed directly after retrieval by gas chromatography gave a negative result. The remaining samples will be evaluated at Kiel.

Stereo-Photography

A total of 292 photographs were taken during the deployment. The photo material has been developed and will be analysed at GEOMAR. The images will be scanned, digitized and merged to a film to detect changes in the faunal distribution and activity during the deployment.

5.6 Deployment of the novel observatories BIGO and FLUFO

S. Sommer, O. Pfannkuche, P. Linke, S. Gubsch, T. Viergutz, B. Bannert, M. Pieper, M. Poser, W. Queisser, A. Kähler, D. Hägele

Introduction

Within the LOTUS project TP-1 we designed two new benthic observatories to study the temporal variability of physico-chemical and biogeochemical mechanisms, flux- and turnover rates related to the decomposition and formation of surficial gas hydrates embedded in their original sedimentary matrix.

Major objective of the **Fluid-Flux-Observatory** (FLUFO) is to identify and quantify the impact and overall relevance of these parameters on the effective discharge rates of fluids and dissolved chemical species related to the decomposition of gas hydrates (see also chapter 5.4).

With the **Biogeochemical Observatory** (BIGO) the temporal variability of the biologically facilitated methane turnover in the sediment and fluxes across the sediment water interface can be studied *in situ* in two mesocosms. Inside the mesocosms the oxygen content and flow regime can be artificially maintained. This approach represents a major step in the development of benthic chambers from stationary to dynamic systems. The biogeochemical observatory will be used to approach the following objectives and questions:

- Baseline studies of biologically mediated advective and diffusive transport processes and their effect on the degradation kinetics of gas hydrates.
- How far are the degradation velocities of gas hydrates controlled by changes of the supply and availability of organic matter, oxidants and reductants, i.e. by the electron and carbon flow through the benthic community?
- What major biogeochemical pathways can be identified affecting degradation kinetics of hydrates and what are their intensities and time constants?
- To which extent are interfacial flux processes (methane release rates) dependent on bottom water shear stress (chapter 5.7.)?

Methods

Eleven employments of BIGO and FLUFO were conducted at characteristic sites at Hydrate Ridge in depths ranging from 605 – 883 m (Suess et al., 1999; Sahling et al., 2002; Sommer et al., 2002). Additionally to the observatories, sediment samples were obtained using a TV guided multiple corer, MUC. For the precise positions of the employments see List of stations (app.).

Gas hydrate affected sites can be separated into three habitats characterised by dominant key organisms, which colonise along a gradient of diffusive sulfide flux (Sahling et al., 2002). Bacterial mats of *Beggiatoa* sp. occur directly above surficial gas hydrates in association with high diffusive sulfide fluxes of up to $63 \pm 36 \text{ mmol m}^{-2}\text{d}^{-1}$, in zones where the sulfide front reaches the surface of the sediment. These bacterial mats together with the underlying sediment were sampled during BIGO #3/#4/#6, FLUFO #2/#3/#5, and MUC #8/#15 employments (cf. Table 5.6.1). Concurrently with reduced sulfide fluxes ($18 \pm 6.5 \text{ mmolm}^{-2}\text{d}^{-1}$) and a lowering of the sulfide front several centimetres deeper into the sediment, the outer rim of the bacterial mats becomes densely populated by vesicomyid clams of the genus *Calyptogena* sp., hitherto referred to as clam fields (BIGO #2/#4, FLUFO #4, MUC

#22). Sediments with lowest sulfide fluxes are characterised by the presence of the solemyid bivalve mollusc *Acharax* sp. which lives buried in the sediment.

Control samples (BIGO #1, FLUFO #1, MUC #32) were obtained from locations without gas hydrates, a few hundred of meters apart from the hydrate-affected sites. In these sediments dissolved sulfide was not detected (M. Drews pers. comm.).

Novel features of BIGO whose design is based on former GEOMAR Landers which has been successfully deployed during e.g. POSEIDON cruise 260 (Pfannkuche & Utecht, 2001) are the following:

The frame of BIGO is made of titanium, which allows long-term employments. Since titanium is lighter than the formerly used steel more scientific payload and sediment samples can be taken up by the system (Figure 5.6.1).

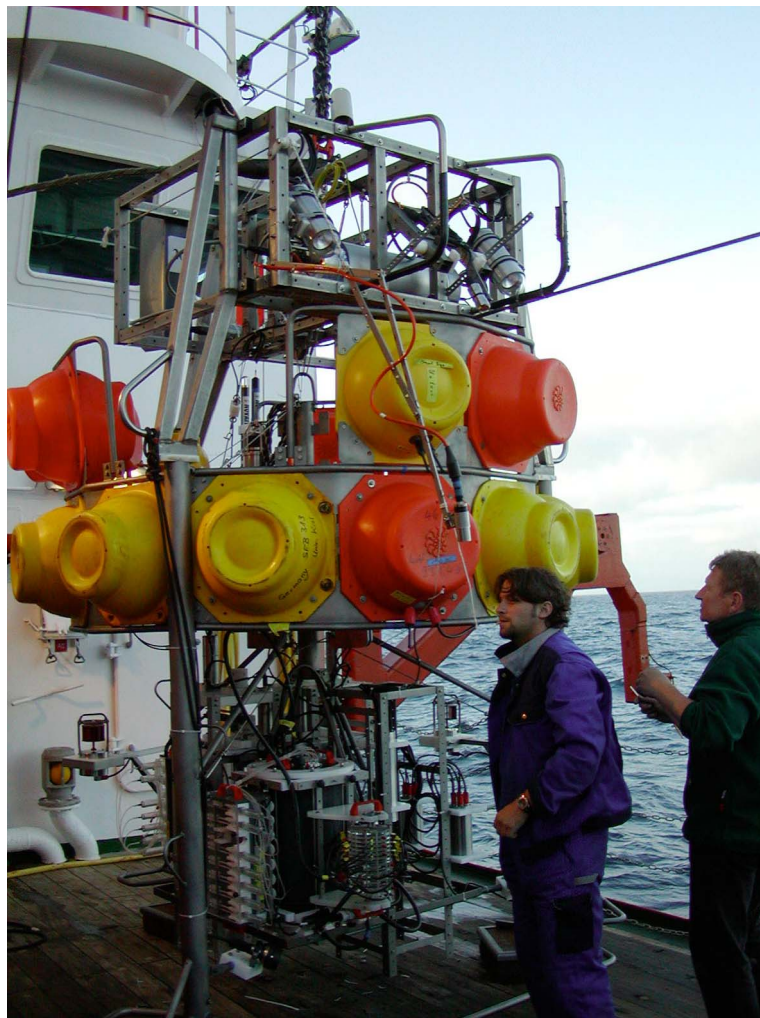


Fig. 5.6.1: BIGO with launching system mounted on it's top.

BIGO contains two circular chambers (mesocosms) with an internal diameter of 30 cm. This size is to minimise smearing effects on the inner sediment core, when the chamber is pushed into the sediment. It provides a surface area of 651,4 cm² for appropriate subsampling of the sediment. As shown by Glud and Blackburn (2002) flux measurements in larger chambers are less susceptible for errors when calculating areal budgets and fluxes based on fewer measurements.

Flux rates of solutes and micro-particulates across the sediment water interface, are highly susceptible to alterations in the flow regime of the overlying water body.

Thus, in cooperation with G. Gust (TUHH, Hamburg) a system mimicking the external flow regime inside the chamber was integrated. The lid of the chamber includes a rotating disc with a skirt, which in dependence of its rotation speed produces a flow regime similar to that outside. The rotation speed of this disc can either be regulated by an external flow sensor (Savonius rotor) or set to fixed values for experimental purposes. For more details see chapter 5.7.

In order to record long-term variability of benthic turnover in semi-closed chamber systems it is of crucial importance to maintain the oxygen supply at natural levels and to avoid severe oxygen depletion. Thus, to compensate for the total oxygen consumption of the enclosed sediment community a gas exchange system (Figure 5.6.2) was designed. This system facilitates oxygen transfer from a reservoir (approx. volume 31.6 l) containing saturated sea-water into the benthic chamber across stacks of silicone membranes. The functionality of the system is based on the counter-current principle as realised in gills of e.g. fish, where oxygen enriched blood and oxygen depleted blood flows counter-currently along a membrane, which is permeable for oxygen. Oxygen transfer is mediated along a concentration gradient via diffusion.

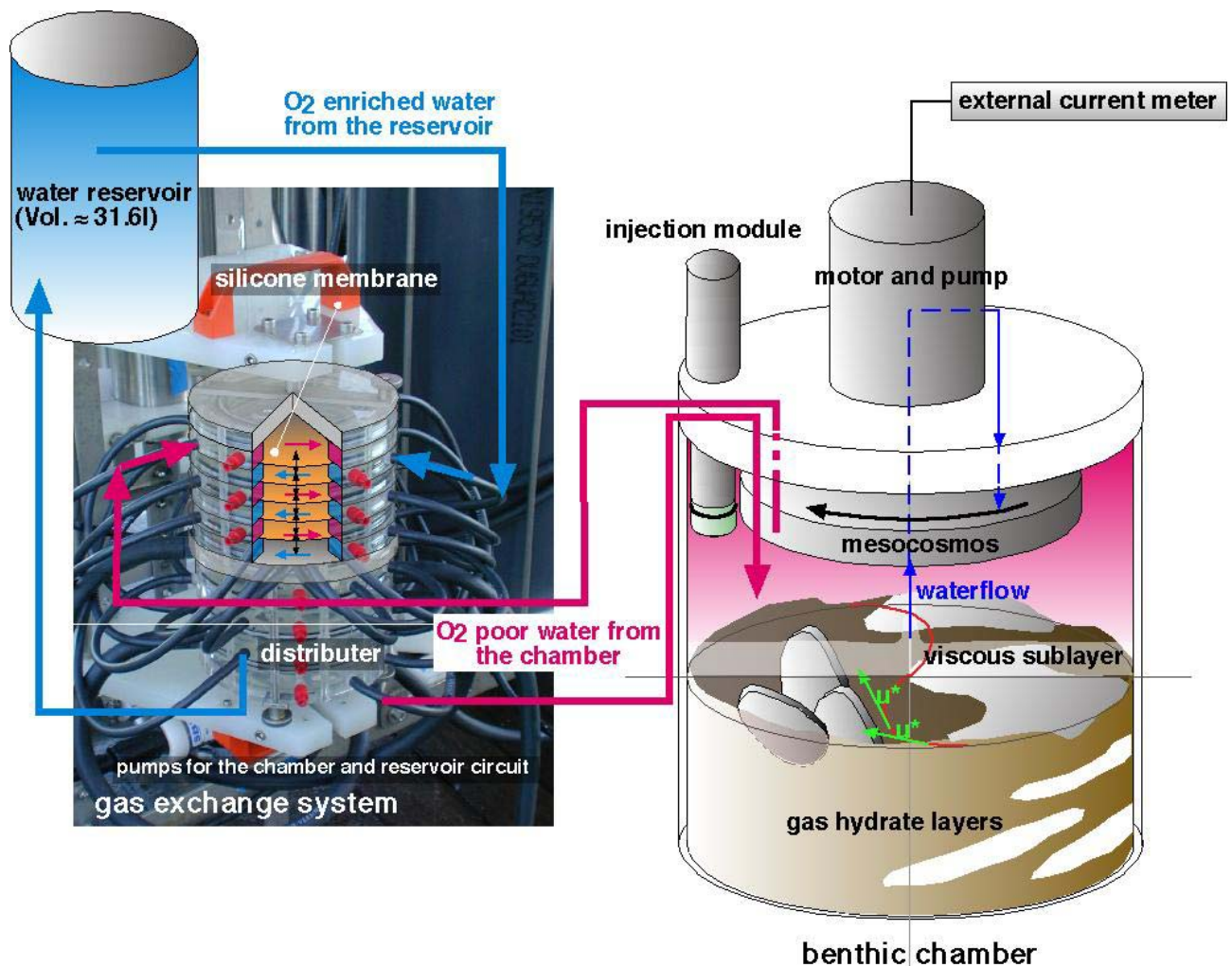


Fig. 5.6.2: Gas exchange system connected with the benthic chamber. The chamber water circle (red) is separated from the reservoir circle (blue) by silicone membranes which allow exchange of methane and oxygen.

The gas exchange system used possesses five membranes supplying a total gas exchange area of 392.7 cm². However, the amount of membrane stacks can be freely chosen in accordance to the activity of the investigation site. The thickness of the membrane is 0,125 mm. Water flow within the chamber- and reservoir circuits is facilitated by Seabird pumps. Prior to the tests the reservoir was filled with filtered seawater to define the start conditions of the measurement more precisely and to reduce microbial contamination in the reservoir circuit. Reservoir water was saturated with oxygen by sparging it with air for several hours. For each BIGO employment the reservoir water was exchanged. Two chambers were integrated into BIGO for each employment, a control chamber without gas exchange system and a chamber fitted with such a system hitherto referred as exchange chamber.

The design of the observatory for the in situ determination of fluid fluxes across the sediment water interface (FLUFO) and preliminary results are described in chapter 5.4.

Biogeochemical analyses

A list of biogeochemical parameters which have been measured in the various sediment/water samples during the cruise is provided in Table 5.6.1. Sediment samples for the measurement of pigments, bioturbation, bioirrigation, exoenzymatical hydrolysis, ¹³CO₂ uptake into the sedimentary organic matter; phospholipids, short chain fatty acids, and meiofauna were taken immediately after recovery of the gear and processed in a cool room at *in situ* temperature (~ 4°C). Sediments retrieved during MUC and BIGO employments were subsampled with cut-off syringes with 1.13 cm internal diameter for the determination of all parameters except meiofauna samples, which were taken with cores of 6 cm internal diameter. Subsamples were sectioned horizontally in 1 cm intervals down to a depth of 10 cm. The number of replicates for all parameters is given in Table 5.6.1.

For the description of additional parameters which have been measured in BIGO sediment samples by M. Drews (GEOMAR) and P. Heinz (University of Tübingen) see chapters 5.8. and 5.17.

Tab.5.6.1: List of parameters measured in samples obtained from the different gears employed. Abbreviations: BI: bioirrigation BT: bioturbation; CO₂ Fix: carbon dioxide fixation in the dark; FDA: exoenzymatical hydrolysis; ICP: MF: meiofauna; oxy: oxygen; optode oxy: oxygen measured with a Aanderaa optode; PIG: plant pigments; SCFA: short chain fatty acids. Bw and ex. ch. refer to measurements in the bottomwater and in the exchange chamber. The numbers denote the number of replicates taken per each chamber and MUC sediment cores.

Gear	Parameter												
	site	oxy.	optode oxy	CH ₄	BT	BI	ICP	PIG	PL	SCFA	FD A	CO ₂ Fix.	MF
BIGO #1	Ref	2		1					3	3	3	2	1
BIGO #2	CF	2	bw	1			1		3	3	2	2	1
BIGO #3	BM	2		1			1		3	3	3	2	1
BIGO #4	BM	2		1			1		3	3	3	2	1
BIGO #5	CF	2	bw	1			1		3	3	3	2	1
BIGO #6	BM	2		1			1		3	3	3	2	1
FLUFO #1	Ref	2		1									
FLUFO #2	BM	2		1									
FLUFO #3	BM	2		1									
FLUFO #4	BM	2		1									
FLUFO #5	BM	2	ex.ch.	1									
BCL #1	BM	2		1				3	3		2		
MUC 8	BM							3	3	3	3	2	1
MUC 15	BM							3	3	3	3	2	1
MUC 22	MF							3	3	3	3	2	1
MUC 32	Ref							3	3	3	3	2	1

Oxygen measurements

From the overlying water column of the control chamber, the exchange chamber and the reservoir water samples were taken at predefined time intervals using syringe water samplers. They allow taking seven sequential water samples at predefined time intervals. The volume of these samples was about 46 ml. During BIGO #5/#6 additional water samples were taken from the bottom water outside the chambers. The inlets of this syringe water sampler were fixed at the Lander frame in a height of about 30 – 40 cm above the sea floor in correspondence to the height of the sampling inlets in the benthic chambers. Oxygen concentrations of these samples were fixed immediately after retrieval of the lander. Until oxygen determination by automated Winkler titration, samples were stored in the dark in a fridge. Storage was at longest one day.

Optode oxygen measurements

During BIGO #2/#5 the oxygen availability in the bottom water was further continuously recorded using a optode (3830), which was kindly provided for test purposes by Aanderaa (A. Tengberg, Göteborg University). The optode was mounted in the lander frame corresponding to a height of about 100 cm above the sediment surface.

During BIGO #6 employment the optode was mounted within the exchange chamber. The optode readings were compensated for salinity and pressure.

Methane measurements

From the water samples of the syringe sampler 10 ml were used for „head space“ methane analyses. Immediately when BIGO and FLUFO were retrieved on board of the ship these samples were carefully, without trapping any gas bubbles, transferred into rubber stoppered 20 ml glass vials. These contained saturated NaCl solution with 1.5 g Na Cl in excess to account for dilution after addition of the sample. The sample to headspace ratio of volumes was 10/4 ml. Within 24 h methane concentrations were determined in cooperation with Dr. J. Greinert and B. Mählich (GEOMAR) using a GC fitted with a FID. Prior to GC measurements the samples were equilibrated for 2h in a shaking table.

Bioirrigation, bioturbation, transportation processes

To determine bioturbational and bioirrigational activity during employments of BIGO, FLUFO and the Benthic Chamber Lander glass beads (60 µm diameter) and bromide (7.24 g) were injected into the chamber shortly after it was pushed into the sediment. During FLUFO deployments no glass beads were added, since this observatory does not recover the enclosed sediment sample.

Chlorophyll *a*

Sediment samples for the determination of chl.a and pheopigment concentrations were taken, they serve as an indicator for the input of phytoplankton derived C_{org.}. Their concentrations were determined using a TURNER fluorometer according to Yentsch and Menzel (1963) and Holm-Hansen et al. (1965) as described by Pfannkuche et al. (1999). Additional identification and quantification of plant pigments will be conducted using HPLC in cooperation with the Institut für Meereskunde, Kiel.

CO₂ dark fixation

To resolve the non-photosynthetic endogenous production of POC in the sediment, chemoheterotrophic and chemoautotrophic ¹³CO₂ uptake into sediment particulate organic matter was analysed. Incubation of the sediment sample (1 cm³) mixed with filtered sea water (3 ml) was conducted in a centrifuge tube (15 ml) under an Argon atmosphere in the dark at *in situ* temperature for 12 h. To each incubation 277 µl of a NaH¹³CO₃ stock solution (90mM, Chemotrade, Leipzig) was added. To halt bacterial activity after incubation, the sediment slurries were centrifuged for 30 min at 4000 rpm. Whereas the liquid phase was kept for latter analysis the sediment pellet was washed in 2 ml filtered seawater and centrifuged again for 10 min at 4000 rpm. The sediment pellet was dried at 60°C for 48 h.

In the home laboratory, these sediment samples were resuspended in 3 ml HCl (10 M) to remove residual NaH¹³CO₃ and CO₂ bound in carbonates and dried at 60°C for 48 h. The sediments were ground using a mortar and pestle and weighed into tin cups. These samples will be measured in a CN-MS in cooperation with the Gesellschaft für Biotechnologische Forschung, Braunschweig (Dr. W.R. Abraham).

Exoenzymatic hydrolytic activity

Potential activity of hydrolytic enzymes was measured fluorimetrically with fluorescein-di-acetate (FDA) as substrate after a slightly modified method of Meyer-Reil and Köster (1992) as specified by Pfannkuche et al. (1999).

Phospholipids

Phospholipids will be determined as biomass parameter of the small sized benthic community comprising fungi, bacteria, protozoans and metazoan meiofauna. PL will be measured following the method described by Boetius et al. (2000a).

Short chain fatty acids

Short chain fatty acids such as acetate, lactate, propionate are thought to represent major intermediate metabolites of sulfate reducing bacteria which in consortia with methanogenic archaea play a key function in the anaerobic oxidation of methane in gas hydrate containing sediments (Boetius et al. 2000b, DeLong 2000)

Preliminary results

At present, the analyses of most biogeochemical parameters of the sediment samples are still in progress, thus this report will focus on water samples taken during BIGO and FLUFO employments.

Oxygen and methane concentrations in the bottom water

The oxygen concentration in the bottom water at the southern summit of Hydrate Ridge was continuously recorded by the optode during employment of BIGO #5. In parallel we took water samples using a syringe water sampler.

Descend and ascend of BIGO #5 back to the surface have been nicely documented, Figure 5.6.3. One meter above the sea floor there was very little variability of the bottom water oxygen concentration recorded by the optode. During the entire 24 h stay of BIGO #5 at the seafloor the average oxygen concentration (optode) of the bottom water was $17.4 \mu\text{mol}\cdot\text{l}^{-1}$ (SD: 0.33). The bottom water oxygen concentrations concurrently determined in water samples by Winkler titration were about $20 \mu\text{mol}\cdot\text{l}^{-1}$ higher than the optode readings and varied between $32.6 - 45.1 \mu\text{mol}\cdot\text{l}^{-1}$. Temperature was about 4°C .

When the chamber is pushed into the sediment enhanced leakage of methane, takes place which is indicated by increased methane concentrations of 820.7ppmV and 495.6ppmV in water samples taken 5 min after chamber insertion during BIGO #5/#6 employments (Figure 5.6.4). After these high concentrations have been oxidised and swept away by bottom currents methane concentrations were much lower in the range of $1.1 - 5.7 \text{ppmV}$ above a clam field and $5.8 - 22.9 \text{ppmV}$ above bacterial mats.

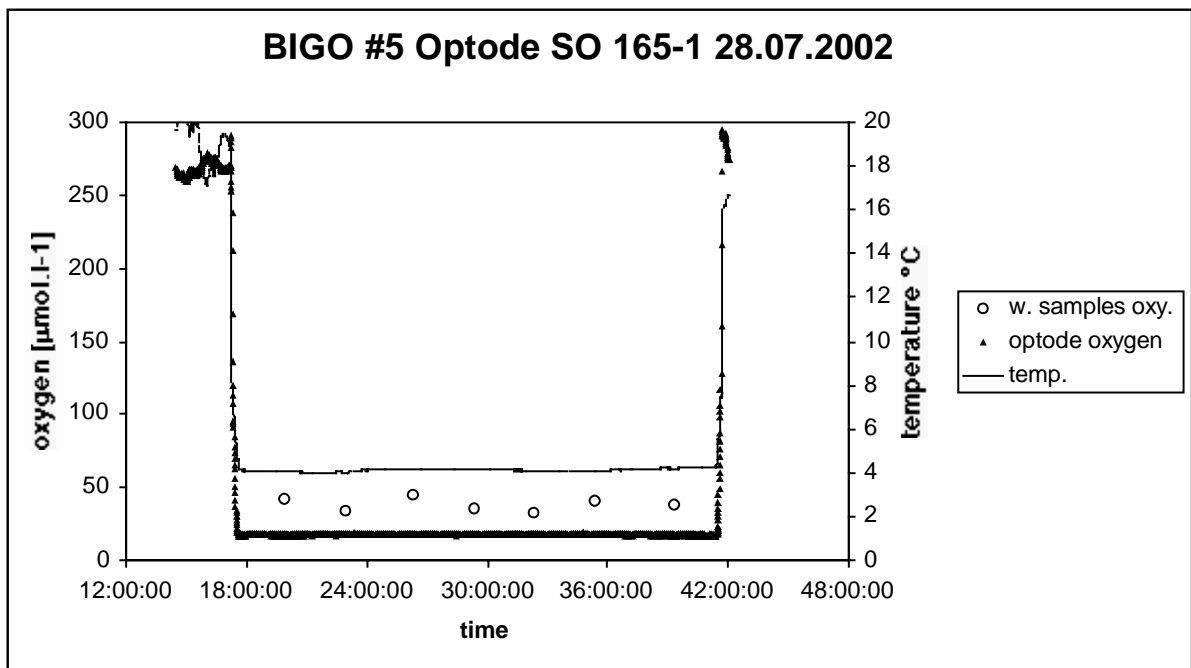


Fig. 5.6.3: Optode oxygen (filled triangles) and temperature (line) measurements in the bottom water during employment of BIGO #5. The sensor was mounted about 1m above the sediment surface. Water samples for oxygen measurements using Winkler titration (open circles) were taken about 30 – 40 cm above the sediment water interface.

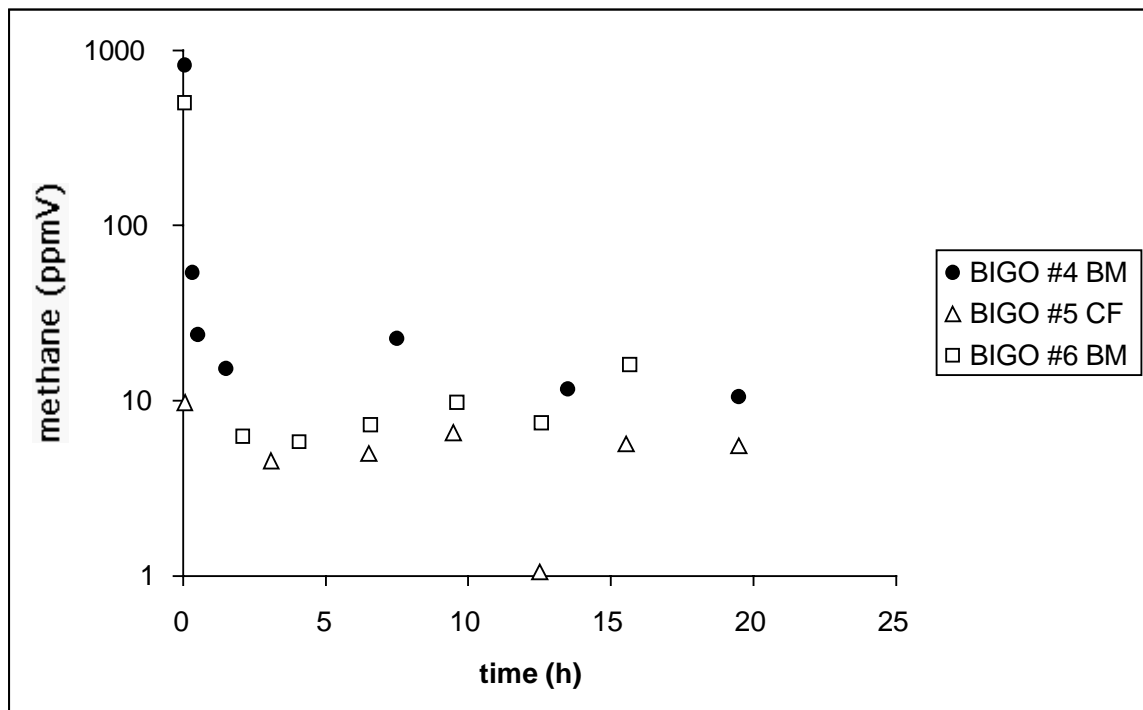


Fig. 5.6.4: Methane concentrations in the bottom water taken 30 – 40 cm above the sea floor during BIGO #4/#5/#6 employments. The observatories were deployed on a clam field and bacterial mats.

Oxygen and methane flux measurements in benthic chambers

Reference site, BIGO #1

In the control chamber oxygen was consumed very slowly, total oxygen uptake (TOU) amounts to $\sim 1.5 \text{ mmol}\cdot\text{m}^{-2}\cdot\text{d}^{-1}$ (Figure 5.6.5). With time the exchange chamber was gradually supplied with oxygen from the reservoir, yielding a maximum oxygen concentration of $130.9 \mu\text{mol}\cdot\text{l}^{-1}$. Obviously the oxygen consumption in the exchange chamber was too low to compensate for this high oxygen input from the reservoir. TOU in the exchange chamber was $19.9 \text{ mmol}\cdot\text{m}^{-2}\cdot\text{d}^{-1}$. It appears that the enhanced oxygen supply stimulates biogeochemical processes within the enclosed sediment/water column, resulting in 13.5 fold higher TOU.

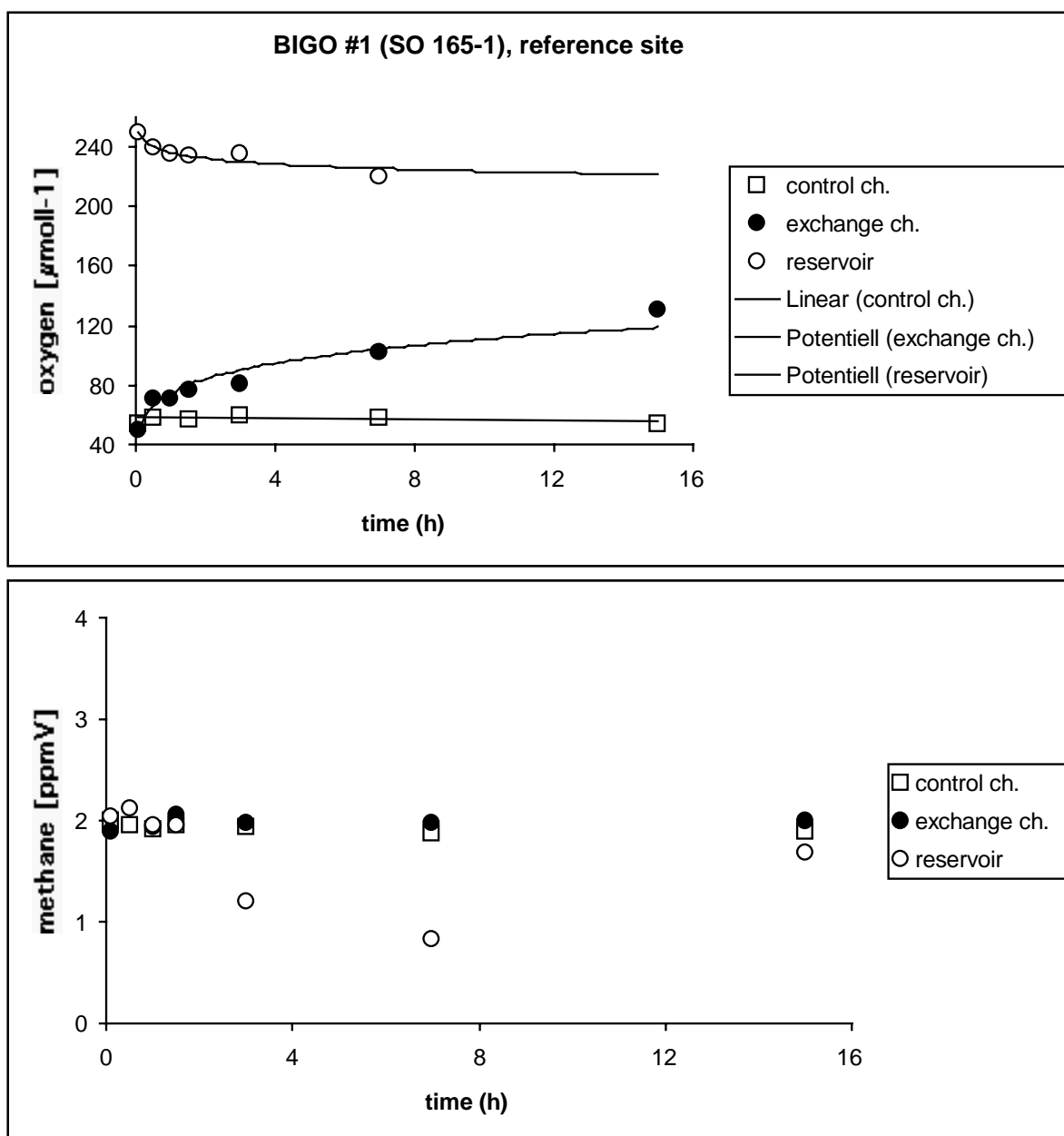


Fig. 5.6.5: Oxygen and methane concentrations over time measured in the control chamber, the exchange chamber and the reservoir during BIGO #1 employment.

At this reference site increased methane concentrations were not detected. Methane concentrations in the control, the exchange chamber and the reservoir during the entire stay of BIGO #1 on the sea floor remained constant at a about 2 ppmV (Figure 5.6.5). This indicates that there was no efflux of methane from the sediment into the water column during employment of BIGO #1. In comparison to this methane background level, methane concentrations in the bottom water above clam fields and bacterial mats were slightly higher.

Clam field, BIGO #5

In the control chamber enclosing a clam field, TOU was only 2.0 mmol·m⁻²·d⁻¹. At the start of the measurements the oxygen supply to the exchange chamber was increased (Figure 5.6.6). However, after about 6 h O₂ consumption in the chamber was in steady state with the O₂ supply from the reservoir at an oxygen level of about 40 μmol·l⁻¹, which corresponds to the ambient bottom water concentration. In the exchange chamber TOU was 17-fold higher than in the control chamber and amounts to 34.1 mmol·m⁻²·d⁻¹. As was already observed during BIGO #1, probably a stimulation of biogeochemical processes induced by increased oxygen supply took place. Concurrently with the steady state in the exchange chamber, the oxygen concentration in the reservoir decreased constantly.

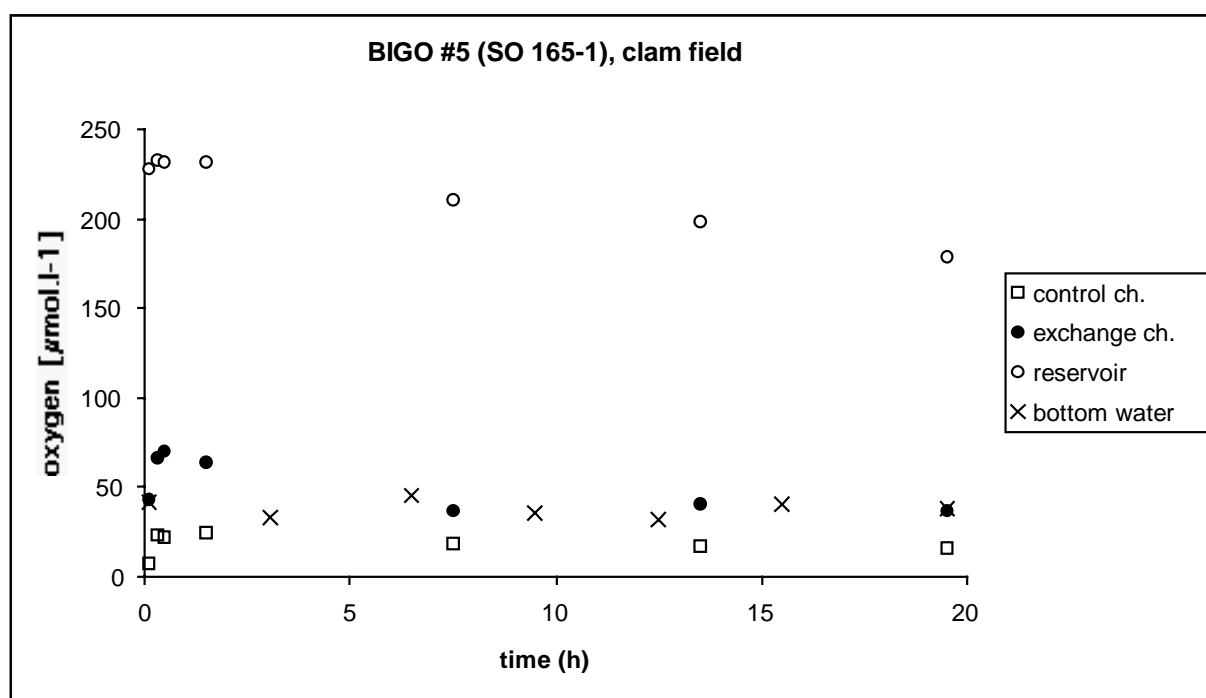


Fig. 5.6.6: Oxygen concentrations over time measured in the control chamber, the exchange chamber and the reservoir during BIGO #5 employment. Ambient bottom water concentrations are shown.

Whereas the methane content in the control chamber increased steadily (Figure 5.6.7) the methane concentration in the exchange chamber including the methane content in the reservoir remained constant at a much lower level.

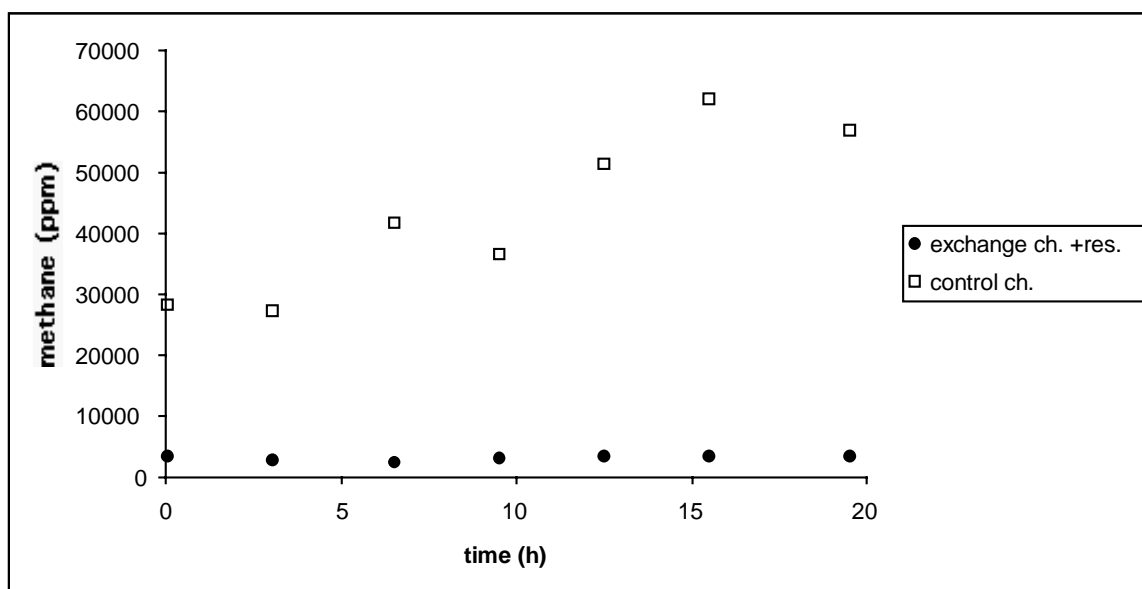


Fig. 5.6.7: Methane content over time in the control chamber in comparison with the exchange chamber (including the reservoir).

Bacterial mat, BIGO #4

The oxygen concentration in the control chamber fell to zero only within 5 minutes after the chamber was pushed into the sediment (Figure 5.6.8). Even in the first syringe water sample no oxygen was detected, thus it is not possible to calculate the TOU in this chamber reliably.

Taking the oxygen concentration of the ambient bottom water as the start value for the incubation an enormously high oxygen consumption rate could be calculated. However, it is uncertain to what extent the enhanced leakage of reduced compounds from deeper sediment strata when the chamber is driven into the sediment affects the TOU in the initial phase of the experiment. Obviously, this bacterial mat sediment is very active and the oxygen demand is much faster than the resilience of the enclosed sediment towards these disturbances. The above phenomenon does not represent a single observation as we made it six times in chambers during employments of FLUFO and a Benthic Chamber Lander (BCL).

Contrastingly, the oxygen supply from the reservoir to the exchange chamber was high enough to cope with these disturbances during the initial phase of the experiment. Within the first 1.5 h the oxygen content reached a maximum of $73.1 \mu\text{mol}\cdot\text{l}^{-1}$ but steadily declined to $55.2 \mu\text{mol}\cdot\text{l}^{-1}$. At the end of the measurements (19.5 h later) TOU was $45.4 \mu\text{mol}\cdot\text{m}^{-2}\cdot\text{d}^{-1}$.

As observed in the clam field (BIGO #5) the methane content in the control chamber was much higher than in the exchange chamber and increased with time (Figure 5.6.9). In the exchange chamber methane content decreased strongly within the first 1.5 h when the oxygen concentrations increased. As the oxygen concentration in the exchange chamber continuously decreased the methane content increased again. The overall methane content in the exchange chamber was about 5 fold higher than that measured in the exchange chamber covering a clam field.

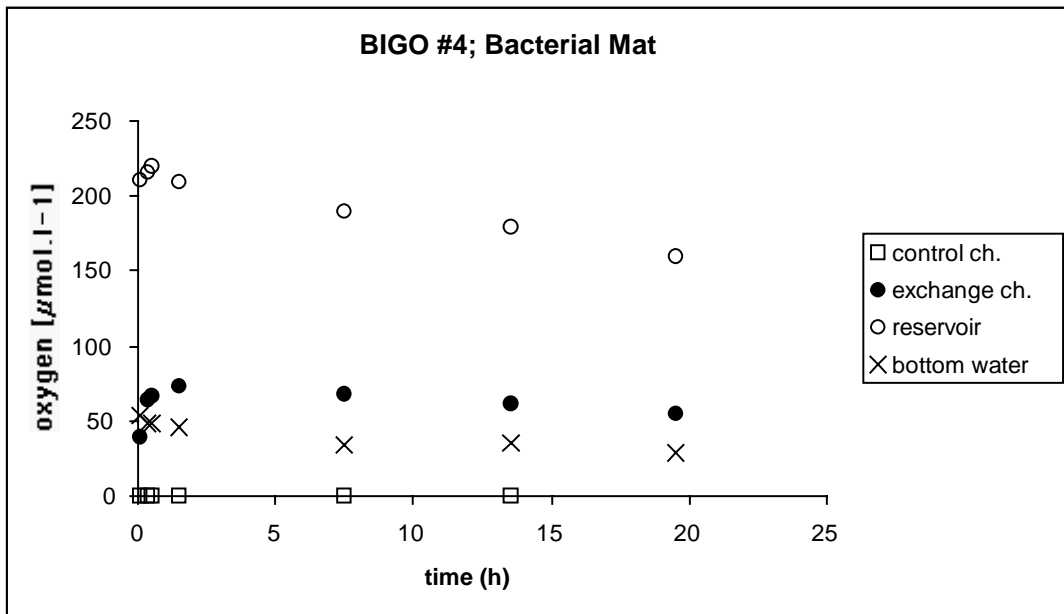


Fig.5.6.8: Oxygen concentrations over time measured in the control chamber, the exchange chamber and the reservoir during BIGO #4 employment. Ambient bottom water concentrations are shown.

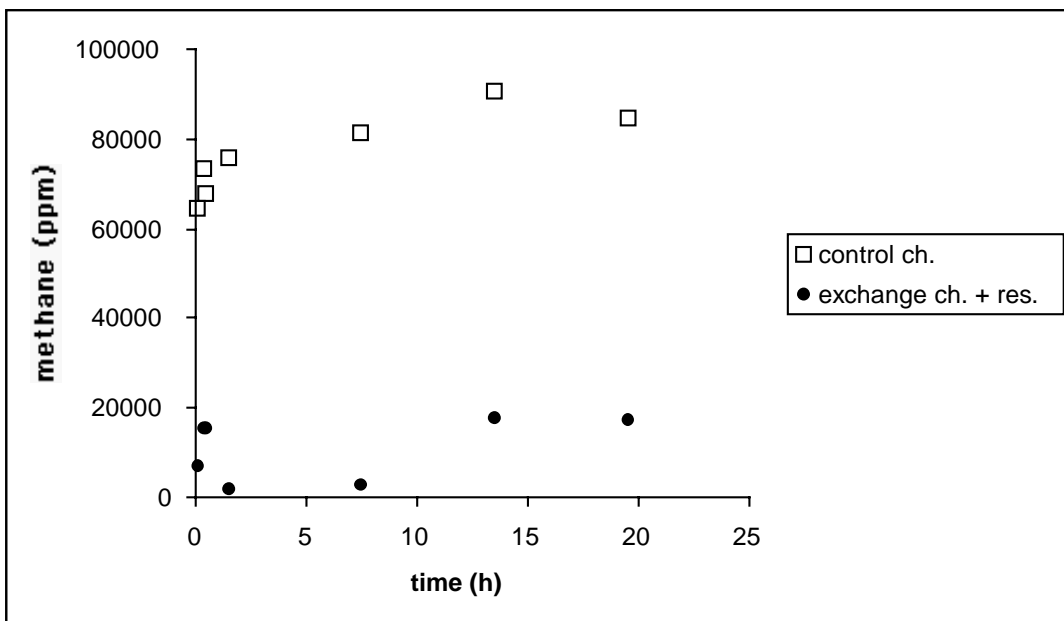


Fig. 5.6.9: Methane content over time in the control chamber in comparison with the exchange chamber (including the reservoir).

Conclusions

In sediments characterised by a lower biogeochemical activity the oxygen supply provided by the gas exchange system was too high and in effect stimulated the enclosed sediment community. Hence in the future BIGO design a self regulating gas exchange system will be developed, which adapts to the actual conditions of the habitat. In more active sediments the gas exchange system was found to work reliably and to prolong the time course during which measurements can be made substantially. Since strong oxygen depletion severely affects the biogeochemistry of

the sediment, in extreme habitats such as the bacterial mats, liable biogeochemical measurements (reflecting natural conditions) without the gas exchange system are possible only to a very limited extent. For future long-term *in situ* experiments in active sediments the above system is indispensable!

We found indications that oxygen availability regulates efflux of methane from the sediment into the water column. Olu et al. (1997) speculate that stable gas hydrates when brought in contact with seawater, will dissociate until methane concentration in the pore water is in equilibrium with the hydrate. Due to the low solubility of methane within the hydrate stability field, leaching of methane from the gas hydrate will only occur when the methane is continuously removed. In addition to diffusive and advective transport, this removal of methane can be “catalysed” by bacterial methane oxidation, probably creating and maintaining steep methane concentration gradients around surficial gas hydrates. We even speculate that rather than passively exploit the methane released from gas hydrates due to chemical dissociation, bacteria actively feed on them. Oxygen availability, which is directly linked to aerobic bacterial turnover and indirectly to anaerobic processes as the ultimate electron acceptor, might highly affect degradation kinetics of gas hydrates and the capability of the “benthic filter”, controlling the flux of methane across the sediment water interface.

5.7 Controlled hydrodynamics inside the chambers of BIGO

T. Viergutz, S. Gubsch

Introduction

The assumption that bottom stress influences the transport of fluid, solutes and particulates across the sediment-water interface initiated the design of a chamber with a homogenous bottom stress distribution (Gust, 1987). This chamber was used in earlier years as a laboratory version to investigate sediment stability and resuspension events. In the LOTUS project TP-1 (BMBF) we redesigned this chamber for in-situ applications with the possibility either to reproduce the external boundary layer stress inside the chamber or to set the internal bottom stress to experimental values independent of the external current. During SO165-1, this *in-situ* system was used after shallow-water tests in deep-sea deployments. Here we describe those aspects of the chambers which were the task of TUHH, particularly chamber adaptations and calibration of its hydrodynamics. For more details of the gas exchange system and lander integration see section 5.6.

Methods

There are two chambers in the BIGO lander, one with gas exchange system and one without gas exchange system (called reference chamber). Each chamber has a diameter of 30 cm. Attached to the lid of the chamber is a disk with 15 cm diameters to which a skirt of 6 cm height is attached.. This disk is turned by a DC-motor. The shaft holding the disk has a central opening through which fluid is removed from the chamber via a centrifugal pump and returned to the chamber at an inlet position. By operating disk and pump at calibrated settings, a spatially homogeneous bottom stress is generated at the bottom of the chamber (Gust & Müller, 1997). For BIGO, a new design with approx. 7,5 cm space remaining between disk and chamber wall was realized, permitting a wider

working/experimenting area for lid-attached sensors to reach the sediment surface. The motors for driving stirrer disk and pump are new developments as well. They are enclosed in titanium housings, transferring their force by means of magnetic couplings and controlled by PWM (pulse width modulation) with feedback pulses. A high reliability in operating mode is thus obtained. The external current in the benthic boundary layer was measured by Savonius rotors (Figure 5.7.1).



Fig. 5.7.1: Savonius rotor

For each chamber a Savonius rotor is attached to the Lander. It records the horizontal flow speed 1m above the seafloor and transfers this information to the electronic control unit based on a Tattletale 8v2 which regulates disk and pump motors. In the operating mode “flow replication”, the friction velocity u^* at the bottom interface of the chamber is matched to the externally measured current.

It is alternatively possible to select preset shear stresses in the chamber or to interrupt the bottom stress replication of the external current for a selected time. To ensure adequate mixing of the fluid inside the chamber, a minimum value of 9 RPM was selected in the chambers. To avoid artefacts on the recovered sediment during ascent and deck operations, the maximum number of revolutions was set to 36 RPM which is equivalent to a mean spatial friction velocity of 0.55 cm/s (15 cm/s horizontal current at 100 cm). One of the design criteria of the benthic chamber was to provide adequate mixing of the water column for complete homogenisation. At the minimum of 9 RPM a mixing time of approx. 300 seconds and at 36 RPM a mixing time of approx. 90 seconds were found to provide this feature (Tengberg et al., to be submitted). This parameter is needed to adequately link the chamber with the gas exchange system.

Results and conclusions

At all six BIGO stations (refer to station list) the operating mode “flow replication” was used. Fig. 5.7.2 shows a typical example of how the inner flow characteristics adjusted in the chamber (BIGO 1 gas exchange system) with a tidally driven external current. The minimum mixing limit of 9 RPM of the disk is well maintained. The link between RPM and u^* is demonstrated in figure 5.7.3. This relationship is determined in the laboratory and refers to a distance of the lower edge of disk to the sediment of 10 cm. In the case of different distances between sediment and disk during deployment, a recalibration with the known penetration

depth will be necessary. Fig. 5.7.4 represents the flow measurements of both Savonius rotors of the BIGO 1. The rotors were located in approx. 150° angular distance around the Lander. It shows that depending upon direction of flow the current meters experience different current speeds since the Lander represents a current obstacle and the current flow is affected by a blocking effect. The bottom stress may be the second relevant parameter (next to the oxygen supply) which essentially contributes to the respiration rates of bacterial mats thru its control of the diffusive sublayer. Jørgensen & Des Marais (1990) reported respiration results where diffusive boundary-layer thickness affected oxygen consumption rates of bacterial mats. At SO165-1, respiration rates near this limit were found inside the exchange chamber (Sommer, section 5.6.) for the given oxygen concentration and flow conditions. These initial results suggest that controlled homogeneous bottom stresses at the bottom of the chamber together with its short mixing times are important conditions for reliable measurements in benthic laboratories.

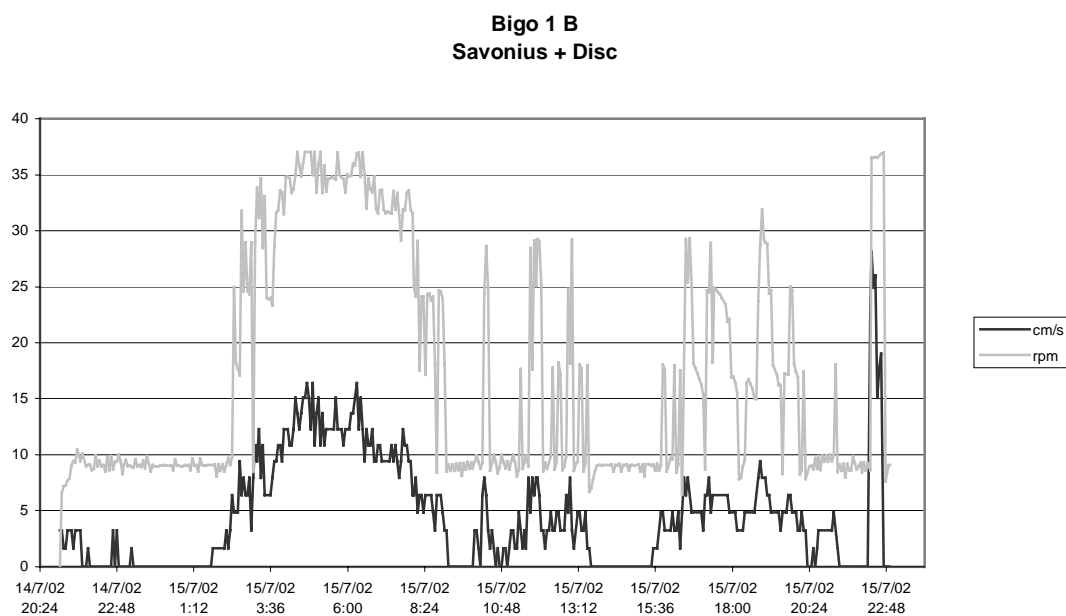


Fig. 5.7.2: External current and RPM of the disk at BIGO 1 gas exchange chamber.

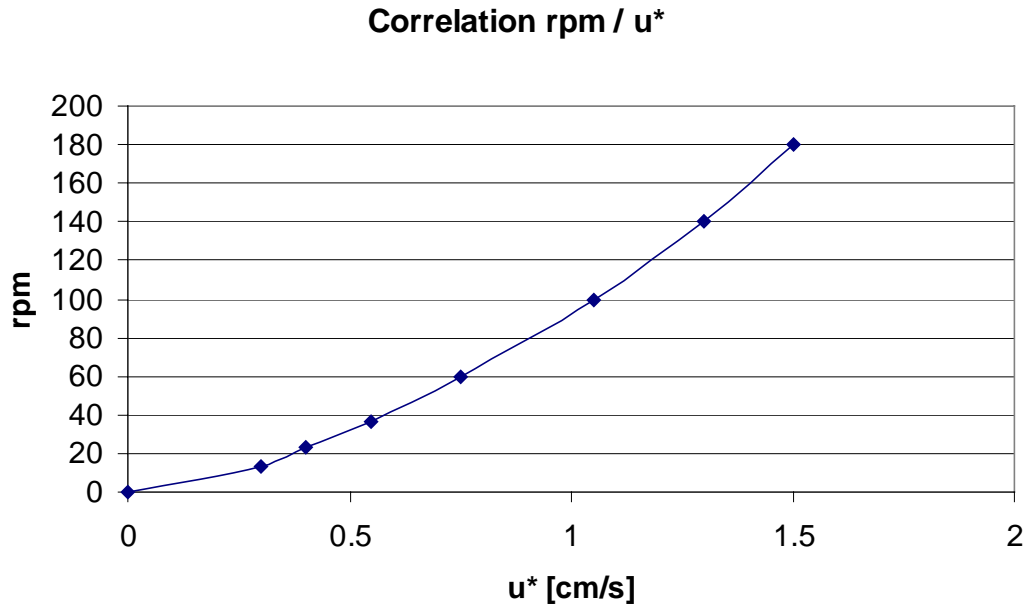


Fig. 5.7.3: Correlation between RPM and u^* with 10 cm distance between the lower edge of disk and sediment surface.

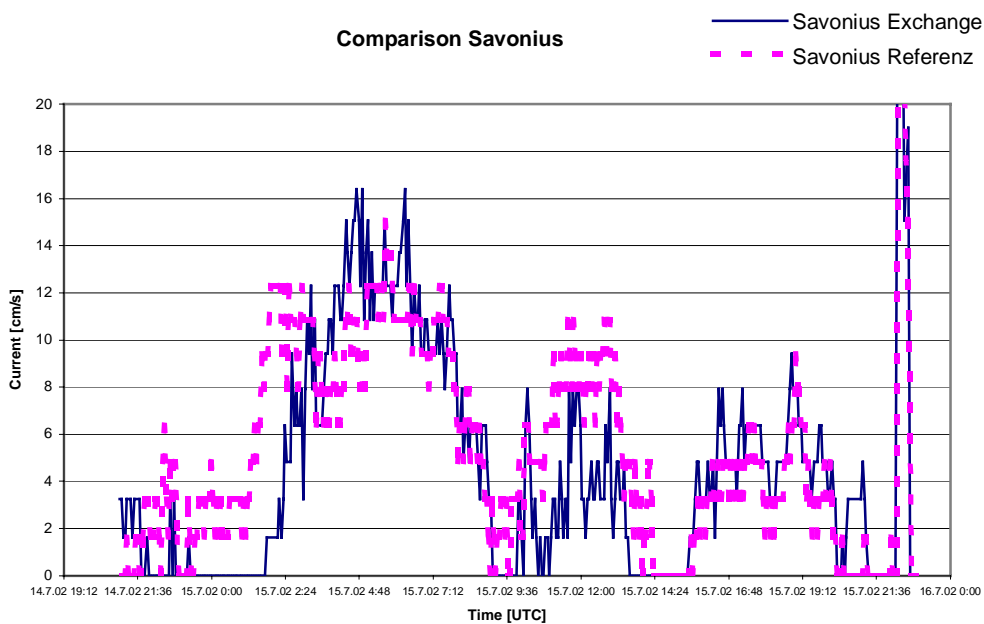


Fig. 5.7.4: Comparison of both Savonius rotors during the BIGO 1 deployment.

Acknowledgements

Thanks go to Mariscope Meerestechnik (Kiel) and Boris Holscher (TUHH) for their assistance in the development of new pumps and motors for depths up to 6000m.

5.8 Sediment Geochemistry

M. Drews, S. Kriwanek, A. Lunau, and M. Treitschke

Introduction

Objective of the geochemistry pore water program was the geochemical characterisation of near surface gas hydrate bearing sediments. Sampling stations were mostly chosen from gas hydrate sites at the Hydrate Ridge and from the Eastern Basin.

Of particular interest during Leg 1 was the combination of pore water geochemistry with the inspection of gas hydrate occurrence and fluid expulsion at venting sites. Sediment samples for geochemical and microbiological analyses were taken from the chambers of the BIGO-Lander and the multicorer. Primary aim of Leg 2 was the pore water geochemistry of long cores taken with the gravity corer to investigate gas hydrate bearing sediments in further depth. This leg's focus was more on the investigation of gas hydrate sediments at the Eastern Basin.

Samples and analytical methods

Sediment analyses were performed on samples taken with an array of different devices, all of which were supplemented with guiding video-equipment except the gravity corer. The devices were the multicorer (TV-MUC), the ocean floor conditions simulating benthic lander BIGO, a sediment grab (TVG), and a gravity corer; undisturbed surface sediment samples could be provided with the multiple corer and the BIGO-lander. The gravity corer was in most cases equipped with a tubular plastic film by which the sediment core could be pulled out in less than 3 minutes after the device was on board. After slicing the tube, the core lay ready for subsampling. Truncated syringes were used for sampling every 5 to 20 cm whereafter they were brought immediately into the cold room for further preparation. The rapid sampling provided opportunity to collect gas hydrate pieces before sediment samples were taken for pore water analyses.

Pore water was squeezed from the sediment in the cold room through 0,2 µm cellulose acetate membrane filters at 4°C and at up to 3 bar pressure using argon gas with a mechanical polypropylen press. Sediment from the multicorer or BIGO push cores was cut into slices of 1–3 cm thickness.

The types of analyses performed on the pore water are listed in Table 2.1. Identical methods have been applied to pore water from former cruises to Hydrate Ridge (Bohrmann et al, 1999, Linke & Suess, 2001) and the Black Sea (Pätzold et al, 2002).

During slicing the sediment pH values were measured; to avoid artifacts from outgassing of H₂S during long time storage. Alkalinity and H₂S concentrations were determined almost immediately after the pore water samples had been collected.

Table 5.8.2.1. Techniques used on board for pore water analysis of freshly gained samples.

Constituent	Method	Reference
pH value	2-point titration	Dickson (1993)
Hydrogen sulphide	Spectrophotometry	Grasshoff <i>et al.</i> (1983)
Alkalinity	Titration	Ivanenkov and Layakhin (1978)
Ammonium	Spectrophotometry	Grasshoff <i>et al.</i> (1983)
Nitrate	Cadmium Reduction Column, Spectrophotometry	Grasshoff <i>et al.</i> (1983)
Silicate	Spectrophotometry	Grasshoff <i>et al.</i> (1983)
Phosphate	Spectrophotometry	Grasshoff <i>et al.</i> (1983)
Chloride	Mohr (AgNO ₃)-Titration	Gieskes <i>et al.</i> (1991)

Spectrophotometric methods

The analytical techniques used on board to determine the various dissolved components are listed in Table 2. Modifications of pore water analyses were necessary for samples with high sulphide contents (above 1 mM). In order to remove H₂S from such samples, the pore water was acidified with suprapure 30 % HCl (10 µl/ 1 ml sample) and left uncapped for 24 to 48 hours in the cold room (4°C). The degassed samples were used to measure silicate, nitrate, and phosphate concentrations applying the standard photometric procedures after Grasshoff *et al.*, (1983). Silicate was determined after the elimination of sulphides by applying the standard manual molybdenum blue method (Grasshoff *et al.*, 1983). Standard photometric methods (Grasshoff *et al.*, 1983) were also used to measure ammonium and phosphate concentrations. For nitrate determination, the pore water was diluted with ammonium chloride buffer and passed through a cadmium reductor column. As the copperized cadmium granules of the reductor decomposed by dissolving sulfide, only sulfide-free samples and acidified samples were analysed for dissolved nitrate; the nitrate data are the sum of nitrate and nitrite concentration.

Titration of chloride

When measuring chloride by titration with silver nitrate, samples with H₂S concentrations of more than 1 mM must be pretreated to avoid corruption by the precipitation of Ag₂S. The pore water samples were diluted 1:2 with 0.1 N suprapure HNO₃ and degassed overnight in the cold room in open vials to remove the H₂S.

Total alkalinity (TA) and pH value

Total alkalinity measurements were performed by direct titration of 1 ml pore water with 0.01 N HCl in an open cell (Ivanenkov and Lyakhin, 1978). The acid was standardised with a IAPSO seawater solution.

A standard pH electrode was used for the determination of pH in the sediment subsamples at 4°C. The electrode was calibrated with a buffer prepared in artificial seawater (Dickson, 1993). For calibration, BIS and 2-Aminopyridine were used as buffers in the neutral pH range (pH 7 to 9).

Analyses in the home laboratory

Acidified subsamples of the pore water (10 µl HCl (30 %) / 1 ml sample) were prepared for ICP analysis (atomic emission spectroscopy with inductively coupled

plasma) of major cations (Na, K, Mg, Li, Ca, Sr and Mn). Concentrations of sulfate, bromide, DIC, delta¹³C, delta¹⁸O and deltaD will be determined on selected subsamples in the home laboratory. The remaining squeezed sediment will be used for C/N/S analysis with a Carlo Erba Element Analyser. Separate aliquots of fresh sediment will be analysed for water content and dry weight.

A synopsis of pore water samples, water samples and geochemical analyses performed on board the ship is shown in Table 2.2 and 2.3.

Table 5.8.2.2. Number of samples taken from cores and type of analyses performed on board the ship during SO165 Leg 1.

Sample	pH sedim.	H ₂ S	TA	NH ₄	NO ₃	PO ₄	SiO ₂	Cl	analysed depth [cm]	No. of samples
BIGO-1-control	X	X	X	X	X	X	X	X	12	10*
BIGO-1-exchange	X	X	X	X	X	X	X	X	10	9*
TV-MUC-7	X	X	X	X	X	X	X	X	5	6
TV-MUC-9	X	X	X	X	X	X	X	X	26	15
TV-MUC-12	X	X	X	X	X	X	X	X	20	10
BIGO-2-control	X	X	X	X	X	X	-	X	7.5	6
BIGO-2-exchange	X	X	X	X	X	X	-	X	5.5	5
TVG-1	X	X	X	X	-	X	-	X	12.5	6
TV-MUC-13	X	X	X	X	X	X	X	X	19	14
TV-MUC-17	X	X	X	X	X	X	X	X	23	15
BIGO-3-control	X	X	X	X	X	X	X	X	19	14
BIGO-3-exchange	X	X	X	X	X	X	X	X	16.5	12
BIGO-4-control	X	X	X	X	X	-	-	X	9	8
BIGO-4-exchange	X	X	X	X	X	-	-	X	12.5	8
TV-MUC-25	X	X	X	X	X	X	X	X	22	15
BCL-1-chamber-1	X	X	X	X	X	X	X	X	13.5	9
BCL-1-chamber-2	X	X	X	X	X	X	X	X	11	8
TV-MUC-26	X	X	X	X	X	X	X	X	22	15
BIGO-5-control	X	X	X	X	X	X	X	X	13.5	9
BIGO-5-exchange	X	X	X	X	X	X	X	X	9	6
TV-MUC-30	X	X	X	X	X	X	X	X	25.5	16
TV-MUC-33	X	X	X	X	X	X	X	X	26	10
BIGO-6-control	X	X	X	X	X	X	X	X	17.5	11
									total no. of samples	237

The numbers for TV MUC and BIGO-Lander samples include bottom water samples except for the numbers marked with an “*”. sedim. = sediment; BIGO-exchange means samples taken from the one BIGO-chamber which was supplied with oxygen by the “gill system”; BIGO-control means samples taken from the control chamber which was not provided with oxygen.

Table 5.8.2.3. Number of samples taken from cores and analyses performed on board the ship during SO165 Leg 2.

Sample (station no.)	pH sedim.	H ₂ S	TA	NH ₄	NO ₃	PO ₄	SiO ₂	Cl	analysed depth [cm]	No. of samples
TV-MUC-38	X	X	X	X	X	X	X	X	23	15
SL-2 (st.160-2)	X	X	X	X	X	X	X	X	116	7
SL-3 (st.160-3)	X	X	X	X	X	X	X	X	111	8
KL/SL-1 (st.167-1)	X	X	X	X	X	X	X	X	107	10
TV-MUC-43	X	X	X	X	X	X	X	X	32	20
KL/SL-5 (st.176-3)	X	X	X	X	X	X	X	X	152	14
SL-5 (st. 184-1)	X	X	X	X	X	X	X	X	189	15
TV-MUC-47	X	X	X	X	X	X	X	X	245	16
SL-10 (st. 202)	-	X	X	X	X	X	X	X	320	10
SL-13 (st. 209-2)	-	X	X	X	X	X	X	X	53	6
SL-14 (st. 210-1)	-	X	X	X	X	X	X	X	279	13
SL-15 (st. 215)	-	X	X	X	X	X	X	X	269	9
SL-16 (st. 216)	-	X	X	X	X	X	X	X	340	10
SL-18 (st 228-1)	-	X	X	X	X	X	X	X	100	11
SL-19 (st. 228-2)	-	X	X	X	X	X	X	X	86	10
									total no. of samples	174

The numbers for TV-MUC samples include bottom water samples.

Preliminary Results and Discussion

Altogether 12 TV-guided multicores, one TV grab, 12 gravity corers, one Benthic Chamber Lander and 9 BIGO-Lander sediment samples were retrieved from the Southern Summit of Hydrate Ridge and the Eastern Basin. From these the pore water was analysed for its constituents. A summary of the cores with amounts of samples and geochemical analyses performed on board is given in Table 2 for leg 1 and in Table 2 for leg 2. Selected depth profiles of chemical constituents in pore waters are shown in Figures 1 to 3 and discussed here.

A characterisation of the cores is given in Table 3.1 (leg 1) and 3.2 (leg 2). The attribution of the cores to a certain community type as described by Sahling *et al.* (2002) (*Beggiatoa*, *Calyptogena* or *Acharax* community) is often impossible due to transitional stages.

Table 5.8.3.1: Surface description and sulfide concentration maxima of all cores taken during SO165-1. SH: Southern Hydrate Ridge; NHR: Northern Hydrate Ridge; EB: Eastern Basin

Sample	Region; water depth	Sediment surface characterisation	Maximum sulfide concentration in appropriate depth
BIGO-1-control	SH; 832 m	Amphipods and polychaetes on surface, bioturbated sediment	4,7 mM in 11.5 cm
BIGO-1-exchange	SH; 832 m	Few <i>Calyptogena</i>	0.05 mM in 9.3 cm
TV-MUC-7	EB; 878 m	<i>Calyptogena</i> , small snails, carbonate pieces on the surface	1.5 mM in 4.5 cm
TV-MUC-9	EB, 880 m	<i>Calyptogena</i> , small snails, carbonate pieces on the surface and inside the sediment	5.7 mM in 24.5 cm
TV-MUC-12	EB; 885 m	Small snails, small carbonate pieces inside the sediment	6.4 mM in 12.5 cm
BIGO-2-control	NHR; 605 m	Dense <i>Calyptogena</i> colony (mussel field)	0.53 mM in 6.5 cm
BIGO-2-exchange	NHR; 605 m	Dense <i>Calyptogena</i> colony (mussel field)	0.82 mM in 4.8 cm
TVG-1	SH; 776 m	Surface disturbed, few distributed gashydrate pieces	3,3 mM in 7 cm
TV-MUC-13	SH; 776 m	Living <i>Calyptogena</i>, few <i>Beggiatoa</i>	14.2 mM in 8.5 and 17.5 cm
TV-MUC-17	SH; 778 m	<i>Beggiatoa</i> , small snails, <i>Calyptogena</i>, carbonate on the surface, partly overgrown with <i>Beggiatoa</i>	12.1 mM in 8.5 cm
BIGO-3-control	EB; 883 m	Few <i>Beggiatoa</i>, small snails, polychaets and worm tubes on the surface, carbonate pieces inside the sediment	12.4 mM in 13.5 cm
BIGO-3-exchange	EB; 883 m	<i>Beggiatoa</i> , small snails, polychaetes and worm tubes on the surface; carbonate pieces inside the sediment	17.8 mM in 15.3 cm
BIGO-4-control	SH; 778 m	<i>Beggiatoa</i> mat, carbonate pieces on the surface and inside the sediment	15.5 mM in 8.5 cm
BIGO-4-exchange	SH; 778 m	<i>Beggiatoa</i> mat, small snails, carbonate crust on the surface and inside the sediment	15.6 mM in 11.5 cm
TV-MUC-25	SH; 776 m	Carbonate pieces on the surface and inside the sediment, worm tubes on the surface	17.1 mM in 20.5 cm
BCL-1-chamber-1	SH; 779 m	Carbonate crust on the surface and inside the sediment, small snails, few <i>Beggiatoa</i>, <i>Calyptogena</i> shells on the surface	16.3 mM in 10 cm
BCL-1-chamber-2	SH; 779 m	Carbonate crust on the surface and inside the sediment, <i>Beggiatoa</i>, worm tubes and <i>Calyptogena</i> shells on the surface	17.2 mM in 3.8 cm
TV-MUC-26	SH; 776 m	Living <i>Calyptogena</i>, small carbonate pieces on the surface, worm tubes, few <i>Beggiatoa</i> filaments on the surface	11.1 mM in 17.5 cm
BIGO-5-control	SH; 777 m	Living <i>Calyptogena</i> (mussel field), few <i>Acharax</i>, small carbonate pieces below 4.5 cm	12.4 mM in 12.3 cm
BIGO-5-exchange	SH; 777 m	Living <i>Calyptogena</i> (mussel field)	6.6 mM in 6.8 cm
TV-MUC-30	SH; 776 m	Reference station, worm tubes on the surface	0.11 mM in 21.8 cm
TV-MUC-33	SH; 778 m	Reference station (position of BCL2)	0.6 mM in 24.5 cm
BIGO-6-control	SH; 782 m	<i>Beggiatoa</i> mat, carbonate pieces	11.8 mM in 16.0 cm

Table 5.8.3.2: Surface description and sulfide concentration maxima of all cores taken during SO165-2. SH: Southern Hydrate Ridge; EB: Eastern Basin

Sample	Region; water depth	Sediment characterisation	Maximum sulfide concentration in appropriate depth
TV-MUC-38	SH; 779 m	Gas hydrates below 12 cm depth, carbonate crust on sediment surface	13.6 mM in 6.3 cm
SL-2	SH; 776 m	Reference, carbonate pieces in surface layer, clay	3.3 mM in 115 cm
SL--3	SH; 776 m	Reference, carbonate pieces in surface layer, clay; mussel shell debris in layers	11.3 mM in 110 cm
KL/SL-1	SH, 775 m	Gas hydrate layer below 49 cm depth	14.1 mM in 63 cm
TV-MUC-43	SH; 776 m	Gas hydrate layer below ca. 24 cm depth, <i>Beggiatoa</i> mat on surface	12.3 mM in 18 cm
KL/SL-5	SH; 776 m	Gas hydrate layer in 112 to 114 cm depth	11.1 mM in 142 cm
SL-5	EB; 880 m	Gas hydrate layer in 183 to 189 cm depth, mussel shell debris 133 to 135 cm depth, carbonate pieces in different layers	12.2 mM in 229 cm
TV-MUC-47	SH; 780 m	Carbonate pieces up to 7,5 cm, carbonate crusts in 7.5 to 8.5 cm depth	0,009 mM in 5.8 cm
SL-10	Northern slope SH; 782 m	Reference, deep sea clay	1.5 mM in 20 cm
SL-13	EB; 874 m	Reference, carbonate in 40 to 60 cm depth	2.2 mM in 51.5 cm
SL-14	EB; 879 m	Gas hydrate layer in 138 to 163 cm depth, carbonate pieces below 160 cm depth	6.4 mM in 185 cm
SL-15	Eastern slope SH; 816 m	Reference, deep sea clay	0.003 mM in 266 cm
SL-16	Between SH and EB; 1218 m	Reference, deep sea clay	4.4 mM in 335.5 cm
SL-18	SH; 776 m	Gas hydrate layer in 59 to 67 cm depth	9.2 mM in 95.5 cm
SL-19	SH; 775 m	Finely dispersed gas hydrates from 65 to 80 cm, massive gas hydrate layer in 68 to 72 cm depth	15.1 mM in 66.5 cm

Southern Summit

The sulfide gradient is known to play a prominent role in the colonisation of gas hydrate and off vent sites. Detailed studies on macrofauna and bacterial mat colonisation were carried out in 1999 during the TECFLUX cruises to the Hydrate Ridge (Sahling *et al.*, 2002). There highest sulfide fluxes were found at *Beggiatoa* sites ($23 \pm 13 \text{ mol m}^{-2} \text{ yr}^{-1}$), lower fluxes at *Calyptogena* sites ($6.6 \pm 2.4 \text{ mol m}^{-2} \text{ yr}^{-1}$) and lowest at *Acharax* dominated stations ($0.05 \pm 0.05 \text{ mol m}^{-2} \text{ yr}^{-1}$). Our new studies focussed on *Beggiatoa* sites because these white to orange bacterial mats are believed to be an indication of gas hydrates below the surface. Gas hydrates cropping out from the seafloor were not seen during the video surveys, however. The depth where the hydrate began to occur seems to have often been below what our sampling devices (multicorer and lander chambers) could reach. On the other hand, where gas hydrate was found at shallower depth, it could, due to its stiffness, not be penetrated by the sampling gear.

Pieces of **gas hydrate** were found in cores from stations TV-MUC-17, TVG-1, MUC-38, KL/SL-5, SL-18, and SL-19. The sediment showed heavy degassing of methane, which appeared as ascending bubbles, evidencing the original high content of gas hydrate which partly dissolved before the samples could be taken on board.

Chloride concentrations lower than normal bottom water concentrations—a negative chloride anomaly—were observed in the core from station TV-MUC-17 below 7.5 cm sediment depth (Figure 2). At the core's bottom the chloride concentration dropped down to 441 mM (background sea water concentration: 556 mM) as a consequence of dissolution of gas hydrate and the release of diluting fresh water into the sediment. Likely, a deeper intrusion of the gear was inhibited by a massive gas hydrate layer below the core bottom at 22 cm depth. The gas hydrates in the sediment of station TVG-1 seemed mostly to be dispersed and already dissolved when the grab was opened on board. Therefore the measured chloride concentration did not change significantly with depth.

Alkalinity profiles of all analysed sediment cores more or less followed the sulfide concentration profiles. Highest alkalinity values were found at the sulfidic stations BIGO-3 (oxygen exchange chamber) and BIGO-4 (control chamber), at both of which the sediment surface was covered with a *Beggiatoa* mat and exhibited **carbonate** precipitates within the sediment (BIGO-3-exchange chamber) or on the surface (BIGO-4-control chamber). Hydrogen carbonate concentrations and therefore the total alkalinity increased with sediment depth as a consequence of anaerobic methane oxidation ($\text{CH}_4 + \text{SO}_4^{2-} \rightarrow \text{HCO}_3^- + \text{HS}^- + \text{H}_2\text{O}$). Bicarbonate released during anaerobic methane oxidation increases alkalinity and supports the precipitation of authigenic carbonates ($\text{Ca}^{2+} + 2\text{HCO}_3^- \rightarrow \text{CaCO}_3(\text{s}) + \text{CO}_2 + \text{H}_2\text{O}$).

At gas hydrate site TV-MUC-17 the **ammonium concentration** was highest at the surface (56 μM). This substantiates the hypothesis of increased organic carbon degradation at the surface; low ammonium values in further depth and low ammonium/alkalinity and ammonium/sulfide ratios pointed to anaerobic methane oxidation which produces sulfide and alkalinity without generating ammonium and phosphate or other organic matter degradation products. Figure 3.1 shows the depth profile of alkalinity drawn against ammonium at station TV-MUC-17 and reference station TV-MUC-33.

Probably due to the high storing capacity for nitrate inside the vacuoles of *Beggiatoa* cells (up to 160 mM, McHatton *et al.*, 1996), the **nitrate concentration** is highest in the surface sediment layers up to 3 cm depth. At *Beggiatoa* sites the nitrate concentration reached high values at the sediment surface (23 μM at TV-MUC-13, 48 μM at TV-MUC-17, 170 μM in the BIGO-4-control chamber).

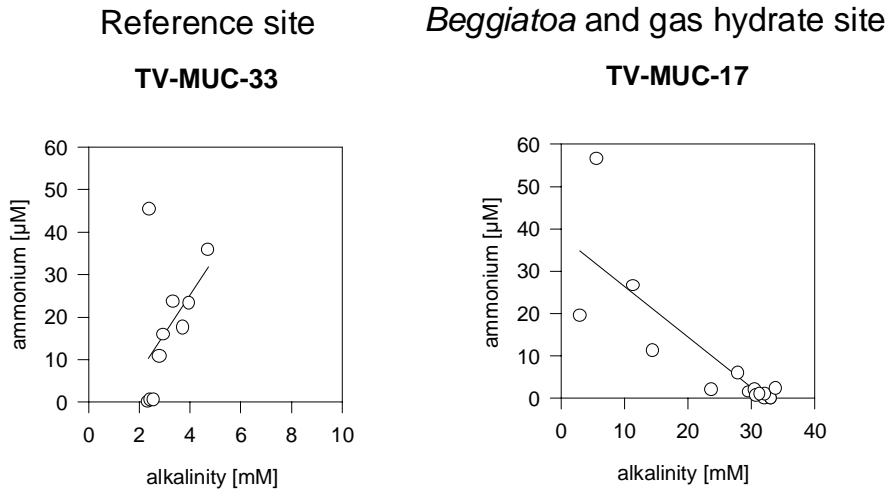


Fig. 5.8.3.1: Alkalinity drawn against ammonium at gas hydrate station TV-MUC-17 and reference station TV-MUC-33 located at the Southern Summit of Hydrate Ridge.

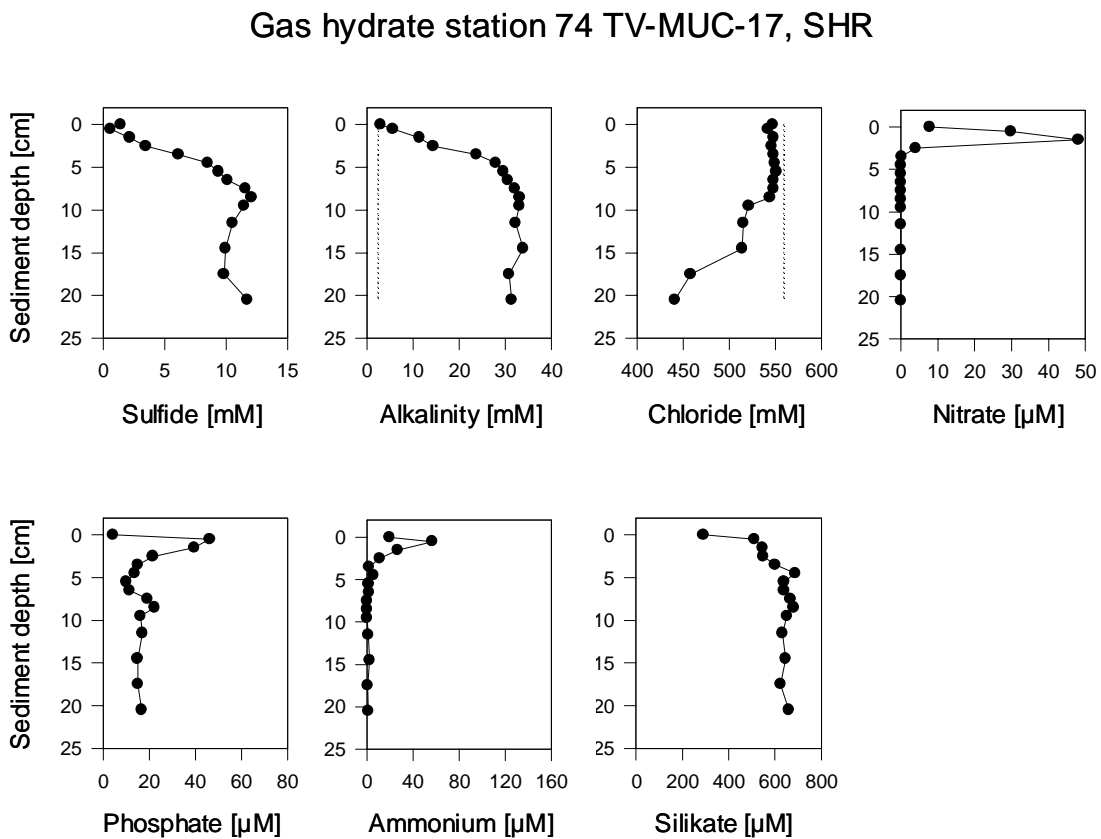


Fig. 5.8.3.2: Pore water chemistry profiles of gas hydrate site TV-MUC-17 at the Southern Summit of Hydrate Ridge.

Reference station TV-MUC-30. Even though only 68 meters apart from gas hydrate station TV-MUC-17, the core from reference site TV-MUC-30 (Figure 5.8.3.3) did not resemble cores from any gas hydrate sites at all. Worm tubes standing out from the sediment surface were found in a bioturbated sediment. Sulfide concentrations were much lower than at *Calypptogena* or *Beggiatoa* sites; chloride concentrations resembled the seawater background level from sediment surface to depth; alkalinity increased below 10 cm (maximum concentration 3 mM) as did the ammonium concentration; nitrate occurred until 15 cm depth, reaching 14 μM in 10 cm.

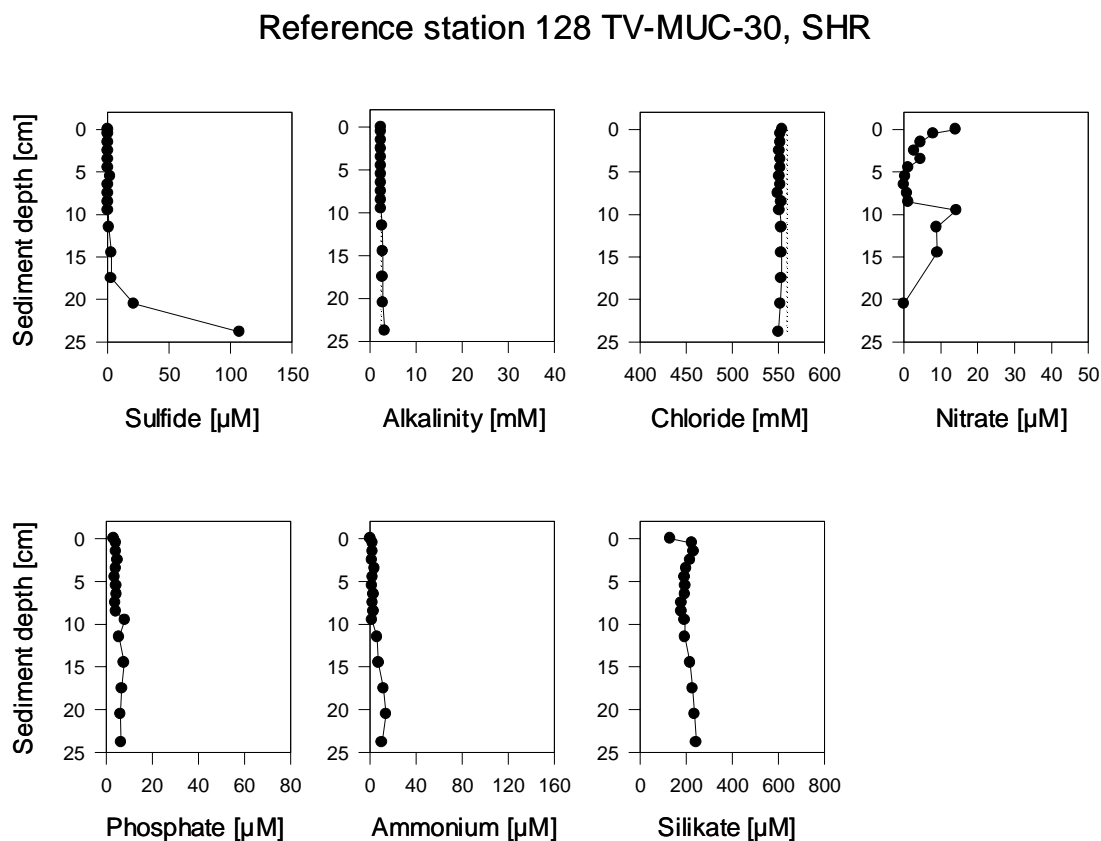


Fig. 5.8.3.3. Pore water chemistry profiles of the reference station TV-MUC-30 at the Southern Summit of Hydrate Ridge.

Eastern Basin

During the previous TECFLUX cruise SO148 in 1999 one gravity core from the Eastern Basin (76-SL-1) showed gas hydrates between 50 and 90 cm depth (Linke & Suess, 2001), but only gas hydrate samples were taken, no pore water profiles. During the current SO165 cruise we intensified the geochemistry pore water program with one BIGO, three TV-MUCs and three gravity core deployments. During the first leg we were not able to find chloride anomalies or surface near gas hydrates (BIGO-3, TV-MUC-7, -9, -12), while leg 2 of the cruise discovered gas hydrates below 1 m sediment depth (cores SL-14 and SL-5) when gravity cores were used.

Copmared to the wide areas of the Southern Summit only small scale areas at the Eastern Basin were characterised by bacterial mats (BIGO-3) and *Calypptogena* fields (TV-MUC-7, -9). Numerous specimens of small snails (Gastropoda) were

found on the sediment surface of all sites. The analysed cores showed carbonate pieces on the surface (TV-MUC-7, -12) and inside the core (TV-MUC-9, BIGO-3).

***Beggiatoa* mat station BIGO-3.** Here very high sulfide concentrations occurred in both cores from the BIGO-Lander, which were covered with a *Beggiatoa* mat. These concentrations indicated intensive sulfate reduction, driven by anaerobic methane oxidation and intense degradation of organic material. Unexpectedly, the same cores showed nitrate concentrations below the detection limit even in the bottom water. This possibly was caused by intensive denitrification and little storage of nitrate inside the cells or by a low density of the *Beggiatoa* mat anyway. The silicate concentration increased from the surface to depth up to a plateau value of 1000 to 1200 μM depending on the opal solution kinetics (e.g. the availability of dissolved aluminium) and the transport processes in the sediment. This indicated that siliceous organisms like diatoms and radiolarians are a prominent component of the biogenic input into the sediment.

At station BIGO-3 ammonium concentrations remained below 5 μM while the alkalinity reached more than 40 mM (BIGO-3-exchange chamber). Here again low ammonium/alkalinity and ammonium/sulfide ratios showed clearly that anaerobic methane oxidation is the main cause for sulfide production in this highly anoxic habitat.

The differences of the two cores from BIGO-3, which were taken only a few decimeters apart, may be explained by erosion and rearrangement of material through lateral particle transport and small scale patchiness of the sediment.

Gas hydrate station SL-5. This core from the eastern slope of the Eastern Basin was marked by one pronounced chloride depletion due to a compact but thin gas hydrate layer in 183–189 cm depth (Figure 5.8.3.4). In contrast, at site SL-14 (close to SL-5) gas hydrates were situated in a diffuse layer between 138 and 163 cm depth. Below this zone the sediment of core SL-14 was riddled with carbonate concretions with some chloride enrichment in the pore water.

Gas hydrate station 184-1 SL-5, Eastern Basin

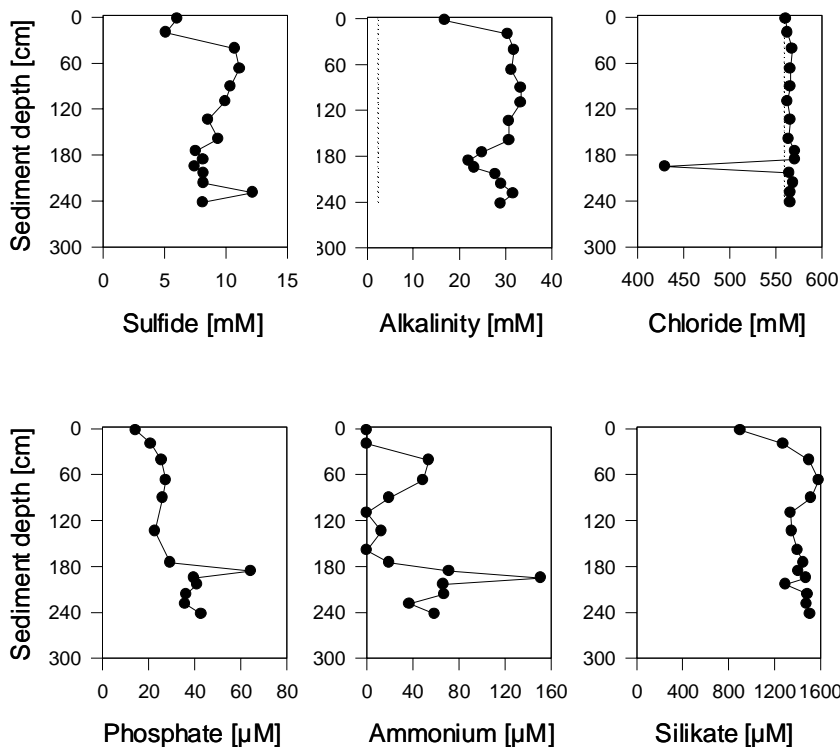


Fig. 5.8.3.4. Pore water chemistry profiles of gas hydrate site SL-5 at the eastern slope of Eastern Basin.

Northern Summit

The area near the Northern Summit was only examined at the central station BIGO-2 where the chamber Lander obtained undisturbed sediment surface, which was covered with living *Calyptogena* mussels and polychaetes. Sulphide values reached up to 800 μ M, much less than at *Beggiatoa* sites. The depth profiles of chloride showed no anomaly with mean values of about 550 mM chloride.

Microsensor measurements

Ex situ measurements of microprofiles were performed with Unisense[®] oxygen (OX 50; 50 μ m tip) and sulfide (H_2S 50; 50 μ m tip and H_2S needle electrode) microsensors. The sensors were provided by the LOTUS subproject 1.

A manual micromanipulator enabled to measure in 100 μ m steps up to 6 cm sediment depth. The core from station TV-MUC-36 showed worm tubes and living specimens of *Nuculana sp.* (Bivalvia) on the surface; a few *Beggiatoa* filaments arranged in nets and tufts were found. The oxygen penetration depth varied between 2.3 and 2.6 cm (Fig. 5.8.4.1). In contrast to the parallel shape of both oxygen profiles the sulfide profiles varied considerably (Fig. 5.8.4.2). Below 1.7 cm sulfide was detected with concentrations increasing from 110 to 304 μ M in 4 cm depth. These values are in the same order of magnitude as values found at station TV-MUC-9 where carbonate crusts and *Calyptogena* were found on the sediment surface.

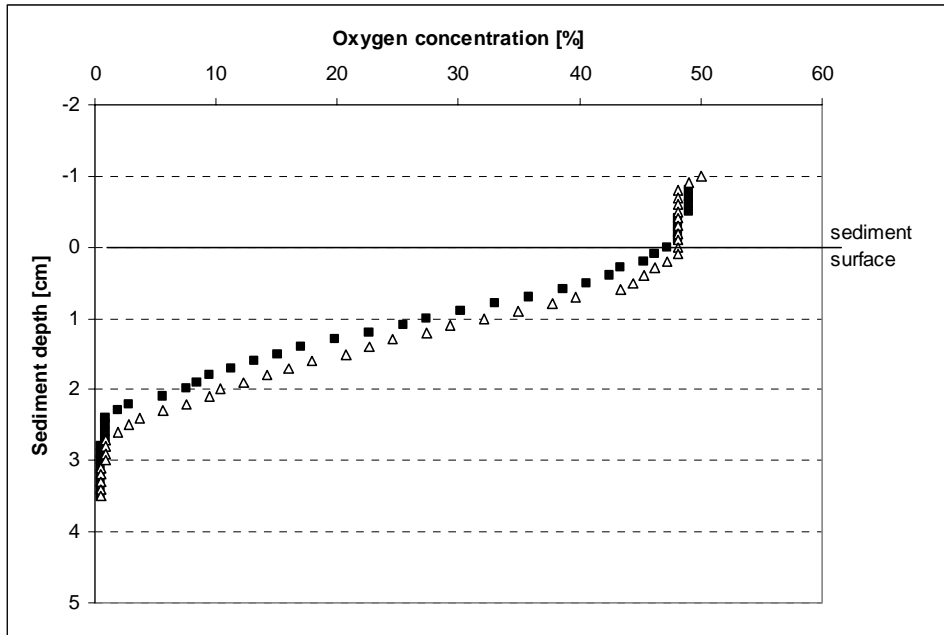


Fig. 5.8.4.1: Oxygen microprofiles in a core from station TV-MUC-36. Two profiles were taken from the core center. The oxygen microsensors were calibrated with nitrogen sparged sea water for 0 % and atmospheric air sparged sea water for 100 % oxygen concentration.

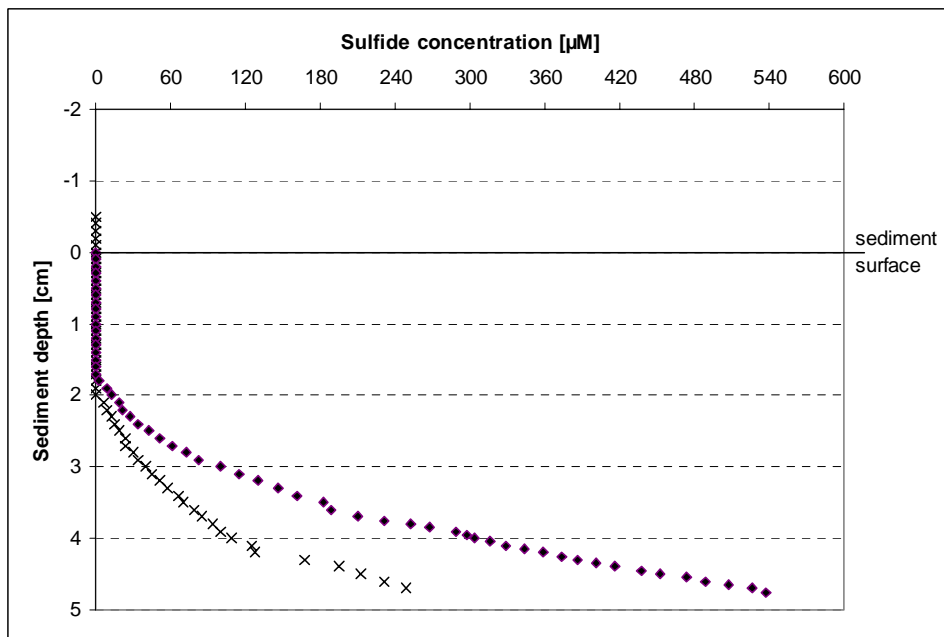


Fig. 5.8.4.2: Sulfide micro profiles in a core from station TV-MUC-36. Two profiles were taken from the core centre. The sulfide microsensors were calibrated with a NaS_2 standard dissolved in oxygen free salt water for a range of 0 to 1 mM sulfide.

5.9 Hydrate Detection and Stability Determination (HDSD)

- a Tool For In Situ Hydrate Destabilization

T. Mörz, W. Brückmann, P. Linke, M. Türk

Introduction

There are two major problems in today's hydrate research and evaluation of exploration of shallow marine deep sea hydrates:

1) Different theoretical stability models (e.g. Sloan, 1982 and Equiphase Hydrate v. 5.0) differ considerably in their PT fields when calculations are applied for a given hydrate deposit and assumed gas composition. Hence the amount of energy needed to mobilize and extract gas from gashydrate is only approximately known.

2) Even though seismic imaging (location of the BSR) and vent faunas are good indicators for shallow hydrates thin sediment covers often prevent a direct observation.

As a response to the above limitations a new device is developed within SFB 574 (Volatiles and Fluids in Subduction Zones: Climate Feedback and Trigger Mechanisms for Natural Disasters), HDSD (Hhydrate Detection and Stability Determination) will be capable of identifying and quantifying near-surface hydrate layers through local heating and continuous thermal and resistivity profiling. In its final stage, the unit will be highly flexible in its mode of operation (Lander based for long-term deployments or on a winch for short-term mapping) due to a fully modular configuration with easily exchangeable components.

Principal Tool Conception

The HDSD device is an add-on to the existing self-sustaining GEOMAR Benthic Chamber Lander. Video guided deployment and recovery is therefore based on approved technology. The prototype HDSD configuration for the SO165 deployment comprises four principal components:

The rectangular in situ experimental chamber acts as a limited thermal shielding (wall thickness 1 cm) and is inserted into the sediment by a motordrive (penetration depth ~ 30 cm).

An electric heating unit mounted on the inner part of the upper lid of the experimenting chamber that consists of Konstantan coils embedded into an isolating plastic carrier with an aluminum heat exchanger pointing toward the sediment surface. Typical power ratings are 50-100 W. The heating unit can be pre-programmed to generate a constant thermal field. Energy is provided by conventional batteries with a total capacity of up to 1800 Wh, allowing operation times of 24-36 h.

A central sensor carrier (sensor lance, 12 mm diameter) is mounted vertically from the chamber top and is equipped with two rows of miniature temperature (PT 1000) and resistivity sensors (vertical Wenner Array). The sensor arrays provide a fast and close spaced vertical control of the migrating temperature signal and the resistivity response of hydrate layers within the experimenting chamber.

A data logging and control unit is situated above the experimenting chamber and transfers time stamped sensor data to the flash memory of the GEOMAR Benthic Chamber Lander (BCL) control unit.

After deployment in its passive state, the sensor array is monitoring temperature and resistivity profiles allowing detailed insights in the inhomogeneous structural

relationship of sediment and interlacing massive hydrate layers of the uppermost 0.3 meters below the seafloor. During this stage thermal equilibration after the insertion of the chamber is documented. After the equilibration phase ambient temperature and resistivity profiles are recorded. These profiles will then be used as references to quantify the time-dependant perturbation of the temperature and resistivity profiles during subsequent heating. In its active stage, the heating unit will be initialized to generate a steep temperature gradient that allows to monitor and determine the vertical thermal conductivity in various sediment types and settings including hydrate bearing zones.

Optional gas and fluid flow meters can monitor and quantify the amount of gas and fluid released during operation.

Setup and First Results of Prototype Deployment

Even though the instrument's design and construction phase prior to SO165 has been very short (6 month) and only limited laboratory tests of the heating unit without the sensor string have been made, we took SO-165 as an opportunity to gain first *in situ* testing experience and understanding of technical deep sea requirements.

The first two weeks of the cruise were spent to finish: a microcontroller based provisional data acquisition and experiment control software, calibrate the temperature sensors and to test the electrical resistivity sensor string in fresh Hydrate Ridge sediments recovered from various TV-MUC deployments (Fig. 5.9.1). During SO165 we deployed the HSDS system twice.

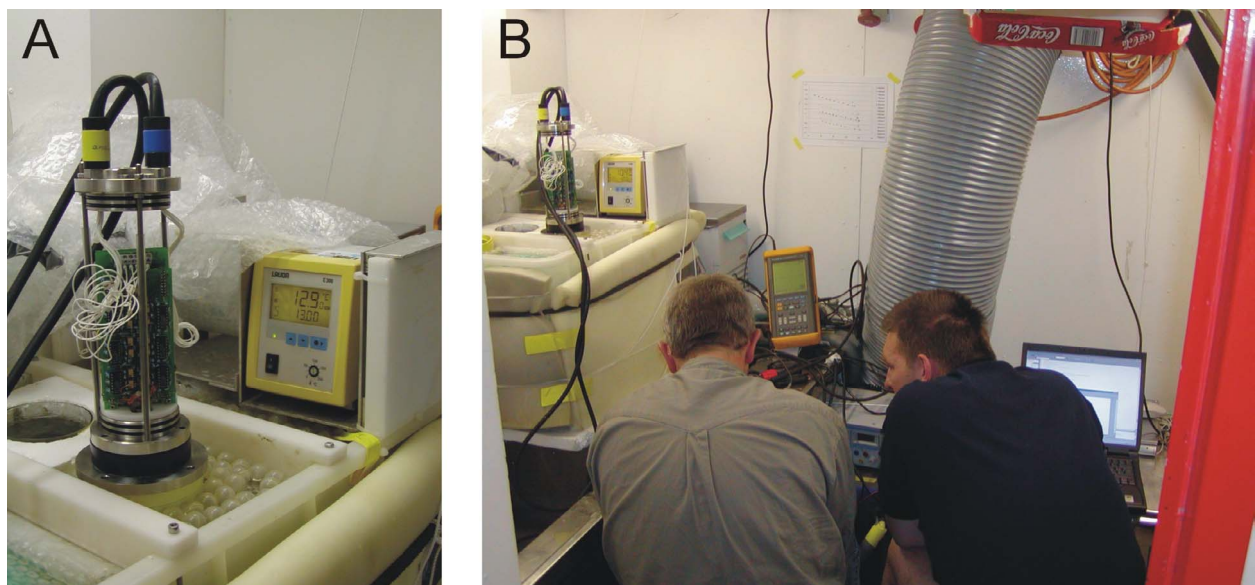


Fig. 5.9.1: The HSDS signal conditioning unit with attached sensor lance in the temperature calibration bath (A). Engineers M. Türk and M. Poser during data recording tests with the new tool (B).

The setup for the first deployment used three battery equipped benthos glass spheres with a total of 1800 Wh for heating and the motor drive of the chambers. Heating timing, motor control and data acquisition has been provided by a single microcontroller unit. In addition a thermal GEOMAR micro flow meter and a Seabird 25 CTD have been attached to the chamber outflow openings to monitor

fluid and gas outflow. The modified BCL Lander was deployed in 778 meter water depth on the Southern Summit (Station 132) on top of a bacterial mat to maximize chances of finding hydrates in the first 0.3 mbsf. Deployment duration was 46.67 h and the active heating experiment lasted 24 hours.

Upon recovery of the Lander several severe malfunctions were detected which could be grouped into accidental- and principal tool design causes. Accidental causes: Flooding of one battery sphere (Fig. 5.9.2) and a drop of saltwater in data acquisition pressure vessel. Principal tool design failures: failure of current source of the chamber motor drive, severe saltwater corrosion of heating wires in the heating unit, minor creep current leaks along the sensor lance due to moistening of glass fibers.



Fig. 5.9.2: Deformed and flooded Ni-Cd cells recovered during the first HDSD deployment.

We changed and modified several tool components for the second deployment (30.07. – 01.08., Southern Summit, water depth: 778 m, Fig. 5.9.3).

- 1) The main energy source for the heating experiment was now provided by 2 industry standard deep sea batteries (each nominal 230Ah).
- 2) The chamber drive control and energy supply were separated from the data acquisition and heating control unit.
- 3) New flexible sealing were used for the heating coil and heat exchanger. For the second deployment a location between a mussel field and a clam mat was chosen (deployment time was 42.16 h, heating time 34 h).

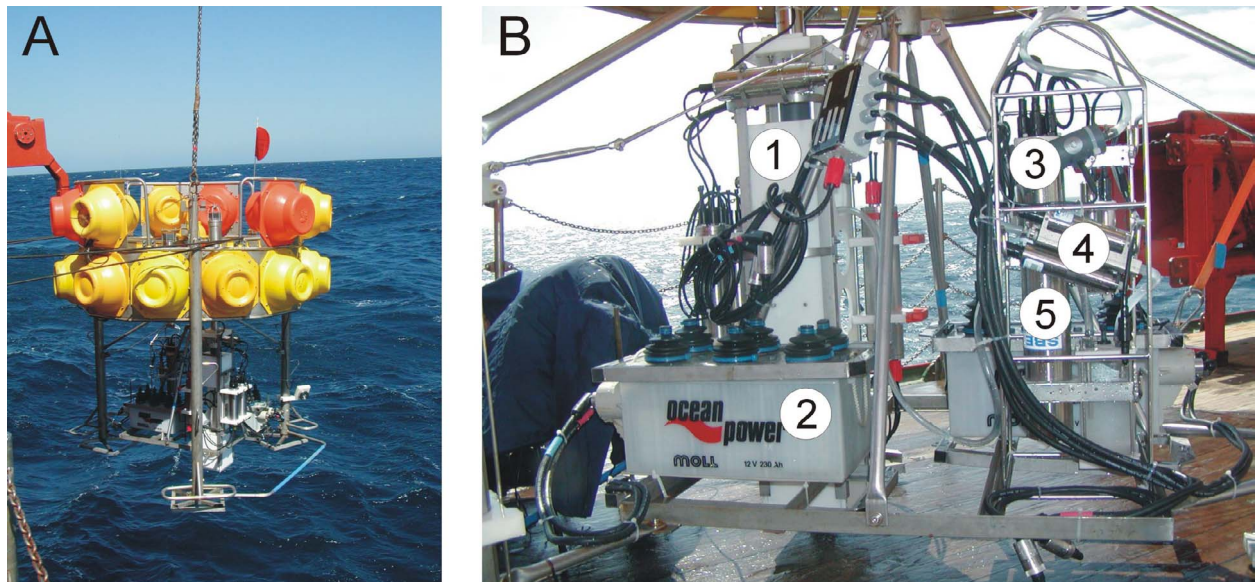


Fig. 5.9.3: The fully equipped BCL Lander with the HDSD system during the buoyancy test (no launcher unit attached, A). (B) Close-up on the HDSD components. 1) HDSD chamber with sensor lance inside. 2) Deep sea batteries. 3) GEOMAR flow sensor for outflow detection of fluids and gases. 4) Electrical resistivity sensor attached to detect salinity changes in the outflow water. 5) Seabird CTD for pressure and bottom water temperature recording.

After a smooth recovery of the Lander we found the chamber properly retracted and mud remnants between heat exchanger ribs clearly confirmed a fully penetration of the chamber and the sensors (Fig. 5.9.4). Data recovery of the HDSD unit was also successful and current and voltage sensors recorded a smooth general experimental run (Fig. 5.9.5). Four of 13 temperature sensors showed anomalies (sensor 3, 4 & 7) or failed to record any data (sensor 11, Fig. 5.9.6). The remaining eight temperature sensors showed an expected temperature increase over time and depth for sediments with a thermal conductivity of $0.6 \text{ W}/(\text{m}^2 \cdot \text{k})$. Unfortunately the electrical conductivity sensor array recorded values outside the range of the analog – digital converter.

In order to verify the data from the HDSD deployment a TV-MUC (TV-MUC 33) was deployed next to the HDSD-BCL Lander position. All recovered cores showed no signs of gas hydrate and also pore water analyses performed by M. Drews (see chapter 5.8) did not support a gas hydrate presence in the first 30 cmbsf. Even though the second HDSD deployment was partly successful no hydrates have been destabilized due to a lack of occurrence within the range of our tool.

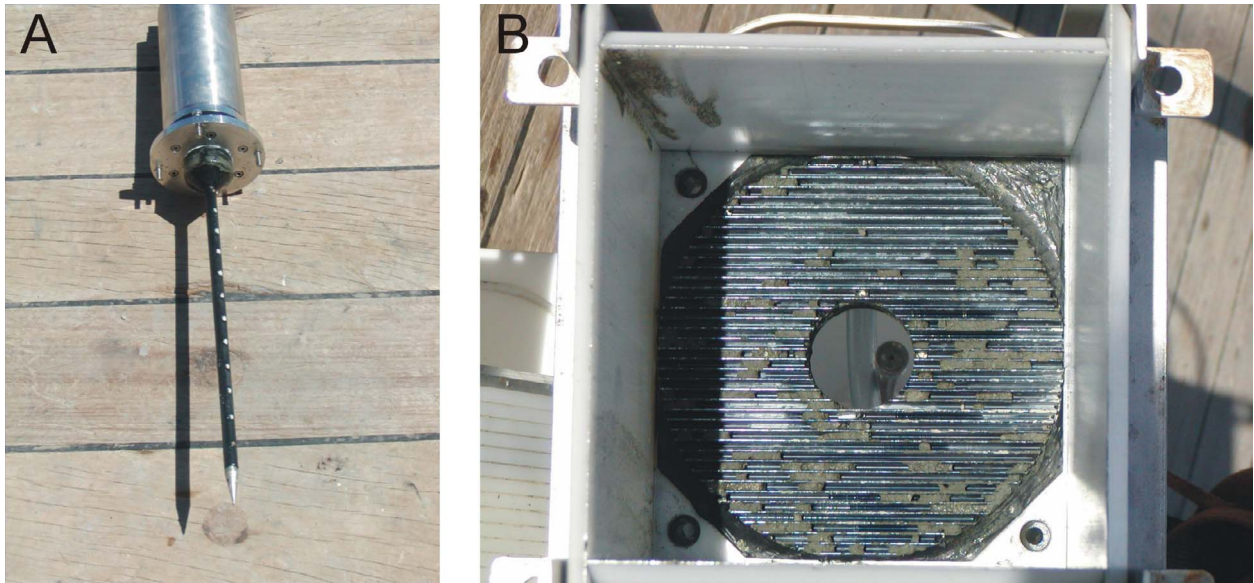


Fig. 5.9.4: Mud traces along the sensor lance (A) and between the heat exchanger lamellae (B) testify a successful chamber and lance penetration during the second HDSD deployment.

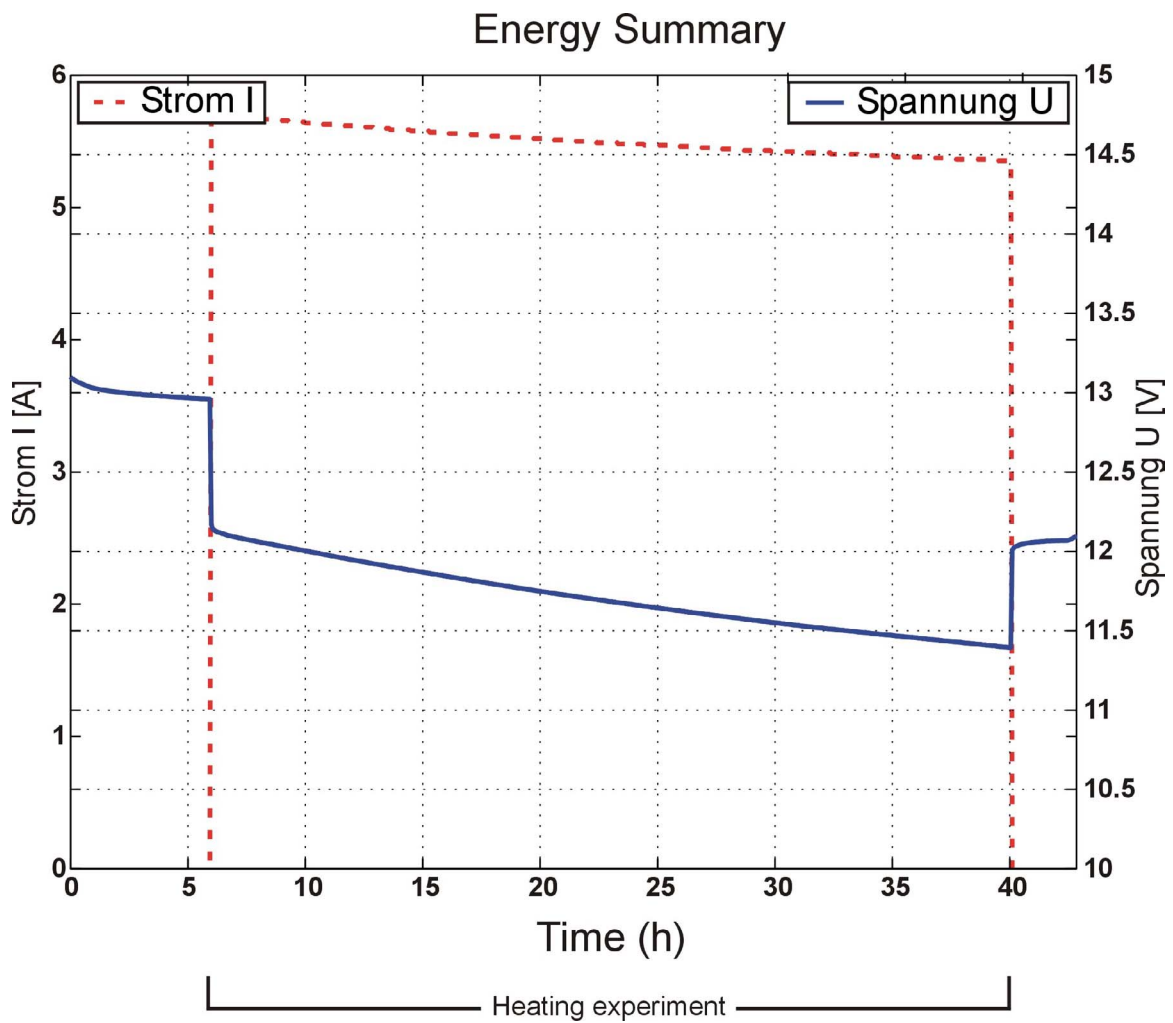


Fig. 5.9.5: Energy consumption during the second HDSD deployment. Note the sharp drops in battery voltage during active heating

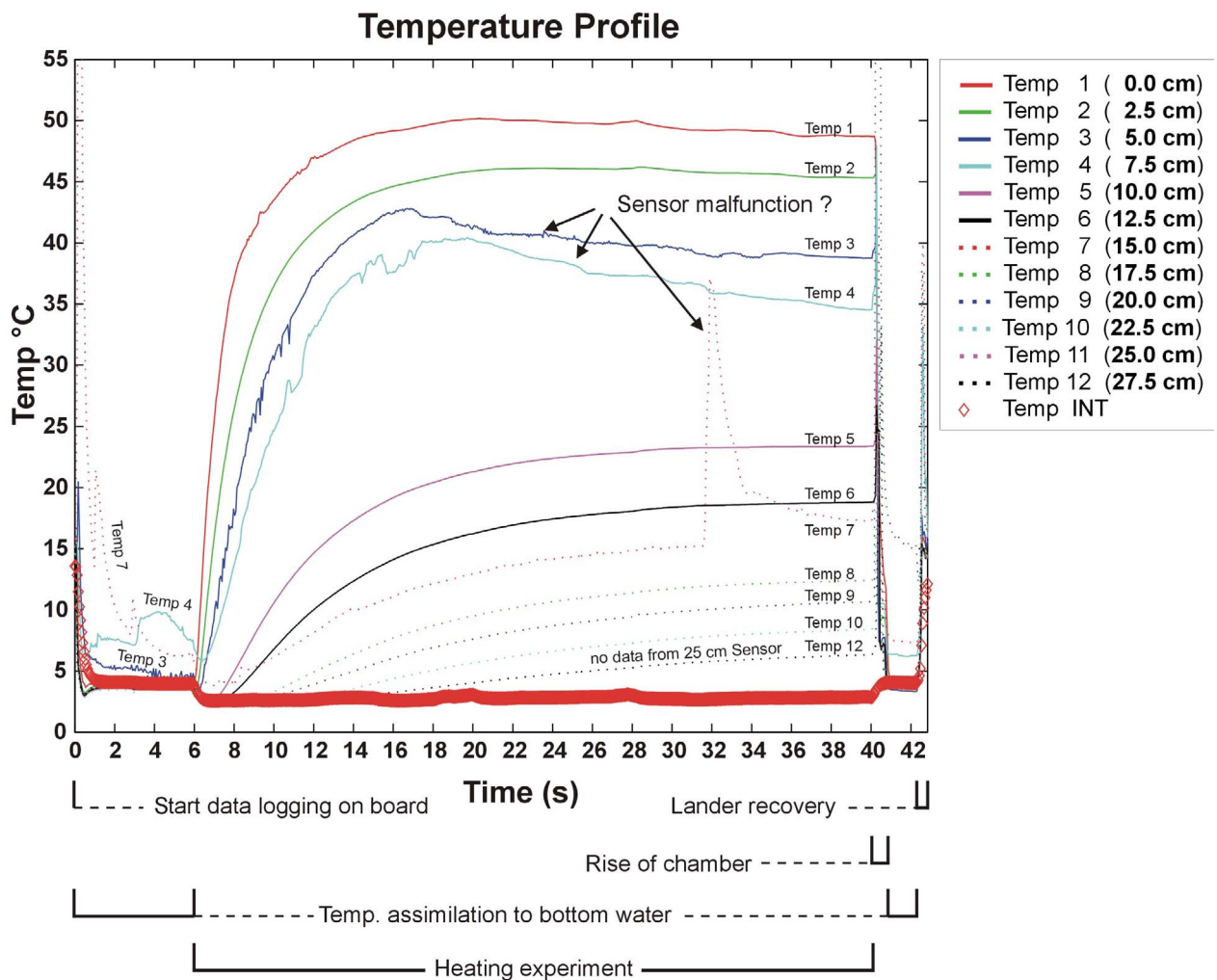


Fig. 5.9.6: Temperature profile of all sensors over time and depth. The different stages of the deployment are indicated below the diagram. Temperature versus time behavior shows no indication for the presence of hydrates.

Upcoming Developments

Further developments under the HDS concept include a new heating and sensor geometry with greater penetration depth of up to 100 cm. Three parallel lances will produce and monitor a radial heat field that is generated during successive step wise increase of the heating power. The new geometry will improve the heat transfer to greater depth and reduce experiment times by factor 10. In addition faster deployments and greater penetration depth will increase the chance of finding hydrates by conducting more deployments in the same ship-time over a larger seafloor area.

5.10 Sediment coring and physical properties

W. Brückmann, R. Luff, F. Abegg, I. Albrecht, V. Liebetrau

Introduction

Sediment coring during leg 2 concentrated on three study areas, the Southern Summit of Hydrate Ridge, the top of SE Knoll, and the basin east of Hydrate Ridge. The TV-Grab, a TV-MUC and a gravity corer were used to recover gas hydrates, sediments, and massive carbonate boulders in these working areas. Observations and results from TV-MUC deployments are discussed elsewhere (5.15), as their primary purpose was oriented towards microbiology. TV-G deployments are covered under items 5.13 (gas hydrate sampling) and 5.14 (carbonate sampling). Gravity coring served several purposes: i.e. sampling for complete sections of gas hydrate rich sediments, sampling for geochemical reference studies (sleeve liners), physical properties reference profiles, sampling for physical property studies, biogeochemical studies, and carbonate studies. An overview of coring stations is given in Tab. 5.10.1 and depicted in a map (Fig. 5.10.1). Two different types of gravity coring equipment were used, a gravity corer with a standard set of weights, and gravity corer with added surplus set of weights. For several deployments, the normal gravity corer was replaced by the head of a piston corer. The advantage is the higher weight of 3 t compared to 1.5 t of the gravity corer, which promised a deeper penetration. Because of the missing flap valve on top of the piston, no vacuum could be created inside the barrel when lifting the corer. For this reason some cores were lost and the core catcher was damaged. The largest number of cores were taken in the southern part of Hydrate Ridge over a very small area on the top of the Summit (Fig. 5.10.1), a smaller number of cores was collected in the Eastern Basin at water depths of around 1000m, primarily as background and reference stations. Different liner types and lengths were utilized depending on sediment composition and sampling requirements: standard tube liners with lengths of 3m, 5m, and 6m, pre-cut tube liners of 2m length, and sleeve liners of 3m length for reconnaissance and test coring. After description, documentation, and sampling sediment cores were returned to the sea, because decaying gas hydrate layers quickly destroyed or altered primary sediment structures and composition, making archival of cores impractical.

Preliminary Observations and Results:

Caveat regarding gravity coring of gas hydrate rich sediments

A dangerous incident occurred after the recovery of gravity core 184-2 SL-2. During the normal process of liner removal on deck, problems became apparent when removing the nails from the core cutter. After the last nail had been removed, the core cutter was abruptly shot across the deck and was only stopped when hitting another instrument after a distance of approximately fifteen meters. This "explosion" was apparently caused by overpressure which had built up inside the core barrel where a stone got stuck in the head of the corer. In this position it blocked the head and further decomposition of the gas hydrate increased the pressure inside the barrel, so that the core cutter burst off after the removal of its fixings.

After this incident, several holes were drilled into the steel barrel to avoid overpressure in case such a blockage happened again. It should be discussed whether a piston corer is a safe tool for coring of gas hydrates.

Description of recovered gas hydrate bearing sediments

Five cores showed pervasive occurrence of gas hydrates in finely laminated layers. Detailed core descriptions of these exceptionally complex sediment-hydrate successions were prepared and are presented below.

Gravity cores

Tab. 5.10.1: Sediment sample stations during SO165-2 (SL = gravity cores; KL = box cores)

Station	Date	Tool	Latitude	Longitude	Depth	Recovery	Remarks
SO165-2	###		°N	°W	(m)	(cm)	
160-1	07.08.	SL-1, 3 m tube	44:34.1670	125:08.8130	776	64	
160-2	07.08.	SL-2, 3 m tube	44:34.1471	125:08.8140	776	113	
160-3	07.08.	SL-3, 3 m tube	44:34.2110	125:08.8090	776	110	
160-4	07.08.	SL-4, 3 m liner	44:34.21	125:08.8100	776.2	60	gas hydrate released by cover floating on sea surface
167-1	08.08.	KL/SL-1, 3 m tube	44:34.2040	125:08.8120	775	115	missing flap valve at the top; defect of core catcher
167-2	08.08.	KL/SL-2, 5 m liner	44:34.2090	125:08.8120	775	20	banana, due to lack of flap valve at the top sediment was washed out and only large pieces of gas hydrate remained in the core liner
176-1	09.08.	KL/SL-3, pre-cut liner	44:34.2050	125:08.8060	776.2		coring successful, but only small amount of gas hydrate; sample not frozen
176-2	09.08.	KL/SL-4, 2 m pre-cut liner	44:34.2060	125:08.8140	776		core with gas hydrate
176-3	09.08.	KL/SL-5, 2 m pre-cut liner	44:34.204	125:08.807	776	173	core with layers of gas hydrate
184-1	10.08.	SL-5, 6 m tube	44:34.2850	124:59.9010	879.6	250	core recovered, gas hydrates
184-2	11.08.	SL-6, 6 m liner	44:34.2830	124:59.9010	878		core under pressure, exploded; gas hydrate, carbonates
194-1	12.08.	SL-7, 6 m liner	44:34.2830	124:59.9090	878.9		few carbonates
194-2	12.08.	SL-8, 6 m liner	44:34.2800	124:59.9060	877	251	
194-3	12.08.	SL-9, 6 m pre-cut liner	44:34.276	124:59.9000	878	165	gas hydrate
202	13.08.	SL-10, 6 m tube	44:34.3650	125:08.7670	782	320	
203	13.08.	SL-11	44:34.3610	129:49.9980	403	37	
209-1	14.08.	SL-12, 6 m	44:34.3600	124:59.8700	877		no core, few small pieces of carbonate (not collected)
209-2	14.08.	SL-13, 6 m tube	44:34.3580	124:59.8710	874	60	banana
210-1	14.08.	SL-14, 3 m tube	44:34.2900	124:59.8960	879	280	
215	15.08.	SL-15, 3 m tube	44:34.2660	125:08.3950	816	270	
216	15.08.	SL-16, 3 m tube	44:34.2470	125:04.3940	1218	340	
222	16.08.	SL-17, 3 m liner	44:34.2040	125:08.8050	775	120	
228-1	17.08.	SL-18, 3 m tube	44:34.2110	125:08.8140	776	100	
228-2	17.08.	SL-19, 3 m tube	44:34.2090	125:08.8060	775	100	

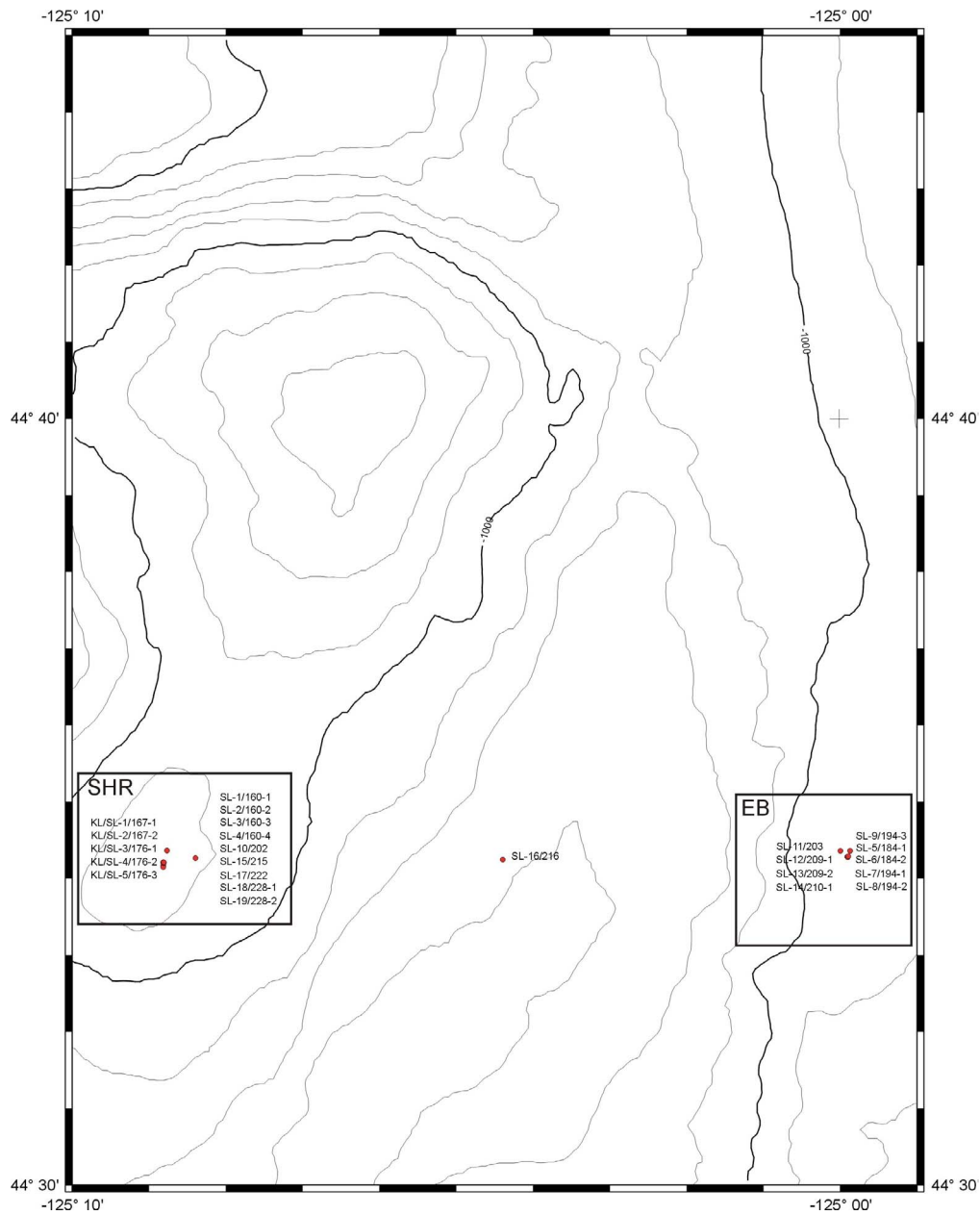


Fig. 5.10.1: Gravity corer stations during SO165-2 (SHR = Southern Hydrat Ridge; EB = Eastern Basin)

Station 176-3 (core SL5)

Gravity core SL5 recovered 173cm of intercalated olive green to gray soft and hard clays from the Southern Summit. Small gas hydrate layers were observed over two depth intervals of the core (Fig. 5.10.2, Fig.5.10.3). Temperature measurements clearly identified horizons with hydrate occurrence. Dry clays with characteristic scaly fabric occurred in shallow parts of the section. As hydrate was present only in very small amounts its exact position was difficult to detect.

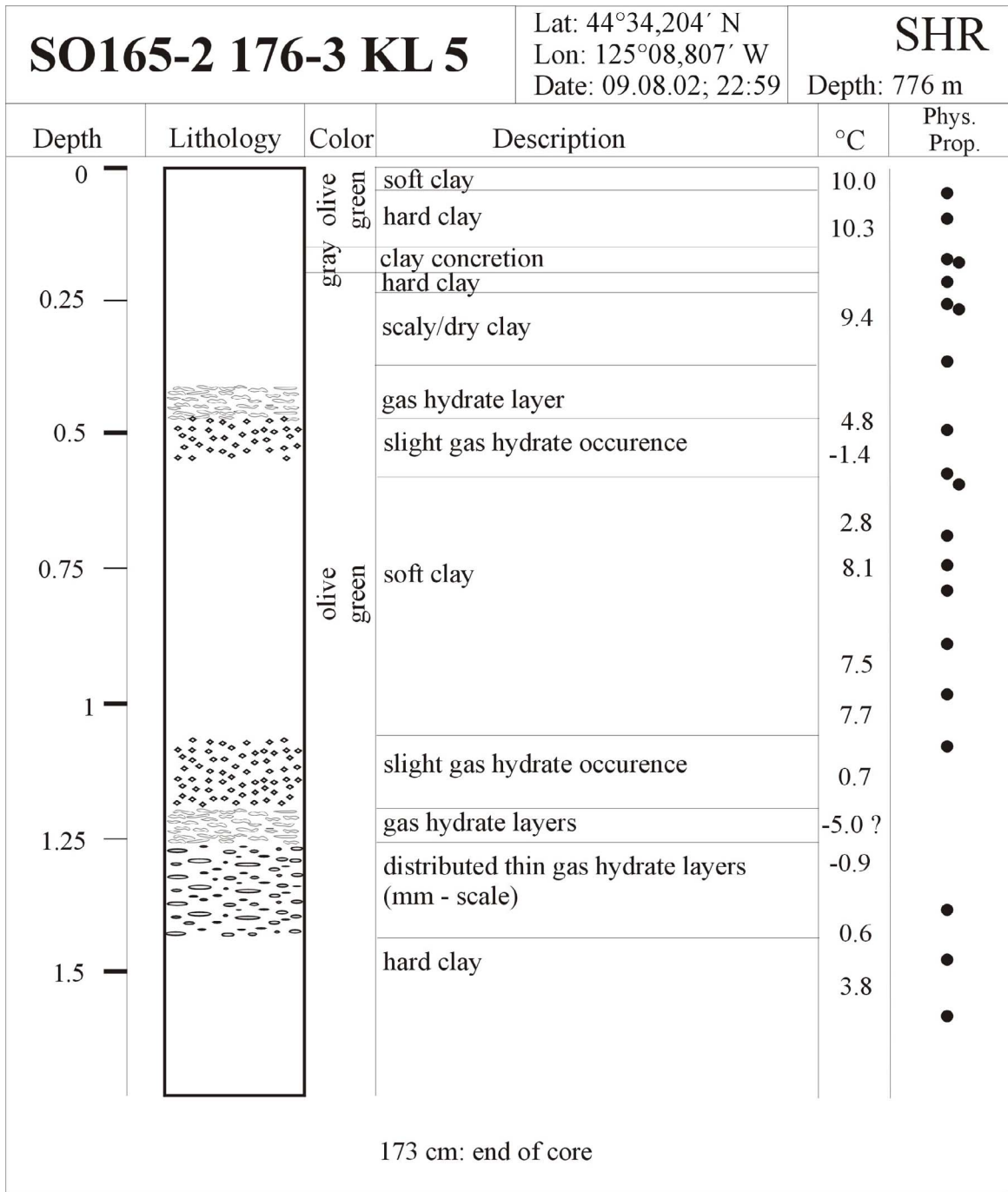


Fig. 5.10.2: Lithostratigraphy of core KL5



Fig. 5.10.3:Detail of gravity core KL5 (station 176-3)

Station 184-1 (core SL5)

This gravity core recovered 2.5m of sediment from the eastern basin (Fig.5.10.3). Predominant lithology is succession of olive green hard and soft clays with individual layers of intermediate to large carbonate pieces. A pronounced layer of gas hydrate is found at around 185cm below sea floor immediately above a layer of black clay, presumably indicating anoxic conditions at the time of deposition.

Tab.5.10.2: Carbonate samples collected from core SO165-2 184-1 SL5, the number (e.g.: MD-POS42) refers to samples taken by M. Drews, the VL number (e.g.: VL-CARB-37) refers to the carbonate piece number of V. Liebetrau.

Depth [cm]	Piece number	Description
133-135	MD-POS42-VL-CARB-37	
183-189	MD-POS45-VL-CARB-38	
202-207	MD-POS75-VL-CARB-36	Breccia
215-218	VL-CARB-41	undefined small split pieces
228-230	MD-POS49-VL-CARB-39/40	undefined small split pieces
241-243	MD-POS74-VL-CARB-35	grid structure
245-253	MD-POS75-VL-CARB-34	porous, mussel, tube filling

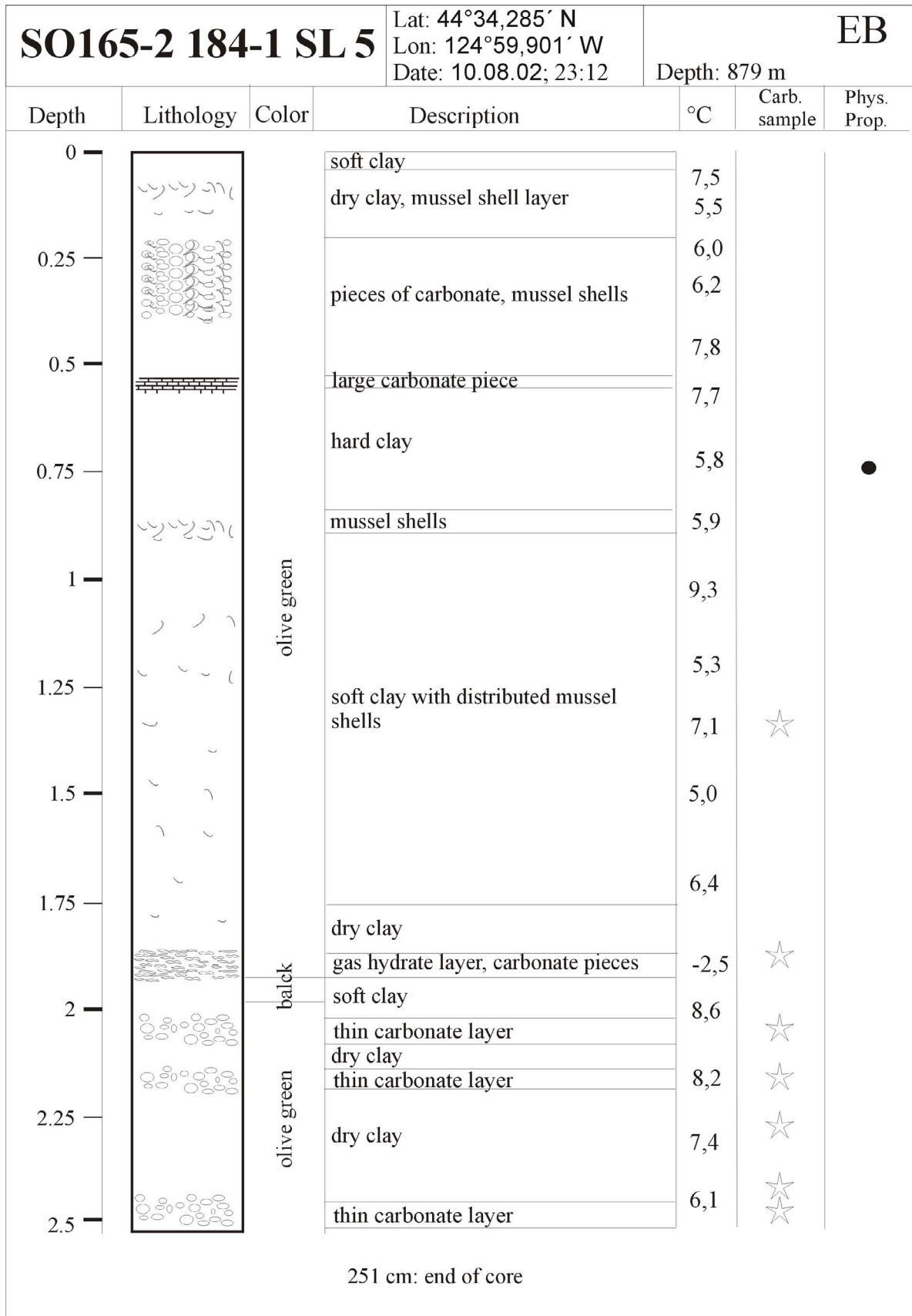


Fig. 5.10.4: Lithostratigraphy of core SL5

Station 194-2 (core SL8)

This gravity core recovered one of the most interesting sediment sections of SO165-2 as it contained a very intricate 251cm succession of carbonate layers, thin and massive gas hydrate layers, and intervals with small to massive carbonate pebbles (Fig. 5.10.5). It was thoroughly sampled for sediment physical property, carbonate and geochemical studies. Dry clay throughout the core displayed typical scaly fabric indicative for gas hydrate dessication (Figs. 5.10.5 and 5.10.6).

Tab.5.10.3: Carbonate sample description of core SO165-2 194-2 SL8

Depth [cm]	Piece number	Description
0-10	VL-CARB-52 (1-2)	breccia
10-20	VL-CARB-53 (1-4)	breccia + sieved sediment
20-30	VL-CARB-54	big breccia
30-40	VL-CARB-55 (1-2)	breccia
60	VL-CARB-56	flat breccia
70	VL-CARB-57	flat breccia
90	VL-CARB-58	filled tube
100	VL-CARB-59	aragonite porous
107	VL-CARB-60	aragonite
115	VL-CARB-61	sieved sediment
130	VL-CARB-62	open tube, fillings
150	VL-CARB-63	tube, filling
170	VL-CARB-64	breccia
190	VL-CARB-65	porous and rimm carbonate, close to gas hydrate
215	VL-CARB-66	Orbulina shell
234-337	VL-CARB-67	gas hydrate filled carbonate tube
270	VL-CARB-68	carbonate tube, filling, Orbulina shell

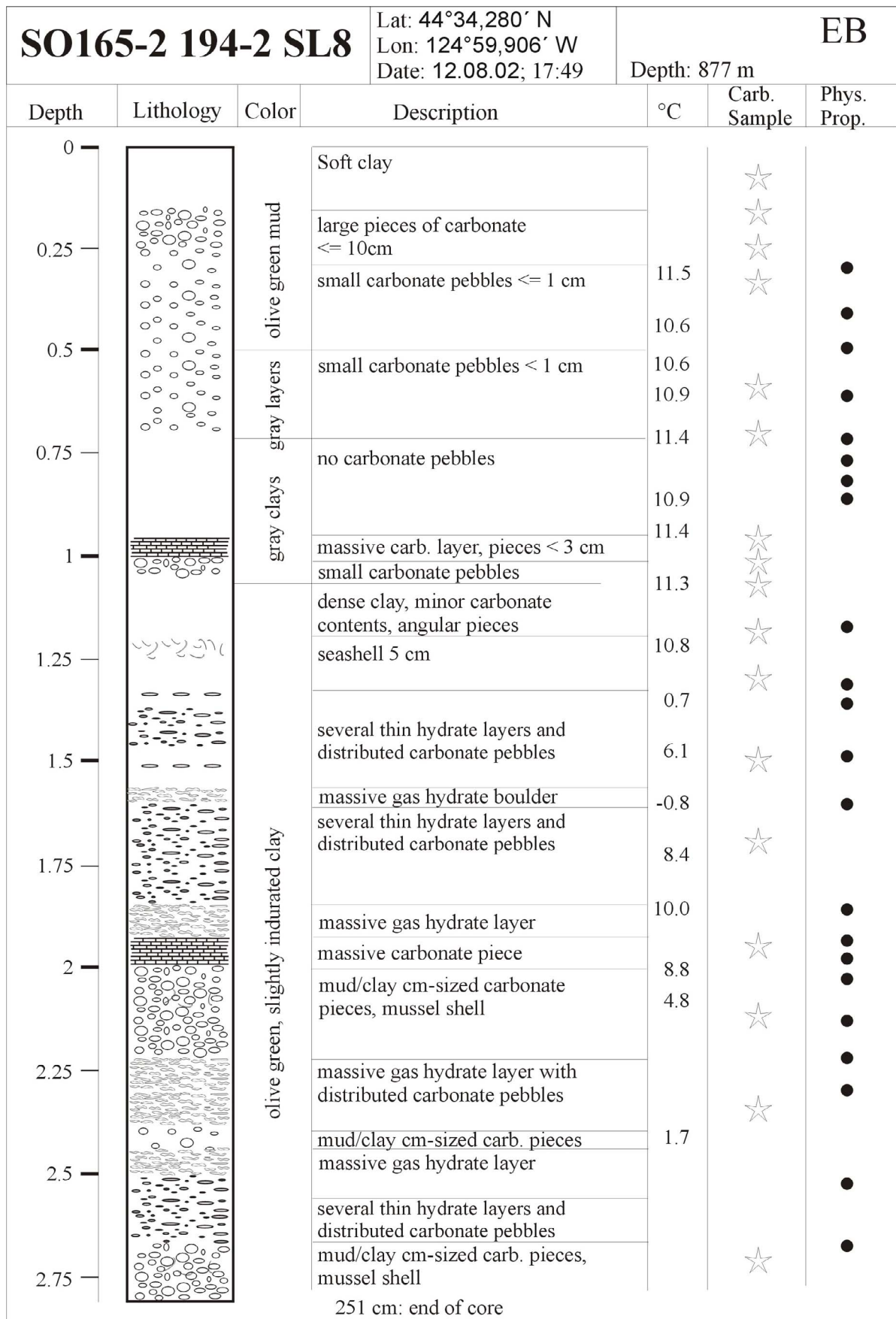


Fig. 5.10.5: Lithostratigraphy of core SL8

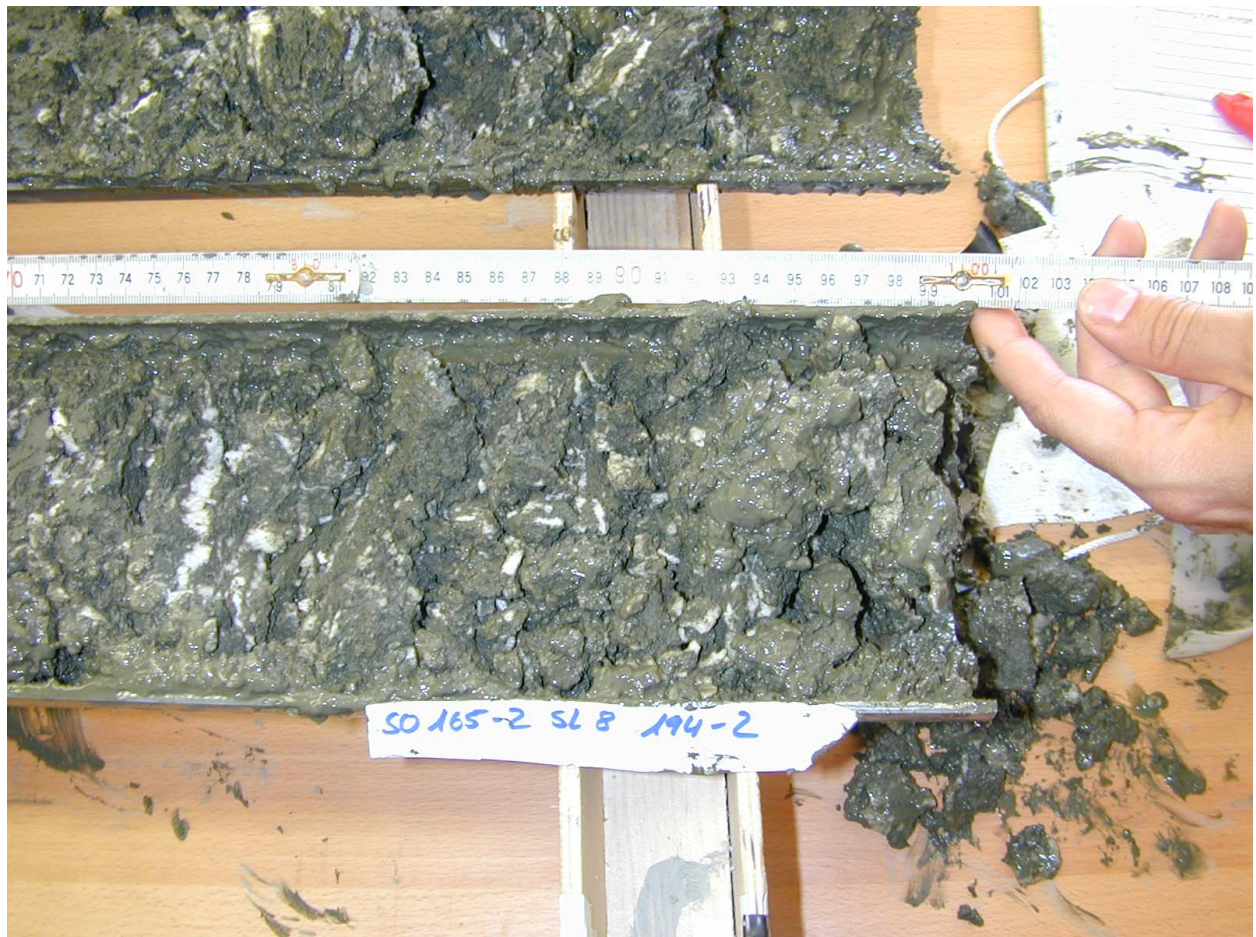


Fig. 5.10.6: Detail of gravity core SL8 (station 194-2)

Station 209-2 (core SL13)

At station 209-2 we recovered a short 60cm long core in the eastern basin of mostly dark green clay with several layers of massive carbonate pieces and Acharax shells (Fig. 5.10.7).

Tab.5.10.4: Carbonate samples taken from core SO165-2 209-1 SL13

Depth [cm]	Piece number	Description
0-1	VL-CARB-82 (1-2)	flat surface plate
43	VL-CARB-38 (1-4)	breccie horizon

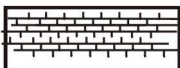



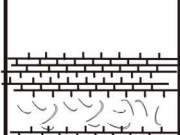


SO165-2 209-2 SL13		Lat: 44°34,358' N Lon: 124°59,871' W Date: 14.08.02; 22:24		EB Depth: 874 m		
Depth	Lithology	Color	Description	Carb. sample		
0		dark green/brown	massive carbonate piece (10 x 6.5 cm), small carbonate piece, soft clay	★		
0.10			massive carbonate piece (7 x 3 cm), soft clay Acharax shells			
0.20			clay			
0.30			clay			
0.40			carbonate pieces and mussel shells cm scale Acharax shells	★		
0.50			clay Acharax shells			
0.60			clay			
			60 cm: end of core			

Fig. 5.10.7: Detail of gravity core SL13 (station 209-2)

Station 222-1 (core SL17)

Core SL17 yielded a 120cm core of olive-green clays with two layers of gas hydrates shallow in the section and a zone of thinly distributed small nodules and veins of gas hydrate at about 100cm depth (Figs. 5.10.9 and 5.10.10).

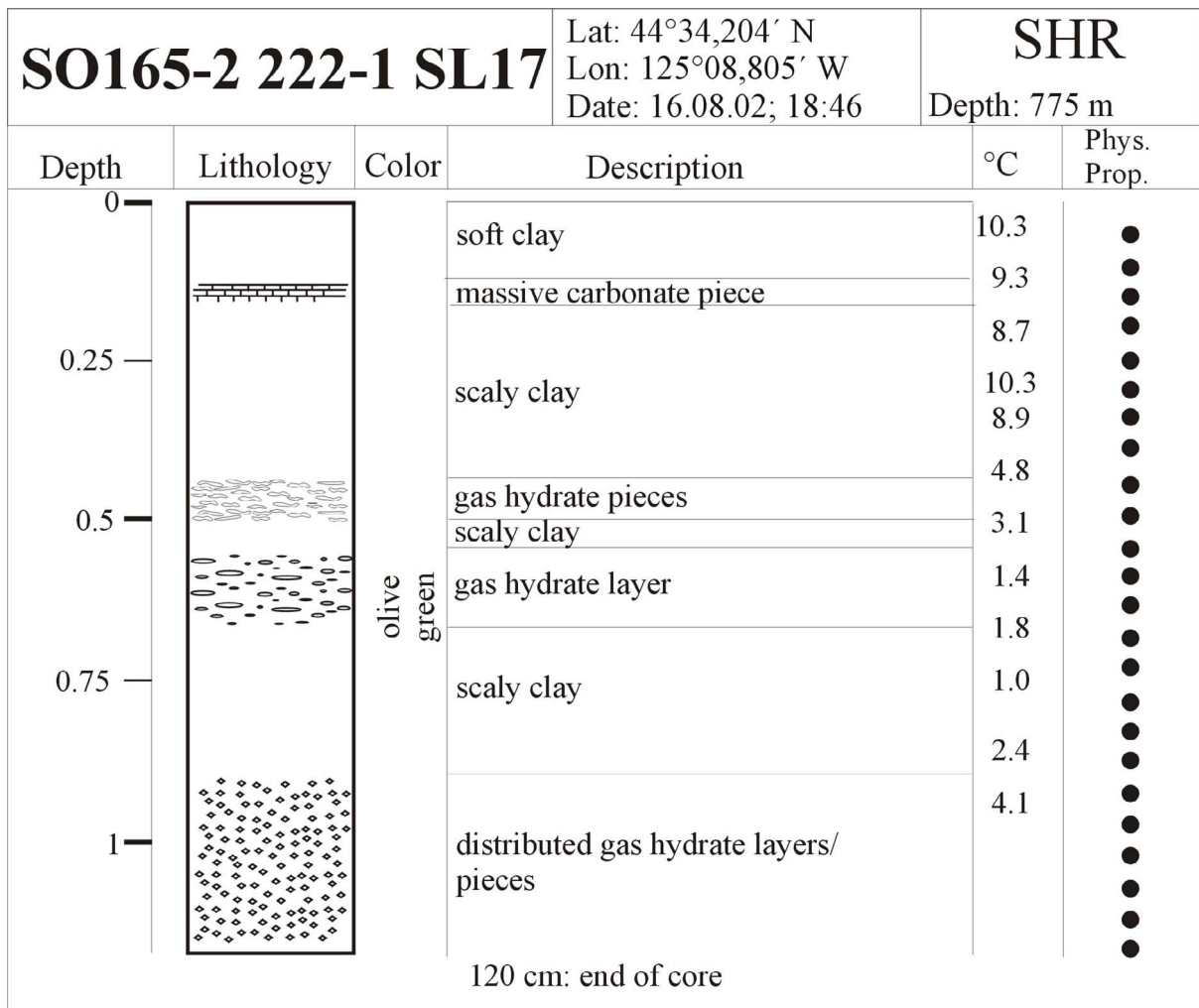


Fig. 5.10.8: Lithostratigraphy of core SL17

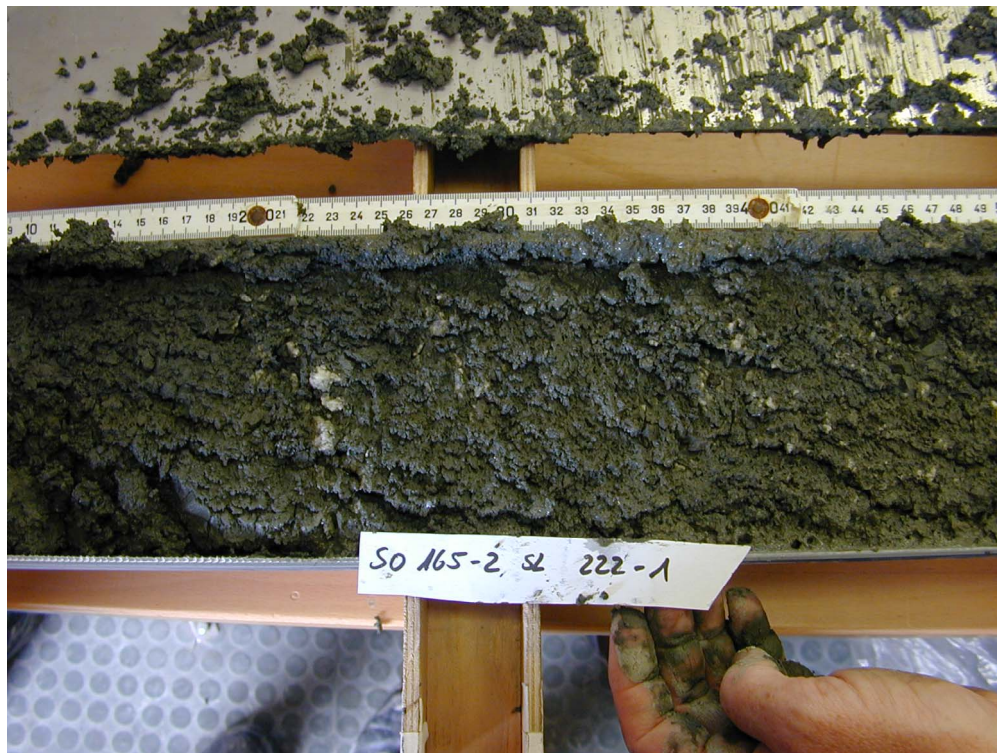


Fig. 5.10.9: Detail of gravity core SL17 (station 222-1)

5.11 In-situ Measurements with GSPT

H. Christian, W. Brückmann

Background

The measurement of geotechnical parameters in situ has met with increasing success in the past few years in concert with the development of more compact but more capable dataloggers, which can now be operated on a fully autonomous basis.

The collection of core samples can in many cases, lead to erroneous interpretations of geotechnical properties, which may be sensitive to sampling disturbance effects, including the necessary reduction in back pressure. However, a commentary on the causes and effects of sampling disturbance in gravity and piston cores is beyond the scope of this report, which summarizes only the application of an in situ test system for the investigation of the benthic hydrologic regime.

The SwordFish design has evolved from a previous evolution developed by the Geological Survey of Canada, known as Excalibur, which is no longer operational. The testing apparatus can undertake specific testing of the zone of sediment immediately surrounding a filter stone mounted near a probe tip, which is installed into the seafloor.

Equipment and Methods

SwordFish comprises a deployment frame housing the system electronics package, an acoustic modem for uplinking to the surface vessel and a variable-length lance, through which pore water pressure enters the hydraulic lines to permit measurement during the test.

The seabed frame is rigidly connected to the lance, which can be varied from 1.4 to 6.4 m in length and is 76 mm in diameter, narrowing to 35 mm at the location of the porous filter. The larger-diameter part of the lance provides bending stiffness should partial penetration into the seafloor occur and the smaller-diameter part of the lance allows for more rapid pore pressure decay, which is monitored at the start of testing. The lance is tightly braced onto the lower baseplate by six turnbuckles, which give additional rigidity to the overall system, but provide a primary function in preventing the lifting wire from getting fouled underneath the baseplate during recovery from the seafloor.

The frame is about 1.5 m in height and is mounted on steel spacer rods arranged around the edge of the frame baseplates in a hexagonal pattern. Lifting eyes are attached to the top ends of these steel spacer rods. The frame is connected to a lifting ring and swivel, which are shackled onto the main winch wire for deployment and recovery. A safety lifting bridle is also attached onto the top plate, in case the primary lifting bridle should fail.

The sensor suite includes an absolute pressure transducer for monitoring hydrostatic pressure during descent through the water column. A differential pressure sensor measures the dynamic pore pressure response at the tip after penetration into the sediment (stage 1). The absolute pressure gauge measures the pressure during pore fluid sampling (stage 2). Other sensors used to determine probe attitude include a 20g vertical-axis accelerometer and an inclinometer, giving roll and pitch.

Pressure data is passed through a gain preamplifier then sent to an A/D converter and datalogger (Onset Tattletale 8). The operator can preset the data sampling rate to be any value, so long as it is less than 1 Hz. Incoming data are stored in a

circular buffer for 60 scans, then written to Flash memory (Persistor CF8) in appending binary format. After instrument recovery, three data files are downloaded to a host computer (data header file, raw sensor data file and a system message file) for processing and interpretation. Details on the conduct and interpretation of test data will be given later in this summary.

Initialization and Lowering through the Water Column

On deck, after the hydraulic lines have been saturated, the sample cylinder flushed and charged with neon gas at 1 bar, the system presets have been enabled, the testing times input into the datalogger and the data logging program started, the instrument is ready for deployment.

SwordFish is lowered through the water column by paying out the winch wire at a rate of about 1 m/s to a set depth above the seafloor (nominally 100 to 200 m), for a 5-minute stabilization period. Baseline transducer readings from this period are used in the post-processing of test data (especially the accelerometer and the differential pressure readings which define the zero transducer offset).

The apparatus is then lowered at about 0.5 m/s until it penetrates the seafloor and comes to rest; additional wire is payed out until there is no chance of tugging on the instrument during vessel dynamic positioning. This condition is maintained for the duration of the testing, which typically takes 1 to 2 hours in fine-grained sediments.

Stage 1: Lance penetration and dynamic pore pressure measurement

The measurement of sediment pore pressure response to lance penetration is an important part of the testing, giving highly representative information for geotechnical and hydrodynamic analysis.

The absolute pressure transducer is a Data Instruments Model AB/HP 13.8 MPa, with a sensitivity of 0.25% of the full-scale output (+/- 34.5 kPa). Other gauges with different ranges can be installed for shallower water depths, giving increased sensitivity. This transducer is used for detection of the trigger depth for test initialization and for monitoring the pressure response during pore fluid sampling.

This means that the pressure measurement system used for monitoring the water column is too insensitive for also measuring the dynamic pore pressure response, which likely never exceeds 80 kPa within the uppermost 5 m of the sediment column. Therefore, a special differential pressure transducer (Validyne Model DP300, 80 kPa range, sensitivity of +/-0.25% differential full scale output, or +/- 0.2 kPa) is installed between the probe tip filter and the water column. This sensor is only enabled during stage 1 of the test and is isolated from the hydraulic line to the tip during stage 2, to prevent it from being overloaded.

Probe penetration into a clayey deposit initiates a full-displacement undrained failure, producing a positive excess pore pressure response which begins to decay only once the lance has come to rest at the full penetration depth. The peak excess pore pressure can be accurately correlated to the sediment undrained shear strength, using cone penetration test theory. The dynamic pore pressure typically peaks at a value of between 6 and 9 times the undrained shear strength, depending on sediment plasticity.

The time-dependent decay (dissipation) of the excess pore pressure gives a value for the coefficient of consolidation. The pore pressure dissipation test data can be numerically modeled by applying cavity expansion theory. After the decay curve has equalized and remains constant with time, the measured pore pressure at the lance

filter can then be compared against the hydrostatic pressure, which is equal to the total water depth. Any remaining positive pore pressure difference is concluded to be an indication of a sediment overpressured condition that existed before penetration of the SwordFish lance and reflects upward migration of pore water toward the seafloor.

A net negative measurement indicates that seawater is migrating into the sediment column from the water column. Most situations involve dewatering of marine sediments through gravitational compaction, hence fluid movements are generally upward. Pore waters may also be advecting from depth in response to a pressure gradient that is unrelated to sediment compaction (e.g. plate subduction). Hence the measurement of excess pore pressure is a parameter of considerable interest to geotechnical researchers.

The time for full pore pressure dissipation relates to the sediment plasticity, clay content, clay mineralogy and most of all, the probe diameter. In fact, the time for dissipation increases according to the square of the filter radius. The SwordFish design seeks to minimize this dimension, in order to shorten dissipation and as a result, the overall testing times. However, in dense or cemented sediments, use of the small-diameter lance extension may result in its being damaged. Several probe tip sizes are available, including 5, 16 and 35 mm diameter, for various sediment conditions as required. A filter for the 76 mm lance would be a useful option for testing of cemented or indurated sediments, as it is capable of surviving penetration without damage, if it is sufficiently short.

Stage 2: Pore water and gas sampling

At the end of the pore pressure dissipation stage, which is either defined by the operator prior to deployment or by direct command over the acoustic link, the pore fluid sampling is begun. A motorized valve is opened, allowing formation pore fluid to enter the hydraulic lines through the cylindrical porous filter mounted on the lance tip (diameter equal to the probe extension installed; height of filter is 19 mm). The filter has an average grain porosity of between 25 and 40 microns, with an overall range of 2 to 75 microns. The filter is fabricated from compressed porous polypropylene. Prior to sampling, the hydraulic lines and filter are backfilled with deaired distilled water (minimum standing volume estimated to be 12 ml). During sampling, approximately 30% of this system charging water is pushed through the valve into the sample collection cylinder and therefore causes some dilution of the actual sampled pore fluid.

The tip pressure response is continuously monitored during sampling, to provide data for interpretation of the coefficient of hydraulic conductivity (permeability). As the cylinder fills with pore fluid (water and gas) an equilibrium pressure condition is re-established across the porous filter and inflow stops. The filter effectively prevents sediment particles from entering the sampling system. The in situ permeability is obtained from the final part of the pressure equalization response, where hydraulic gradient falls below the critical hydraulic gradient, at which level Darcy's law is applicable.

From the assembled test results, we obtain the undrained shear strength (in fine-grained sediments), the coefficient of consolidation, the residual porewater pressure and direction of fluid migration within the sediment column, the in situ hydraulic gradient relative to the seafloor and the coefficient of permeability. From Darcy's law we then may calculate the seepage velocity within the zone of measurement. It

must be noted that these results are only applicable in the immediate vicinity of the filter on the probe and should be considered as spot measurements.

The trapping of pore gas within the sampled volume offers an opportunity for detection of hydrocarbons which may have been present in situ as either dissolved compounds or as free phase gas. At the end of fluid sampling, the valve is closed, locking in whatever pressure level has been achieved within the hydraulic lines. The pressurized cylinder is removed from the seabed frame after instrument recovery and depressurized into a gas transfer bag, after which the collected water sample can be drained off and analyzed. The gas in the bag can be injected into a GC-MS for detailed analysis. The geochemistry of the porewater sample can be obtained. From the GC data, it is possible to calculate the unit volume of gas that existed in situ, based on observed headspace concentrations and the in situ pressure and temperature conditions. A useful parameter applicable to slope stability studies then is the degree of saturation, which reports how much free gas exists within a unit volume of the pore water at the tested depth.

Recovery

The apparatus is simply pulled out of the bottom by the winch, with as near a vertical wire angle as possible. Once on deck, the serial communications cable is reconnected to the system electronics package and data logging is halted. The test data are transferred to the host computer at a baud rate of 9600 bps. Each test can record about 17 hours of data at a sampling rate of 1 Hz. The batteries are capable of several deployments before they need to be replaced.

The sample cylinder is removed from the seabed frame and handled very carefully, as it may hold a high shut-in pressure.

GSPT operations on SO165-2

August 4

Loading of SwordFish equipment in Portland, OR.

August 6

Complete assembly and deployment of the SwordFish in 777 m water depth over a known gas hydrate deposit. Probe returned to surface showing tip broken off at threads between lower and upper push rods, inside nosecone. Tubing inside push rod crimped at break in rods, such that no flow was possible, despite the sampling valve operating correctly. Our conclusion is that the seabed contains layers or lumps of carbonate and hydrate material, which are capable of stopping probe penetration.

Upon opening the pressure case, observed seawater intrusion around both impulse connectors. Pressure record shows that the depth at which the leak occurred was about 730m. Considerable corrosion evident on main circuit board.

Electronics washed of salt water and stripped out of system for evaluation and possible repair. Valve is showing a continuous voltage forcing it to rotate, as if the MossFet switch was damaged and is now stuck in the Hi position. Both pressure transducers are non-responsive,

suggesting damage has occurred to the pre-amplifying circuitry. Surface mount components on board are not repairable and no spare circuit board is available, as the only other board was used for electronics development purposes.

August 7

Search onshore for replacement electronics or an alternate datalogger. The spare circuit board is an earlier version which was abandoned due to wiring errors made during fabrication. The surface mount design means it may not be possible to make it serviceable or have a new one manufactured. Attempts are being made onshore to provide us with an operational main circuit board, or an alternative datalogging capability. Options being pursued include mobilizing an earlier version of a fluid sampling electronics, an early version of the Brooke Ocean Technology Ltd. Free Fall Cone Penetrometer, a standard industry piezometer datalogger, or upgrading the early main circuit board for SwordFish.

August 8

Conducted a successful pressure test to 740 m depth of empty pressure case (electronics removed, lower motor assembly left intact); no leaks evident except an insignificant accumulation of water around valve mount on lower endcap. This was accomplished by refacing endcap connector o-ring seats on lathe in ship's machine shop and tightening the connectors to maximum torque. The connectors themselves show that they can withstand the pressure, therefore the leaks occurred around their o-ring seals, which were newly installed prior to mobilization.

Summary

The SwordFish equipment was mobilized and loaded onto the FS Sonne and operated to a depth of about 730 m, at which point a pressure case leak developed, which disabled the electronics system. The leak occurred at the endcap connectors and resulted in about 0.5 litres of seawater entry. The main analogue circuit board was damaged beyond repair and no spare board was available. This prevented the SwordFish system from being used again during the cruise.

The first deployment was over a supposedly soft sediment location, with little perceived risk of damage, as carbonate and hydrates were thought to be present only as isolated lumps or lenses. The 35 mm lance extension was snapped off at the threaded connection with the 76 mm lance, indicating that it had encountered something dense or hard (hydrate or carbonate) during penetration. The inner hydraulic line was crimped closed at the break, but stayed attached to the filter adapter, so that the entire tip assembly was recovered with the instrument. However, no pore fluid was able to enter the cylinder because of the damaged line.

5.12 Sediment coring with autoclave technology

H.-J. Hohnberg, H. Mudrack

The Multi Autoclave Corer (MAC, Figure 5.12.1) was developed for sampling, recovering, storing and evaluating of sediment cores from the deep sea under *in situ* conditions.



Fig. 5.12.1: Deployment of the MAC with two cores

Synopsis

The MAC system by TUB/MAT was developed for simultaneous sampling of four sediment cores from the upper seafloor (max. 55 cm) in water depths of up to 1400 m. The cores are trapped in pressure chambers and hauled inboard under pressure, thus staying close to *in situ* conditions. The MAC consists of a deployment frame with a damping system including a pull rope releaser system and eight further large structural components, namely the four coring units and the four pressure chambers. In addition, every pressure container is equipped with a pressure preserving system (accumulator) supporting the closure of the pressure chambers during the coring procedure and enabling pressure preservation over several weeks. Each of the cores is kept in a liner which is pulled into the respective pressure chamber and trapped inside in vertical direction. The MAC was deployed on the deep sea cable. When the system hits the seafloor, left to rest there for a certain time and before hoisted back. Function groups are activated that control the

processes of coring, pulling the liner into the pressure chamber, sealing the pressure chamber and hauling under in situ pressure. Each of the four pressure chambers is enclosed by a transparent mantle tube which is filled with sea water, providing sufficient cooling of the pressure chamber. Cooling is especially vital for sediment samples that contain gas hydrate. The sediment cores can be used for various physical, chemical or biological examinations. For example, they can be scanned using non-invasive technology or they can be released from the pressure chamber for description and analysis immediately after recovery. The pressure chambers were checked and approved by the Berlin TÜV (Technischer Überwachungsverein, technical inspection authority of Germany). Stored in a safe transport box, they are suitable for transport by sea or road.

Materials used for the MAC:

The deployment frame including damping system, releasing system and coring system consist of stainless steel (1.4571 und 1.4301), partly hot zinc dipped. The parts of the pressure chambers exposed to inner pressure were made of highly firm stainless steel (1.4462) and GRP tubes. The mantle tubes around the pressure tubes, which are exposed to tractive force, are made of a highly firm aluminium alloy. (AlMgSi1). All materials used for the pressure chambers have been approved by the TÜV and classified by 3.1b oder 3.1a certificates.

MAC-testing procedure

All sediment coring tests were supported by a video telemetry system provided by GEOMAR. Different weather conditions (swell) can be compensated by changing the lowering/ hoisting speed. The different structural components are so variable that alterations are possible as a response to the test results. The following components can be adjusted during a series of tests:

- Position of the piston within the liner.
- Position of the sealing sleeve within the liner, determining when the water column in the liner above the sediment surface is sealed.
- Installation of a catching or releasing socket in the head of the pressure chamber, which means an anticipatory determination of the position of the liner within the pressure tube.
- The damping and thus the speed at which the corers enter the sediment can be adjusted by changing the internal flow resistance.
- The sealing characteristics of the pressure chamber immediately after the coring can be changed by variable pre-adjustment of the initial accumulator pressure.
- The base height of the deployment frame is adjustable, allowing for a flexible reaction to different types of sediment with different solidity which might affect the stability of the system.
- The cutting force can be changed by adding more or less lead weight, which also means a change of cutting speed.
- Installation of a core catcher.
- 4 corers can be deployed simultaneously, so that a maximum of four different samples can be examined and compared under identical sampling conditions.

MAC Tests

Eight deployments were made during leg 2 (Tab. 5.12.1). Various combinations of almost all of the above-mentioned options were tried during the test series.

Table 5.12.1: List of MAC deployments

Nr.	Station	Date	Time (UTC)	Position at seaf. contact (N;W)
MAC 01	161	07.08.02	21:36 to 22:50	44°36.169'; 125°08.810',
MAC 02	170	09.08.02	02:00 to 03:05	44°34.210'; 125°08.810',
MAC 03	179	10.08.02	03:41 to 04:49	44°34.210'; 125°08.830',
MAC 04	196-1	12.08.02	22:51 (broken off)	
MAC 04	196-2	12.08.02	23:49 to 01:00	44°34.233'; 125°08.836',
MAC 05	200	13.08.02	14:01 to 15:13	44°34.216'; 125°08.828',
MAC 06	221	16.08.02	17:16 (broken off)	
MAC 07	223	16.08.02	19:40 to 21:00	44°34.211'; 125°08.810',
MAC 08	229	17.08.02	17:25 to 18:25	44°34.209'; 125°08.824',

Results of MAC testing

Coring success as well as pressure stability varied during the test series. The variations were partly caused by the system or by assembly errors. In addition, deployment positioning on the seafloor and recovery of the MAC were affected by different swell conditions.

At station 161, one of the four pressure chambers was retrieved under pressure (60 bar), two others had been decompressed because of mud in the closing flap, the fourth was open because the end piece of the liner had been torn off, so that the liner could not be pulled inside.

For the following stations the MAC was equipped each with two corers because one of the units had suffered mechanical damage and because this approach enabled a more effective use of the time allocated for each station

We got two good cores at station 170, yet they were not under pressure due to an assembly error.

Two cores were recovered at station 179. One chamber showed 40 bar, the other one 10 bar at the beginning, which increased to 20 bar after a leakage had been closed.

Station 196 yielded two cores, yet they were partly lost on their way upwards because none of the two flaps had closed completely. In one of the corers, we found a fist-size piece of gas hydrate. Both chambers were decompressed.

Station 200 marked a first full success. Both chambers were under pressure at 65 bar, with cores inside. When trying to extract the cores, however, problems were encountered that could not be solved satisfactorily on board.

At station 223 the liners were equipped with core catchers for the first time. The station turned out to be problematic due to high swell. The MAC had two touchdowns, on the monitor we could observe it being knocked over by the deep sea cable. Yet, two cores were recovered, but both without pressure. In one of the chambers, pressure built up within an hour. When the degassing ventile was opened, a substantial amount of gas escaped, which proved to be burnable.

Station 229 corroborated the success of station 200. Both chambers were under pressure at 65 bar. The core quality could not be checked on board. Both pressure chambers were kept refrigerated in the cool lab. They underwent computer tomography in San Francisco and again a few weeks later in Kiel (see chapter 5.13)

Stations 196-1 und 221 had to be broken off due to malfunctions of the video telemetry.

Conclusions

The test series has shown that a special core catcher solution will be necessary to core sediments containing gas hydrate. The deployment frame should have finer damping properties for adjustment to different swell conditions. A new solution must be found for extracting the cores immediately after decompression on board. The flap works satisfactorily, small changes are recommendable to improve operational reliability. The pressure preservation over longer periods of time is satisfactory.

5.13 Sampling of gas hydrates and investigation of their internal structure

F. Abegg, W.Brückmann, M. Drews, A. Eisenhauer, J. Greinert, H.-J. Hohnberg, V. Liebetrau, R. Luff, H. Mudrack, A. Petersen, T. Treude, S. Schenck

Aim of Investigation

The internal structure of gas hydrate samples is investigated to determine the different environments of gas hydrate genesis as expressed by different structures. Additionally, the respective amounts of gas hydrate, gas and ambient sediment will be determined. Special attention focusses on the question of the proportions under in situ conditions. So far, their determination has always been influenced by possible variations due to changes of temperature and pressure during sample recovery.

Methods

Shipboard work was limited to high quality rapid sampling of gas hydrates. Because of the inhomogeneous distribution of the gas hydrate in the seafloor, most sites were sampled using video-guided tools such as the TV Grab or the newly developed TV-MAC, for details see 5.12. Mats of *Beggiatoa* are used as an indicator for the presence of gas hydrate. Sites for gravity corer sampling of gas hydrate were chosen by precise determination of coring locations by OFOS investigations and depended on perfect positioning of the ship.

Bulk gas hydrate samples obtained with the TV Grab and core segments obtained by gravity coring were preserved in liquid nitrogen immediately after recovery. Samples from the TV Grab went through a provisional cleaning from mud before they were frozen. As a special technique, plug samples were drilled from pieces of gas hydrate. An electric drilling machine was used with a 3 cm inner diameter drill. This technique provided plugs of gas hydrate with a length of approximately 3 cm which will be used for permeability tests.

The gravity corer was used with a pre-cut liner with a segment length of up to 55 cm which was determined by the storage capacity of the liquid nitrogen dewars. Upon retrieval of the corer the segments are pulled out of the barrel, closed with caps and put into a bag with ropes. In these bags the samples are lowered into the liquid nitrogen. A core with four segments can be processed within six minutes after corer retrieval.

All the frozen samples will be examined in Germany. Sampled stations are listed in Tab. 5.13.1.

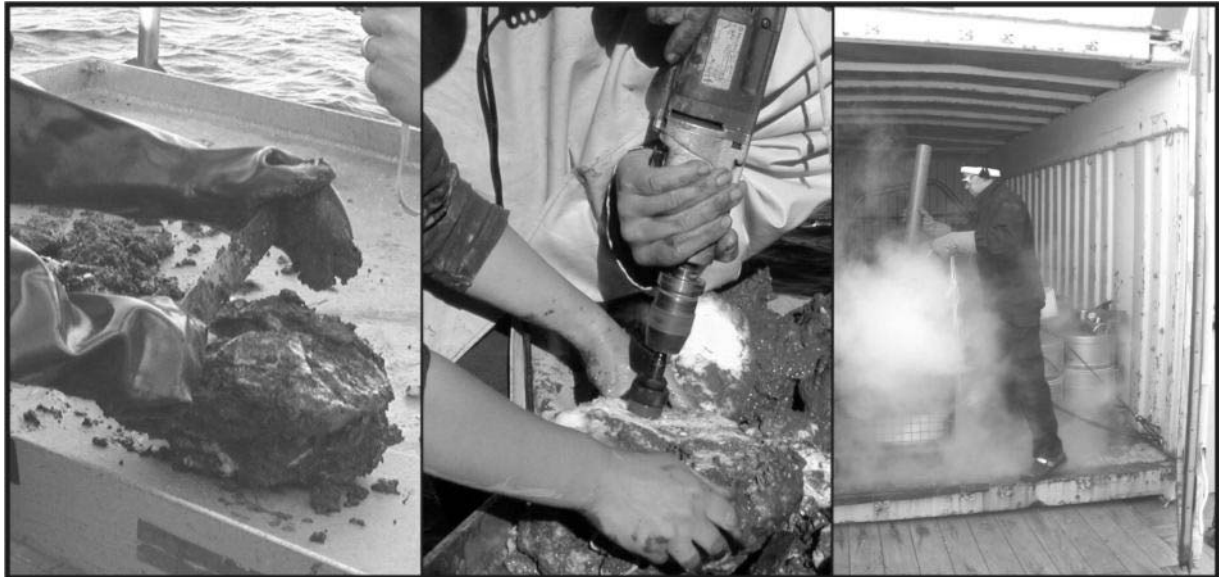


Fig. 5.13.1: left: cleaning from mud; middle: drilling of plugs; right: freezing

A lot of attention was attracted by the pressurised MAC cores. Finally, a set of two cores could be taken from the Southern Summit. After recovery, they were under a pressure of 65 bar (non-calibrated gauges). The pressure increased up to 70 bar during dismounting of the laboratory transfer chambers (LTCs) and transported into the cold storage of the SONNE. Inside the cold storage at +4°C the pressure dropped to a constant value of 60 bar.

In order to avoid any risk due to our lack of experience with the new pressure coring device, computerised tomographic imaging (CT) of the samples was performed after arrival in San Francisco. A clinic in Palo Alto had been chosen because they were running the same type of scanner as had been used for such investigations in Kiel. The main uncertainties regarding the MAC samples concerned pressure loss and changes of the samples due to consolidation or diagenetic changes during the transport from USA to Germany.

For the transport from the ship to the clinic, the LTCs had been placed in a wooden box. To avoid extended heating of the samples, dry ice had been placed inside the box. During scanning, which took approximately one hour for each LTC, the internal pressure increased up to 62 bar.

The first step of the CT scanning produces an overview of the core, called surviue. It contains all information projected into one layer. Showing the whole core, it serves as a planning tool for the following scans. Based on this surviue, start and end points for the single slices are determined.

Preliminary Results

Table 5.13.1 provides an overview of the gas hydrate samples. Except for the pressurized cores all samples are stored in liquid nitrogen and will go through subsequent examinations.

Tab. 5.13.1: List of gas hydrate samples

Station No.	Instrument	Area	Samples
154-1	TV-G-2	Southern Summit	many sub samples
162-1	TV-G-3	Southern Summit	many sub samples
167-2	KL/SL-2	Southern Summit	piece of gas hydrate
169	TV-G-4	Southern Summit	many sub samples
176-2	KL/SL-4	Southern Summit	4 core segments frozen
184-2	SL-6	Eastern Basin	piece of gas hydrate
194	SL-9	Eastern Basin	3 core segments frozen
197	TV-G-8	Southern Summit	many sub samples
229	TV-MAC-8	Southern Summit	2 pressurized cores

Investigation of the LTCs proved that both cores were well-positioned within the scanning window (area of thin aluminium walls) of the LTC and showed an undisturbed structure as can be seen in Fig. 5.13.2.

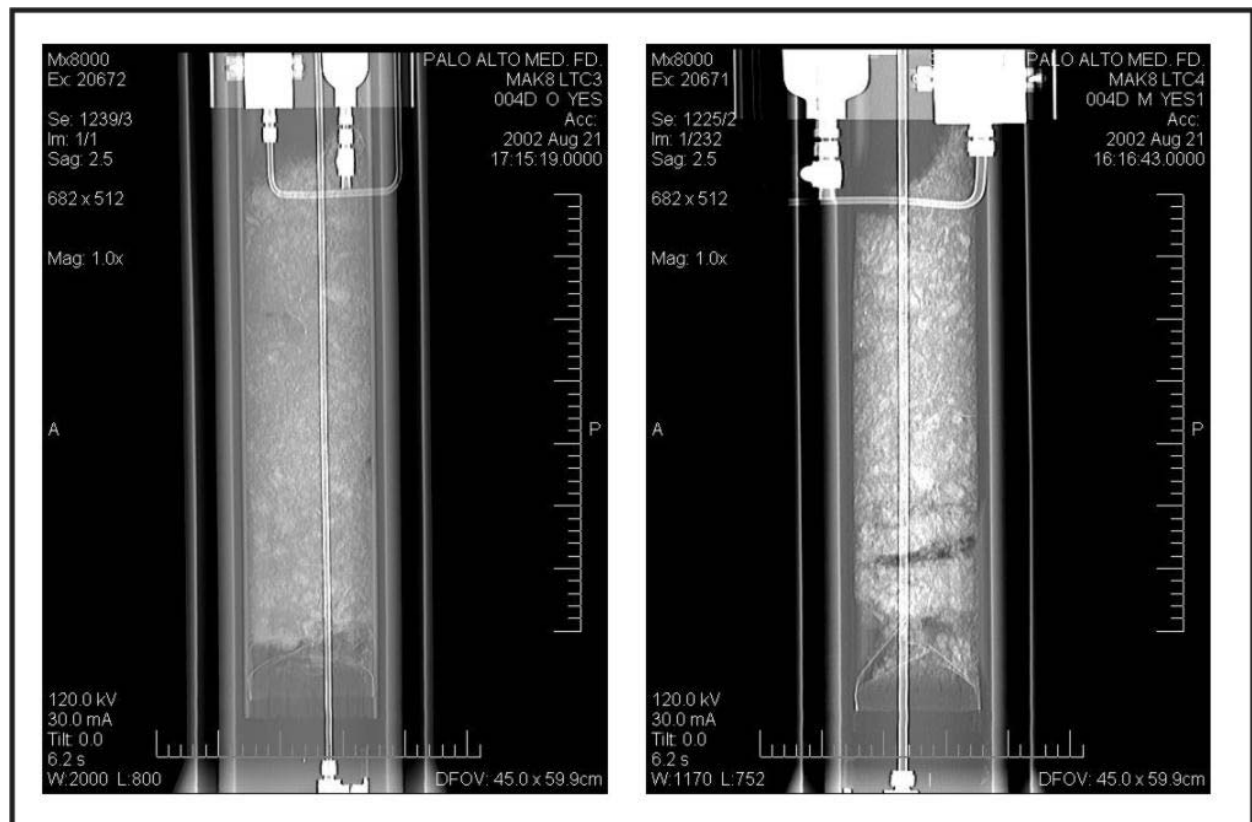


Fig. 5.13.2: left panel: surview of LTC 3, right panel surview of LTC 4.

Core LTC 3 has a length of 39,5 cm and has been scan-cut into 440 slices. Core LTC 4 has a length of 35 cm and has been cut into 464 slices. Looking at both surviews a black horizon is apparent in LTC 4. This horizon consists of gas hydrate. The

uppermost gas hydrate in LTC 4 was detected at 10 cm subseafloor depth. LTC 3, in comparison, does not show such a distinct gas hydrate horizon. The determination of gas hydrate volume will be achieved by subsequent data processing.

A very striking feature observed in these scans taken under in situ conditions are gas bubbles inside the gas hydrate. Fig. 5.13.3 provides a view of a single slice where bubbles are indicated by black spots. Gas hydrate occurs in dark grey and mud in light grey.

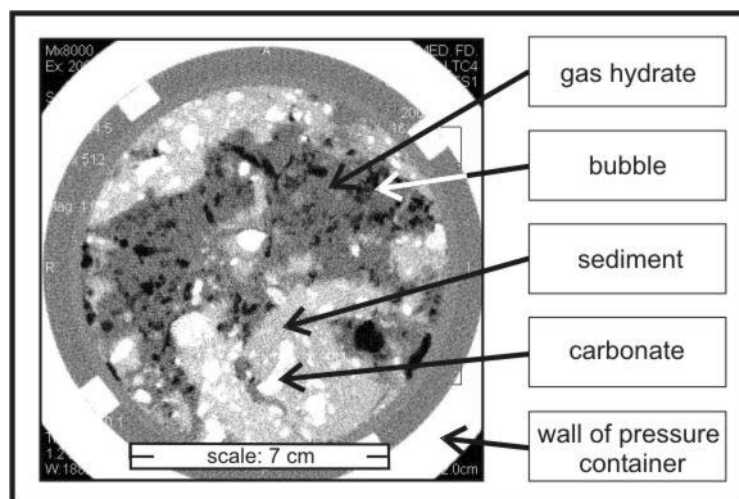


Fig. 5.13.3: Single slice from core SO165-2, Station 229, MAC8, LTC4 in 29 cm subseafloor depth.

Bubbles detected in this core may reach a size of up to 1cm in horizontal direction and 1.5 cm in vertical direction.

5.14 Authigenic Carbonates

V. Liebetrau & A. Eisenhauer

Introduction

The main goal of LOTUSsubproject 3 is to constrain life span and ages of gas hydrate vent sites in order to quantify the time variability of chemical fluxes and the efficiency of local gas hydrate venting systems. Gas hydrate carbonates dated by U/Th-disequilibrium and $^{226}\text{Ra}_{\text{excess}}/\text{Ba}$ -methods are suitable archives in order to get the necessary chronological information. An increasing age data set for different carbonates from different sampling sites allows constrains on timing and identification of the major geological vent-controlling processes. In order to investigate the chemical dynamics of a typical vent site in high time resolution, detailed geochronological profiles of single carbonate built-ups are necessary.

Specific aims for SO165 were:

1. Recovery of large carbonate built-ups for high resolution geochronological profiles covering different time windows of venting activity.
2. Co-sampling of recent to subrecent gas hydrate related carbonates from gas hydrate recoveries and sediment cores in order to investigate different carbonate precipitation processes and the chemical interaction of carbonate and gas hydrate.
3. Sampling of gas hydrate, bottom water and methane enriched water column to study the chronometer related isotope systematics (U, Th, Ra, Ba) of different venting related phases and source tracer like Sr, U, REE-pattern and trace elements. Pore water samples were depending on new in situ sampling techniques described in chapter 5.13.
4. Close cooperation with other subprojects to provide direct link of data sets (this report: 5.3, 5.8, 5.10, 5.12, 5.13, 5.15)

Material and Methods:

Large carbonate blocks and near surface gas hydrates were recovered with the TV guided grab sampler (TV-G; successful application due to expertise of F. Abegg, 5.13). Carbonates of sedimentologically documented settings were sampled from different gravity cores (coord. with 5.8 and 5.10). Some of these are of specific interest for carbonate/gas hydrate interaction (aragonite plates in contact to and inside of gas hydrates, gas hydrate filled tubes). TV-guided multi corer (TV-MUC) and TV-guided multi autoclave corer (TV-MAC) provided carbonate and bottom water samples in correlation to different biological settings (coord. with 5.8, 5.10 and 5.13). From CTD tracks (coord. with 5.3) for methane analyses of the water column (depth resolved profile) and the bottom water (tow-jo CTD) 2 liter aliquots of water samples were separated.

A complete list of samples including remarkable observations concerning the scientific potential for subproject 3 is given below. Detailed information about the sampling sites are compiled in the official station list of SO165 (chapter 7).

Tab. 5.14.1: Sampling and processing protocol.

Stat.	gear	sample-code	no. of pieces volume (ml)	sample type	sample origin / depth	sample curator
160-2	gravity corer	SO165-VL-carb-14	1	carb.	90 - 110 cm	Brückmann
160-2	gravity corer	SO165-VL-carb-15	1	carb.	90 - 110 cm	Brückmann
160-4	gravity corer	SO165-VL-carb-11	1	carb.	max. 100 cm	Brückmann
160-4	gravity corer	SO165-VL-carb-12	1	carb.	max. 100 cm	Brückmann
160-4	gravity corer	SO165-VL-carb-13	1	carb.	max. 100 cm	Brückmann
161	TV-MAC-1-1	VL-SO165-2/k-10	30-50ml	water	bottom water	Abegg
161	TV-MAC-1-2	VL-SO165-2/k-10	30-50ml	water	bottom water	Abegg
162-1	TV-G-3	SO165-VL-carb-1	1	carb.	surface grab	VL-AE
162-1	TV-G-3	SO165-VL-carb-2 to 8	7	carb.	surface grab	VL-AE
162-1	TV-G-3	SO165-VL-carb-9	1	carb.	surface grab	VL-AE
162-1	TV-G-3	SO165-VL-carb-10	1	carb.	surface grab	VL-AE
168-1	TV-MUC-41	VL-SO165-1/1-11	> 1000 ml	water	bottom water	Nauhaus
168-1	TV-MUC-41	VL-SO165-1/1-12	> 1000 ml	water	bottom water	Nauhaus
168-1	TV-MUC-41	VL-SO165-1/1-13	> 1000 ml	water	bottom water	K. Nauhaus
168-1	TV-MUC-41	VL-SO165-1/1-14	> 1000 ml	water	bottom water	K. Nauhaus
168-2	TV-MUC-42	VL-SO165-1/1-8	> 1000 ml	water	bottom water	T. Treude
168-2	TV-MUC-42	VL-SO165-1/1-9	> 1000 ml	water	bottom water	T. Treude
168-2	TV-MUC-42	VL-SO165-1/1-10	> 1000 ml	water	bottom water	T. Treude
169	TV-G-4	VL-SO165-2/k-11 to 13	3 * 100 ml	water	Gas hydrate melt	F. Abegg
169	TV-G-4	VL-SO165-2/k-15	1 * 100 ml	water	Gas hydrate melt	F. Abegg
169	TV-G-4	VL-SO165-2/k-16 to 18	3 * 100 ml	water	Gas hydrate melt	F. Abegg
169	TV-G-4	VL-SO165-2/k-20 to 21	3 * 100 ml	water	Gas hydrate melt	F. Abegg
169	TV-G-4	SO165-VL-carb-16 to 30	15	carb.	surface grab	VL-AE
170	TV-MAC 2	SO165-VL-carb-31	1	carb.	on top	M. Drews
	TV-MAC 3	SO165-VL-carb-32	1	carb.	not defined	M. Drews
	TV-MAC 3	SO165-VL-carb-33	1	carb.	not defined	M. Drews
	TV-MAC 3	SO165-VL-k-MAC3	40 ml	water	bottom water	M. Drews
175-1	TV-MUC-43	VL-SO165-1/1-19	> 1000 ml	water	bottom water	M. Drews
175-2	TV-MUC-44	VL-SO165-1/1-24	> 1000 ml	water	bottom water	K. Nauhaus
175-2	TV-MUC-44	VL-SO165-1/1-25	> 1000 ml	water	bottom water	K. Nauhaus
175-2	TV-MUC-44	VL-SO165-1/1-26	> 1000 ml	water	bottom water	K. Nauhaus
175-2	TV-MUC-44	VL-SO165-1/1-27	> 1000 ml	water	bottom water	K. Nauhaus
178	CTD	VL-SO165-1/1-67 to 94	> 1000 ml	water	water col. prof.	J. Greinert
184-1	gravity corer	SO165-VL-carb-34 to 41	8	carb.	see core log	Brückmann
184-2	gravity corer	SO165-VL-carb-42 to 46	5	carb.	see core log	Brückmann
188-1	TV-G-5	SO165-VL-carb-47 (1-20)	20	carb.	surface grab	VL-AE
188-1	TV-G-5	SO165-VL-carb-48	1	carb.	surface grab	VL-AE
188-2	TV-G-6	SO165-VL-carb-49 & 50	2	carb.	surface grab	VL-AE
190-1	TV-MUC-46	VL-SO165-1/1-29 & 30	> 1000 ml	water	bottom water	K. Nauhaus
190-2	TV-MUC-47	VL-SO165-1/1-28	> 1000 ml	water	bottom water	M. Drews
190-2	TV-MUC-47	SO165-VL-carb-69 to 76	8	carb.	1 - 20 cm	M. Drews
190-3	TV-MUC-48	VL-SO165-2/2-97 & 98	> 1000 ml	water	bottom water	K. Nauhaus
191-2	CTD-63	VL-SO165-1/1-31-49/2-56-66	> 1000 ml	water	tow-jo CTD	J. Greinert
194-1	gravity corer	SO165-VL-carb-51(1-5)	5	carb.	complete core	Brückmann
194-2	gravity corer	SO165-VL-carb-52 to 68	22	carb.	see core log	Brückmann
197-1	TV-G-8	SO165-VL-carb-77 to 81	5	carb.	surface grab	VL-AE
197-1	TV-G-8	VL-SO165-2/k-36	60 ml	water	Gas hydrate melt	VL-AE
200	TV-MAC 5	VL-SO165-2/k-37	80 ml	water	bottom water	M. Drews
200	TV-MAC 5	VL-SO165-2/Glasampulle 1		gas	gas of bottom water	J. Greinert
209-2	gravity corer	SO165-VL-carb-82 & 83	6	carb.	0-1 cm & 43 cm	Brückmann
210	gravity corer	SO165-VL-carb-84 & 85	2	carb.	100 cm & 200 cm	Brückmann
218-2	TV-G-11	SO165-VL-carb-86	1	carb.	surface grab	VL-AE
218-2	TV-G-11	SO165-VL-carb-87	1	carb.	surface grab	VL-AE
218-2	TV-G-11	SO165-VL-carb-88	6	carb.	surface grab	VL-AE
218-2	TV-G-11	VL-SO165-1/1-52		sponge	surface grab	VL-AE
218-3	TV-G-12	SO165-VL-carb-89	1	carb.	surface grab	VL-AE
230-1	TV-G-13	SO165-VL-carb-90	1	carb.	surface grab	VL-AE
230-1	TV-G-13	SO165-VL-carb-91	1	carb.	surface grab	VL-AE
230-2	TV-G-14	SO165-VL-carb-92	1	carb.	surface grab	VL-AE
230-2	TV-G-14	VL-SO165-1/1-45	1	div. biol.	surface grab	VL-AE

Sample Processing and First Results:

SO165 was for subproject 3 a pure sampling campaign and no on-board analytics could be conducted.

Carbonate samples were mechanically cleaned, washed with seawater, air-dried under dust avoiding coverage and wrapped in kim wipes and cling film before package in closed transport boxes.

Water samples were on-board filtered (0.45 μm mesh size) under Argon atmosphere directly after recoverage and acidified to 3% of HNO_3 (p.a. double distilled).

The Thermal Ionisation Mass Spectrometer (TIMS) measurements of U, Th, Ra and Sr isotopes are in progress at the GEOMAR research center and samples for thin section, XRD mineral identification, REE-pattern and trace element analyses are under preparation.

First priority is given to the time series investigation of two large carbonate samples (each approx. 300 kg and covering 1 m growth profile from different sites of the SE-Knoll) and aragonite precipitates which were sampled in direct contact with gas hydrate. The subsequent analytical strategy is depending on these results.

5.15.1 *Microbial Ecology*

T. Treude, W. Ziebis

Anaerobic oxidation of methane in the sediment

The major aim of this study was the investigation of microbial anaerobic oxidation of methane (AOM) and sulfate reduction (SR) in methane enriched surface sediments at Hydrate Ridge. At this site methane is oxidized with sulfate by a consortium of methane-oxidizing archaea and sulfate reducing bacteria (Boetius et al., 2000) via the following net equation:



Fields with distinct bacterial mats (*Beggiatoa*) and clams (*Calyptogena* or *Acharax*) were sampled to investigate the coupling of methane and sulfate cycles. The presence of *Beggiatoa*, *Calyptogena* and *Acharax* indicates a high production of hydrogen sulfide in the surface sediment as these organisms use sulfide as an energy source. Fluxes of sulfide are highest at *Beggiatoa*-fields, followed by *Calyptogena*- and *Acharax*-fields (Sahling et al., 2002). The production of sulfide at Hydrate Ridge is directly coupled with SR and therefore as well with AOM.

Methods

Samples were obtained from sediment cores, which were retrieved by a TV-guided multicorer (Tab. 5.15.1.1). Three parallel cores were investigated per each multicorer. One of the three cores was taken prior to subsampling to measure microsensor profiles in the undisturbed sediment at in-situ temperature. Carbonates, which were located at the top of the sediment and might result from AOM, were frozen for biomarker investigations. Altogether 18 subcores (with an inner diameter of 2.6 cm) were taken out of the three cores. Six subcores were split into 1 cm intervals and fixed for the following measurements:

- sediment methane concentration
- sediment sulfate concentration
- $\delta^{13}\text{C}$ of the sediment methane and carbon dioxide
- porosity of the sediment
- bacteria counts
- fluorescence in situ hybridization (FISH, molecular identification method for bacteria)

To measure AOM and SR, radioactive tracers of methane ($^{14}\text{CH}_4$) and sulfate ($^{35}\text{SO}_4$) were injected separately into 5 subcores and incubated for 24 h at in situ temperature. After incubation, the subcores were split into 1 cm intervals and fixed to stop the microbial activity. Control subcores were first fixed and then added with radiotracers. Another method, using silver foils (Krumholz et al., 1997), was used to get a high resolution of SR in subcores added with $^{35}\text{SO}_4$. All samples will be analyzed in the home laboratory. A preliminary result of beta-imager measurements of the silver foils is shown in Fig. 5.15.1.1. The beta-imager picture shows counts per minutes of radioactive sulfur on the foil.

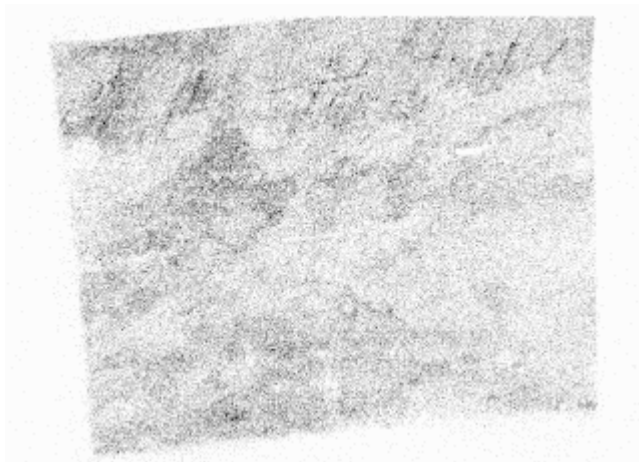


Fig.: 5.15.1.1. Beta-imager picture of the SR-silver foil.

Microprofiles

O₂ and H₂S microgradients as well as pH profiles were measured in intact cores immediately after retrieval in the cold room at 3 °C.

O₂ microgradients

Vertical oxygen distribution was measured by Clark-type microelectrodes provided with a built-in reference and a guard cathode (Revsbech and Jørgensen, 1986; Revsbech, 1989). The electrodes were purchased from UNISENSE, Denmark and had a sensing tip of 15 – 20 μm, a stirring sensitivity of < 2% and a 90% response time ≤ 1s. Electrode currents had a linear response to 0% and 100 % air saturation of O₂. Linear calibration was done at 3°C in 100% saturated seawater (35‰) and nitrogen purged seawater with 0 % oxygen saturation.

H₂S microgradients

The H₂S microsensors are miniaturized amperometric sensors with an internal reference and a guard anode (Jeroschewsky et al., 1996).

Calibration is performed after the sensor signal has stabilized during pre-polarization. The H₂S microsensors respond linearly over a certain range. A stock solution of S²⁻ (i. e. 100 mM) is prepared from dissolving Na₂S in N₂-flushed 0.1 M NaOH in a closed container. The final concentration of stock solution was determined spectrophotometrically (Cline 1969). The signal zero is obtained by immersing the sensor tip into the calibration buffer. Further calibration points are prepared by injecting suitable amounts of the S²⁻ stock solution into a defined volume of calibration buffer (100 mM phosphate buffer, pH 7) with a micro-syringe. These H₂S sensors have been successfully applied in marine ecology (Kuehl et al., 1998) and were purchased from UNISENSE, Denmark.

A new hydrogen sensor (UNISENSE) was also successfully used for high resolution measurements in intact cores, the results are being processed.

Parallel to H₂S microprofiles, pH was measured with long Needle Combination pH Electrode (Diamond General) at 1-mm to 5-mm intervals.

The electrodes were attached to a micromanipulator, which was driven by a stepping motor (Oriental Motor), signals were amplified and transformed to mV by a picoammeter (Unisense PA 2000) and data were collected directly on a computer.

Measurements were performed in vertical increments of typically 100 μm -200 μm for oxygen and 200 μm to 500 μm for H_2S .

Preliminary results of microsensors measurements

1. Micro profiles were measured in cores retrieved from *Beggiatoa*- or *Calyptogena*-fields prior to geochemical analyses and sub-coring for incubation experiments of sulfate reduction and methane oxidation rate determinations (cores from TV-MUC stations # 27, 52, 60, 76, 110, 115, 138). Some profiles are shown in Fig. 5.15.1.2, 3, 4 and 5.

2. In addition, high-resolution measurements were performed in cores from *Beggiatoa*-fields that were subsequently used for microbiological investigations of the filamentous sulfur oxidizing bacteria. The focus of these measurements were high resolution oxygen and sulfide gradients through the bacterial mat (cores from TV MUC stations # 41, 75, 109, 125). Some profiles through mats can be seen in Fig. 5.15.1.6 and 7.

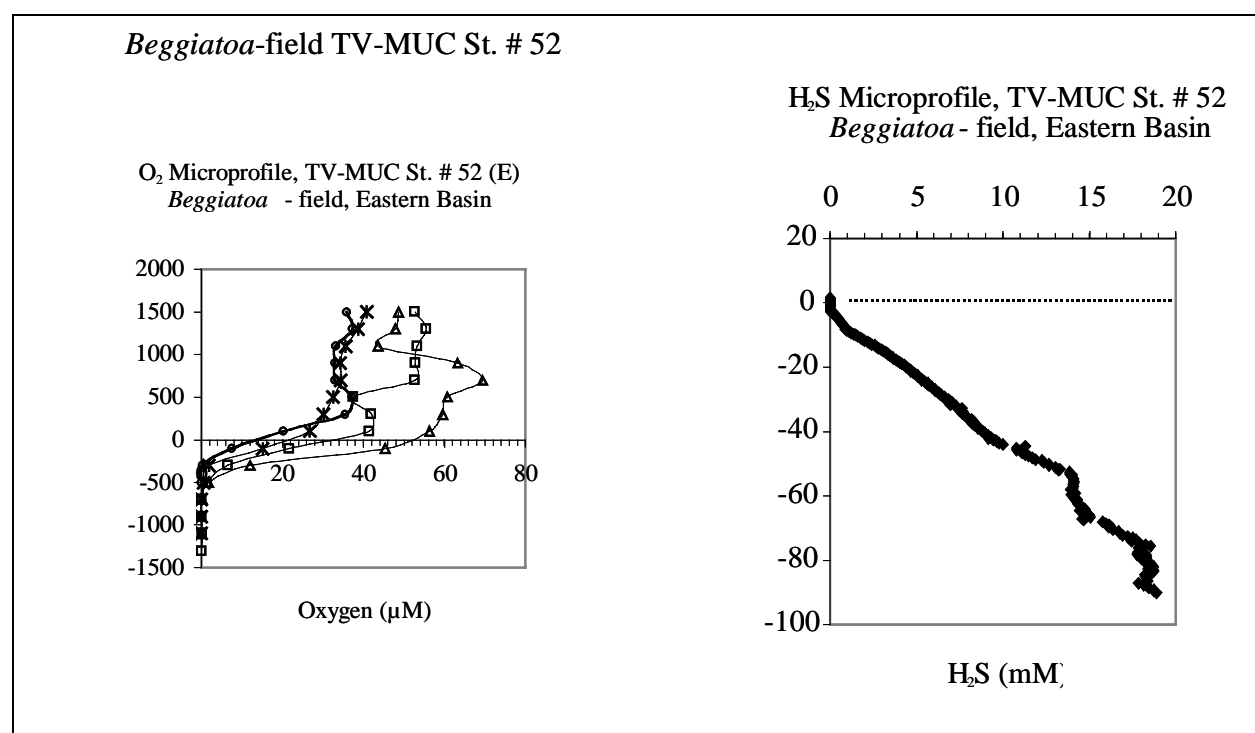


Fig. 5.15.1.2: Oxygen and H_2S -profile of station # 52 (*Beggiatoa*-field).

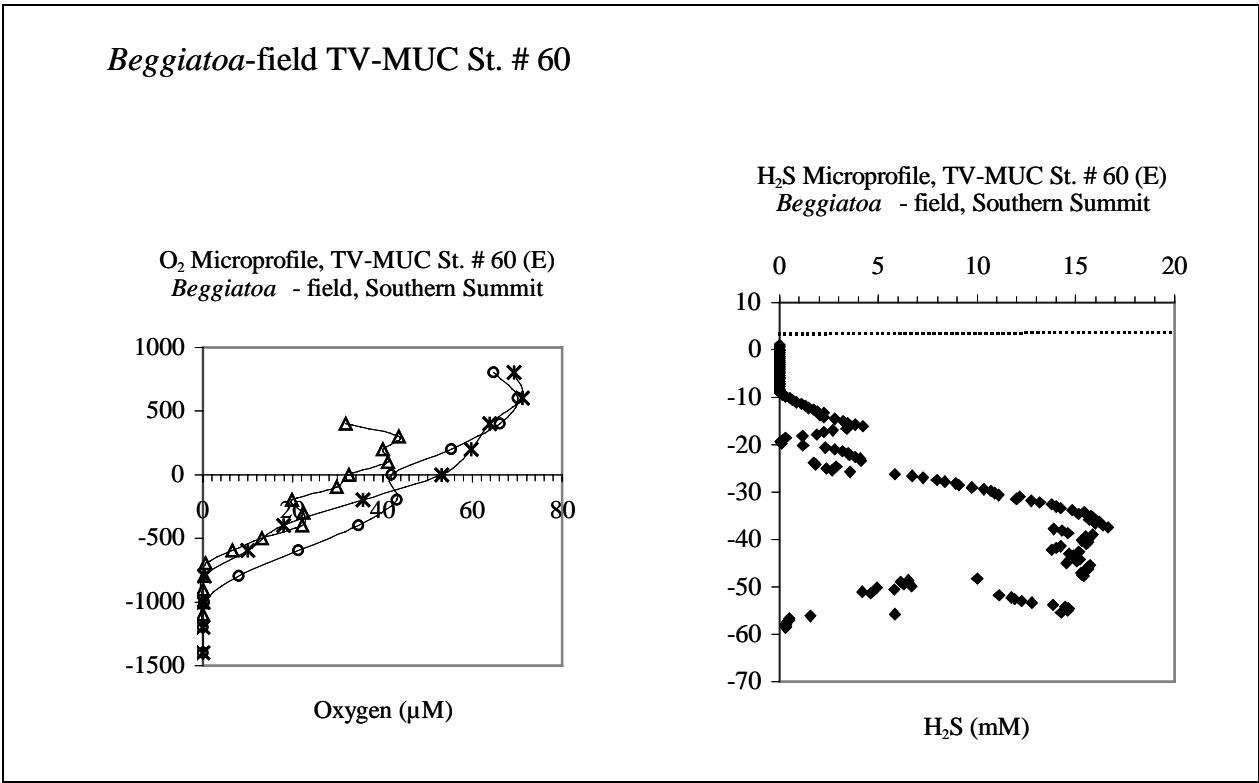


Fig. 5.15.1.3: Oxygen and H₂S-profile of station # 60 (*Beggiatoa*-field).

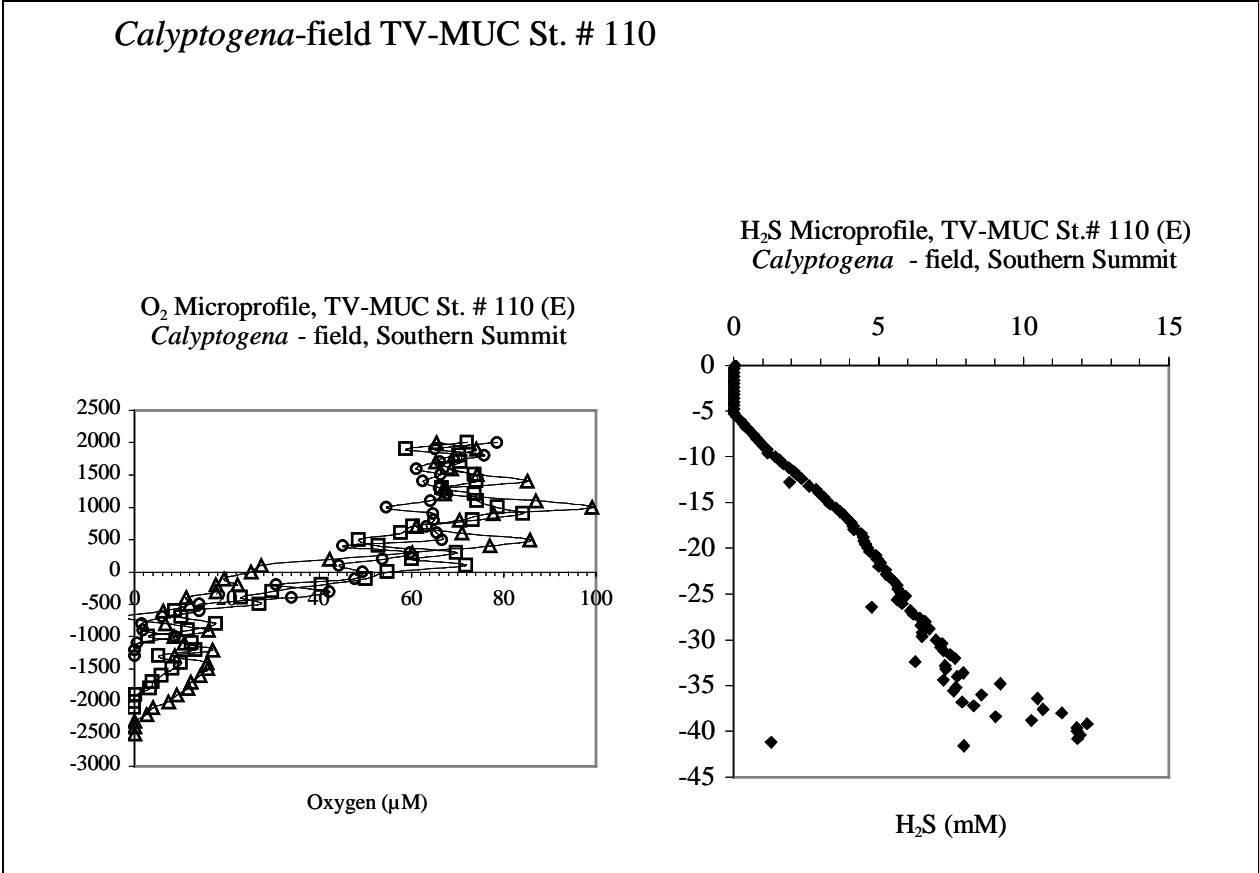


Fig. 5.15.1.4: Oxygen and H₂S-profile of station # 110 (*Calyptogena*-field).

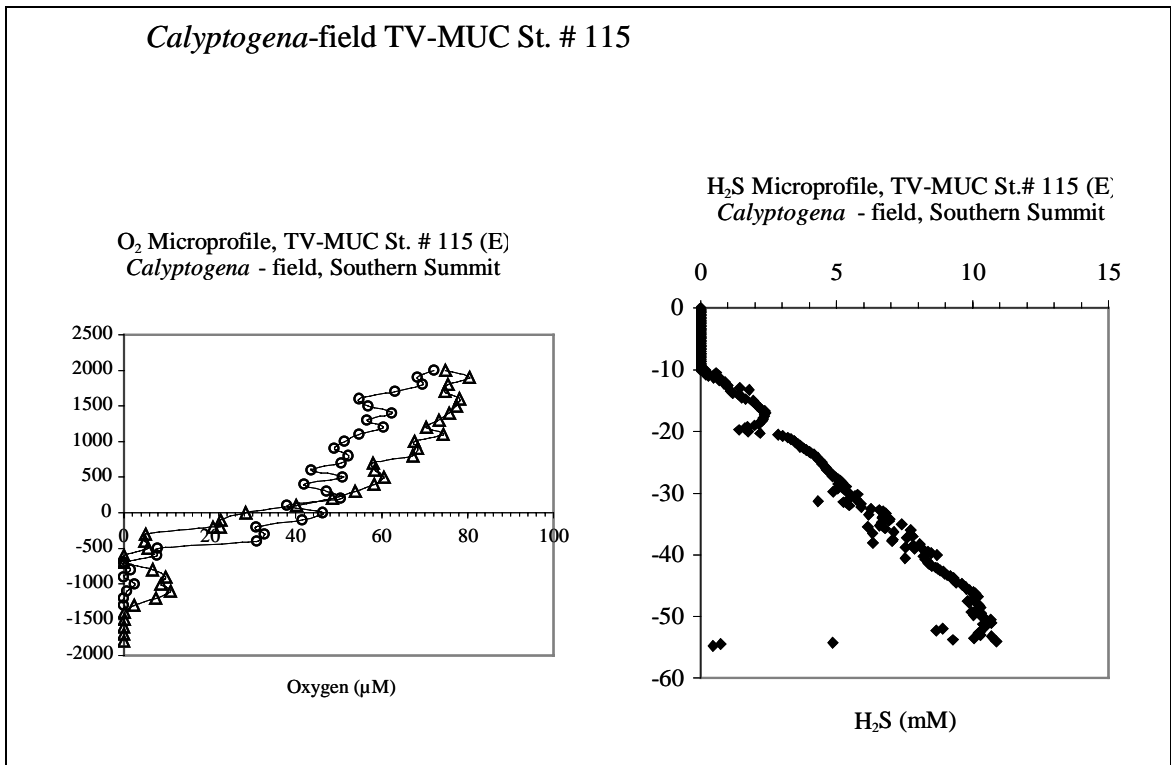


Fig. 5.15.1.5: Oxygen and H₂S-profile of station # 115 (*Calyptogena*-field).

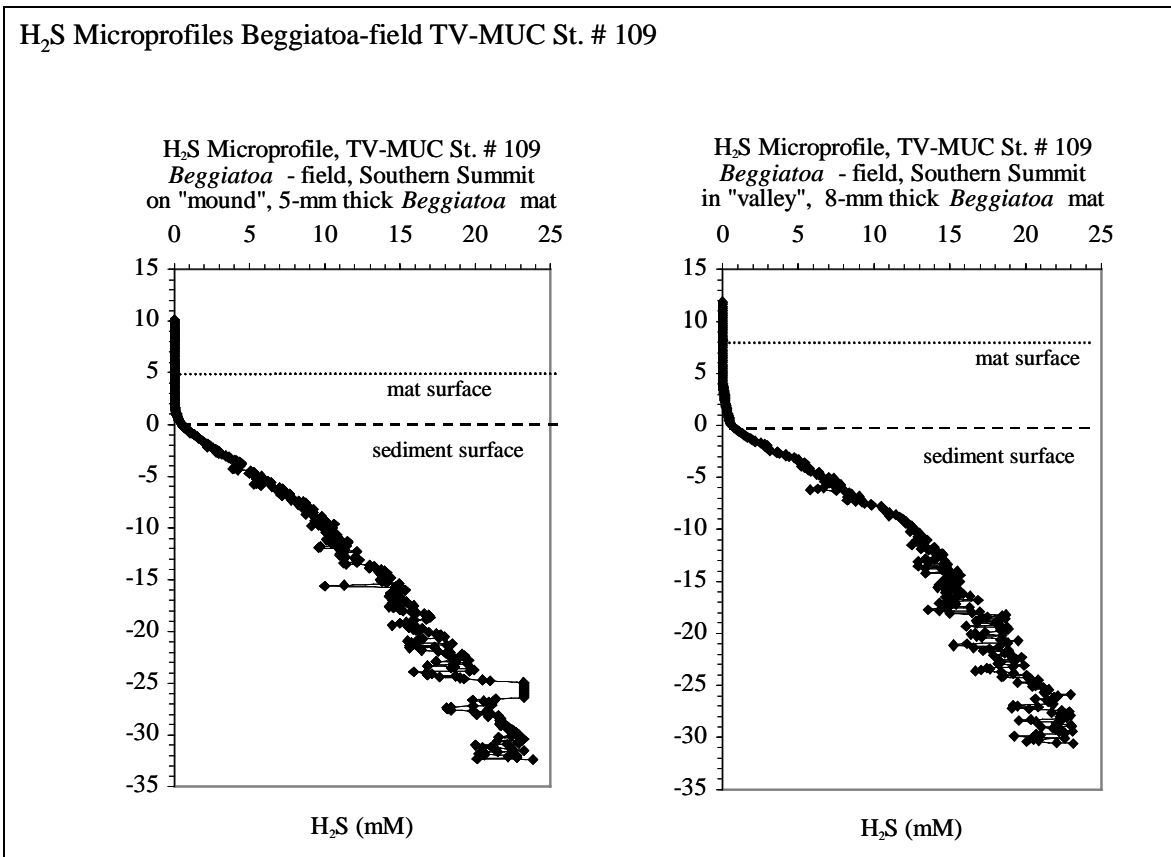


Fig. 5.15.1.6: Focus on bacterial mat: oxygen and H₂S-profile of station # 109 (*Beggiatoa*-mat and sediment).

O₂/H₂S Microprofiles (detail), TV-MUC St. # 109,
Beggiatoa-field, Southern Summit

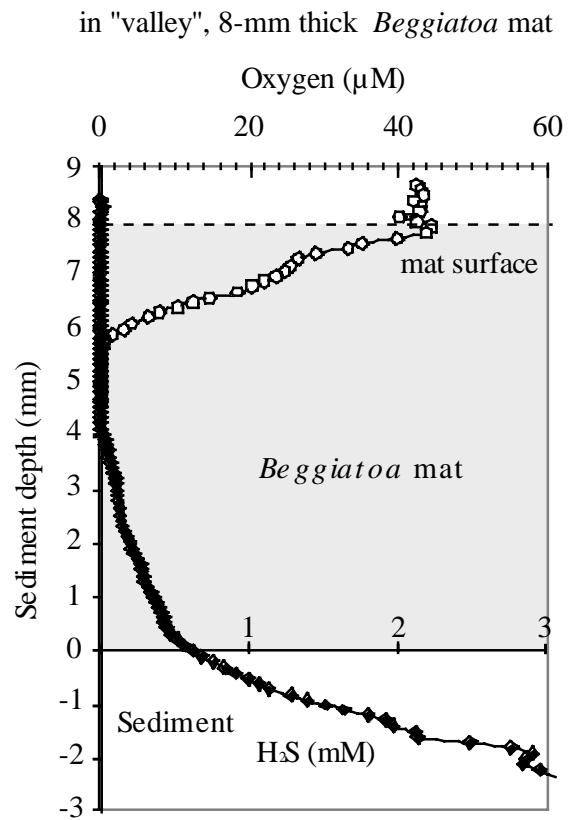
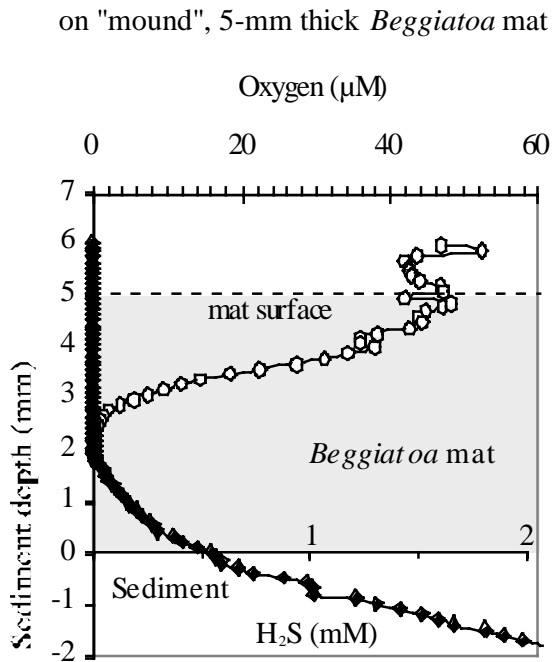


Fig. 5.15.1.7: Focus on bacterial mat: oxygen and H₂S-profile of station # 109 (detailed profile through the *Beggiatoa* mat).

The core from station # 109 had a thick (5 – 8 mm) bacterial mat (Fig. 5.15.1.8). The sediment surface was characterized by a strong topography of „mounds“ and „valleys“ that had bacterial mats of different thicknesses.



Fig. 5.15.1.8: Bacterial mat on top of the sediment of core station # 109.

The core from station # 41 was taken in the Eastern Basin. The surface of the core looked at first sight like a bacterial mat, but all the filamentous bacteria (most probably *Thiotrix*) were attached to hard substrates, predominantly to the shells of living snails (Fig. 5.10.1.9, scale bar 1 cm). There were 39 snails on the surface of this core, all of them had a fur of bacteria. The microsensor profile of this special core is shown in Fig. 5.15.1.10.

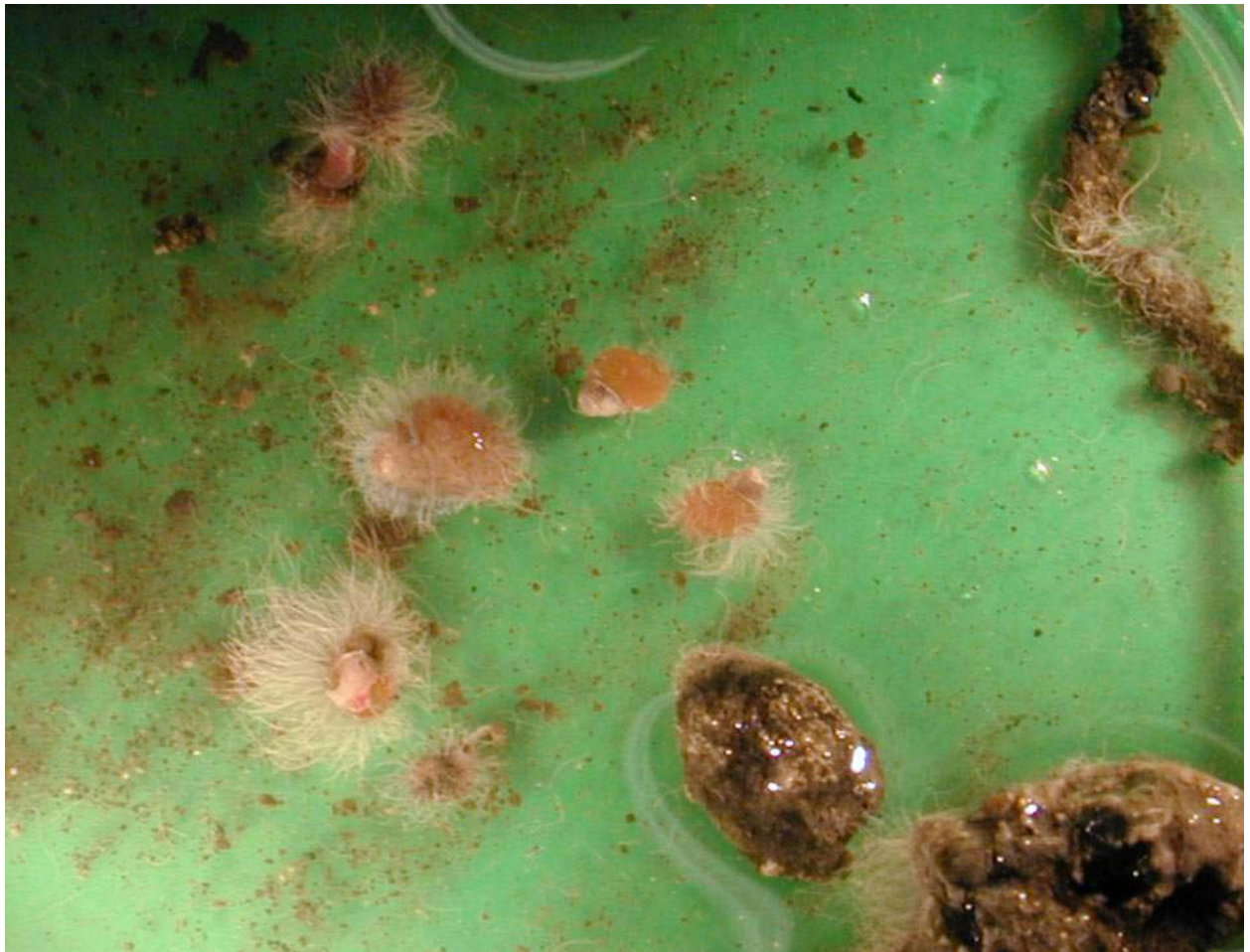


Fig. 5.15.1.9: Snails with attached filamentous bacteria from core station # 41.

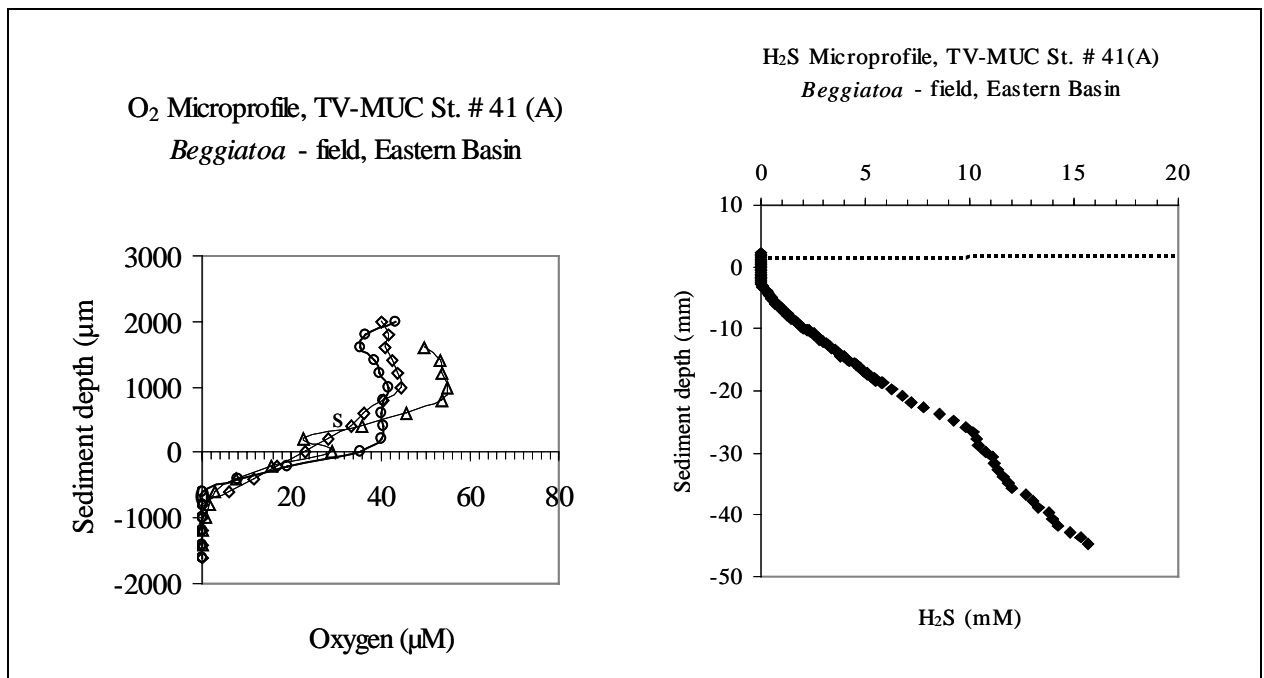


Fig. 5.15.1.10: Oxygen and H₂S-profile of station # 41.

Anaerobic oxidation of methane in gas hydrates

Gashydrate samples, taken either from TV-grabs or gravity cores (Tab. 5.10.1.1) were investigated for microbial activity. Until now no data are available about AOM and SR activities in pure gas hydrates or in the sediments located between gas hydrates. Three types of gas hydrates were sampled: 1) gas hydrates without sediment, 2) gas hydrates with small amounts of sediment 3) gas hydrates with large amounts of sediment (the amount of sediments will be defined by the porosity of the samples). The gas hydrates were melted anaerobically in a 1L glass bottle with an outlet for the expanding gas. Subsamples of the gas hydrate-water or gas hydrate-water-sediment mixture were taken to measure the parameters already described for multicorer samples. AOM and SR was measured in 5 ml Hungate-tubes. All samples will be analyzed in the home laboratory.

Calyptogena sulfide uptake

The vesicomid clams of *Calyptogena* at Hydrate Ridge are chemoautotrophic symbionts (Sahling et al., 2002). They harbor sulfide-oxidizing bacteria in their gills. The bacteria are supported with oxygen and sulfide via the blood circulation of the clam. Sulfide passes the clam via its foot, which is usually drilled into the sulfidic sediment horizon. To demonstrate the sulfide uptake by the clams and sulfide oxidation by the bacterial symbionts, respectively, specimens of *Calyptogena* were incubated in a 1 L aquarium filled with about 0.5 L sulfidic sediment (sampled from *Calyptogena* covered sediment cores) and 0.5 L bottom water. Radioactive sulfate ($^{35}\text{SO}_4$) was injected into the sediment. The radioactive sulfate, reduced to sulfide by sulfate reducing bacteria in the sediment, diffused into the food of the clam. After some days of incubation at in situ temperature, the clams were fixed in 4% formaldehyde and stored in 1:1 PBS/Ethanol. In the home laboratory the clams will be sliced and radioactivity of the slices will be measured by betaimaging.

Aerobic oxidation of methane in the water column

The major part of methane, which passes the sediment-water interface, is microbiologically oxidized with oxygen before it reaches the atmosphere. Water samples of CTD hauls (Tab. 5.10.1.1) were incubated with radioactive methane (C^3H_4) to measure the rates of aerobic oxidation of methane (AEOM) in the water column above Hydrate Ridge. Vertical CTD's, located at different sites above Hydrate Ridge, as well as horizontal CTD's drawn across the southern and northern summit, respectively, were investigated. The samples were incubated for 4 days at 4°C. After incubation the samples were fixed with 37% formaldehyde. Controls were first fixed and then added with radioactive methane. All samples will be analyzed in the home laboratory.

5.15.2 *Beggiatoa* mats at Hydrate Ridge

A. Preisler, W. Ziebis,

Aim of study

The aim of this study was to investigate the biomass and the size class composition of *Beggiatoa*-mats, how deep they move down into the sediment and how they depend on the sulfide and oxygen gradients.

At Hydrate Ridge *Beggiatoa*-mats are taken as an indicator for subsurface gas hydrates. High sulfide concentrations, reaching the surface, in combination with low oxygen concentrations in the water column provide favorable conditions for the formation of *Beggiatoa*-mats.

Methods

At 6 different stations sediment cores, taken by a video-guided multiple corer, were used to investigate the biomass of *Beggiatoa*. The biomass was calculated by counting and measuring *Beggiatoa* filaments in a defined sample volume. The species composition was determined by randomly taking out about 50 filaments, and measuring width and length by microscoping. One core was transported back in a cooling chamber for DNA analysis. Some *Beggiatoa* filaments of each size class were picked out and frozen in distilled water for analysis of internal nitrate and the corresponding cations. At all stations sulfide and oxygen profiles were measured and samples were taken to determine porosity, elemental sulfur and pore water nitrate (Tab.5.10.2.1).

Preliminary results

The *Beggiatoa*-mats of Hydrate Ridge showed patchiness. The biomass was restricted to the surface and no *Beggiatoa* was found deeper than 2 cm. The mats of highest biomass (89 g/m² - station 125; 41.8 g/m² station 75) contained *Beggiatoa* filaments of 50-75 µm width. In a *Calyptogenia*-field, which was neighboring a *Beggiatoa*-mat, the size classes of *Beggiatoa* filaments were the same but the biomass was one order of magnitude lower (7.5 g/m² - station 129).

At station 42 and 50 the biomass and the size classes of *Beggiatoa* filaments were clearly smaller as well (station 42: biomass: 2.2 g/m²-, filament width: 3-5µm/10µm; station 50: biomass: 4.9 g/m², filament width: 10µm/30µm) (Figure5.15.3.1).

The biggest filaments were found at station 29 (115 µm width).

At stations with conspicuous *Beggiatoa*-mats, sulfide was consumed inside the mat showing a concave up profile. Oxygen penetrated the mat only few millimeters (Figs 5.15.1.6 and 5.15.1.7 of station 109 in chapter 5.15.1).

Tab 5.15.2.1: Sample processing protocol.

Date	Station No.	Instrument	Latitude (°N)	Longitude (°W)	Water depth (m)	Analysis
17.7.	42	TV-MUC 7	44:34.2401	125:08.7734	878.3	a) biomass b) filament size c) analysis of internal and environmental nitrate and sulfur d) internal kations e) porosity
18.7.	50	TV-MUC 10	44:34.3441	124:59.8228	880	a) biomass b) filament size c) analysis of internal and environmental nitrate and sulfur d) internal kations e) porosity
22.7.	75	TV-MUC 18	44:34.2141	125:08.7740	777.8	a) biomass b) filament size c) internal kations d) porosity
30.7.	124	TV-MUC 28	44:34.1610	125:08.7990	778	a) biomass (reference) b) filament size c) analysis of internal and environmental nitrate and sulfur d) porosity
30.7.	125	TV-MUC 29	44:34.2225	125:08.7944	779.8	a) biomass b) filament size c) analysis of internal and environmental nitrate and sulfur d) internal kations e) porosity
30.7.	129	TV-MUC 31	44:34.1935	125:08.7692	775.5	a) biomass b) filament size c) analysis of internal and environmental nitrate and sulfur d) porosity
16.7.	29	TV-MUC 5	44:34.1600	125:08.8160	776	analysis of internal kations
17.7.	41	TV-MUC 6	44:34.2770	124:59.9590	878.3	a) analysis of environmental nitrate and sulfur b) porosity
24.7.	88	TV-Muc20	44:34.2831	125:59.9470	885	nitrate consumption experiment (reference)
28.7.	109	TV-Muc24	44:33.2162	125:08.1100	779	a) filament size b) analysis of internal and environmental nitrate and sulfur c) porosity d) nitrate consumption experiment (failed) e) DNA analysis
28.7.	113	BCL-1				filament size

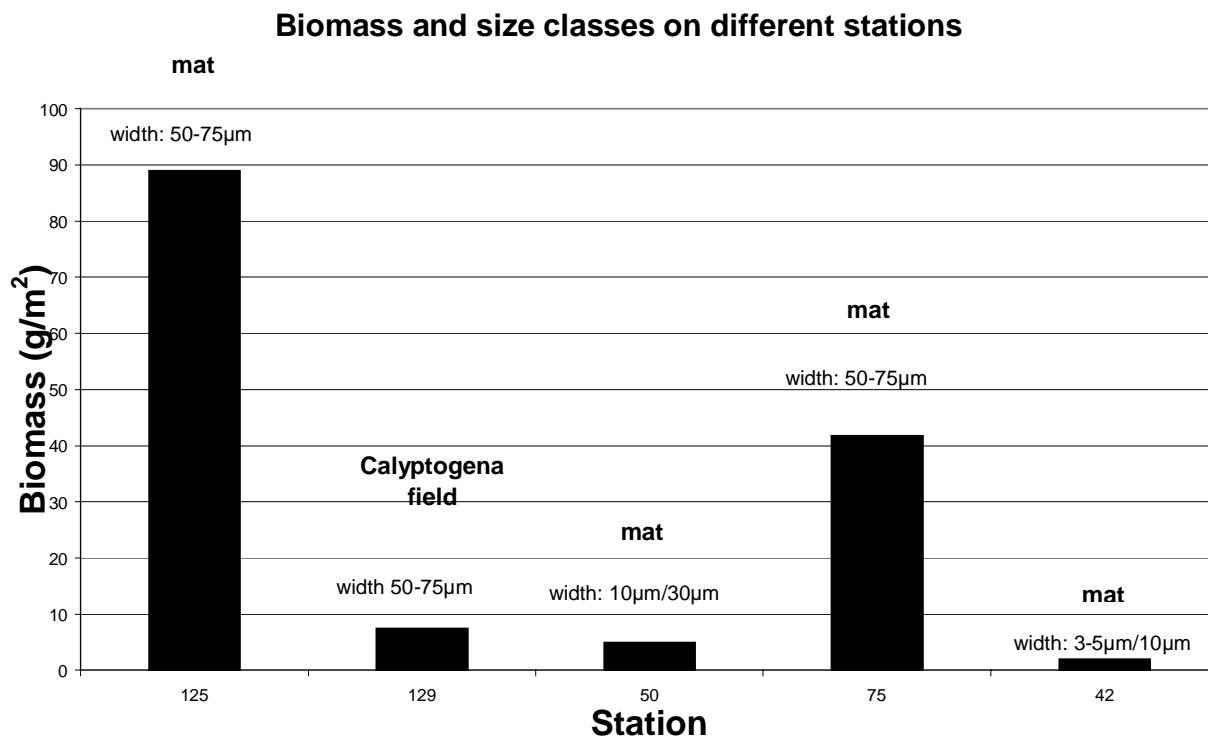


Fig. 5.15.2.1. Biomass and size classes at different stations.

5.15.3 Microbial Ecology and Physiology

K. Nauhaus

Aim of the Study and Sample Material

In vitro depth profiles of anaerobic oxidation of methane in the sediment

The anaerobic oxidation of methane (AOM) coupled to the reduction of sulfate is a long known process in marine sediments. However the establishment of a laboratory culture or enrichment was never successful. With samples from the TECFLUX Cruise SO148 it was for the first time possible to establish the process of AOM *in vitro* under laboratory conditions (Nauhaus et al. 2002). Some first physiological experiments were carried out with sediment slurry incubations. Investigations will now concentrate on the *in vitro* measurement of depth profiles with fresh sediment samples from different locations at the southern summit of the Hydrate Ridge. A covering with mats of the sulfide oxidizing bacterium *Beggiatoa* indicates sites with high sulfide concentrations due to high AOM activity. These will be compared to sites with lower AOM activity indicated by sediment colonization with the vesicomid clams *Calyptogena* or with the solemyid bivalves *Acharax* (Sahling et al. 2002). Both of these organisms harbor symbiotic sulfide oxidizing bacteria. Also a reference site with no indication for elevated sulfide concentrations will be investigated. The sediment samples were taken from multicorers at depth intervals of 0-1 cm, 1-4 cm, 4-10 cm, 10-15 cm and 15-20 cm from the top of the core. The experiments will be carried out in the home laboratory.

In vitro AOM activity in gashydrates and the associated sediment

AOM activity and cells of the AOM consortium have so far only been detected in sediments above gas hydrate deposits. A new aspect will be to investigate the *in vitro* and *ex situ* (see also Tina Treude, this report) activity and the abundance of bacteria (see also Tina Lösekann, this report) performing AOM directly associated with gas hydrates. Gas hydrates without sediment, with a small amount of surrounding sediment and sediment containing gashydrates were sampled to investigate the *in vitro* AOM activity in these habitats. The hydrates were sampled from TV-Grab samples into glass bottles and melted under anoxic conditions with a gas outlet. The melted hydrate was stored anoxically at 4°C. Some samples were incubated during the cruise. For the length of the cruise no activity could be observed. Most of the experiments will be carried out in the home laboratory.

AOM activity in deeper sediment layers

Multicorer samples only reach a depth of about 20 to 30 cm. Gashydrates in the sediment and sulfate in the porewater are strong arguments for AOM activity to occur in deeper sediment layers. *In vitro* experiments will be carried out with samples from a 1.5 m piston corer modified as a gravity corer. The core contained distinct gashydrate layers at about 1 and 1.2 m depth and was sampled in 5 cm intervals in this section and in 10 cm intervals in the remaining core. The sediment was stored in 5 ml syringes and in aluminum bags which were sealed after intensive gassing with N₂ to remove the oxygen and stored at 4°C, until further processing in the home laboratory.

Material and Methods

Sediment samples were taken from multiple corers, TV-grabs and gravity cores (Tab. 5.15.3.1). The Sediment was stored in glas bottles under anoxic conditions at 4°C until further processing in the home laboratory.

Tab. 5.15.3.1: List of samples, stations and devices

device	Nr.	Station	Position N	Position W	Sample type
TV-Muc	39	153-3	44°34,1274	125°08,8178	Beggiatoa
	41	168-1	44°34,1956	125°08,8326	Beggiatoa
	43	175-1	44°34,2102	125°08,7967	Beggiatoa
	44	175-2	44°34,1990	125°08,7820	Calypptogena
	46	190-1	44°34,2100	125°08,7762	Acharax
	48	190-3	44°34,2918	125°08,7536	Reference
	53	220	44°34,2070	125°08,8035	Beggiatoa
TV-Grab	2	154	44°34,2114	125°08,8031	Gashydrate
	4	169	44°34,2027	125°08,0900	Gashydrate
	8	197-1	44°34,2100	125°08,8120	Gashydrate
Piston corer modified as gravity corer	1	167-1	44°34,2040	125°08,8120	Sediment
	5	176-3	44°34,204	125°08,807	Sediment

All experiments are and will be carried out in glass tubes (20 ml) with sediment or melted gashydrate, artificial seawater medium and methane in the gas-phase. Sulfide as the product of the reduction of sulfate with methane as the electron donor, is determined as an indicator for AOM activity via the copper-sulfate method (Cord-Ruwisch 1985).

5.15.4 *Molecular Ecology*

T. Lösekann

Objectives

The major aim of this study was to investigate the microbial diversity and community structure in sediments/gas hydrates of Hydrate Ridge applying molecular techniques.

Previous studies have shown that the anaerobic oxidation of methane (AOM) in methane enriched surface sediments of Hydrate Ridge is apparently mediated by highly structured microbial consortia (Boetius *et al.*, 2000). These AOM consortia consist of an inner core of methane-oxidizing archaea (ANME2-group) and an outer shell of sulfate-reducing bacteria (*Desulfosarcina/Desulfococcus* group). However, further microbial associations are known to be capable of oxidizing methane anaerobically (e.g. Michaelis *et al.*, 2002; Orphan *et al.*, 2002). Hitherto no data are available about microorganisms mediating AOM in deeper methane enriched sediment layers or in direct association with gas hydrates. In this study we will focus on the identification of methanotrophic microorganisms in these habitats.

Materials and Methods

All samples were taken at the Southern Summit of Hydrate Ridge. Sites with differences in AOM activity are marked by different sulfide-dependent, chemoautotrophic communities (*Beggiatoa sp.*, *Calyptogenia sp.*, *Acharax sp.*). Surface sediment cores were sampled with TV-guided multicorer, deeper gas hydrate bearing sediment layers were obtained by gravity cores (Tab. 5.15.4.1).

Gas hydrate samples were retrieved by either TV-grabs or gravity cores (Tab. 5.15.4.1). Different kinds of gas hydrates were sampled: a) gas hydrate contaminated with large amounts of associated sediment, b) gas hydrates with small amounts of associated sediment, and c) almost pure gas hydrates. The samples were prepared aboard to perform the following experiments in the home laboratory:

Comparative 16S rDNA analysis. In order to analyze the microbial diversity, sediment and gas hydrate samples will be used for DNA extraction with subsequent construction of 16S rDNA libraries for Archaea and Bacteria and comparative, phylogenetic sequence analysis.

Fluorescence *in situ* hybridization (FISH). FISH experiments allow *in situ* the phylogenetic identification of single microbial cells, the quantification of their abundance, and the detection of potential interactions between different species. Therefore, fixed samples will be stained with DAPI for total cell counts and hybridized with fluorescently labeled 16S rRNA targeted oligonucleotide probes in order to investigate the vertical distribution of different taxonomic groups (e.g. Archaea, Bacteria, sulfate-reducing bacteria, ANME1/2-groups). The abundance of AOM associated microorganisms/consortia in different methane enriched habitats (especially deeper sediment layers, gas hydrates) will be of particular interest.

Sample preparation procedure aboard.

Sediment cores: Sediment subsamples from certain depth intervals (Tab. 5.15.4.1) were stored at 4°C or -20°C, respectively, for subsequent nucleic acid extraction in the home laboratory. In addition, corresponding subsamples were fixed with 3% (w/v) formaldehyde in order to carry out fluorescence *in situ* hybridization experiments in the home laboratory. For this purpose the samples were incubated for 2-4 h in formaldehyde at 4°C, washed twice with 1xPBS and stored in abs. Ethanol/1xPBS (1:1) at -20°C.

Gas hydrates: Gas hydrates with different degrees of purity were melted at 4°C. Subsamples were taken for nucleic acid extraction or fixed for FISH in the home laboratory (see above).

Tab. 5.10.4.1: Sampling protocol

Station No.	Instrument	Sample type	FISH Sediment horizon (cm)
153-4	TV-MUC-40	thin <i>Beggiatoa</i> mat	0-10/10-18 (1/2 cm layers)
154-1	TV-Grab-2	Gas hydrate, low purity*	-
162-1	TV-Grab-3	Gas hydrate, medium purity*	-
167-2	Gravity core-2	Gas hydrate, highest purity*	-
168-1	TV-MUC-41	thin <i>Beggiatoa</i> mat/ <i>Calyptogena</i> field (2 clams)	0-10/10-20 (1/2 cm layers)
169	TV-Grab-4	Gas hydrate, medium purity*	-
175-1	TV-MUC-43	thick <i>Beggiatoa</i> mat	0-10/10-16 (1/2 cm layers)
175-2	TV-MUC-44	<i>Calyptogena</i> field (2 clams)	0-10/10-20 (1/2 cm layers)
176-3	Gravity core-5	Sediment, Gas hydrate bearing	3-148 (5/10 cm layers)
190-1	TV-MUC-46	<i>Acharax</i> field (3 clams)	0-10/10-16 (1/2 cm layers)
190-3	TV-MUC-48	Reference	0-10/10-16 (1/2 cm layers)
197-1	TV-Grab-8	Gas hydrate, medium purity*	-

*purity with respect to the extent of associated sediment

Preliminary results

First FISH experiments confirm the abundance of AMNE1-group archaea and ANME2-group archaea in pure melted gas hydrate samples. The archaeal cells have not been counted yet, but these AOM mediating groups seemed to be predominant in the microbial community.

ANME1-cells were detected as filamentous free-living rods (Fig. 5.15.4.2). Archaea of the ANME2-group were found in associations (Fig. 5.15.4.1). In contrast to the known highly structured Hydrate Ridge consortia, these cells are easily aggregated with apparently no close contact to Eubacteria.

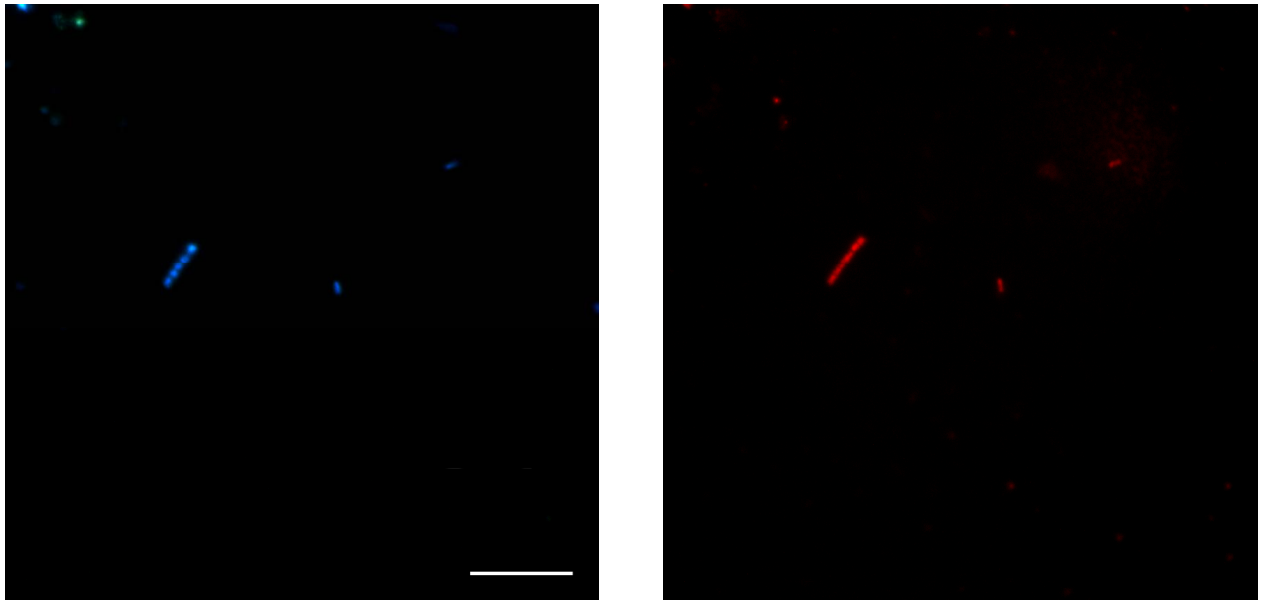


Fig. 5.15.4.1: Epifluorescence micrographs of ANME1-cells in pure melted gas hydrates, DAPI stained (left) and hybridized with a fluorescently labeled oligonucleotide probe specific for the ANME1-cluster (right). Scale bar, 10 μm .

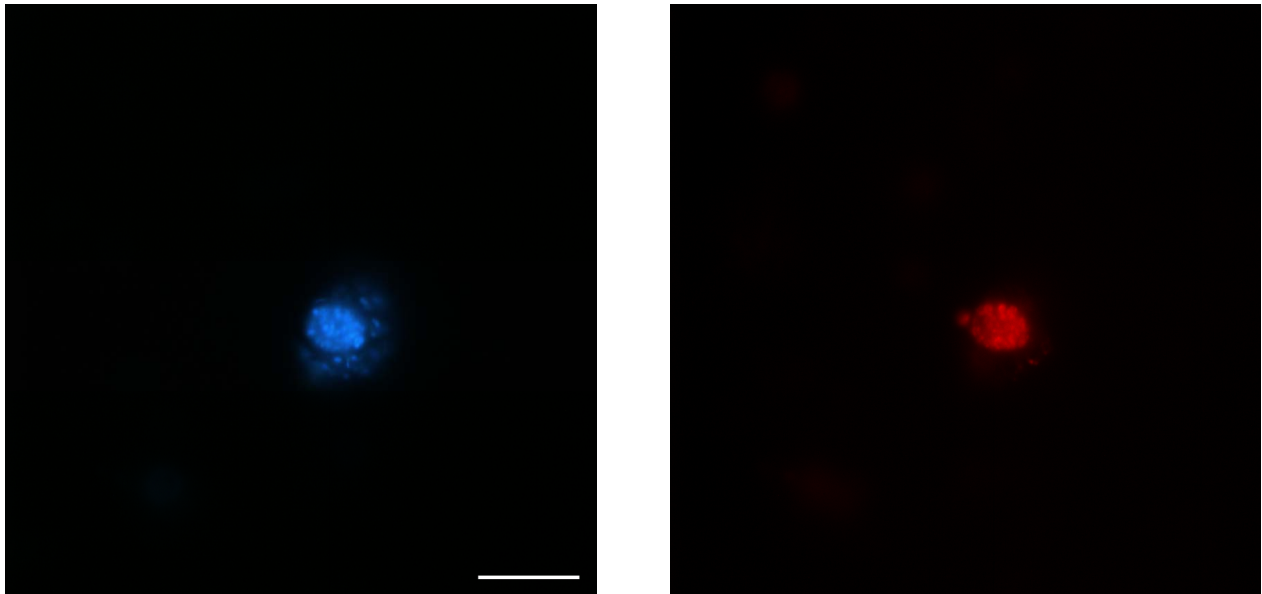


Fig. 5.10.4.2: Epifluorescence micrographs of ANME2-cells in pure melted gas hydrates, DAPI stained (left) and hybridized with a fluorescently labeled oligonucleotide probe specific for the ANME2-cluster (right). Scale bar, 10 μm .

5.16 *Benthic foraminifera*

Petra Heinz

Introduction

Benthic foraminifera are among the most abundant organisms living in deep-sea sediments (Thiel, 1975, 1983; Gooday, 1986; Alongi and Pichon, 1988). Their species composition, abundance and distributional patterns mainly depend on environmental factors, such as food supply and oxygen distribution (e.g. Jorissen *et al.*, 1985). Faunal assemblages of benthic foraminifera in extreme habitats like cold seeps or zones of methane hydrate occurrences are hardly investigated yet. Gas hydrate areas show a high variability of environmental conditions in a very narrow region. The exposure of gas hydrates near the sediment surface and venting processes in the area provides an enormous nutrient and energy pool for benthic life, leading to the formation of a unique ecosystem, where ecological niches and a biological zonation of meio- and macrofauna can establish (Suess *et al.*, 1997, 1999, Bohrmann *et al.*, 2000, Sahling *et al.*, 2002). We want to determine and compare assemblages of benthic foraminifera between these ecological niches, habitat relationships between single niches and between epi- and infaunal communities, and live to dead assemblages (early diagenesis). Results will be compared with those of different other regions and environmental conditions in the deep sea. Methane hydrate and free methane, originating from these hydrates, show very negative carbon isotopic values, that are typical for biogenic produced methane (Cicerone and Oremland, 1988, Kvenvolden, 1995). In fossil records, benthic foraminiferal carbon isotopic oscillations reflected periods of increased sedimentary methane outgassing (Kennett *et al.*, 2000). To study this phenomenon in recent samples, we want to analyse stable isotopes in shells and biomass of foraminifera and compare values with investigated bottom water samples.

Material and methods

For faunal analysis and isotopic studies of foraminiferal shells, cores collected with a TV guided multicorer were taken. Sediment was sliced in half centimetre intervals for the top two centimetres and thereafter in one centimetre slices. The upper 10 cm were stained with a solution of ethanol and Rose Bengal (1 g Rose Bengal in 1 l Ethanol) for fixation and staining of the cytoplasm (to distinguish living and dead specimens). This solution was added to the sediment in approximately equal volume. The Rose Bengal staining method (after Walton, 1952) has its limitations, because it is still under discussion how much time proteins need to degrade after the death of an animal and how long a dead foraminifer will be stained, especially in low oxic and anoxic sediments (Douglas *et al.*, 1980, Bernhard, 1988). To be sure that foraminifera can survive and inhabit these low oxygen but methane and sulfide enriched sediments, some specimen were tested for vitality directly on board using a spectrofluorometry method (Geslin *et al.*, 2001). Sediments were washed very carefully with chilled seawater and vital looking individuals were picked out from different sediment depths and transferred into artificial seawater containing a fluorogenic probe (1 μ M FDA, dissolved in DMSO). After an incubation for 30-36 h, active specimen can be recognised by a colour change of the medium (from white transparent to yellow), that can be measured with a spectrofluorometre.

To analyse stable isotopic values in the bottom water, the overlying water of each core was sampled and each sample was poisoned with mercury chloride. Sediment samples were obtained from lander deployments for isotopic investigations of foraminiferal biomass. Samples were cut in 0.5-cm-slices for the first 2 centimetre and in 1.0 cm slices for the 3. - 5. centimetre. All slices were sieved over a 30 µm mesh screen with seawater and were immediately frozen after sieving. The samples were transported frozen to our laboratory in Tübingen.

Station works

Collected sediment samples were summarised in Table 5.16.1. Sediment and water samples were prepared and fixed immediately after arriving on board and will be analysed in our home laboratory. Vital tests were made with specimens from 2 different biozones: from bacterial mats and from control sediment without bacteria or clams.

Tab. 5.16.1: Collected samples during SO 165-1.

instrument	sample collection		
	faunal analysis	isotopic analysis	vital test
BIGO-1	no	biomass	
BIGO-2	no	biomass	
BIGO-3	no	biomass	
BIGO-4	no	biomass	
BIGO-5	no	biomass	
BIGO-6	no	biomass	
TV-MUC-5	yes	bottom water / shell	
TV-MUC-6	yes	bottom water / shell	
TV-MUC-9	yes	bottom water / shell	
TV-MUC-10	yes	bottom water / shell	yes
TV-MUC-14	yes	bottom water / shell	
TV-MUC-17	yes	bottom water / shell	
TV-MUC-20	yes	bottom water / shell	yes
TV-MUC-21	yes	bottom water / shell	
TV-MUC-24	yes	bottom water / shell	
TV-MUC-27	yes	bottom water / shell	
TV-MUC-28	yes	bottom water / shell	
TV-MUC-29	yes	bottom water / shell	
TV-MUC-30	yes	bottom water / shell	
TV-MUC-31	yes	bottom water / shell	
TV-MUC-33	yes	bottom water / shell	
TV-MUC-35	yes	bottom water / shell	
TV-MUC-36	yes	bottom water / shell	

Preliminary Results

A first analysis of species composition was made with specimens collected for the vital test. Most taxa in sediment covered by bacterial mats were calcareous species. Main dominant was *Uvigerina peregrina*. Other important genera were *Globocassidulina*, *Cassidulina*, *Bulimina*, *Chilostomella* and *Fissurina*. The investigated control sediment, that was not influenced by bacterial mats and clams, shows a different preliminary faunal analysis. Again, *Uvigerina peregrina* was the

dominating taxon. But it was not as abundant as in the bacterial mat sediment. Other calcareous genera can also be found: *Globocassidulina*, *Bulimina*, *Chilostomella* and *Bolivina*. Additionally, agglutinated genera were observed: *Cribrostomoides*, *Glomospira*, *Reophax*, *Eggerelloides*, and *Textularia*. Control sediment seems to have a higher diversity. High amounts of *Uvigerina*, *Bulimina* and *Bolivina* indicate low oxygen conditions and high amounts of organic material (Lutze 1986, Lutze and Coulbourn 1984, Schmiedl 1995)

In both vital tests, about 30 good looking individuals were tested. Additionally, 10 individuals were killed before (dried and washed in distilled water) and incubated as a background control. Only 2 individuals from the bacterial mat sediments showed a positive reaction and were surely active and living (*U. peregrina*, from 0-1 cm sediment depth, even demonstrating pseudopods, and *Globobulimina* sp., 1-2 cm). Four individuals from the control sediment were positive (2 *U. peregrina*, 2 *Eggerelloides*, from 1-3 cm sediment depth), but additionally, one dead specimen (*Eggerelloides*) showed colour change of the medium). Most tested foraminifera did not respond, although a healthy shell filled with cytoplasm was observed. It is not clear if foraminifera died during sampling and handling procedure or if they were dead before. But at least two living individuals were found at bacterial mats, indicating that they inhabit this environment. Field studies in Monterey Bay found living foraminifera in hydrocarbon and cold seep areas (Bernhard *et al.*, 2001). Different independent methods were used in these investigations, that showed unequivocally that benthic foraminifera can live under these conditions. Additionally, very similar faunal assemblages were observed, compared to our preliminary analysis.

6. References

- Alongi, D.M., Pichon, M., 1988. Bathyal meiobenthos of the western Coral Sea: distribution and abundance in relation to microbial standing stocks and environment factors. *Deep-Sea Research* 35, 755-790.
- Bernhard, J., Buck, K.R., Barry, J.P., 2001. Monterey Bay cold-seep biota: Assemblages, abundance, and ultrastructure of living foraminifera. *Deep-Sea Research I* 48, 2233-2249.
- Bernhard, J.M., 1988. Postmortem vital staining in benthic foraminifera: duration and importance in population and distributional studies. *Journal of Foraminiferal Research* 18 (2), 143-146.
- Blondel, P. and Murten B.J., 1998. *Handbook of seafloor imagery*. John Wiley and Sons Ltd, West Sussex, England, 314 p.
- Boetius, A., Lochte, K. 2000a. Regional variation of total microbial biomass in sediments of the deep Arabian Sea. *Deep-Sea Research II* 47, 149-168.
- Boetius, A., Ravensschlag, K., Schubert, C., Rickert, D., Widdel, F., Gieseke, A., Amann, R., Jørgensen, B. B., Witte, U. & Pfannkuche, O. (2000). A marine microbial consortium apparently mediating anaerobic oxidation of methane. *Nature* 407, 623-626.
- Boetius, A., Ravensschlag, K., Schubert, C.J., Rickert, D., Widdel, F., Gieseke, A., Amann, R., Jørgensen, B.B., Witte, U., Pfannkuche, O. 2000b. A marine microbial consortium apparently mediating anaerobic oxidation of methane. *Nature* 407, 623-626.
- Bohrmann, G., Linke, P., Suess, E., Pfannkuche, O., and cruise participants 1999. RV SONNE cruise report SO 143, TECFLUX-I-1999, GEOMAR Report 93.
- Carson, B., Seke, E., Paskevich, V. and Holmes, M.L., 1994. Fluid expulsion sites on the Cascadia accretionary prism: Mapping diagenetic deposits with processes GLORIA imagery. *Journal of Geophysical Research*, 99 (B6), 11959-11969.
- Cicerone, R.J., Oremland, R.S., 1988. Biogeochemical aspects of atmospheric methane. In: Oremland, R.S. (Ed.), *Special section on Methane biogeochemistry*. Global Biogeochemical Cycles 2, American Geophysical Union, Washington, DC, United States, 299-327.
- Cline J.D., 1969. Spectrophotometric determination of hydrogen sulfide in natural waters. *Limnology and Oceanography* 14, 454-458.
- Cord-Ruwisch, R., 1985. A quick method for the determination of dissolved and precipitated sulfides in cultures of sulfate-reducing bacteria. *Journal of Microbiological Methods* 4, 33-36.
- DeLong, E.F. 2000. Resolving a methane mystery. *Nature* 407, 577-579
- Dickson, A. D. (1993) pH buffers for sea water media based on the total hydrogen ion concentration scale. *Deep-Sea Research I*, 40: 107-118.
- Douglas, R., Liestman, J., Walch, C., Blake, G., Cotton, M.L., 1980. The transition from live to sediment assemblage in benthic foraminifera from the Southern California borderland. In: Field, M., Bouma, A., Colburn, I., Douglas, R., Ingle, I. (Eds.), *Quaternary depositional environments of the Pacific coast*, Pacific Coast Paleogeography, Symposium 4, Pac. Sect., SEPM, p. 257-280.
- Findlay, R.H., King, G.M., Watling, L. 1989. Efficacy of phospholipid analysis in determining microbial biomass in sediments. *Applied and Environmental Microbiology* 55, 2888-2893.
- Geslin, E., Heinz, P., Hemleben, C., 2001. Response of deep-sea foraminifers to anoxic conditions (Laboratory study). XI international congress of Protozoology ICOP, Salzburg, Austria, 71.
- Gieskis, J. M., Gamo, T. and H. Brumsack (1991) Chemical methods for interstitial water analysis aboard JOIDES Resolution, ODP Technical Notes 15: College Station, TX (Ocean Drilling Program).
- Glud, R.N., Blackburn, N. 2002 The effects of chamber size on benthic oxygen uptake measurements: A simulation study. *Ophelia* 56, 23-31.
- Gooday, A.J., 1986. Meiofaunal foraminiferans from the bathyal Porcupine Seabight (northeast Atlantic): size, structure, taxonomic composition, species diversity and vertical distribution in the sediment. *Deep Sea Research* 33 (10), 1345 - 1373.
- Grasshoff, K., Ehrhardt, M. and K. Kremling (1983) *Methods of seawater analysis*, 2nd edition, Verlag Chemie, Weinheim, 419 pp.
- Gust, G. 1987, "Verfahren und Vorrichtung zum Erzeugen von definierten Bodenschubspannungen", Patent DE 3717969 C1.
- Gust, G. and Kozerski, H.-P. (2000): In situ sinking particle flux from collection rates of cylindrical traps. *Marine Ecology Progress Series* 208:93-106.
- Gust, G., Müller, V. 1997 "Interfacial Hydrodynamics and Entrainment Function of currently used erosion devices", in Burt, N.; Parker, R.; Watts, J.(Eds.): "Cohesive Sediments – Proc. 4th

- Nearshore and Estuarine Cohesive Sediment Transport Conference INTERCOH '94, Wallingford, 1994", John Wiley & Sons, pp. 149-174
- Holm-Hansen, O., Lorenzen, C.J., Holmes, R.W., Strickland, J.D.H. 1965. Fluorometric determination of chlorophyll. *Journal du Conseil Permanent International pour l'Exploration de la Mer* 30, 3-15.
- Ivanenkov, V.N. and Yu. I. Lyakhin (1978) Determination of total alkalinity in seawater. In: Bordovsky, O.K. and V.N. Ivanenkov (eds.): *Methods of hydrochemical investigations in the ocean*. Nauka Publ. House, Moscow, 110–114 (in Russian).
- Jeroschewsky, P., Steuckart C., and Kuehl, M., 1996. An Amperometric Microsensor for the determination of H₂S in Aquatic Environments. *Analytical Chemistry* 68, 4351 – 4357
- Johnson, H.P. and Helferty, M., 1990. The geological interpretation of sidescan sonar. *Reviews in Geophysics*, 28, 357-380.
- Johnson, J.E. and Goldfinger, C., 2002. The influence of structure on the distribution and morphology of authigenic carbonates in the Hydrate Ridge region, Cascadia margin. *Marine Geology*, submitted.
- Jørgensen, B.B., & Des Marais, D.J. 1990, "The diffusive boundary layer of sediments: Oxygen microgradients over a microbial mat.", *Limnology and Oceanography*, 35, 1343-1355.
- Jorissen, F.J., de Stigter, H.C. and Widmark, J.G.V., 1995. A conceptual model explaining benthic foraminiferal microhabitats. *Marine Micropaleontology* 26, 3 - 15.
- Kennett, J.P., Cannariato, K.G., Hendy, I.L., Behl, R.J., 2000. Carbon isotopic evidence for methane hydrate instability during quaternary interstadials. *Science* 288, 128-133.
- Krumholz L.R., McKinley J.P., Ulrich, G.A., Suflita J.M., 1997. Confined subsurface microbial communities in Cretaceous rock. *Nature* 386, 64-66.
- Kuehl, M., Steuckart C., Eickert G. and Jeroschewsky P., 1998. A H₂S microsensor for profiling biofilms and sediments: application in an acidic lake sediment. *Aquatic Microbial Ecology* 15, 201-209.
- Kvenvolden, K.A., 1995. A review of the geochemistry of methane in natural gas hydrate. *Organic Geochemistry* 23 (11-12), 997-1008.
- Linke, P., Suess, E. and cruise participants (2001) RV SONNE cruise report SO 148, TECFLUX-II-2000, GEOMAR Report 98.
- Lutze, G.F., 1986. *Uvigerina* species of the eastern North Atlantic; In: van der Zwaan, G.J., Jorissen, F.J., Verhallen, P.J.J.M., von Daniels, C.H. (Eds), *Atlantic-European Oligocene to Recent Uvigerina: taxonomy, paleoecology and paleoceanography*. Utrecht Micropaleontological Bulletin 35, 21-46.
- Lutze, G.F., Coulbourn, W., 1984. Recent benthic Foraminifera from the continental margin of northwest Africa: community structure and distribution. *Marine Micropaleontology* 8, 361-401.
- McHatton, S. C., Barry, J. P., Jannasch, H. W. and D. C. Nelson (1996) High nitrate concentrations in vacuolate, autotrophic marine *Beggiatoa* spp. *Appl. Environ. Microbiol.* 62: 954–958.
- Michaelis, W., Seifert, R., Nauhaus, K., Treude, T., Thiel, V., Blumenberg, M., Knittel, K., Gieseke, A., Peterknecht, K., Pape, T., Boetius, A., Amann, R., Jørgensen, B.B., Widdel, F., Peckmann, J., Pimenov, N.V., Gulin, M.B. 2002. Microbial reefs in the Black sea fueled by anaerobic oxidation of methane. *Science* 297, 1013-1015.
- Nauhaus, K., Boetius, A., Krueger, M., Widdel, F., 2002. In-vitro demonstration of anaerobic methane oxidation coupled to sulfate reduction in a methane rich marine sediment. *Environmental Microbiology* 4 (5), 296 – 305.
- Olu, K., Lance, S., Sibuet, M., Henry, P., Fiala Médioni, A., Dinet, A. 1997. Cold seep communities as indicators of fluid expulsion patterns through mud volcanoes seaward of Barbados accretionary prism. *Deep-Sea Research I* 44, 811-841.
- Orphan, V. J., House, C. H., Hinrichs, K.-U., McKeegan, K. D. & DeLong, E. F. (2002) Multiple archaeal groups mediate methane oxidation in anoxic cold seep sediments. *Proceedings of the National Academy of Sciences of the United States of America* 99, 7663-7668.
- Pätzold et al. 2002. Expeditionsheft METEOR 52. Institut für Meereskunde der Universität Hamburg, Leitstelle METEOR. pp.40.
- Pfannkuche, O., Boetius, A., Lochte, K., Lundgreen, U., Thiel, H. 1999. Responses of deep-sea benthos to sedimentation patterns in the North-East Atlantic. *Deep-Sea Research* 46, 573-596.
- Pfannkuche, O., Utecht, C. (eds.) 2001. FS Poseidon Cruise Report POS 260, biogeochemical transport of matter and energy in the deep sea.. GEOMAR Report 100, pp. 67.

- Revsbech N.P. and Jørgensen B.B., 1986. Microelectrodes: their use in microbial ecology. In: K.C. Marshall(ed.). *Advances in Microbial Ecology* Vol. 9. Plenum Publishing Corporation, New York, 293-352.
- Revsbech, N.P., 1989. An oxygen sensor with a guard cathode. *Limnology and Oceanography* 34, 474-478.
- Sahling, H., Rickert, D., Raymond, W.L., Linke, P., Suess, E., 2002. Macrofaunal community structures and sulfide flux at gas hydrate deposits from the Cascadia convergent margin, NE Pacific. *Marine Ecology Progress Series* 231, 121-138.
- Sahling, H., Rickert, D., Linke, P., Suess, E., Lee, R.W., 2002. Community structure at gas hydrate deposits at the Cascadia convergent margin, NE Pacific. *Marine Ecology Progress Series* 231, 121-138.
- Schmiedl, G., 1995. Rekonstruktion der spätquartären Tiefenwasserzirkulation und Produktivität im östlichen Südatlantik anhand von benthischen Foraminiferenvergesellschaftungen. *Bericht zur Polarforschung* 160, 1-207.
- Sommer, S., Pfannkuche, O., Rickert, D., Kähler, A. 2002. Ecological implications of surficial marine gas hydrates for the associated small sized benthic biota at the Hydrate Ridge (Cascadia Convergent Margin, NE Pacific). *Marine Ecology Progress Series* 243, 25-38.
- Suess, E., Bohrmann, G., 1997. FS Sonne Fahrtbericht SO 110 SO-RO. Geomar Report 59, 181 pp.
- Suess, E., Torres, M.E., Bohrmann, G., Collier R.W., Greinert, J., Linke, P., Rehder, G., Trehu, A., Wallmann, K., Winckler, G., Zuleger, E., 1999. Gas hydrate destabilization: enhanced dewatering, benthic material turnover and large methane plumes at the Cascadia convergent margin. *Earth and Planet Science Letter* 170 (1-2), 1-15.
- Tengberg, A., et al., to be submitted, "Intercalibration of benthic flux chambers I. Accuracy of flux measurements and influence of chamber hydrodynamics", *Progress in Oceanology*.
- Thiel, H., 1975. The size structure of the deep-sea benthos. *Internationale Revue der gesamten Hydrobiologie* 60, 575 - 606.
- Thiel, H., 1983. Meiobenthos and nanobenthos of the deep-sea. In: Rowe, G.T. (Ed.), *Deep-sea biology*, 157 - 230.
- Walton, W.R., 1952. Techniques for recognition of living foraminifera. *Contributions from the Cushman Foundation for Foraminiferal Research* 3, 56-60.
- Yentsch, C.S., Menzel, D.W. 1963. A method for the determination of phytoplankton chlorophyll and phaeophytin by fluorescence. *Deep-Sea Research* 10, 221-231.

7. List of stations

Date	St. No.	Instrument	Time (UTC)				Duration	Begin / on seafloor		End / off seafloor		Water depth (m)	Recovery, remarks / Sample held by
			Begin	on seafloor	off seafloor	End		Latitude °N	Longitude °W	Latitude °N	Longitude °W		
2002	SO165/		Begin	on seafloor	off seafloor	End	(hh:mm)	Latitude °N	Longitude °W	Latitude °N	Longitude °W		
13. 7.	1-1	CTD-1	13:00	13:20		13:39	0:39	44:37.9500	125:10.0200	44:37.9900	125:09.9900	1153	24 bottles
13. 7.	1-2	CTD-2	14:00	14:30		15:00	1:00	44:37.9900	125:10.0100	44:38.0000	125:10.0000	1159	24 bottles
13. 7.	2	LR-1	16:45	17:18		17:42	0:57	44:37.2820	125:07.9890			875	deployed
13. 7.	3	Posidonia-1	18:29	19:20	19:35	20:30	2:01	44:37.0000	125:10.0060	44:37.0000	125:10.0000	1240	successful test
13. 7.	4	TV-MUC-1	21:30	23:01	23:03	23:30	2:00	44:34.1760	125:08.8240			780	4 cores, 10-20 cm
13. 7.	5	TV-MUC-2	23:50	0:26	0:29	0:50	1:00	44:34.2030	125:08.8340			780	6 cores, 5-15 cm
14. 7.	6	BIGO	6:00			9:00	3:00	44:34.1150	125:08:8400				cancelled, technical problems
14. 7.	7	CTD-3	7:13	7:20		7:27	0:14	44:49.9600	124:30.0100	44:50.0000	124:30.0300	185	7 bottles
14. 7.	8	CTD-4	8:11	8:18		8:24	0:13	44:46.0000	124:30.0300	44:46.0200	124:30.0100	163	6 bottles
14. 7.	9	CTD-5	9:07	9:12		9:17	0:10	44:41.9900	124:29.9950	44:42.0300	124:29.9200	131.8	5 bottles
14. 7.	10	CTD-6	9:55	10:01		10:07	0:12	44:38.0110	124:30.0240	44:38.0240	124:30.0030	111.9	5 bottles
14. 7.	11	CTD-7	10:48	10:51		10:55	0:07	44:34.0210	124:30.0480	44:34.0570	124:29.9410	95.9	4 bottles
14. 7.	12	CTD-8	11:44	11:47		11:51	0:07	44:30.0200	124:29.9700	44:30.0600	124:29.9160	82.3	4 bottles
14. 7.	13	CTD-9	12:27	12:30		12:34	0:07	44:25.9770	124:29.9760	44:25.9680	124:30.0340	79.3	4 bottles
14. 7.	14	BIGO-1	19:15	20:43		21:10	0:55	44:33.9800	125:08.3800			832	deployed, reference station
14. 7.	15	DOS	22:12			22:44	0:32	44:34.0300	125:08.4800				
15. 7.	16	FLUFO	1:37			1:39	0:02	44:34.1200	125:08.8600				cancelled, bad weather conditions
15. 7.	17	CTD-10	4:40	4:45		4:50	0:10	44:26.0000	124:39.9500	44:26.0400	124:39.9500	116.1	5 bottles
15. 7.	18	CTD-11	5:42	5:50		5:58	0:16	44:29.9900	124:40.0300	44:29.9600	124:40.0000	193.7	7 bottles
15. 7.	19	CTD-12	6:39	6:49		6:59	0:20	44:33.9800	124:40.0100	44:34.0000	124:40.0200	290.3	8 bottles
15. 7.	20	CTD-13	8:02	8:07		8:46	0:44	44:42.0100	124:40.0700	44:41:9900	124:40.0000	303.7	8 bottles
15. 7.	21	CTD-14	9:51	9:59		10:51	1:00	44:49.9700	124:40.0500	44:50.0300	124:40.0100	373.2	9 bottles
15. 7.	22	CTD-15	12:12	12:19		12:26	0:14	44:37.9900	124:40.0200	44:38.0000	124:40.0100	231.8	7 bottles
15. 7.	23	CTD-16	13:22	13:29		13:37	0:15	44:46.0500	124:40.0200	44:46:0200	124:39.9900	260.5	7 bottles
15. 7.	24	FLUFO-1	16:20	17:47		18:10	1:50	44:34.0000	125:08.8600			779.0	deployed
15. 7.	25	DOS	19:07			21:10	2:03	44:39.8800	125:06.0900			605.0	failed
15. 7.	26	BIGO-1	22:12		22:17	22:42	0:30						recovery, two chambers filled
15. 7.	27	TV-MUC-3	23:20	0:01	0:04	0:29	1:09	44:34.1900	125:08.7900			778.0	4 cores, ~20 cm, Calyptogena-field
16. 7.	28	TV-MUC-4	0:50	2:45	2:48	3:10	2:20	44:33.8500	125:08.9500			774.0	reference
16. 7.	29	TV-MUC-5	3:25	3:49	3:52	4:13	0:48	44:34.1600	125:08.8160			776.0	some Beggiatoa
16. 7.	30	18kHz survey	5:15			11:00	5:45	44:40.1700	125:05.8000			~ 600	Northern Summit; Gusher Site 1; Gusher Site & another (Ghost Flare)
16. 7.	31	CTD-17	11:49	12:34		13:34	1:45	44:38.0000	125:15.0200	44:38.0100	125:15.0100	2263.4	24 bottles
16. 7.	32	DOS-1	16:10	16:40	16:42	17:00	0:50	44:39.8700	125:06.0670			606.0	deployed, clam field
16. 7.	33-1	OFOS-1	18:25	19:00	19:22	19:44	1:19	44:34.1100	125:08.4100	44:34.2800	125:08.4100	820.0	
16. 7.	33-2	OFOS-2	20:30	20:54	21:25	21:58	1:28	44:34.4110	125:08.8400	44:34.3500	125:08.8400	779.0	
16. 7.	34	OFOS-3	22:10	22:34	0:03	0:20	2:10	44:34.0900	125:09.1000	44:34.2400	125:09.0000	~ 800	
17. 7.	35-1	Posidonia-2	1:23			1:37	0:14	44:38.0000	125:16.0000			2300.0	calibration antenna, transponder deployed
17. 7.	35-2	CTD-18	2:15	2:45		3:38	1:23	44:41.9800	125:14.9900	44:41.9800	125:15.0600	1573.4	24 bottles
17. 7.	35-3	Posidonia-3	4:20			5:30	1:10	44:38.0000	125:16.0000			2300.0	calibration antenna failed
17. 7.	36	CTD-19	5:49	6:09		6:31	0:42	44:37.7800	125:15.1600	44:37.8000	125:12.1200	2271.1	9 bottles
17. 7.	37	18kHz survey	7:20			13:06	5:46	44:34.2200	125:08.8000			780.0	Southern Summit; Bubble site; two flares seen several times
17. 7.	38	CTD-20	13:27	13:51		14:24	0:57	44:34.0000	125:10.0000	44:34.000	125:09.940	907.0	24 bottles
17. 7.	39	FLUFO-1	14:50		14:55	15:25	0:35					809.0	recovery, 14 syringes
17. 7.	40	Posidonia-3	16:35			17:15	0:40					2300.0	recovery transponder
17. 7.	41	TV-MUC-6	18:30	19:14	19:15	19:45	1:15	44:34.2770	124:59.9590			875.0	4 cores, 25-30 cm
17. 7.	42	TV-MUC-7	19:55	20:24	20:26	20:52	0:57	44:34.2840	124:59.9460			878.3	3 cores, 5-10 cm
18. 7.	43	BIGO-2	0:30	1:08		1:38	1:08	44:39.8670	125:06.1150			605.0	deployed, clams
18. 7.	44-1	Posidonia-4	1:45			2:15	0:30	44:40.0400	125:06.0400			605.0	transponder test successful

7. List of stations

Date	St. No.	Instrument	Time (UTC)			Duration	Begin / on seafloor		End / off seafloor		Water depth (m)	Recovery, remarks / Sample held by	
			Begin	on seafloor	off seafloor		End	(hh:mm)	Latitude °N	Longitude °W			Latitude °N
2002	SO165/												
18. 7.	44-2	Posidonia-5	2:55			3:25	00:30	44:35.0000	125:03.0000		1250.0	transponder deployed	
18. 7.	44-3	Posidonia-6	3:25			6:11	2:46	44:35.0000	125:03.0000		1230.0	calibration successful	
18. 7.	45	CTD-21	9:08	9:16		9:35	0:27	44:49.9800	124:50.0100	44:50.0100	124:50.0000	399.7	11 bottles
18. 7.	46	CTD-22	12:12	12:48		13:45	1:33	44:49.9700	125:14.9700	44:50.0100	125:15.0400	1868.1	24 bottles
18. 7.	47	GQ-1	18:05	19:31		19:54	1:49	44:40.1250	125:05.8250			605.0	deployed
18. 7.	48	TV-MUC-8	21:12	21:48	21:50	22:15	1:03	44:34.3200	124:59.8690			879.0	4 cores, 25-27 cm, Beggionatoa-mat
18. 7.	49	TV-MUC-9	22:28	23:04	23:06	23:32	1:04	44:34.3640	124:59.8760			880.0	2 cores, 27-30 cm
18. 7.	50	TV-MUC-10	23:42	0:19	0:22	0:50	1:08	44:34.3441	124:59.8228			880.0	3 cores, 15-20 cm
19. 7.	51	TV-MUC-11	1:11	1:50	1:53	2:28	1:17	44:34.3060	124:59.8860			882.0	4 cores, ~ 30 cm
19. 7.	52	TV-MUC-12	2:37	3:42	3:44	4:06	1:29	44:34.3196	124:59.9588			885.0	3 cores, ~ 30 cm, Beggionatoa-field, Eastern Basin
19. 7.	53	DTS-1-1	6:11	7:08	13:30	14:57	8:46	44:25.8600	125:08.3900			700-1630	
19. 7.	54	BIGO-2	16:25		16:30	17:00	0:35						recovery, two chambers filled
19. 7.	55	TV-G-1	18:30	19:15		19:45	1:15	44:34.2010	125:08.7710			776.0	gas hydrate chips
19. 7.	56-1	Posidonia-7	20:53			21:39	0:46						recovery transponder
19. 7.	56-2	CTD-23	22:15	22:34		23:09	0:54	44:33.9900	125:0.0100	44:33.990	124:59.980	880.2	24 bottles
20. 7.	57	FLUFO-2	0:20	1:20		1:45	1:25	44:34.3060	125:59.8640			880.0	deployed
20. 7.	58-1	DTS-1-2	3:35	4:58	10:01	10:01	6:26	44:29.1520	125:07.6990	44:44.0000	125:07.0170	1200-600	
20. 7.	58-2	DTS-1-3	10:01	11:55	17:13	18:10	8:09	44:44.0000	125:09.5000	44:28.8980	125:09.5590	1200-600	
20. 7.	59-1	CTD-24	19:13	19:30		19:54	0:41	44:30.0300	125:10.0000	44:29.9800	125:10.0200	902.3	24 bottles
20. 7.	59-2	CTD-25	20:14	20:43		21:22	1:08	44:29.9800	125:10.0100	44:29.9800	125:10.0100	1167.0	24 bottles
20. 7.	60	TV-MUC-13	22:20	22:44	22:47	23:10	0:50	44:34.1911	125:08.7871			776.0	4 cores, ~20 cm, Beggionatoa/Calyptogena-field
20. 7.	61	TV-MUC-14	23:25	23:53	23:56	0:10	0:45	44:34.1810	125:08.7690			776.0	17-23 cm, reference
21. 7.	62	TV-MUC-15	0:30	1:00	1:05	1:41	1:11	44:34.2077	125:08.8200			770.0	3 cores, Beggionatoa, heavy bubbling
21. 7.	63	TV-MUC-16	1:40	2:04	2:07	2:31	0:51	44:34.2402	125:08.9041			784.0	failed
21. 7.	64	CTD-26	4:52	5:17		5:32	0:40	44:26.0000	124:50.0100	44:26.0100	124:56.0100	377.8	10 bottles
21. 7.	65	CTD-27	8:20	8:51		9:52	1:32	44:25.9800	125:15.0100	44:26.0100	125:15.0000	1702.0	24 bottles
21. 7.	66	CTD-28	12:50	13:42		15:12	2:22	44:41.9900	125:30.0000	44:42.0100	125:30.0300	2829.0	24 bottles
21. 7.	67	TV-MUC											cancelled, position occupied
21. 7.	68	GQ-1	18:30		18:40	19:00	0:30						recovery
21. 7.	69	BIGO-3	21:45	22:14		22:48	1:03	44:34.2893	124:59.8887			883	deployed, Beggionatoa-mat
21. 7.	70	FLUFO-2	22:50		23:00	23:25	0:35						recovery
22. 7.	71-1	18kHz survey	1:45			4:38	2:53	44:44.6660	124:55.3040			560	Search for a flare seen during CTD transit, the flare was not seen during the survey
22. 7.	71-2	swath bathymetry	5:15			14:01	8:46	44:41.2250	124:59.7150	44:41.0000	125:01.8000	800-1200	4 profiles N-S
22. 7.	71-3	18kHz survey	14:11			15:55	1:44	44:40.0070	125:06.6530	44:40.2060	125:05:7890	00:00	Northern summit, Gusher site 2, flare seen several times
22. 7.	72	CTD-29	16:05	16:22		17:07	1:02	44:40.5700	125:05.9300	44:40.5600	125:05.9000	624.1	24 bottles
22. 7.	73	METS- Mooring-1a	17:20			17:41	0:21	44:40.5460	125:05.9000			630.0	2 METS sensors deployed (30 m + 60 m above bottom)
22. 7.	74	TV-MUC-17	18:48	19:17	19:20	19:43	0:55	44:34.1580	125:08.8280			777.7	4 cores, 17-25 cm, gas hydrate
22. 7.	75	TV-MUC-18	19:58	20:40	20:41	21:06	1:08	44:34.2141	125:08.7740			777.8	4 cores, Beggionatoa-field, heavy bubbling
22. 7.	76	TV-MUC-19	21:20	21:46	21:49	22:14	0:54	44:34.2240	125:08.8550			787.0	4 cores, ~30 cm, Beggionatoa-field
22. 7.	77	CTD-30	23:39	0:01		0:32	0:53	44:25.9900	125:05.0600	44:26.0200	125:04.9500	963.7	21 bottles
23. 7.	78	18kHz survey	1:02			3:00	1:58	44:26.9900	125:01.8900			700.0	SE Knoll flare search: no flare seen
23. 7.	79	DTS-1-4	3:37			5:21	1:44	44:27.1400	125:06.8200	44:30.9500	125:06.2400	1200-600	
23. 7.	80	CTD-31	9:19	10:11		11:29	2:10	44:50.0100	125:30.0900	44:49.9700	125:29.9700	2795.2	24 bottles
23. 7.	81	CTD-32	15:49	16:00		16:11	0:22	44:42.0300	124:50.1100	44:42.0100	124:50.1000	263.0	12 bottles
23. 7.	82	BIGO-3	18:05		18:10	18:35	0:35						recovery, two chambers filled
23. 7.	83	FLUFO-3	22:50	23:48		0:07	1:17	44:34.2270	125:08.7920			779.2	deployed

7. List of stations

Date	St. No.	Instrument	Time (UTC)				Duration	Begin / on seafloor		End / off seafloor		Water depth (m)	Recovery, remarks / Sample held by
			Begin	on seafloor	off seafloor	End		Latitude °N	Longitude °W	Latitude °N	Longitude °W		
24. 7.	84	GQ-2	0:59	1:49		2:08	1:09	44:34.1802	125:08.8371			778.0	deployed
24. 7.	85	LR-1	2:41			3:17	0:36						recovery
24. 7.	86-1	DTS-1-5	4:48	5:54	11:01	11:01	6:13	44:44.0000	125:10.4800	44:29.0000	125:10.4000	800-1600	
24. 7.	86-2	DTS-1-6	11:01	12:54	17:38	19:13	8:12	44:30.0300	125:06.9020	44:44.0000	125:06.8800	800-1400	
24. 7.	87	LR-2	21:34	22:02	22:03	22:34	1:00	44:34.1970	125:08.4740			807.0	deployed
24. 7.	88	TV-MUC-20	23:31	1:17	1:19	1:43	2:12	44:34.2831	125:59.9470			885.0	4 cores, 25-29 cm
25. 7.	89	TV-MUC-21	1:55	2:27	2:29	2:55	1:00	44:34.2910	124:59.9140			882.0	4 cores, 8-12 cm
25. 7.	90-1	Apstein-net-1	3:40			3:48	0:08	44:34.0007	125:04.9775			1196.0	2 parallels, 30 m depth, 20 µm mesh
25. 7.	90-2	Apstein-net-2	3:50			3:55	0:05	44:34.0205	125:04.9877			1192.0	2 parallels, 30 m depth, 20 µm mesh
25. 7.	90-3	CTD-33	3:55	4:22		4:48	0:53	44:34.0100	125:04.9610	44:34.0000	125:04.9800	1191.0	24 bottles
25. 7.	90-4	CTD-34	5:36	6:03		6:49	1:13	44:34.0200	125:05.0000	44:34.0100	125:05.0100	1173.0	24 bottles
25. 7.	91	CTD-35	9:38	10:29		13:05	3:27	44:25.9600	125:30.0900	44:26.0100	125:30.0000	2918.6	24 bottles
25. 7.	92	18kHz survey	16:02			19:35	3:32	44:43.1320	125:14.7130	44:45.4800	125:13.8210	1200	NW Knoll; 5 profiles in NNW-SSE direction; no flare
25. 7.	93	CTD-36	21:22	21:43		22:16	0:54	44:50.0300	124:59.9400	44:50.0300	124:59.9600	1142	24 bottles
25. 7.	94	METS-Mooring-1b	23:51			0:10	0:19						recovery
26. 7.	95-1	DTS-1-7	2:15	3:35	7:50	7:50	5:35	44:29.0300	125:05.9910	44:44.0050	125:05.9100	800-1400	
26. 7.	95-2	DTS-1-8	7:50	9:43	13:44	15:05	7:15	44:44.0100	125:05.0100	44:32.9190	125:05.0110	800-1400	
26. 7.	96	LR-2	17:35			19:10	1:35						recovery
26. 7.	97	BIGO-4	19:40	20:30		20:51	1:11	44:34.2303	125:08.7705			778.0	deployed, Beggatoa-mat
26. 7.	98	BCL-1	23:06	23:52		0:10	1:04	44:34.2200	125:08.8200			779.0	deployed
27. 7.	99	FLUFO-3	0:15		0:25	0:50	0:45						recovery
27. 7.	100	TV-MUC-22	1:08	1:41	1:42	2:05	0:57	44:34.1980	125:08.8231			777.0	4 cores, 18-30 cm, clams
27. 7.	101	TV-MUC-23	2:10	2:50	2:54	3:18	1:08	44:34.2183	125:08.8004			777.6	2 cores, 5 cm,
27. 7.	102	CTD-37	5:22	6:13		7:11	1:49	44:46.0000	125:19.9300	44:46.0100	125:19.9800	2303.0	24 bottles
27. 7.	103	CTD-38	11:02	11:11		11:22	0:20	44:29.9800	124:49.9700	44:30.0000	124:50.0100	217.3	8 bottles
27. 7.	104	METS-Mooring-2a	13:36			13:51	0:15	44:33.9900	125:08.7000	44:34.0000	125:08.7000	787.8	3 METS sensors deployed (30 m, 60 m, 90 m above bottom)
27. 7.	105	18kHz survey	14:53			18:35	3:42	44:40.0070	125:06.6530	44:40.2060	125:05.7890	~600	Gusher Site 3, ghost flare
27. 7.	106	CTD-39	19:41	20:15		21:02	1:21	44:46.0000	125:10.0000	44:46.0200	125:10.0200	1740.3	24 bottles
28. 7.	107	FLUFO-4	0:30	1:16		1:36	1:06	44:34.1867	125:08.7730			777.0	clam field
28. 7.	108	BIGO-4	1:40		1:41	2:13	0:33						recovery, two chambers filled
28. 7.	109	TV-MUC-24	2:22	3:11	3:12	3:35	1:13	44:33.2162	125:08.1100			779.0	4 cores, Beggatoa-mat
28. 7.	110	TV-MUC-25	3:43	4:14	4:15	4:38	0:55	44:34.1830	125:08.8040			776.0	4 cores, 22 cm, Calyptogena field
28. 7.	111-1	CTD-40	5:02	5:37		6:14	1:12	44:32.0100	125:04.1000	44:31.9900	125:04.1900	1259.0	12 bottles
28. 7.	111-2	DTS-1-9						44:32.0000	125:04.1000				failed
28. 7.	111-3	18kHz survey	10:10			17:04	6:54	44:28.0000	125:03.0000	44:28.0190	125:01.6020	650-900	SE Knoll, one flare seen
28. 7.	112	DOS-1	19:00		19:04	19:28	0:28						recovery
28. 7.	113	BCL-1	21:45		21:46	22:17	0:32						recovery
29. 7.	114	BIGO-5	0:00	0:46		1:05	1:05	44:34.2105	125:08.7800			777.0	deployed, clams
29. 7.	115	TV-MUC-26	1:37	2:10	2:12	2:37	1:00	44:34.1868	125:08.7885			776.3	4 cores, 25 cm, Calyptogena field
29. 7.	116	TV-MUC-27	3:08	3:49	3:51	4:10	0:58	44:34.2006	125:08.7904			778.8	3 cores, 11-26 cm, Beggatoa-mat
29. 7.	117	CTD-41	6:26	7:21		8:27	2:01	44:33.9800	125:30.0900	44:34.0100	125:30.0600	2877.5	24 bottles
29. 7.	118	CTD-42	10:54	11:10		11:50	0:56	44:25.9900	125:09.9000	44:26.0800	125:10.0200	1310.1	24 bottles
29. 7.	119	METS-Mooring-2b	13:07			13:50	0:43						recovery
29. 7.	120	CTD-43	16:01	16:18		16:38	0:37	44:45.9800	124:49.9700	44:46.0000	124:50.0100	482.0	14 bottles
29. 7.	121-1	CTD-44	19:10	19:23		19:40	0:30	44:30.0000	125:04.4960	44:30.0400	125:04.9800	1173.0	12 bottles
29. 7.	121-2	CTD-45	19:51	20:17		20:43	0:52	44:30.0200	125:5.0100	44:30.0500	125:4.9800	1173.0	24 bottles + O2 sensor Optode
29. 7.	121-3	Modem-Test	20:50			22:10	1:20	44:30.2500	125:4.8900			1183.0	Test with 1200 baud o.k. without ships acoustics !

7. List of stations

Date	St. No.	Instrument	Time (UTC)				Duration	Begin / on seafloor		End / off seafloor		Water depth (m)	Recovery, remarks / Sample held by
			Begin on seafloor	off seafloor	End	(hh:mm)		Latitude °N	Longitude °W	Latitude °N	Longitude °W		
29. 7.	122	GQ-2	22:20			23:45	1:25					recovery	
30. 7.	123	BIGO-5	0:15		0:16	0:45	0:30					recovery, two chambers filled	
30. 7.	124	TV-MUC-28	1:11	1:32	1:34	1:50	0:39	44:34.1610	125:08.7990		778.0	4 cores, 20 cm, reference	
30. 7.	125	TV-MUC-29	2:00	2:43	2:45	3:10	1:10	44:34.2225	125:08.7944		779.8	3 cores, Beggiatoa-mat	
30. 7.	126-1	Parasound-1	3:49			5:24	1:35	44:32.0240	125:10.4080	44:42.0390	125:10.4020	800-1300	
30. 7.	126-2	Parasound-2	5:39			7:21	1:42	44:42.0420	125:09.5120	44:31.8780	125:09.5010	800-1200	
30. 7.	126-3	Parasound-3	7:41			9:21	1:40	44:32.0780	125:07.7120	44:42.0800	125:07.7200	700-1250	
30. 7.	126-4	Parasound-4	9:33			11:13	1:40	44:41.9600	125:08.5800	44:31.9290	125:08.6030	693.5-1222.22	
30. 7.	126-5	Parasound-5	11:29			12:49	1:20	44:32.0150	125:06.7930	44:40.0000	125:06.7980	> 600	
30. 7.	127	FLUFO-4	13:30		13:32	14:00	0:30					recovery	
30. 7.	128	TV-MUC-30	15:05	15:30	15:32	15:56	0:51	44:34.1506	125:08.7825		776.3	4 cores, 20-26 cm, reference	
30. 7.	129	TV-MUC-31	16:00	17:26	17:29	17:55	0:55	44:34.1935	125:08.7692		775.5	3 cores, 20 cm, dead Calyptogena-Field	
30. 7.	130	TV-MUC-32	18:00	18:25	18:27	18:50	0:50	44:34.1549	125:08.8597		776.0	3 cores, ~ 28 cm, reference	
30. 7.	131	FLUFO-5	21:05	21:50		22:11	1:06	44:34.2044	125:08.8183		777.0	deployed, bacterial mat	
30. 7.	132	BCL-2	23:10	23:45		0:10	1:00	44:34.2063	125:08.7800		778.0	deployed	
31. 7.	133	BIGO-6	4:10	4:51		5:15	1:05	44:34.2401	125:08.7734		782.0	deployed, bacterial mat	
31. 7.	134	CTD-46	6:48	7:42		8:49	2:01	44:25.9900	125:19.9300	44:26.0600	125:19.9300	2881.8	
31. 7.	135	CTD-47	11:26	12:09		12:56	1:30	44:49.9800	125:20.0000	44:50.0000	125:20.0200	2191.0	
31. 7.	136	NTTA-1	14:20	14:42		20:08	3:48	44:40.1600	125:05.9000	44:40.0000	125:05.6200	590.0	
31. 7.	137	TV-MUC-33	21:00	21:33	21:36	22:00	1:00	44:34.2179	125:08.7852		778.0	4 cores, ~ 30 cm, next to BCL	
31. 7.	138	TV-MUC-34	22:15	22:43	22:46	23:15	1:00	44:34.2024	125:08.7918		776.0	4 cores, ~ 30 cm, Beggiatoa-mats and gas hydrates, touched FLUFO during recovery	
31. 7.	139	TV-MUC-35	23:25	23:46	23:48	0:15	0:50	44:34.1768	125:08.7746		779.0	3 cores, * 30 cm, Calyptogena	
01. 8.	140	BIGO-6	0:15		0:21	0:46	0:31					recovery, one chamber filled	
01. 8.	141	CTD-48	1:58	2:52		4:16	2:18	44:29.9600	125:20.0000	44:30.0100	125:20.0000	2840.3	
01. 8.	142	CTD-49	7:21	7:35		7:46	0:25	44:37.9500	124:50.0200	44:37.9900	124:50.0300	383.2	
01. 8.	143	CTD-50	10:00	10:50		11:45	1:45	44:38.0100	125:20.0000	44:38.0200	125:19.9600	2728.7	
01. 8.	144	FLUFO-5	14:05		14:06	14:30	0:25					recovery	
01. 8.	145	TV-MUC-36	14:50	16:13	16:15	16:38	1:48	44:34.2109	125:08.8064		780.0	3 cores, 25 cm, Beggiatoa-mat	
01. 8.	146	TV-MUC-37	16:47			17:15	0:28					failed, bottles closed in the water	
01. 8.	147	BCL-2	17:20		17:26	17:50	0:30					recovery	
01. 8.	148	GQ-3	19:15	20:06		20:27	1:12	44:40.1400	125:05.8580		597.0	Gusher Site is target	
01. 8.	149	METS-Mooring-3a	13:36			14:15	0:39	44:40.400	125:06.000		616.0	NNW of Gusher Site	
06.08.	150	CTD-51	7:49	8:02		8:17	0:28	44:33.9800	124:49.9700	44:34.0000	124:50.0000	401.5	
06.08.	151	CTD-52	10:23	11:22		12:41	2:18	44:34.0020	125:20.0200	44:38.9800	125:19.9700	2877.3	
06.08.	152	18 kHz survey	13:40			17:11	3:31	44:40.4480	125:06.6360	44:39.9300	125:05.878	~600	
06.08.	153-1	18 kHz survey	18:38			19:20	0:42	44:34.4900	125:09.5100	44:34.2000	125:08.7800	~780	
06.08.	153-2	TV-MUC-38	19:32	20:05	20:07	20:30	0:58	44:34.2319	125:08.8416		779	4 cores C = 25 cm, E = 23 cm, G = 15 cm, A = 15 cm / 1 core Drews (E)	
06.08.	153-3	TV-MUC-39	20:41	21:15	21:18	21:41	1:00	44:34.1274	125:08.8178		776	3 cores, 1 leaked out A = 27 cm, C = 26 cm, E = 33 cm / 1 sample (0-10 cm) Maggiulli/TUB (E)	
06.08.	153-4	TV-MUC-40	21:52	23:07	23:09	23:32	1:40	44:34.1892	125:08.7990		780	4 cores, A = 23 cm, C = 23 cm, E = 27 cm, G = 19 cm	

7. List of stations

Date	St. No.	Instrument	Time (UTC)				Duration	Begin / on seafloor		End / off seafloor		Water depth (m)	Recovery, remarks / Sample held by
			Begin	on seafloor	off seafloor	End		Latitude °N	Longitude °W	Latitude °N	Longitude °W		
2002	SO165/		Begin	on seafloor	off seafloor	End	(hh:mm)	°N	°W	°N	°W		
07.08.	154-1	TV-G-2	0:15	2:06	2:06	2:22	2:07	44:34.2114	125:08.8031			776	large amounts of gas hydrate; several pieces of carbonate/ Abegg (gas hydrate); Liebetau/Eisenhauer (carbonates). Nauhaus/ Treude (gas hydrate)
07.08.	155	GSPT-1	4:15	4:54	7:32	7:55	3:40	44:34.1900	125:08.8000			777	Tip of tool broke off, no sample records. Rope: 795,0m, tension 6.3 UN, 5.6 UN upon seafloor contact.
07.08.	156	CTD-53	9:01	9:26	9:57	0:56	0:56	44:29.9600	125:00.0200	44:30.0200	125:00.0300	814.6	22 bottles closed
07.08.	157	18 kHz survey	10:50			12:38	1:48	44:34.1700	125:08.7000	44:34.0900	125:09.2300	880-780	
07.08.	158	CTD-54	12:35	13:02		14:00	1:25	44:34.1900	125:08.8500	44:34.2500	125:08.8400	773.8	Yoyo in flare: 24 bottles closed
07.08.	159	METS-Mooring-3b	14:44			15:10	0:26			44:40.4200	125:05.9100	604	recovery
07.08.	160-1	SL-1, 3 m tube	16:15	16:36	16:37	16:45	0:30	44:34.1670	125:08.8130			776	64 cm of grey-olive mud /Brückmann: 1 sample (0-10 cm) Maggiulli/TUB
07.08.	160-2	SL-2, 3 m tube	17:25	17:43	17:45	18:02	0:37	44:34.1471	125:08.8140			776	107 cm
07.08.	160-3	SL-3, 3 m tube	18:43	19:01	19:03	19:18	0:35	44:34.2110	125:08.8090			776	>28cm
07.08.	160-4	SL-4, 3 m liner	19:40	19:57	19:58	20:15	0:35	44:34.21	125:08.8100			776.2	gas hydrate released by cover floating on sea surface /1 sample (0-10 cm) Maggiulli/TUB: Drews
07.08.	161	TV-MAC-1	21:36	22:15	22:15	22:50	01:14	44:36.1690	125:08.8140			776.7	1 pressure tube 60 bar
07.08.	162-1	TV-G-3	23:24	23:50	23:51	00:09	00:45	44:34.1710	125:08.7910			775	large amounts of gas hydrate /Abegg, Brückmann, Lösekann (gas hydrate); Treude, Liebetau (carbonates); Maggiulli/TUB (0-10 cm)
08.08.	163	CTD-55	02:43	03:24		04:09	01:26	44:49.9900	125:05.0000	44:50.0100	125:05.0100	1835.5	24 bottles closed
08.08.	164	OFOS-2	05:36	05:52	10:48			44:39.9290	125:05.5160	44:40.322	125:05.5690	625	the uppermost top of the northern summit still shows the most bacteria mats
08.08.	165-2	CTD-56	12:17	13:12		14:27	02:10	44:42.0000	125:20.0100	44:42.0100	125:20.0000	2660.6	24 bottles closed
08.08.	166	GQ-3b	15:37		15:37	16:03	00:26			44:40.0000	125:05.9900	620	recovery
08.08.	167-1	KL/SL-1, 3 m tube	17:37	17:56	17:57	18:15	00:38	44:34.2040	125:08.8120			775	missing flap valve at the top: defect of core catcher
08.08.	167-2	KL/SL-2, 5 m liner	19:02	19:21	19:22	19:35	00:33	44:34.2090	125:08.8120			775	banana, due to lack of flap valve at the top sediment was washed out and only large pieces of gas hydrate remained in the core liner
08.08.	168-1	TV-MUC-41	20:23	21:17	21:19	21:44	01:21	44:34.1910	125:08.2460			776	4 cores, A = 20 cm, C = 25 cm, E = 21 cm, G = 25 cm / Treude; Abegg
08.08.	168-2	TV-MUC-42	21:56	22:42	22:45	23:08	01:12	44:34.1973	125:08.8108			778	3 cores o.k., E disturbed, A = 25 cm, C = 27 cm, G = 24 cm / sample taken at marker 13
09.08.	169	TV-G-4	23:24	00:03	00:07	00:30	01:06	44:34.2070	125:08.0900	44:34.1713	125:08.7685	776	large amounts of gas hydrate
09.08.	170	TV-MAC-2	02:00	02:27	02:31	03:05	01:05	44:34.2100	125:08.8100			775	assembly error, blocking device wrongly placed: pressurized sampling not possible
09.08.	171	GSPT-2	03:45			04:25	00:40	44:34.2100	125:08.8100			776	pressure housing test / 1 sample (0-10cm) Maggiulli (TUB)
09.08.	172	CTD-57	05:50	06:10		06:29	00:39	44:46.0000	125:00.0100	44:46.0000	124:59.9900	839	22 bottles closed
09.08.	173	Simrad-6	07:59			12:10	04:11	44:29.0000	125:04.0100	44:29.0000	125:01.2200	1200-700	5 profiles N-S; target: SE-Knoll
09.08.	174	CTD-58	13:46	14:16		15:18	01:32	44:45.9800	125:05.0000	44:46.0100	125:05.0000	1403.1	24 bottles closed
09.08.	175-1	TV-MUC-43	16:30	18:18	18:21	18:43	02:13	44:34.2102	125:08.7967			776	3 cores, Beggiaoa and gas hydrates taken exactly next to two TV-grab sites (holes visible)

7. List of stations

Date	St. No.	Instrument	Time (UTC)				Duration	Begin / on seafloor		End / off seafloor		Water depth (m)	Recovery, remarks / Sample held by
			Begin	on seafloor	off seafloor	End		Latitude °N	Longitude °W	Latitude °N	Longitude °W		
2002	SO165/		Begin	on seafloor	off seafloor	End	(hh:mm)	Latitude °N	Longitude °W	Latitude °N	Longitude °W		
09.08.	175-2	TV-MUC-44	18:57	19:20	19:23	19:47	00:50	44:34.2027	125:08.7711			776	4 cores, A = , C = , E = , G =
09.08.	176-1	KL/SL-3, pre-cut liner	20:28	20:53	20:55	21:10	00:42	44:34.2050	125:08.8060			776.2	coring successful, but only small amount of gas hydrate: sample not frozen
09.08.	176-2	KL/SL-4, 2 m pre-cut liner	21:25	21:43	21:44	21:57	00:32	44:34.2060	125:08.8140			776	core with gas hydrate, 160cm / Lösekann; 1 sample(0-10cm) magiulli (TUB)
09.08.	176-3	KL/SL-5, 2 m pre-cut liner	22:20	22:59	23:00	23:13	00:53	44:34.204	125:08.807			776	core with layers of gas hydrate / Abegg, four liner segments frozen in liquid N2
10.08.	177	METS-Mooring 4a	00:13			00:44	00:31	44:40.1500	125:05.8000			589.01	4 METS sensors, 30 m/ 60 m/ 90 m over bottom/ Nauhaus; Treude; Lösekann; Drews; Albrecht; 1 sample (0-10 cm) Maggiulli/TUB
10.08.	178	CTD-59	01:10			02:20	01:10	44:42.0100	125:05.0000	44:42.0100	125:05.0000	907	
10.08.	179	TV-MAC-3, 2 x LTC	03:41	04:26	04:30	04:49	01:08	44:34.2100	125:08.8300			774	2 cores, 1) 40 bar, 2) 10 bar, rising to 20 bar after closing leakage / 1 sample (0-10 cm) Maggiulli/TUB
10.08.	180	Simrad-7	23:00			04:38	05:38	44:46.0900	125:15.2700	44:42.0000	125:12.5000		target: NW-knoll, 6 profiles in N-S direction
10.08.	181	OFOS-3	12:10	12:32	14:42	15:06	02:56	44:43.8780	125:13.8980	44:44.9220	125:13.8940	900-1000	NW-knoll, S-N track
10.08.	182	CTD-60	16:12	16:38		17:16	01:04	44:41.9800	124:59.9900	44:41.9900	125:00.0000	917.7	24 bottles closed
10.08.	183	OFOS-4	18:10	18:35	21:45	22:15	04:05	44:34.3100	125:00.5100	44:34.4780	124:59.8000	~900	Eastern Basin: very few bacterial mats, carbonates
10.08.	184-1	SL-5, 6 m tube	22:50	23:12	23:13	23:33	00:43	44:34.2850	124:59.9010			879.6	2,5 m core recovered, gas hydrates
11.08.	184-2	SL-6, 6 m liner	00:10	00:28		00:45	00:35	44:34.2830	124:59.9010			878	core under pressure, exploded; gas hydrate, carbonates / M.Drews
11.08.	185-1	MUC-45	02:19	02:46	02:48	03:13	00:54	44:34.2760	124:59.8372			877.6	TV system failed, 4 water samples / Liebetau (gas hydrate, carbonates)
11.08.	186	OFOS-5	04:55	05:12	11:25	11:48	06:53	44:34.3530	125:08.7650	44:34.3100	125:08.7960	781	survey of the Southern Summit, 4 sightings of holes (drill holes?)
11.08.	187	CTD-61	13:25	14:02		15:05	01:40	44:49.9900	125:10.0000	44:50.0000	125:09.9800	1760.4	24 bottles closed
11.08.	188-1	TV-G-5	17:46	18:00	19:35	19:50	02:04	44:27.0810	125:01.8220			620	South East Knoll
11.08.	188-2	TV-G-6	20:20	20:35	20:58	21:15	00:55	44:27.0560	125:01.7780			618	South East Knoll, TV-G not completely closed, 1 carbonate sample, massive + veins / Eisenhauer; Liebetau
11.08.	188-3	TV-G-7	21:20	21:35	21:51	22:08	00:52	44:27.0880	125:01.6880			612	failed, batteries empty (2nd run, 188-2 + 188-3)
11.08.	189	CTD-62	23:01	23:22		23:47	00:46	44:25.9710	125:00.0100			820.9	21 bottles closed / Eisenhauer , Liebetau
12.08.	190-1	TV-MUC-46	01:02	01:34	01:36	02:00	00:58	44:34.1994	125:08.7610			778.5	
12.08.	190-2	TV-MUC-47	02:10	02:42	02:45	03:07	00:57	44:34.2420	125:08.7467			780	4 cores, reference
12.08.	190-3	TV-MUC-48	03:16	03:54	03:58	04:23	01:07	44:34.2918	125:08.7536			783	3 cores, A = 19 cm, C = 13 cm, E = 17 cm / Lösekann, Nauhaus
12.08.	191	CTD-63	06:45			09:00	02:15	44:34.2050	125:08.8180	44:34.1730	125:08.8550	776	24 bottles closed, Tow-yo CTD / Drews, Luff (8 pieces of Acharax)
12.08.	192	CTD-64	10:46	12:24		13:50	03:04	44:27.5300	125:29.0000	44:27.5700	125:28.8000	2928.4	no bottles, winch problems
12.08.	193	18 kHz survey	15:23			15:58	00:35	44:33.8180	125:09.3030	44:33.9100	125:08.4400	770	no flare, 33 kHz used
12.08.	194-1	SL-7, 6 m liner	16:42	17:03	17:05	17:27	00:43	44:34.2830	124:59.9090			878.9	few carbonates
12.08.	194-2	SL-8, 6 m liner	17:30	17:49	17:51	18:12	00:42	44:34.2800	124:59.9060			877	~2.5 m
12.08.	194-3	SL-9, 6 m pre-cut liner	18:33	18:52	18:53	19:07	00:34	44:34.276	124:59.9000			878	1,45 m, gas hydrate
12.08.	195	TV-MUC-49	19:59	20:25	20:26	20:45	00:46	44:34.2880	124:59.8440			879	4 cores / Brückmann, Albrecht
12.08.	196-1	TV-MAC-4	22:51			23:08	00:17	44:34.2100	125:08.8000			777	TV system defective / Abegg, three segments frozen in liquid N2

7. List of stations

Date	St. No.	Instrument	Time (UTC)				Duration	Begin / on seafloor		End / off seafloor		Water depth (m)	Recovery, remarks / Sample held by
			Begin	on seafloor	off seafloor	End		Latitude °N	Longitude °W	Latitude °N	Longitude °W		
2002	SO165/		Begin	on seafloor	off seafloor	End	(hh:mm)	Latitude °N	Longitude °W	Latitude °N	Longitude °W		
12.08.	196-2	TV-MAC-5	23:49	00:27	00:27	01:00	01:11	44:34.2330	125:08.8360			777	no pressure, 2 cores / Albrecht
13.08.	197-1	TV-G-8	01:27	01:49	01:50	02:06	00:39	44:34.2100	125:08.8120			775.7	gas hydrate
13.08.	198	OFOS-6	05:01	05:13	10:20	10:30	05:29	44:51.9300	124:55.9300			446-500	very nice video, unfortunately too short / 1 sample (0-10 cm) Maggiulli/TUB
13.08.	199	CTD-65	12:17	12:38		13:04	00:47	44:37.9800	125:05.0000	44:38.0000	125:05.0000	883.1	24 bottles closed / 1 sample (0-10 cm) Maggiulli/TUB
13.08.	200	TV-MAC-5	14:01	14:36	14:37	15:13	01:12	44:34.2160	125:08.8280			775	2 cores under pressure (65 bar)
13.08.	201-1	TV-MUC-50	16:17	16:56	16:59	17:25	01:08	44:34.0848	125:08.7782			778	4 cores, A = 15 cm, C = 17 cm, E = 16 cm, G = 15 cm
13.08.	201-2	TV-MUC-51	17:31	17:57	18:00	18:25	00:54	44:33.9880	125:08.8223			779.5	4 cores, A = 12 cm, C = 27 cm, E = 26 cm, G = 27 cm / 1 sample (0-10 cm) Maggiulli/TUB
13.08.	202	SL-10, 6 m tube	16:56	19:13	19:14	19:30	02:34	44:34.3650	125:08.7670			782	320 cm / Albrecht
13.08.	203	SL-11	20:54	21:04	21:05	21:14	00:18	44:34.3610	129:49.9980			403	Albrecht
13.08.	204	METS-Mooring-4b	22:34			22:55	00:24	44:39.9600	125:05.8700			608.5	recovery / Drews, Brückmann
14.08.	205	CTD-66	00:26	00:54		01:31	01:05	44:46.0100	125:15.0300	44:46.0000	125:15.0000	1335.4	24 bottles closed / geochemistry profile
13./	206	Simrad-8	19:00			04:08	09:08	44:47.0000	125:11.0650	44:28.0000	125:12.6800		2 N-S profiles 7 Drews
14.08.	207	CTD-67	11:32	12:11		13:03	01:31	44:30.0600	125:15.0200	44:30.1000	125:14.9500	1913.3	24 bottles closed
14.08.	208-1	TV-G-9	14:12	14:30	14:50	15:07	00:55	44:27.0860	125:01.7560			623	7 grabs SE flank: thin mats (44°27.0670/ 125°01.7690), shells and linear mat (44°27.0800/ 125°01.7770): fault zone
14.08.	208-2	TV-G-10	15:26	15:40	17:41	17:55	02:29	44:27.0180	125:01.7980			623	12 grabs; several steel ropes at the SSE end of the SE Knoll: grab caught in fishing net
14.08.	209-1	SL-12, 6 m	21:23	21:43	21:44	22:04	00:41	44:34.3600	124:59.8700			877	no core, few small pieces of carbonate (not collected)
14.08.	209-2	SL-13, 6 m tube	22:06	22:24	22:25	22:45	00:39	44:34.3580	124:59.8710			874	banana / large rock grabbed, which fell of upon reaching
14.08.	210-1	SL-14, 3 m tube	23:04	23:21	23:22	23:43	00:39	44:34.2900	124:59.8960			879	280 cm / the sea surface and touching the ship
15.08.	211	TV-MUC-52	00:36	01:04	01:07	01:31	00:55	44:34.2183	125:08.7996			778.5	failed
15.08.	212	CTD-68	02:20	02:35		04:00	01:40	44:40.1110	125:05.8510	44:40.0970	125:05.8060	596	Tow-yo CTD Gusher Site 24 bottles closed
15.08.	213												Drews
15.08.	214	CTD-69	12:17	12:56		13:57	01:40	44:34.0000	125:14.9700	44:34.0100	125:15.0100	1987.5	23 bottles closed
15.08.	215	SL-15, 3 m tube	14:36	14:54	14:55	15:15	00:41	44:34.2660	125:08.3950			816	270 cm
15.08.	216	SL-16, 3 m tube	15:58	16:24	16:25	16:51	00:53	44:34.2470	125:04.3940			1218	
15.08.	217	METS-Mooring 5a	17:31		17:56	18:09	00:38	44:39.8890	125:05.7990			615	deployed south of Gusher Site
15.08.	218-1	TV-G-10	19:31		19:59	20:14	00:43	44:27.0470	125:01.7860			615	SE-Knoll: 3 grabs; failure of TV system
15.08.	218-2	TV-G-11	20:35	21:01	21:01	21:22	00:47	44:27.0710	125:01.7950			615-620	5 grabs including 218-1 (same set of batteries) ; recovery of carbonate block (300-500 kg) / Drews
15.08.	218-3	TV-G-12	21:55	23:54	23:55	00:13	02:18	44:27.0560	125:01.8030			606	11 grabs, sample grabbed at 44°27.0560/ 125°01.8070 (598 m rope length, shallowest part) but lost during retrieval / Drews
16.08.	219	Simrad-9	00:48			13:08	12:20	44:28.2500	125:04.2900	44:27.7000	125:20.3500	600-2300	
16.08.	220	TV-MUC-53	15:06	15:37	15:39	16:03	00:57	44:34.2070	125:08.8035			775	2 good cores, 1 short, 1 failed, A = 6 cm, E = 22 cm, G = 25 cm

7. List of stations

Date	St. No.	Instrument	Time (UTC)				Duration	Begin / on seafloor		End / off seafloor		Water depth (m)	Recovery, remarks / Sample held by
			Begin	on seafloor	off seafloor	End		(hh:mm)	Latitude °N	Longitude °W	Latitude °N		
2002	SO165/		Begin	on seafloor	off seafloor	End	(hh:mm)	Latitude °N	Longitude °W	Latitude °N	Longitude °W		
16.08.	221	TV-MAC-6	17:16			18:15	00:59	44:34.2080	125:08.8140				cable flooded, no deployment
16.08.	222	SL-17, 3 m liner	18:30	18:46	18:47	19:05	00:35	44:34.2040	125:08.8050			775	
16.08.	223	TV-MAC-7	19:40	20:20	20:21	21:00	01:20	44:34.211	125:08.810			774	no pressure, 2 cores (leaked out); core catcher did not work
16.08.	224	18 kHz survey	21:59			02:30	04:31	44:39.5900	125:06.5600	44:39.6400	125:06.0200	680-590	Gusher Site, flares seen
17.08.	225	CTD-70	03:06	03:35		04:06	01:00	44:41.9900	125:09.9900	44:42.0100	125:10.0000	1071.7	24 bottles closed
17.08.	226	Simrad-10	05:01			12:35	07:34	44:47.0000	125:03.6530	44:44.8970	125:00.646	1300-700	N-S profiles Eastern Basin
17.08.	227	CTD-71	13:36	14:02		14:36	01:00	44:37.9900	125:10.0000	44:38.0000	125:10.0200	1141.6	24 bottles closed
17.08.	228-1	SL-18, 3 m tube	15:16	15:33	15:34	15:50	00:34	44:34.2110	125:08.8140			776	1 m
17.08.	228-2	SL-19, 3 m tube	16:04	16:20	16:22	16:38	00:34	44:34.2090	125:08.8060			775	1 m
17.08.	229	TV-MAC-8	17:25	17:54	17:55	18:25	01:00	44:34.2090	125:08.8240			774.6	2 cores under pressure; LTC3=39.5cm, LTC4=35
17.08.	230-1	TV-G-13	19:43	20:45	20:46	21:02	01:19	44:27.0440	125:01.8000			615	1 grab (608 m rope): 2 different samples, 1 fresh (porous, similar to 218-2), 1 altered (dense)
17.08.	230-2	TV-G-14	21:04	22:21	22:23	22:47	01:43	44:27.0690	125:01.8240			619	6 grabs incl. 230-1, large rock sample obtained at 609 m rope / Drows: 1 sample (0-10 cm) Maggiulli/TUB
18.08.	231	OFOS-7	01:58	02:13	07:41	08:05	06:07	44:54.2500	124:55.9400	44:56.8500	124:57.4100	476-670	Drows
18.08.	232	Simrad-11	09:08			12:52	03:44	44:47.0000	124:59.8000	44:32.1000	124:59.1800	800-1200	Abegg: left under pressure for CT scanning
18.08.	233	CTD-72	13:33	13:57		14:23	00:50	44:37.9900	125:00.0000	44:37.9900	125:00.0100	976.4	24 bottles closed
18.08.	234	TV-G-15	14:59	15:21	15:22	15:45	00:44	44:34.2860	124:59.9030			879	grab full, did not open: no gas hydrate
18.08.	235	METS-Mooring-5b	16:40			17:10	00:30	44:39.9090	125:05.850			615	recovery
18.08.	236	CTD-73											wrong position, CTD back onboard
18.08.	236	CTD-74	18:55	19:18		19:53	00:58	44:41.9900	124:59.9800	44:41.9900	125:00.0400	914.8	24 bottles closed
18.08.	237	TV-G-16	21:03	22:12	22:13	22:30	01:27	44:34.1110	125:09.1890			789	2 grabs, grab does not open: deployment terminated
18.08.	238	CTD-75	23:21	23:47		00:10	00:49	44:38.0100	125:05.0000	44:38.0000	125:04.9900	886	22 bottles closed